ParisTech
INSTITUT DES SCIENCES ET TECHNOLOGIES
PARIS INSTITUTE OF TECHNOLOGY

TELECOM ParisTech

2013-ENST-0019

EDITE ED 130

Doctorat ParisTech

T H È S E

pour obtenir le grade de docteur délivré par

Télécom ParisTech
Spécialité " Communications et Electronique "

présentée et soutenue publiquement par

Julie KARAKI

le 12 avril 2013

100 Gbps Coherent MB-OFDM for Long-Haul Optical Transmission

Directeur de thèse : **Yves JAOUEN**
Co-encadrement de la thèse : **Raphaël LE BIDAN**

Jury

M. Stefano WABNITZ, Professeur, Università di Brescia	President
M. Andrew ELLIS, Professeur, Aston University	Rapporteur
M. Pascal SCALART, Professeur, ENSSAT/Université de Rennes	Rapporteur
M. Stefano WABNITZ, Professeur, Università di Brescia	Examinateur
M. Bernhard SPINNLER, Dr. Ing., Nokia Siemens Networks	Examinateur
M. Philippe CIBLAT, Professeur, Telecom ParisTech	Examinateur
M. Yves JAOUEN, Professeur, Telecom ParisTech	Directeur de thèse
M. Raphael LE BIDAN, Maître de Conférence, Telecom Bretagne	Co-directeur de thèse
M. Erwan PINCEMIN, Ingénieur, Orange Labs	Invité

T H È S E

Télécom ParisTech
Ecole de l'Institut Télécom – membre de ParisTech
46, rue Barrault – 75634 Paris Cedex 13 – Tél. + 33 (0)1 45 81 77 77 – www.telecom-paristech.fr

Transmission optique longue distance avec le format MB-OFDM cohérent à 100 Gbps

Resumé:

La demande de services à forte bande passante comme la vidéo à la demande, les réseaux sociaux, le cloud,.., est en croissance permanente. Afin de fournir ces services aux utilisateurs, la capacité dans le réseau d'accès doit augmenter, entrainant ainsi une augmentation du débit dans les réseaux de transport métro / cœur.

Dans le passé, la réponse à cette demande de capacité dans le réseau de transport WDM longue-distance a été rendue possible par l'augmentation du débit des canaux NRZ-OOK de 2,5 Gbps à 10 Gbps et par la compensation de la dispersion chromatique (CD). Augmenter encore la capacité des canaux OOK n'était plus possible; la dispersion modale de polarisation (PMD) constitue une contrainte forte à la montée en débit dans les infrastructures de fibre actuelles. Heureusement, la technologie cohérente qui permet la compensation de CD et de PMD dans le domaine électronique et aussi l'utilisation des modulations multi-niveaux a permis de réaliser des transmissions à de très hauts débits. Aujourd'hui, le format « Quadrature Phase Shift Keying » avec multiplexage de polarisation (DP-QPSK) opérant à 100 Gbps est devenue un standard pour la transmission WDM longue distance.
Une alternative au format DP-QPSK permettant d'atteindre des débits de 100 Gbps et au-delà (400 G & 1Tbps) est l' « Orthogonal Frequency Division Multiplexing » (OFDM). Ce dernier est intrinsèquement robuste à la CD et à la PMD et permet d'atteindre une grande efficacité spectrale. Mais, des interrogations subsistent quant à sa robustesse aux effets non linéaires.

Dans cette thèse nous avons étudié le potentiel de la technologie OFDM pour la transmission WDM longue distance à 100 Gbps. Le traitement du signal est détaillé ainsi que la mise en œuvre du transmetteur et récepteur OFDM opérant à 100 Gbps. Nous présentons aussi les résultats expérimentaux de la transmission obtenus dans plusieurs configurations. Dans l'une de ces configurations, le canal modulé avec le format Co-DP-OFDM est multiplexé avec 40 canaux modulés en DP-QPSK à 100 Gbps. Les canaux ont ensuite été transmis sur 1000 km de fibre G.652 sans gestion de la dispersion chromatique. Dans une autre configuration, les canaux Co-DP-OFDM et Co-DP-QPSK sont combinés avec 78 canaux 10 Gbps NRZ-OOK et transmis sur 1000 km de fibre G.652 avec gestion de dispersion.
Nous avons démontré que le Co-DP-OFDM et Co-DP-QPSK ont des performances similaires après une transmission de 1000 km sur une ligne sans gestion de dispersion, et nous avons aussi démontré que la transmission de ces deux formats sur une infrastructure de fibre actuelle (présence des canaux 10 Gbps NRZ-OOK) est possible à condition de réduire de 5 dB la puissance des canaux 10 Gbps NRZ-OOK par rapport aux canaux 100 Gbps Co-DP-OFDM et Co-DP-QPSK.
Ces résultats sont précieux pour la prochaine génération de systèmes WDM à 400 Gbps ou 1 Tbps.

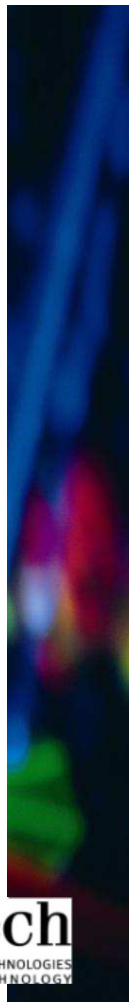

Mots clés: 100Gbps Co-DP-OFDM, 100 Gbps Co-DP-QPSK, transmission WDM.

TELECOM ParisTech

EDITE

ParisTech
INSTITUT DES SCIENCES ET TECHNOLOGIES
PARIS INSTITUTE OF TECHNOLOGY

100 Gbps Coherent MB-OFDM for Long-Haul Optical Transmission

Abstract:

The demand for more broadband services such as video on demand, social networking, cloud/grid computing…is expected to grow up. To support and provide these services to the users, the capacity in access network must increase, driving thus data rate increase in metro/core transport network.
In the past, the demand for more capacity in WDM long-haul transport network has been enabled by increasing the capacity from 2.5 Gbps to 10 Gbps based on the NRZ-OOK modulation, and by overcoming the impact of chromatic dispersion (CD) through the insertion along the transmission line of inline dispersion fiber modules. However, upgrading more the capacity of the OOK channels while keeping the legacy G-652 fiber based infrastructure was not possible due to the detrimental impact of the polarization mode dispersion (PMD) at high data rate. Fortunately, the coherent technology that permits the compensation of CD and PMD in the electronic domain and the use of multi-level modulation has enabled high data-rate transmission. Today the 100 Gbps coherent dual polarization quadrature phase shift keying (DP-QPSK) is standardized as the industrial solution for long-haul WDM transmission.
Another alternative format to DP-QPSK that permits also to reach a data rate of 100 Gbps and beyond (400 Gbps & 1Tbps) is the coherent orthogonal frequency division multiplexing (Co-OFDM) format. This last one is intrinsically robust against CD and PMD and permits high spectral efficiency. However a doubt exists whether the OFDM can be as efficient as QPSK for long-haul WDM transmission due to its supposed higher sensitivity to nonlinear effects.
In this thesis, we have investigated the potential of Co-DP-OFDM for 100 Gbps WDM transport. The digital signal processing algorithms are detailed and also, the different experimental set-ups required to carry out and validate the 100 Gbps transceiver are shown. We also present the transmission results obtained with several configurations. In one of these configurations, the 100 Gbps Co-DP-OFDM channel is multiplexed with forty 100 Gbps DP-QPSK channels and all these channels are transmitted over 1000 km of DCF-free G.652 fiber, while in another configuration, the Co-DP-OFDM and Co-DP-QPSK channels are combined with 78 NRZ-OOK channels and transmitted over 1000 km of dispersion managed G.652 fiber line.
We have demonstrated that OFDM and QPSK have nearly the same performance after a transmission over 1000 km of DCF-free fiber line, and also we have demonstrated that the transmission of these two formats over legacy fiber infrastructure (with the presence of the 10 Gbps NRZ-OOK channels) is possible under the condition of decreasing the 10 Gbps channel power with respect to the 100 Gbps Co-DP-OFDM and Co-DP-QPSK channels by 5 dB.
The results presented in this thesis are very valuable when considering the next generation of 400 Gbps or 1 Tbps for WDM systems.

Keywords : 100 Gbps Co-DP-OFDM, 100 Gbps Co-DP-QPSK, WDM transmission.

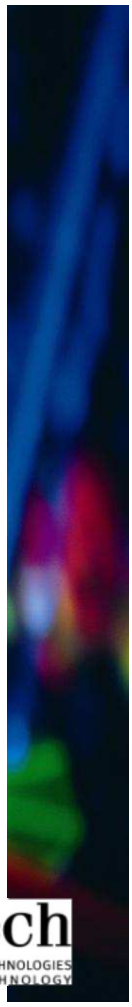

TELECOM ParisTech

ParisTech
INSTITUT DES SCIENCES ET TECHNOLOGIES
PARIS INSTITUTE OF TECHNOLOGY

Acknowledgements

This work would not been possible without the help and contribution of few people.

First of all, I wish to deliver my gratitude to the honorable jury members. I would like to thank Pr. Andrew ELLIS from Aston University of UK and Pr. Pascal SCALLAR from ENSSAT university, for accepting the role of reporters and for their constructive review of my thesis; their comments have helped me to improve the quality of this work. Also I would like to thank Pr. Stefano WABNITZ from Brescia university of Italy that has presided the thesis committee and Dr. Berhnard SPINNLER from Nokia Siemens Networks, Germany and Pr. Philippe CIBLAT from Telecom ParisTech for accepting to be a part of the thesis committee.

I would like to express my sincere gratitude to my thesis supervisor, M. Erwan PINCEMIN for the guidance and continuous encouragement. Many thanks for your suggestions, comments, and interesting and fruitful discussions. Thanks to you I have appreciated the experimental work, and I have found the motivation to do all my best to successfully achieve the thesis objectives. Without forgetting the funny moments we have got either in the SPPCOM conference or in the "Salon de Recherche". I was lucky to have you as a supervisor and also as a friend that I can count on him.

I am grateful to my thesis co-directors Pr Yves JAOUEN and Pr Raphael LE BIDAN. Many thanks for your availability all the time; suggestions and advices received from you were precious for my research. And also big thank for the time you spent on correcting this manuscript.

I would like to thank M. Didier GROT and M. Thierry GUILLOSSOU for their help in carrying out the experimental test-beds and for their cheerfulness.

I would like to thank Dr. Maryse GUENA that is on the head of SOAN team in Orange Labs for accepting me in her team during these three years. And also I would like to thank all the team for their support, help and especially for the good ambiance.

I would like to thank Dior, Jelena, Ahmed, Damien, Sofiene, Mathieu, Ramon, Paul and others who made the lab a friendly environment for working.

I would like to thank my parents Aida and Rizkallah and my two brothers Boudi and Charo, for believing in me, for their love and their supports. Also I would like to thank Jeremy for his patience and support all the time. This work has not been possible without their encouragements and their help.

Table of Contents

Table of Contents 7

Résumé de la thèse 11

Evolution de la capacité dans les transmissions optiques 11
OFDM 12

Principe de l'OFDM 12
Structure du transmetteur et récepteur OFDM 12
Emetteur de l'OFDM optique 13
Détecteur cohérent 14

Dimensionnement 14
Génération d'une sous-bande OFDM multiplexée en polarisation 16

Back-to-back électrique 17
Back-to-back optique 18
Génération d'une bande OFDM à 12.5G 18

Réglage du CMZM 18
Implémentation en back-to-back optique de l'OFDM en multiplexage de polarisation : 20
Détection hétérodyne 21

Transmetteur OFDM à 100 Gbps 22
Impact des effets linéaires sur le signal OFDM 24

Impact de la PMD 24
Impact de la CD et de la PMD 25

Transmission optique 26

Transmission de DP-OFDM et DP-QPSK sur une ligne sans gestion de la dispersion 27

Résultats expérimentaux 28

Transmission de DP-OFDM et DP-QPSK sur une ligne avec gestion de la dispersion 29

Résultats expérimentaux 30

Conclusion 33
Bibliographie 34
List of Abbreviations 35
List of Figures 40
List of Tables 44

1 Introduction 47

2 OFDM for optical communication systems 53

2.1 Capacity evolution of optical transmission 55

2.1.1 What has permitted the EDFA invention? 56
2.1.2 From 2.5 to 10 Gbps based on OOK format 57
2.1.3 Toward 40 Gbps technologies 58

2.1.3.1 10 to 40 Gbps based on OOK format 58
2.1.3.2 The coherent detection revival 59

2.1.4 100 Gbps coherent DP-QPSK systems 60

2.1.5 Beyond 100 Gbps 60
2.2 Main physical impairments in long-haul optical fiber transmission 61
2.2.1 Attenuation 61
2.2.2 Chromatic Dispersion 62
2.2.3 Polarization mode dispersion 63
2.2.4 Optical amplification 66
2.2.5 Nonlinear effects in optical fiber 68
2.2.5.1 Self-phase modulation 69
2.2.5.2 Cross-phase modulation 69
2.2.5.3 Cross-polarization modulation 70
2.2.5.4 Four wave mixing 70
2.3 OFDM for optical transmission 71
2.3.1 Generic principles of OFDM 72
2.3.1.1 OFDM principles 72
2.3.1.2 Transmitter and receiver structures 73
2.3.1.3 OFDM orthogonality concept 75
2.3.1.4 Avoiding ISI: Cyclic prefix concept 75
2.3.2 OFDM for long haul coherent optical transmission 77
2.3.2.1 Appropriate detection technique for long-haul transmission 77
2.3.2.2 Typical OFDM transmitters structures 79
2.3.3 Multi-band optical OFDM approach 80
2.3.4 Optical OFDM experiments: state of the art 81
2.3.5 All-optical OFDM solution 82
2.3.6 No guard interval coherent optical OFDM 83
2.4 Conclusion 85
Bibliography 86
3 Dimensioning & signal processing architecture of the 100 Gbps OFDM format 91
3.1 OFDM parameters design 93
3.1.1 Transmission targets, hardware constraints and design choices 93
3.1.2 OFDM sub-band design methodology and results 96
3.2 Transmitter / receiver set up 99
3.2.1 25 Gbps Transmitter set up 99
3.2.2 Receiver set up 101
3.3 OFDM digital receiver design 101
3.3.1 Transmission impairments and signal processing model 102
3.3.2 Timing Synchronization 104
3.3.2.1 Impact of a timing offset 104
3.3.2.2 Timing synchronization algorithms 107
3.3.3 Frequency synchronization 110
3.3.3.1 Impact of CFO 110
3.3.3.2 CFO estimation and correction 113
3.3.3.2.1 Estimation of the fractional part of the CFO 113

3.3.3.2.2 Estimation of the integer part of the CFO 115
3.3.4 Channel equalization 116
3.3.4.1 Channel equalization for single polarization OFDM transmission 116
3.3.4.2 Extension to CO DP-OFDM transmission 117
3.3.4.2.1 Improving channel estimation 119
3.3.4.2.2 Time domain averaging 119
3.3.4.2.3 Frequency domain averaging 120
3.3.4.2.4 Combination of TD and FD averaging 121
3.3.5 Phase noise compensation 122
3.3.5.1 Impact of phase noise 122
3.3.5.2 Phase noise compensation 123
3.4 Conclusion 125
Bibliography 126
4 Experimental implementation of 100 Gbps MB-OFDM transmitter with polarization diversity coherent receiver 129
4.1 Proposed methodology 131
4.2 Electrical back-to-back arrangement 133
4.2.1 Preliminary experiment 133
4.2.1.1 Clipping and Pre-emphasis 134
4.2.1.2 Results 135
4.2.2 Complete experiment 136
4.3 Single polarization Tx/Rx design and validation 138
4.3.1 Experimental set-up 139
4.3.2 Transmitter adjustments 139
4.3.3 Experimental results 144
4.4 Dual polarization Tx/Rx design and validation 145
4.4.1 Experimental validation with homodyne detection 146
4.4.2 Experimental validation with heterodyne detection 148
4.5 100 Gbps transmitter set-up and validation 150
4.5.1 Multi-band approach for 100 Gbps OFDM signal generation 150
4.5.2 Performance comparison with 100 Gbps DP-QPSK system 152
4.6 Impact of Linear impairments impact 153
4.6.1 First and second PMD impact on the OFDM system performance 153
4.6.2 Impact of PMD and CD on the system performance 155
4.7 Conclusion 157
Bibliography 158
5 100 Gbps Transmission Experiments 159
5.1 Representation of the performance curves 162
5.2 Mixed 100 Gbps DP-MB-OFDM and 100 Gbps DP-QPSK transmission over DCF-free fiber line 163
5.2.1 100 Gbps DP-QPSK transceiver description 163

5.2.2 100 Gbps Transmission performance 164
5.2.2.1 Experimental Results: BER Vs PIN SPAN 165
5.2.2.2 Experimental Results: BER Vs OSNR 167
5.3 Mixed 100 Gbps DP-MB-OFDM and 100 Gbps DP-QPSK transmission over dispersion-managed (DM) fiber line without the presence of 10 Gbps NRZ-OOK channels 168
5.3.1 Transmission performance comparison of the "Single-Channel" configuration with and without dispersion management 169
5.3.2 Performance comparison between "dispersion-managed WDM", "Single-Channel" and "WDM" configurations 171
5.4 100 Gbps DP-MB-OFDM and 100 Gbps DP-QPSK transmission over legacy infrastructure including dispersion-managed (DM) fiber line and presence of 10 Gbps NRZ-OOK channels 173
5.4.1 Impact of the insertion of a guard band between the 10 Gbps NRZ-OOK channels and the 100 Gbps channels 174
5.4.2 Impact of the insertion of a power dissymmetry between the 10 Gbps NRZ-OOK channels and the 100 Gbps channels 175
5.5 Conclusion 178
Bibliography 179
6 Conclusion 181
Publications and patents 186

Résumé de la thèse

La demande toujours plus forte pour des services à forte bande passante (TVHD, streaming HD, peering, jeux en ligne, grid & cloud computing, …) dans les réseaux d'accès pourrait déboucher sur une saturation des réseaux de transport longue distance, qu'il est nécessaire d'anticiper en augmentant toujours plus l'efficacité spectrale des systèmes WDM. Avec la croissance du débit transporté par chaque longueur d'onde, s'accroît également la sensibilité du canal optique à l'interférence entre symboles, et plus particulièrement à la dispersion modale de polarisation (PMD) et à la dispersion chromatique (CD). Récemment, la modulation Polarization-Multiplexing Quaternay Phase Shift Keying cohérente avec multiplexage de polarisation (Co DP-QPSK) est devenue un standard pour la transmission WDM longue distance à 100 Gbps. Grâce à la détection cohérente et à l'égalisation électronique implémentée au niveau du récepteur, cette technologie est robuste à 30 ps de PMD et à 35000 ps/nm de CD. Cependant, une autre technologie, intrinsèquement robuste au CD et PMD, est fort utile quand les contraintes en termes d'efficacité spectrale et d'interférence entre symboles sont importantes: c"est l'OFDM (Orthogonal Frequency Division Multiplexing). Cette technologie semble être une solution préférentielle pour la transmission WDM longue distance pour des débits au delà de 100 Gbps. Mais, des interrogations subsistent quant à sa robustesse aux effets non linéaires. L'objectif de cette thèse est de répondre à ces interrogations en mettant en œuvre une comparaison expérimentale des performances du format multi-bandes OFDM avec multiplexage de polarisation (DP-MB-OFDM) et DP-QPSK à 100 Gbps pour une transmission sur une ligne G.652 de 1000 km avec et sans gestion de dispersion.

Evolution de la capacité dans les transmissions optiques

La demande croissante pour des services à forte bande a nécessité la mise en place de nouvelles technologies et l"utilisation des formats de modulation adéquats permettant l"augmentation de la capacité dans les réseaux métro et cœur. La technologie la plus importante dans l"histoire des télécommunications optiques était l"invention des amplificateurs à fibre dopée Erbium « EDFA ». Les EDFAs permettent d"amplifier le signal de façon toute optique en évitant la conversion optique-électrique-optique. En plus ils ont un gain d"amplification qui s"étale sur une bande passante de 40 THz (bande C) et même sur 80 THz (bandes C et L) permettant d"amplifier plusieurs canaux simultanément et donnant ainsi naissance à une nouvelle technologie appelée multiplexage en longueur d"onde « WDM ». Cette dernière consiste à coupler dans une même fibre un grand nombre de canaux modulés, chacun sur une longueur d"onde différente, ce qui permet d"augmenter la capacité totale des systèmes. Les systèmes WDM ont été déployés dans la moitié des années quatre-vingt-dix. Chaque longueur d"onde portait un débit de 2.5 Gbps et une totalité de 40 canaux modulés en NRZ-OOK ont été transmis sur 600 km de fibre SSMF. Augmenter plus la longueur de transmission tout en augmentant le débit n"est alors plus possible à cause de l"impact de la dispersion chromatique.

De nouvelles techniques ont permis d"augmenter la capacité des systèmes de transmission WDM de 2.5 Gbps à 10 Gbps. Nous pouvons citer la gestion de la dispersion chromatique et les codes correcteur d"erreurs FEC permettant d"augmenter de façon significative la marge tolérable de dégradation des signaux.

Améliorer encore la capacité des canaux OOK n"était plus possible; la dispersion modale de polarisation (PMD) constitue une contrainte forte à la montée en débit dans les

infrastructures de fibre actuelles. Heureusement, la technologie cohérente, introduite par Nortel en 2008, qui permet la compensation de CD et de PMD dans le domaine électronique et aussi l'utilisation des modulations multi-niveaux a permis de réaliser des transmissions à de très hauts débits.
Aujourd'hui, le format DP-QPSK cohérent opérant à 100 Gbps est devenu un standard pour la transmission WDM longue distance.

OFDM

Afin de pouvoir répondre à une demande toujours plus grande de capacité dans le futur, et en raison de la disponibilité du matériel nécessaire pour la mise en place d'un émetteur / récepteur OFDM capable de traiter des signaux électriques aux débits très élevés, la technique OFDM a fait l'objet d'un certain nombre de travaux de recherche dans le domaine de communication optique. Le premier travail expérimental consistant à transmettre un signal OFDM cohérent à un débit de 8 Gbps sur 1000 km de fibre SSMF a été signalé par Shieh et al. [Shi07], rapidement suivie d'une autre expérience de transmission d'OFDM cohérent à 20 Gbps sur 4160 km de SSMF réalisé par Jansen et al. [Jan07]. En 2009, une transmission à 100 Gbps sur 1000 km de SSMF a été décrite [Jan09]. Actuellement, l'OFDM est considéré comme un concurrent au format DP-QPSK pour les hauts débits.

Principe de l'OFDM

Le principe de l'OFDM consiste à répartir l'information à transmettre sur un grand nombre de porteuses en parallèle, individuellement modulées à bas débit. Les spectres de toutes les sous-porteuses résultant d'un filtrage de mise en forme rectangulaire, sont des sinus cardinaux qui se recouvrent mutuellement. On obtient ainsi une excellente efficacité spectrale. Et vu que le signal OFDM vérifie la condition cruciale d'orthogonalité, l'information portée par chaque sous-porteuse peut être extraite sans pâtir d'interférences dûes à la porteuse voisine. L'orthogonalité entre les sous-porteuses nécessite que l'espacement entre deux sous-spoteuses adjacentes soit égal à l'inverse du temps symbole OFDM.

La durée d'un symbole OFDM est généralement beaucoup plus longue que la durée du retard induit par un canal, limitant ainsi l'impact de l'interférence entre symbole (ISI) sur une petite partie de chaque symbole OFDM. Pour éviter complètement l'ISI, un intervalle de garde est inséré entre les symboles OFDM successifs. Sa durée est choisie pour être plus longue que le retard maximal induit par le canal de transmission et il est formé par une extension cyclique du symbole OFDM, d'où l'appellation préfixe cyclique. Le préfixe cyclique permet aussi de maintenir l'orthogonalité entre les sous-porteuses et ainsi d'éviter les interférences entre sous-porteuse (ICI). En optique, le préfixe cyclique donne une robustesse face aux CD et PMD, et sa durée est choisie pour être plus grande que la durée maximale de la CD et du PMD.

Structure du transmetteur et récepteur OFDM

L'architecture du transmetteur OFDM est représentée dans la Figure 1. Les données binaires sont modulées avec une modulation M-QAM, converties en parallèle et après transmises

vers une IFFT (Inverse Fast Fourier Transform). L'IFFT permet de convertir le signal OFDM du domaine fréquentiel au domaine temporel. À la sortie de l'IFFT, on obtient des symboles OFDM complexes ; on sépare les parties réelle (I) et imaginaire (Q) et on les transmet en parallèle vers deux convertisseurs analogiques numériques (DAC). Après, les signaux I et Q analogiques sont filtrés par des filtres passe-bas afin de supprimer les aliasing générés par les DACs. Finalement, I(t) et Q(t) sont modulés par □□□□□□□□ et □ □□□□□□□□respectivement et sont combinés ensemble. Le signal généré est porté par une fréquence intermédiaire□□.

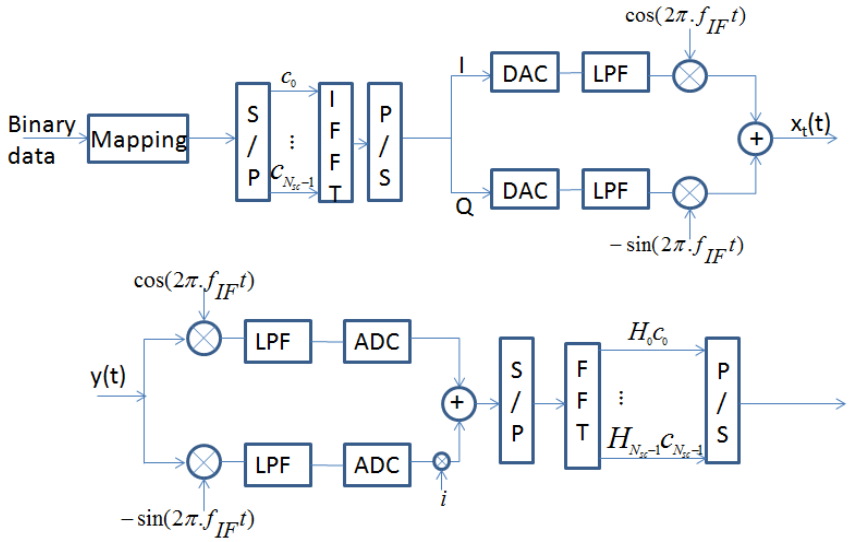

Figure 1: Emetteur et récepteur OFDM

Le récepteur OFDM consiste à envoyer le signal OFDM reçu sur deux branches parallèles ; une branche est multipliée par □□□□□□□□ et l'autre par □ □□□□□□□□. Derrière, deux filtres passe-bas sont mis en place pour supprimer les fréquences élevées. Les deux signaux filtrés sont transmis vers des convertisseurs analogiques numériques (ADC). Les deux signaux à la sortie des convertisseurs sont combinés pour former des symboles OFDM complexes. À ce niveau, une FFT (Fast Fourier Transform) est appliquée à ces symboles. Les données sont donc converties du domaine temporel au domaine fréquentiel, permettant à ce niveau l'implémentation des algorithmes de traitement du signal nécessaires pour retrouver les données émises.

Emetteur de l'OFDM **optique**

L'architecture de l'émetteur présenté ci-dessus donne un aperçu général sur la génération d'un signal OFDM pour toutes sortes d'applications. En optique, la conversion du signal électrique en un signal optique peut être réalisée de deux manières différentes: soit en utilisant un simple modulateur Mach-Zehnder (MZM), ou un MZM complexe (CMZM).
L'émetteur se basant sur un MZM est représenté sur la Figure 2.a. Le signal OFDM porté sur une fréquence RF intermédiaire est converti en un signal optique grâce à un MZM. La conversion génère une bande latérale non souhaitée qui est finalement éliminée par un filtre passe-bande optique (OBPF).
Le deuxième émetteur, représenté sur la Figure 2.b, a été essentiellement motivé par la disponibilité commerciale du CMZM [Fuj07]. Dans cette approche, la conversion est réalisée en combinant optiquement les signaux I et Q par un CMZM. Ainsi, le CMZM

élimine le besoin de l'étape de passage sur une fréquence intermédiaire électrique ainsi que le besoin d'un OBPF (aucune image latérale n'est générée ici). Pour toutes ces raisons, le CMZM est actuellement utilisé par la plupart avec la détection cohérente.

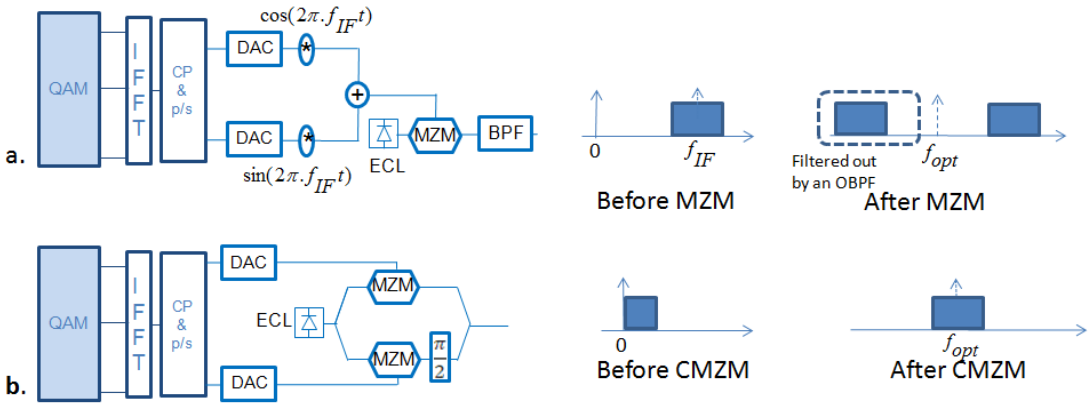

Figure 2: Schémas expérimentaux des émetteurs OFDM optiques : l'émetteur a. utilise un simple modulateur Mach-Zehnder (MZM), alors que l'émetteur b. utilise un MZM complexe (CMZM).

Détecteur cohérent

La détection cohérente est la technique de détection la plus appropriée pour les transmissions longues distances, grâce à sa meilleure sensibilité et à sa grande efficacité spectrale (par rapport à la détection directe). La biréfringence des fibres engendre une fluctuation de la polarisation du signal reçu. Un récepteur cohérent à diversité de polarisation permet de détecter le signal sur la base de 2 polarisations orthogonales

Le détecteur cohérent à diversité de polarisation est constitué de deux hybrides 90° (un pour la polarisation X et un pour la polarisation Y), qui permettent de séparer la composante en phase (I) de la composante en quadrature (Q) dans le signal OFDM. Les sorties des hybrides 90° sont envoyées sur les entrées de quatre photorécepteurs équilibrés, eux-mêmes connectés aux quatre convertisseurs analogiques numériques (ADC).

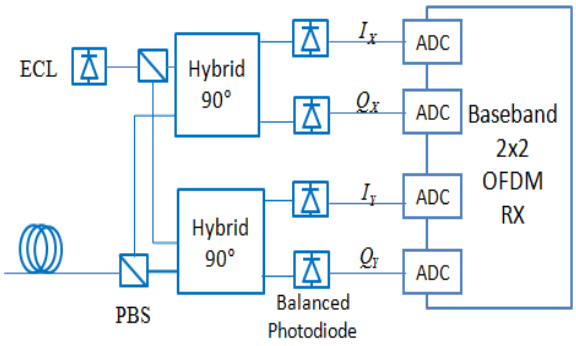

Figure 3 : Détecteur cohérent à diversité de polarisation.

Dimensionnement

En raison de la performance limitée des convertisseurs numériques-analogiques (DAC) embarqués dans les générateurs de signaux arbitraires (AWG), il est aujourd'hui très difficile

de faire tenir 100 Gbps dans une seule sous-bande OFDM. Comme par ailleurs la résolution verticale des DAC (~ 5.5 bits effectifs), le bruit de phase des lasers et surtout le bruit de phase non-linéaire généré par la propagation sur fibre interdisent d'utiliser des modulations de type QAM (Quaternary Amplitude Modulation) avec un nombre élevé d'états dans la constellation, nous avons choisi de partager le débit nominal de 100 Gbps entre quatre sous-bandes OFDM indépendantes multiplexées en polarisation.
Afin d'être compatible avec un espacement entre canaux de 50 GHz, chaque sous-bande a une largeur de 8 GHz dans le domaine optique, tandis que l'espacement entre les sous-bandes est de 10 GHz.
Le débit nominal à adresser lorsque l'on considère 100 GbEthernet de charge utile (payload) avec 4% d"overhead dédié aux protocoles et 7 % pour le codage de canal associé (FEC) est de 111 Gbps. Mais un signal OFDM nécessite un certain nombre d'overheads supplémentaires, liés à l'ajout du préfixe cyclique, des séquences d'apprentissage et des sous-porteuses pilotes. Le préfixe cyclique procure à l'OFDM sa robustesse face à l'interférence entre symboles (PMD et CD), et a été dimensionné ici pour une ligne de 1000 km de fibre G.652 sans compensation périodique de la CD (ce qui correspond à ~ 17000 ps/nm de CD cumulée). Les symboles d'apprentissage et les sous-porteuses pilotes sont là pour permettre la synchronisation, l'estimation de canal, et la compensation du bruit de phase des lasers. Le débit effectif à transmettre est alors de ~ 128 Gbps. Afin de ne pas être trop sensible à l'accumulation du bruit de phase non-linéaire au cours de la propagation et du bruit de phase des lasers, nous avons choisi de faire porter à chaque sous-porteuse une modulation QPSK. Le débit effectif porté par chaque sous-bande sur une polarisation est donc de ~ 16 Gbps. Il est contenu dans ~ 8 GHz de bande passante dans le domaine optique. Le préfixe cyclique, quant à lui, va occuper un slot temporel de 1.5 ns au début de chaque symbole OFDM. Parmi les 256 porteuses, 85 sous-porteuses sont mises à zéro (sur les bords du spectre) afin d'induire un sur-échantillonnage, permettant de séparer le signal OFDM utile de l'aliasing généré par les DACs. Chacune des quatre sous-bandes OFDM compte alors 170 sous-porteuses. A noter que la sous-porteuse centrale est mise à zéro. La durée des symboles OFDM est de 22.75 ns. La fréquence d'échantillonnage des DACs a été fixée à son maximum de 12 GSa/s.
Les valeurs résultant du dimensionnement sont présentées dans le tableau ci-dessous :

Débit nominal	100 Gbps
Nombre de sous-bandes	4 sous-bandes
Débit en comptant les overheads induits par le FEC (7%) et le protocole (4%)	111.28 Gbps
Débit effectif	128 Gbps
Débit porté par chaque sous-bande multiplexée en polarisation	32 Gbps
Modulation utilisée	4-QAM
Bande passante	8 GHz
Bande de base	4 GHz
Fréquence d'échantillonnage f_S	12 GSa/s
Dispersion chromatique cumulée	17000 ps/nm
Taille du préfixe cyclique	18 échantillons
Taille de la FFT	256
Sous-porteuses utilisées	170 sous-porteuses
Sous-porteuses mises à zéro	85 sous-porteuses
Fréquences Pilotes (□□)	5 sous-porteuses
Durée du symbole OFDM sans préfixe cyclique t_s	21.33 ns
Nombre de symboles d'apprentissage formant une séquence d'apprentissage	5 symboles
Nombre de symboles OFDM entre les séquences d'apprentissage	100 symboles
Durée du symbole OFDM avec prefixe cyclique T_S	22.83 ns
Espacement entre sous-porteuses Δf	46.9 MHz
Bande de garde entre deux bandes OFDM	2 GHz
Espacement entre canaux	50 GHz

Tableau 1 : Principaux paramètres du système OFDM proposé.

Génération d'une sous-bande OFDM multiplexée en polarisation

La génération du signal MB-OFDM portant un débit de 100 Gbps nécessite en premier lieu la génération d'une bande OFDM multiplexée en polarisation et ayant un débit de 25 Gbps.

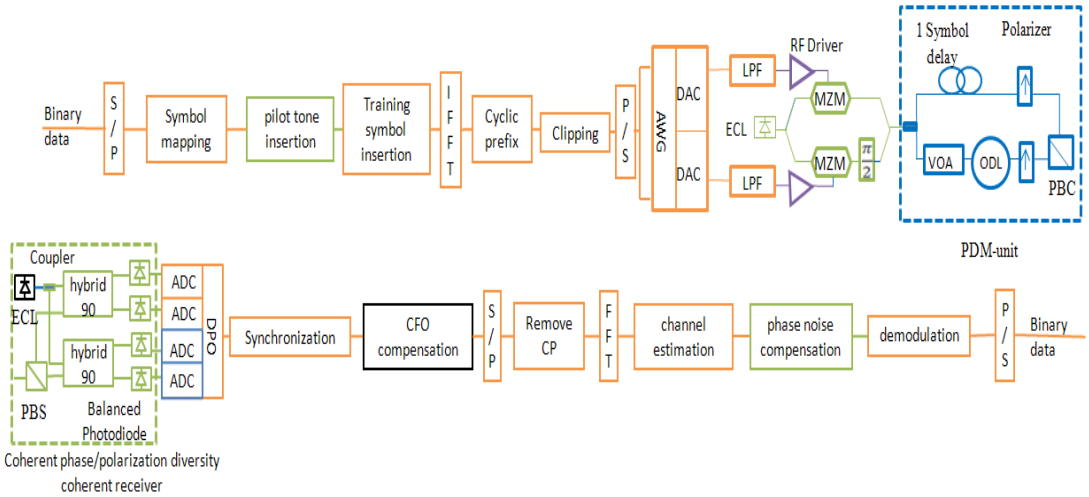

Figure 4 : Schéma expérimental de l'émetteur / récepteur OFDM mis en œuvre pour générer une sous-bande OFDM.

La Figure 4 montre le schéma expérimental de l'émetteur et récepteur OFDM implémenté afin de générer et détecter une sous-bande OFDM. La mise en œuvre expérimentale de ce système était faite en plusieurs étapes successives qui sont identifiées par des couleurs différentes sur cette figure et qui ont été menées successivement afin d'évaluer et valider l'émetteur et le récepteur.
Dans la suite, nous allons développer les différentes expériences expérimentales.

Back-to-back électrique

La première expérience consiste à valider en deux étapes le système en back-to-back électrique. Tout d'abord, les sorties filtrées de l'AWG ont été connectées aux ADCs incorporés à l'intérieur de l'oscilloscope (DPO). Les blocs de cette étape sont repérés par la couleur orange sur la Figure 4.
Le spectre électrique du signal I(t) à la sortie du DAC est illustré sur la Figure 5. Une différence d'intensité de l'ordre de 8 dB est observée entre la première et la dernière sous-porteuse du signal OFDM. Cette atténuation est inacceptable et nécessite une correction de la réponse fréquentielle non idéale des DACs. Plusieurs techniques existent pour faire cette correction. Ici, nous avons choisi de profiter de la fonction d'égalisation fournies par l'AWG et qui permet d'égaliser la puissance des différentes sous-porteuses OFDM. Après égalisation, le spectre est uniforme et il est représenté à droite de la Figure 5.

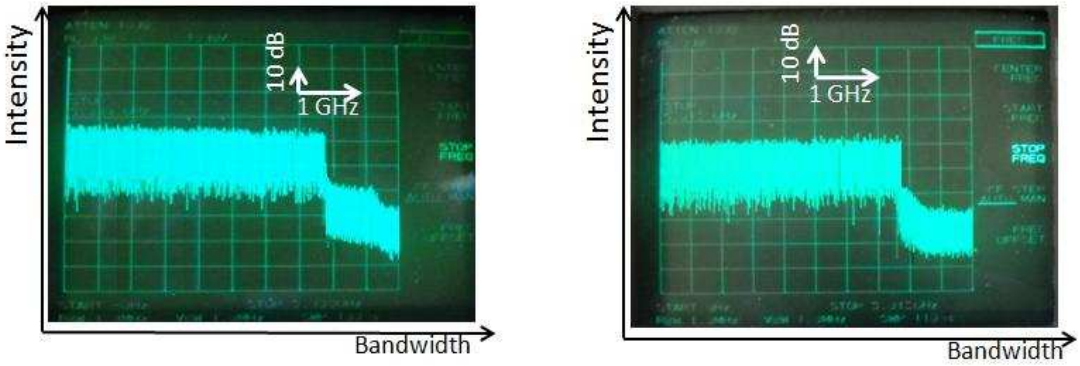

Figure 5 : Spectre de l'OFDM en bande de base observé sur un analyseur de spectre **électrique à la sortie filtrée** d'un des DACs **(à gauche) sans et (à droite) avec égalisation du spectre.**

Dans la deuxième étape de validation du système en back-to-back électrique, nous avons inséré les drivers derrière les filtres du coté transmetteur. A ce niveau, une optimisation des valeurs d'atténuation au niveau des entrées des drivers RF a été nécessaire pour que ces dispositifs fonctionnent dans leur régime linéaire.

Afin d'évaluer les performances du système en back-to-back électrique, nous avons tracé dans la Figure 6 les courbes du taux d'erreur binaire (BER) en fonction du rapport signal à bruit (SNR) pour un canal AWGN. Le bruit a été ajouté au signal OFDM avant de le transmettre aux ADCs. Les courbes sont obtenues dans le cas où les sorties filtrées des DACs sont connectées aux ADCs et dans le cas où le driver est également inséré. Ces courbes ont été comparées avec la courbe théorique. Les trois courbes sont superposées indiquant qu'aucun des composants électriques n'induit de pénalité.

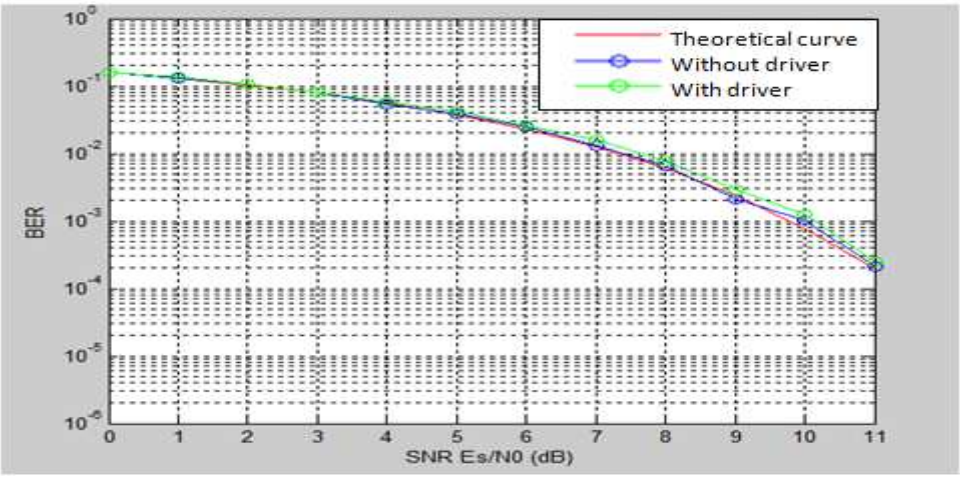

Figure 6 : BER en fonction du SNR du signal OFDM électrique.

Back-to-back optique

Nous allons décrire dans cette section les étapes réalisées successivement pour générer un signal OFDM optique multiplexé en polarisation et portant un débit de 25 Gbps.

Génération d'une bande OFDM à 12.5G

Le passage au domaine optique a nécessité l'insertion d'un modulateur CMZM derrière les drivers et la mise en place du détecteur cohérent. Ce dernier est connecté aux convertisseurs analogiques numériques (ADC) fonctionnant à une vitesse d'échantillonnage de 50 GSa/s. Un laser à cavité externe (ECL), ayant une largeur de raie de ~100 kHz est connecté au modulateur CMZM et au récepteur cohérent. Le laser génère un bruit de phase, et par conséquent induit une erreur de phase commune affectant tous les sous-porteuses dans chaque symbole OFDM. Pour compenser le bruit de phase du laser, nous avons implémenté l'algorithme du CPE (common phase error) [Pet07].
L'étape la plus cruciale dans cette partie était le réglage du transmetteur OFDM et spécialement le CMZM.

Réglage du CMZM

A la sortie des convertisseurs, les deux composants I et Q du signal OFDM empruntent deux trajets différents. Chaque trajet est constitué d'un filtre passe-bas (LPF), un atténuateur, un driver, et un câble RF. Ensuite, les deux signaux I et Q sont optiquement combinés par un CMZM. Par conséquent, plusieurs composants présents dans l'émetteur peuvent être la source d'un déséquilibre IQ. Un déséquilibre IQ est dû à une différence de gain entre les bras I et Q, à une déviation de la phase de 90° entre les deux voies, ou à un retard temporel entre les deux composants du signal OFDM.

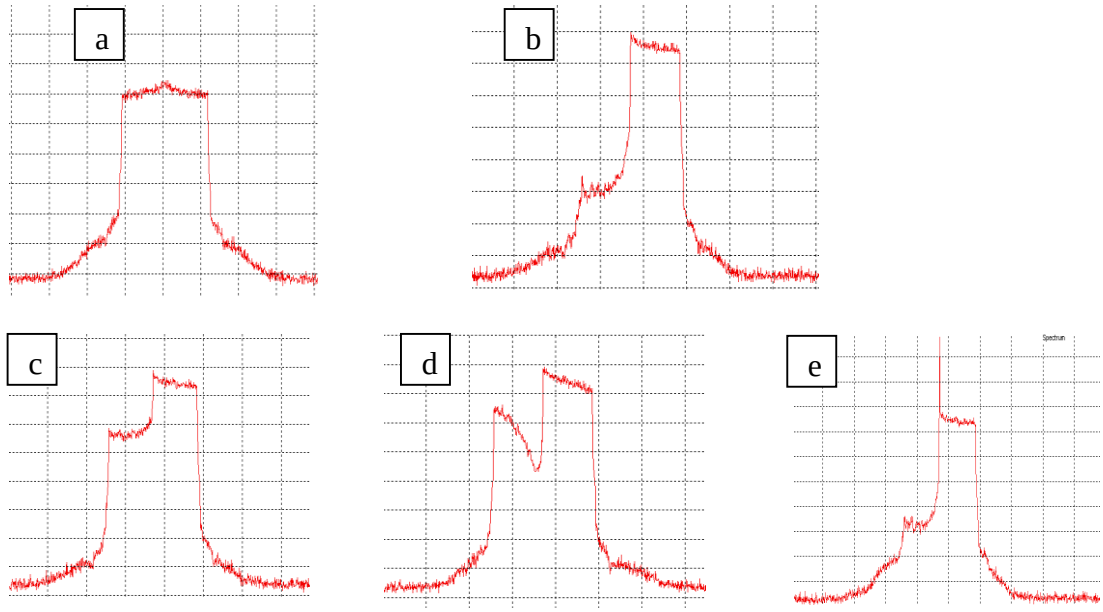

Figure 7 : Spectres de l'OFDM observés sur un analyseur de spectre optique. a) représente le spectre lorsque la composante continue est supprimée du signal. Les autres spectres représentent la bande supérieure du signal OFDM. On identifie dans b) un réglage parfait du transmetteur, dans c) un déséquilibre de phase ou de gain, dans d) un retard temporel entre I et Q, et dans e) la présence de la composante continue dans le signal.

Une différence de gain entre les voies I et Q peut être présente à cause d'une différence légère entre les valeurs des atténuateurs mises en place dans la chaîne RF sur chacune des deux voies I et Q, ou d'une différence des gains des drivers RF. En plus, un petit écart entre la longueur des composants électriques se traduira par un temps de retard entre les signaux I et Q. Enfin, un réglage inexact de tension de déphasage du CMZM peut provoquer une déviation de 90°.
Le réglage du transmetteur OFDM peut se faire d'une façon expérimentale. On envoie sur un analyseur de spectre optique les fréquences positives (ou justement négative) du signal OFDM. La présence d'un déséquilibre IQ se manifeste par la présence des fréquences négatives qui sont une image des fréquences positives par rapport à la porteuse optique.
Pour supprimer le déséquilibre IQ dû à une différence de gain entre les voies I et Q, on régle les tensions du driver de sorte à maximiser la différence de puissance entre la bande des fréquences positives et négatives. Concernant le retard temporel induit entre les deux voies, on insère des lignes de retard sur les deux voies tout en les ajustant pour minimiser la puissance de la bande image. Finalement, pour régler un déphasage de 90°, on ajuste dans le même principe la tension de la phase du CMZM.
Dans l'étape du réglage de transmetteur, il reste à supprimer la composante continue présente dans le spectre du signal. Cette étape est mise en place par un réglage fin de la tension des deux MZMs (qui constituent le CMZM). Une fois que les tensions de polarisation des deux MZMs sont bien réglés au niveau du point d'émission nulle, la porteuse optique est éliminée et on obtient le spectre montré dans la Figure 7 (a ou b).

Le taux d'erreur binaire (BER) a été mesuré en fonction du rapport signal à bruit optique (OSNR) dans une largeur de bande de référence égale à 0.1 nm. La sensibilité en back-to-back mesurée est comparée à la mesure de back-to-back obtenue dans [JanM08]. Dans cette référence, les auteurs ont généré deux sous-bandes OFDM, chacune portant un débit de données brutes de 10 Gbps. Des algorithmes de traitement de signaux numériques très similaires ont été mis en œuvre, exception faite pour la compensation de bruit de phase.

Dans la référence [Jan08], les auteurs ont mis en œuvre la méthode du pilote RF. Les deux courbes de performance sont présentées dans la Figure 8. Nous avons mesuré un BER =10^{-3} pour une valeur d'OSNR de 6,5 dB, alors que dans la référence considérée, l'OSNR est supérieure à 8,7 dB. Généralement, aux petits OSNRs, notre système a de meilleures performances que le système de référence, et des performances similaires sont obtenues à des OSNR élevées, validant ainsi notre système.

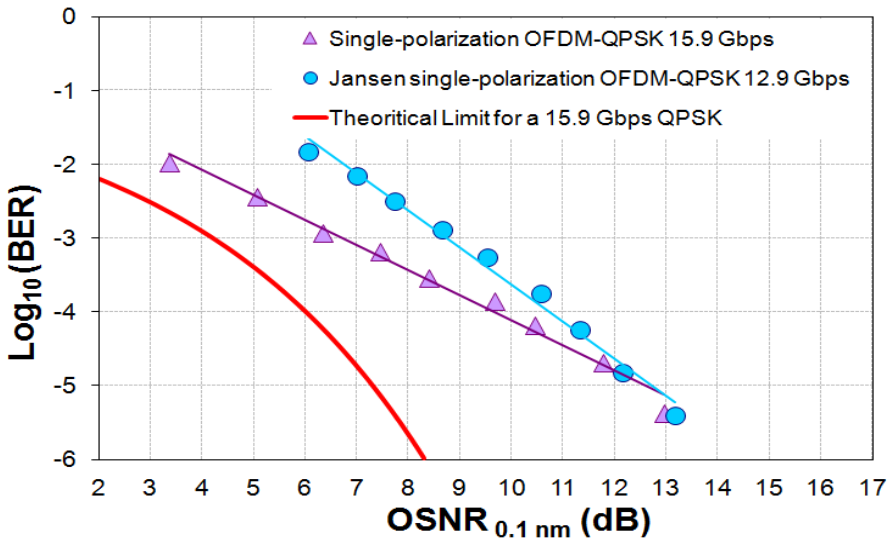

Figure 8 : BER en fonction de l'OSNR (mesuré dans 0.1 nm) en configuration simple polarisation. La courbe de la référence [Jan08] est aussi tracée, ainsi que la limite théorique pour un signal QPSK portant 15.9 Gbps.

Implémentation en back-to-back optique de l'OFDM en multiplexage de polarisation :

La troisième expérience, présentée en bleu dans la Figure 4, a permis la génération d'un signal OFDM multiplexé en polarisation.
Cette étape a nécessité l'insertion du module de multiplexage de polarisation, à la sortie du CMZM, qui est basé sur la mise en œuvre d'un retard temporel d'un temps symbole (correspondant à ~ 22.75 ns) sur l'un des bras du multiplexeur. Du coté software, l'algorithme d'égalisation de canal a été implémenté afin de séparer les deux composantes en polarisation du signal OFDM. Pour ce faire, cinq symboles consécutifs, dont deux symboles portent des données et trois symboles sont vides, sont associés dans la séquence d'apprentissage de la manière présentée dans la Figure 9. Après multiplexage de polarisation et transfert d'énergie entre les deux polarisations, les symboles vides de la séquence d'apprentissage contiennent de l'énergie. En comparant les symboles reçus et le symbole d'apprentissage émis contenant de l'information, on estime le canal, et l'égalisation est faite avec la technique du « Zero Forcing » (ZF).
Deux méthodes ont été combinées pour améliorer l'estimation du canal. La première connue sous le nom de « Intra-Symbol Frequency Averaging » (ISFA) [Liu08] consiste à améliorer l'estimation du canal en moyennant la réponse du canal obtenue sur les sous-porteuses voisines. La réponse du canal obtenue par la méthode ISFA sur chaque symbole est ensuite moyennée sur deux symboles d'apprentissage constituant la séquence d'apprentissage (méthode de moyennage temporel des symboles d'apprentissage). Pour plus de détails, voir le chapitre 3.

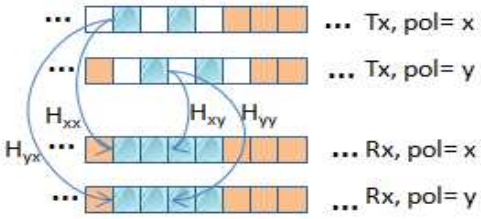

Figure 9 : Structure des séquences d'apprentissage.

La courbe de sensibilité a été tracée et comparée à la courbe en simple polarisation. Etant donné que sur toute la gamme d'OSNR mesurés l'écart entre les deux configurations fluctuent entre 2.7 dB et 3.5 dB, alors la pénalité induite par le processus de séparation de polarisation et l'égalisation ZF est négligeable.

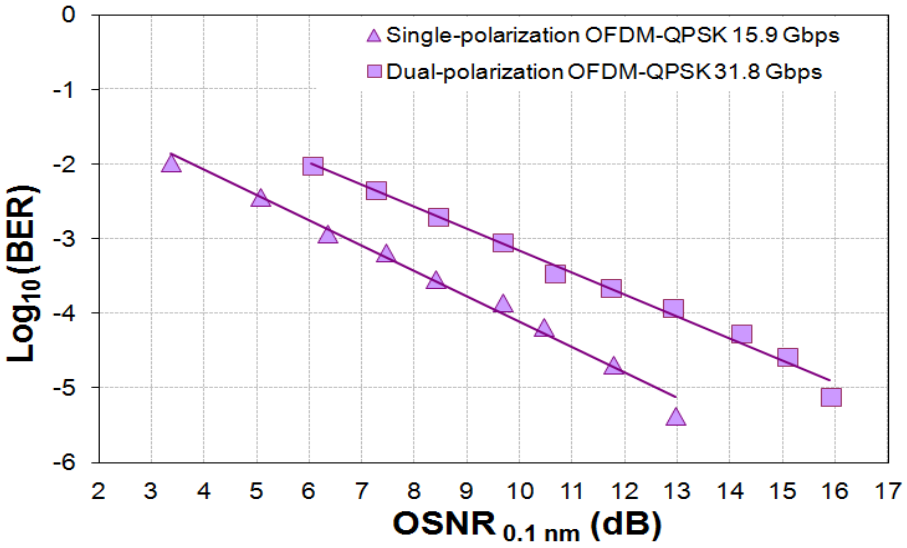

Figure 10 : BER en fonction de l'OSNR (mesuré dans 0.1 nm) en configuration simple et double polarisation.

Détection hétérodyne

Jusqu'à présent, la détection mise en place était une détection homodyne. Dans cette dernière étape, une détection hétérodyne est établie en utilisant deux lasers différents pour le CMZM et le récepteur cohérent. Les blocs supplémentaires nécessaires pour cette expérience sont représentés en noir dans la Figure 4. Le passage de la détection homodyne à la détection hétérodyne induit un offset de fréquence (CFO). La compensation de l'offset de fréquence est une étape essentielle à implémenter derrière la synchronisation du signal OFDM. Une erreur sur l'estimation du CFO peut se traduire par des interférences inter-porteuses ou bien par une dégradation complète de la performance du système.

L'offset de fréquence se décompose en une partie fractionnaire égale à une fraction de l'espacement entre deux sous-porteuses □.□f (□<1) et en une partie entière n.□f (n est entier positif ou négatif), qui peut être au delà de 1 GHz. La partie fractionnaire du CFO (□.□f avec □<1) est estimée par la méthode décrite par [LiY06]. L'estimation de la partie entière du CFO consiste à comparer le spectre émis et reçu. Nous présentons dans la Figure 11 le spectre du signal OFDM à l'émission et à la réception. Nous remarquons que la dernière fréquence du spectre est repérée sur une autre fréquence. Ce décalage est dû à une rotation

du spectre de la bande OFDM à cause du CFO. Après correction de la partie fractionnaire, et après la FFT ce décalage est estimé. La méthode d'estimation et de compensation est bien détaillée dans le chapitre 3.

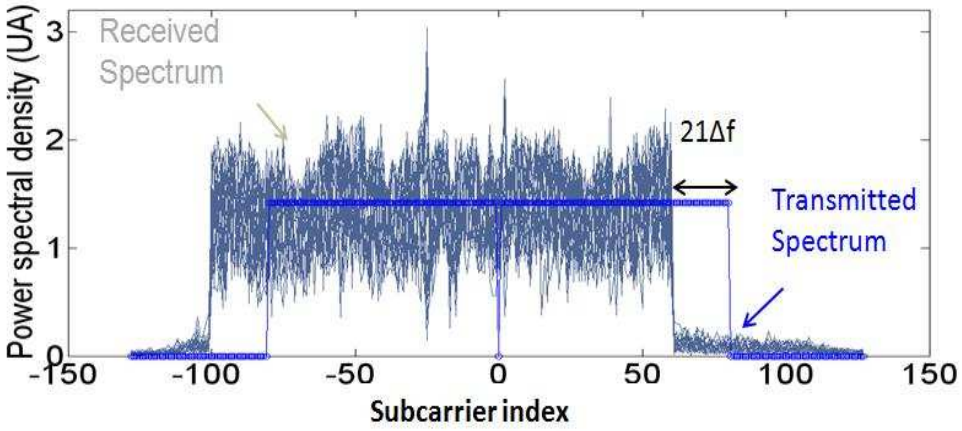

Figure 11 : Superposition des spectres du signal OFDM à l'émission et à la réception. On y visualise la partie entière de l'offset de fréquence **correspondant à 21.Δf**

La Figure 12 montre les courbes du BER en fonction d'OSNR obtenues avec une détection homodyne et une détection hétérodyne. Pour la détection homodyne, l'estimation de CFO n'est pas nécessaire et la courbe de sensibilité correspondant (carré rose sur la Figure 12) est utilisée comme référence. Nous n'avons pas observé de différences significatives entre les deux courbes de performance. Ceci valide l'efficacité de notre méthode de compensation du CFO.

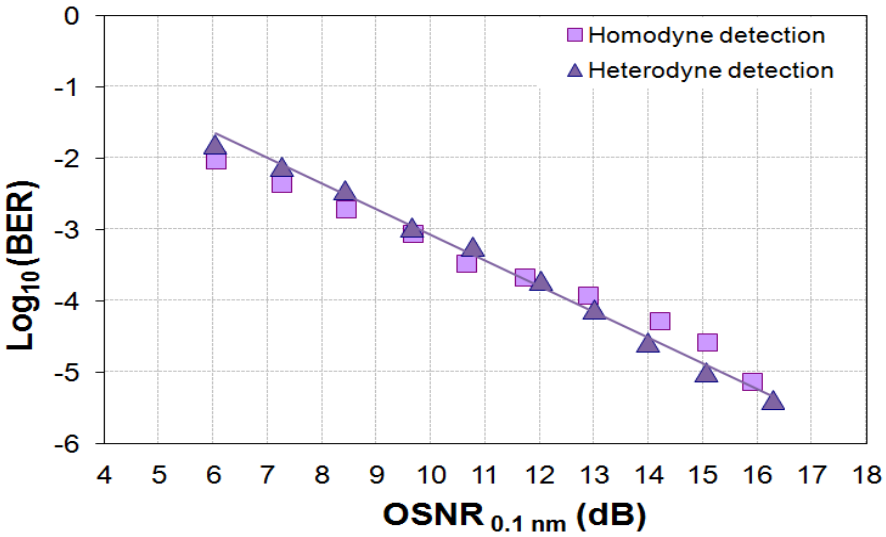

Figure 12 : BER en fonction de l'OSNR (mesuré dans 0.1 nm) en configuration double polarisation mesuré avec détections homodyne et hétérodyne.

Transmetteur OFDM à 100 Gbps

La Figure 14 montre le montage expérimental de l'émetteur permettant de générer le signal MB-OFDM avec multiplexage de polarisation opérant à 100 Gbps. Un peigne de porteuses

optiques espacées de 10 GHz (Figure 13) est généré grâce à un modulateur Mach-Zehnder (MZM) alimenté par une fréquence RF à 10 GHz ayant une grande amplitude, selon les recommandations de la référence [Sak07]. Cependant, l'aplatissement spectral est établi en réglant finement la tension de polarisation du MZM.

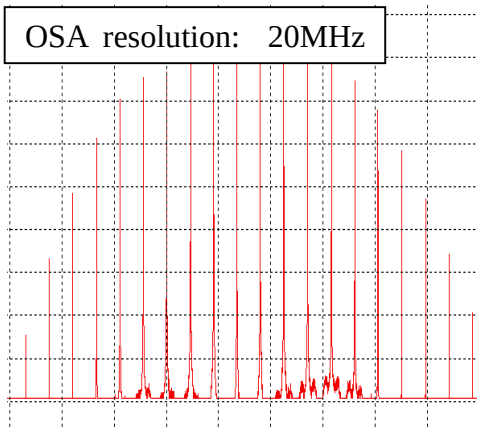

Figure 13 : Peigne de sous-porteuses espacées de 10 GHz obtenu à la sortie du MZM.

Une combinaison des lignes à retard interférométrique et à maintien de polarisation de 20 GHz et 40 GHz (PM-DLI) permet de diviser le peigne initial de sous-porteuses espacées de 10 GHz en quatre peignes de sous-porteuses espacées de 40 GHz. Chaque peigne est modulé individuellement par un CMZM, et les quatre signaux optiques obtenus à la sortie des CMZMs sont combinés ensemble par l'utilisation d'un coupleur à maintien de polarisation 04:01.
En ce qui concerne la génération des signaux OFDM en bande de base, nous profitons du fait que les AWGs peuvent fournir à la fois un signal I / Q complexe et son complément. Ainsi, globalement, deux AWGs, AWG1 et AWG2, (au lieu de 4) sont suffisants pour générer les 4 signaux complexes correspondant aux quatre sous-bandes. Afin d'assurer que les données transportées par les sous-bandes voisines sont décorrélées, AWG1 génère des données pour les première et troisième sous-bandes et AWG2 génère les données pour les deuxième et quatrième sous-bandes. Un amplificateur EDFA à maintien de polarisation (PM-EDFA) compense les pertes introduites par le MZM, les DLI, les CMZMs et le coupleur et alimente le module de multiplexage de polarisation. A la sortie de ce module, un filtre passe-bande optique (BPF) de bande passante de ~ 40 GHz est utilisé pour sélectionner les quatre sous-bandes OFDM. Le spectre de notre signal 100 Gbps DP-MB-OFDM à la sortie de l'émetteur est affiché dans l'encart de la Figure 14.

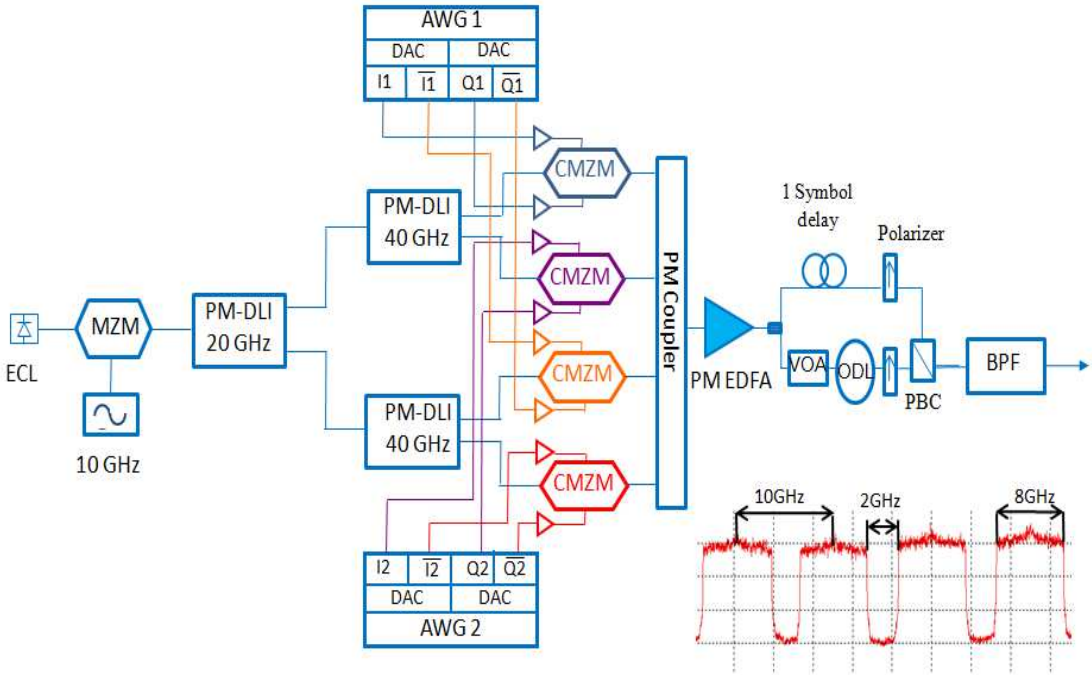

Figure 14 : Schéma expérimental de l'émetteur OFDM mis en œuvre pour générer quatre sous-bandes OFDM multiplexées en polarisation et portant un débit total de 100 Gbps.

Impact des effets linéaires sur le signal OFDM

Dans cette section, nous étudions l'impact de la PMD du premier et du second ordre sur la performance du système cohérent 100 Gbps PM-MB-OFDM avec détection homodyne. La polarisation du signal est brouillée par un brouilleur de polarisation (PS) permettant de varier l'état de polarisation à une vitesse de 70 ° / ms. Le PS est placé avant l'émulateur de la PMD.

Dans la deuxième partie de cette section, nous évaluons, dans le cadre d'une détection hétérodyne, la performance du système en présence de la PMD du premier et second ordre et aussi de la CD.

Une sous-bande OFDM à 25 Gbps, choisie au milieu du multiplex MB-OFDM, a servi pour étudier l'impact des effets linéaires sur notre système.

Impact de la PMD

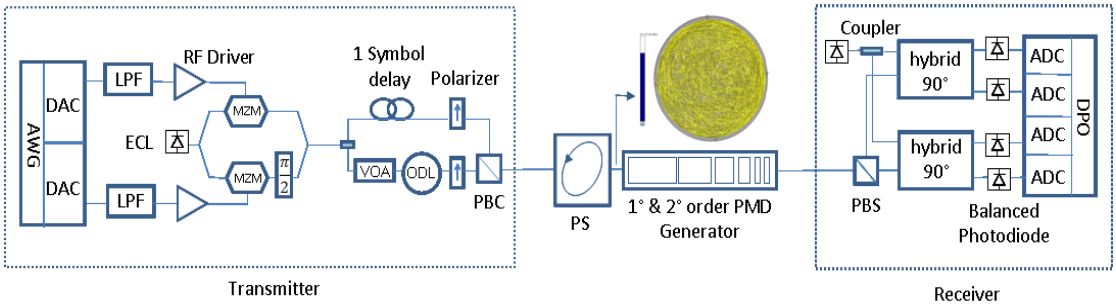

Figure 15 : Montage expérimental. La trace de l'état de polarisation sur la sphère de Poincaré à la sortie du brouilleur de polarisation (PS) est aussi donnée.

Afin de stresser le signal avec la PMD tout en se mettant dans les conditions réalistes du terrain, un brouilleur de polarisation suivi d'un émulateur de PMD ont été insérés en amont du récepteur cohérent. Le brouilleur permet de modifier la vitesse de variation de l'état de polarisation. Il est capable d'atteindre une vitesse de 70°/ms qui est la plus grande valeur mesurée sur le terrain, et l'émulateur de PMD est capable d'émuler une valeur de PMD de premier ordre (FOPMD) égale à 180 ps et de PMD du second ordre (SOPMD) égale à 8220 ps².

L'impact de la PMD sur une bande OFDM multiplexées en polarisation a été évalué. La Figure 16 nous montre les courbes de sensibilités mesurées avec quatre différentes configurations de PMD du premier et second ordre : 0 ps / 0 ps², 180 ps / 0 ps², 112.6 ps / 6052 ps², et 128.4 ps / 8220.6 ps².
Les courbes de sensibilité ont montré qu'aucune combinaison de PMD du premier ordre avec la PMD du second ordre n'a un impact sur le signal OFDM.

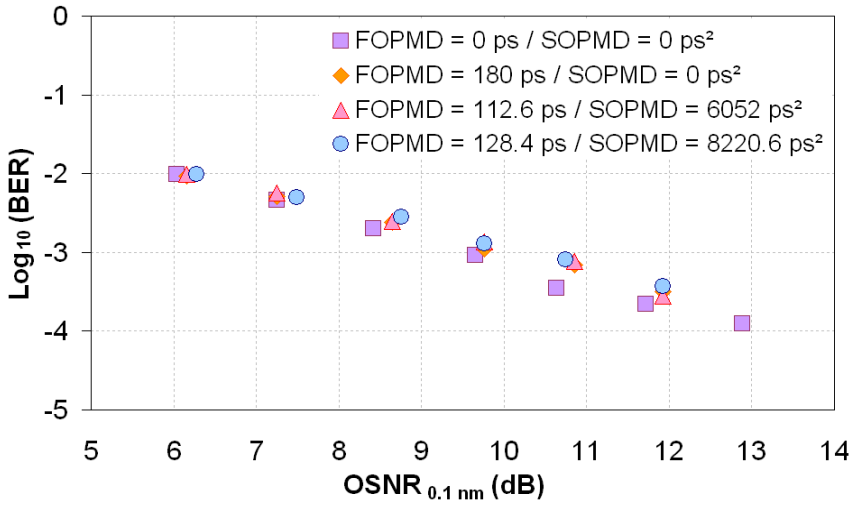

Figure 16 : BER en fonction de l'OSNR (mesuré dans 0.1nm) mesuré avec différentes configurations de **PMD du premier et second ordre et avec une vitesse de brouillage de polarisation de 70°/ms.**

Impact de la CD et de la PMD

Dans cette dernière expérience de caractérisation du système en back-to-back, nous avons inséré en plus du brouilleur de polarisation (PS) et de l'émulateur de PMD, un émulateur de la dispersion chromatique à base de fibres de Bragg (Teraxion ClearSpectrumTM DCMEX) émulant une valeur fixe de CD de 10000 ps/nm. Le but ici était d'évaluer l'impact de la CD et de la PMD sur le signal OFDM en l'absence des effets non-linéaires. Le montage expérimental correspondant est décrit dans la Figure 17.

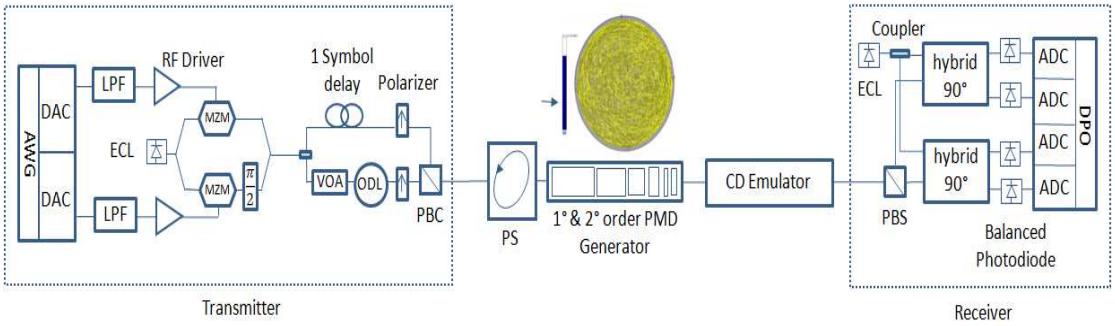

Figure 17 : Montage expérimental.

Le BER en fonction d'OSNR est évalué dans différentes configurations. Le système a été stressé par: 10000 ps / nm de CD uniquement, -10000 ps / nm de CD et 180 ps de FOPMD, 10000 ps / nm de CD, 128 ps de FOPMD et 8220 ps² de SOPMD. Les résultats sont présentés dans la Figure 18. Les courbes de sensibilités obtenues en back-to-back avec détections homodyne et hétérodyne et sans la présence des effets linéaires sont tracées pour fournir une référence.
Aucune pénalité d'OSNR n'a été observée pour des BER de valeurs supérieures à 10^{-4}. Par contre pour des valeurs de BER inférieurs, un plancher d'erreur apparaît autour de 10^{-5}, montrant que les valeurs élevées de CD et de PMD ont un impact sur la performance du système.

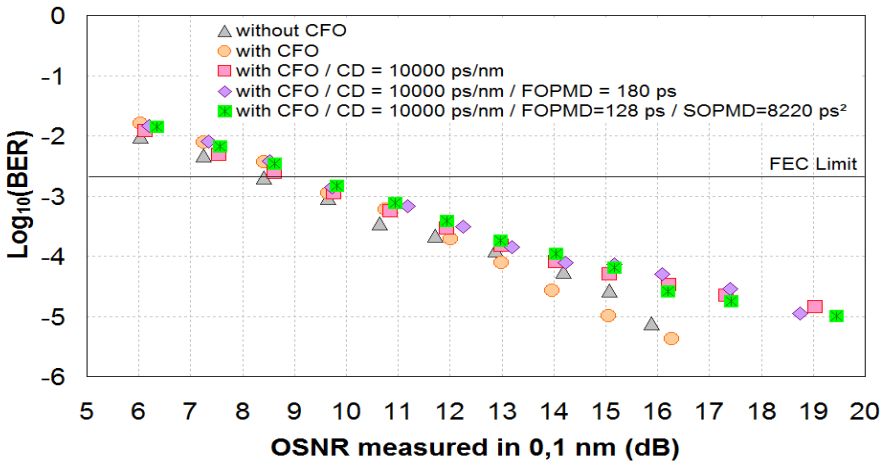

Figure 18 : BER en fonction de l'OSNR (mesuré dans 0.1nm) mesuré avec différentes configurations de PMD et de CD et avec une vitesse de brouillage de polarisation de 70°/ms.

Transmission optique

Dans cette section, nous comparons les performances des signaux cohérents 100 Gbps DP-MB-OFDM et 100 Gbps DP-QPSK après une transmission de 10x100 km sur une fibre G.652 sans insertion des modules de compensation de la dispersion (DCM). Ce type de configuration de la ligne est connu sous le nom de transmission DCF-free. Deux systèmes différents sont ainsi étudiés: le premier correspond à la configuration "Single-Channel" dans lequel seulement deux canaux bien espacés portant chacun un débit de 100 Gbps sont transmis (un portant le format DP-MB-OFDM et l'autre le format DP-QPSK), tandis que les autres longueurs d'onde ne transportent pas de données, le second correspond à la configuration "WDM", où les deux canaux précédents sont couplés avec des longueurs

d'ondes espacées de 50 GHz et modulés avec 100 Gbps DP-QPSK. Nous démontrons que le 100 Gbps DP-MB-OFDM est aussi robuste que le 100 Gbps DP-QPSK pour une transmission de 1000 km avec les configurations "Single-Channel" et "WDM": ces résultats apportent une réponse claire aux suppositions prédisant que l'OFDM est plus sensible aux effets non-linéaires dans la fibre.

Un deuxième apport original de notre travail provient de la comparaison des performances des deux formats cohérents DP-MB-OFDM et DP-QPSK pour une transmission avec un débit de 100 Gbps sur une ligne G.652 avec insertion des modules de gestion de la dispersion (DM). Dans un premier temps, seuls les canaux à 100 Gbps, DP-MB-OFDM et DP-QPSK, ont été transmis sur cette ligne. Cette configuration fournit une référence pour les expériences qui ont été faites dans une seconde étape. Ces expériences reproduisent les mêmes configurations de transmission sur les infrastructures de fibre existantes, qui sont constituées de fibre G.652 à gestion de dispersion et un système WDM avec des canaux 10 Gbps NRZ-OOK. Dans ce schéma, les canaux à 100 Gbps sont multiplexés avec les 78 canaux à 10 Gbps. Cette configuration permet d'effectuer une augmentation de débit des systèmes WDM déployés à 10 Gbps d'une façon douce et progressive.
Nous comparons ainsi les performances de ces deux techniques de modulation sur une fibre G.652 à gestion de dispersion et de longueur 10x100 km. Nous montrons que les deux signaux à 100 Gbps ne sont pas en mesure d'opérer sous le seuil FEC même en présence d'une bande de garde entre les canaux à 10 Gbps et à 100 Gbps. Cependant, en réduisant la puissance des canaux NRZ-OOK par rapport à celle des signaux à 100 Gbps, le DP-MB-OFDM et DP-QPSK gagnent un peu de performance et peuvent être considérés comme exempts d'erreurs (après FEC). Pour cette configuration particulière, nous montrons que le 100 Gbps cohérent DP-MB-OFDM n'est pas désavantagé par rapport au 100 Gbps cohérent DP-QPSK.

Transmission de DP-OFDM et DP-QPSK sur une ligne sans gestion de la dispersion

Le signal 100 Gbps DP-MB-OFDM décrit précédemment est porté par la longueur d'onde à 1552,93 nm et est introduit dans un multiplex de quarante longueurs d'onde espacées de 50 GHz et modulées en 100 Gbps DP-QPSK (Figure 19). Un seul canal DP-QPSK à 100 Gbps est modulé par un ECL à 1548,11 nm, tandis que les trente-neuf autres canaux sont modulés par des laser diodes (LD). Les canaux 100 Gbps DP-QPSK pairs et impairs sont multiplexés séparément, indépendamment modulés, et combinés avec le 100 Gbps DP-MB-OFDM via un coupleur. La ligne de transmission est constituée de 10 spans de 100 km de G.652 séparés par des amplificateurs EDFA. Au milieu de la ligne est inséré un égalisateur de gain afin d'aplatir la puissance des canaux optiques après une transmission de 1000 km.

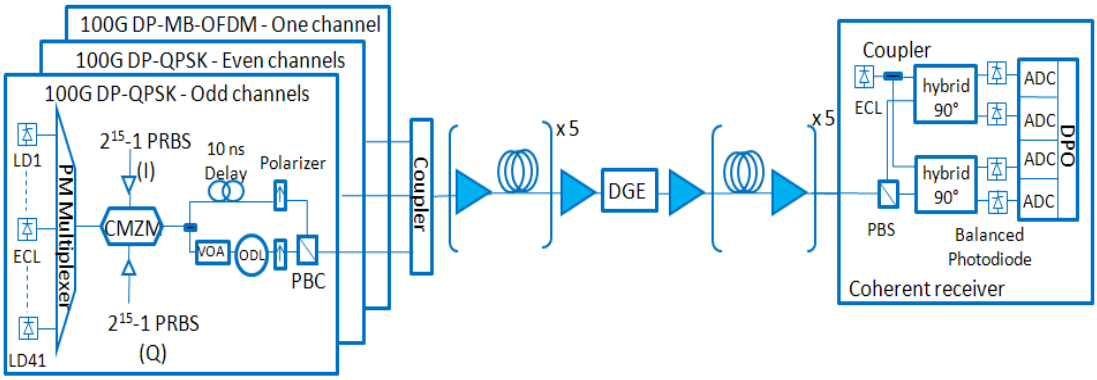

Figure 19 : Montage expérimental des émetteurs de DP-MB-OFDM et DP-QPSK, de la ligne de transmission et du détecteur cohérent.

Les signaux DP-MB-OFDM et DP-QPSK sont détectés par un détecteur cohérent et le traitement offline des signaux est réalisé.

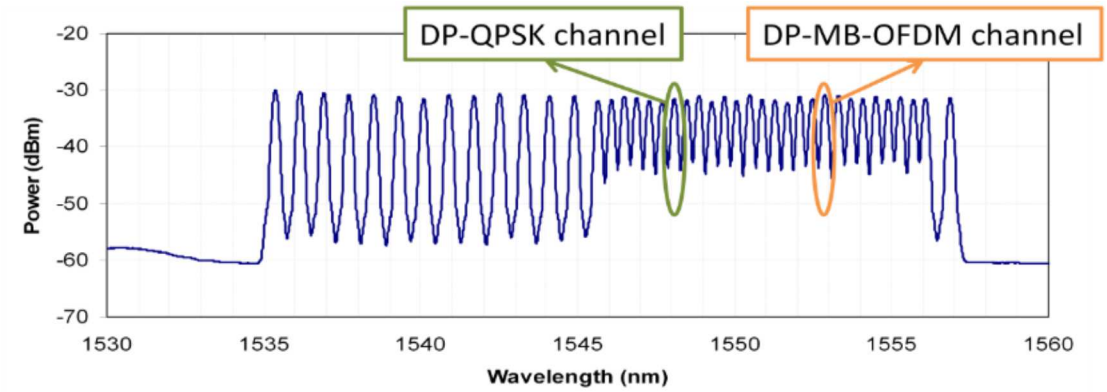

Figure 20 : Spectre des 41 canaux portant chacun un débit de 100 Gbps y compris les deux canaux DP-MB-OFDM et DP-QPSK qui font l'objet de toutes les mesures.

Résultats expérimentaux

Deux configurations ont été évaluées ; la première notée sur la Figure 21 par « Single Channel » correspond au cas où juste les deux canaux 100 Gbps DP-MB-OFDM et 100 Gbps DP-QPSK sont transmis avec 39 canaux non modulés. La deuxième configuration notée par « WDM » correspond au cas où tous les canaux sont modulés.

Afin de comparer la performance des signaux DP-MB-OFDM et DP-QPSK dans ces deux configurations, les courbes de BER en fonction de la puissance injectée par canal (PIN SPAN) ont été tracées. A noter qu"un canal OFDM correspond à un multiplex de 4 sous-bandes OFDM.

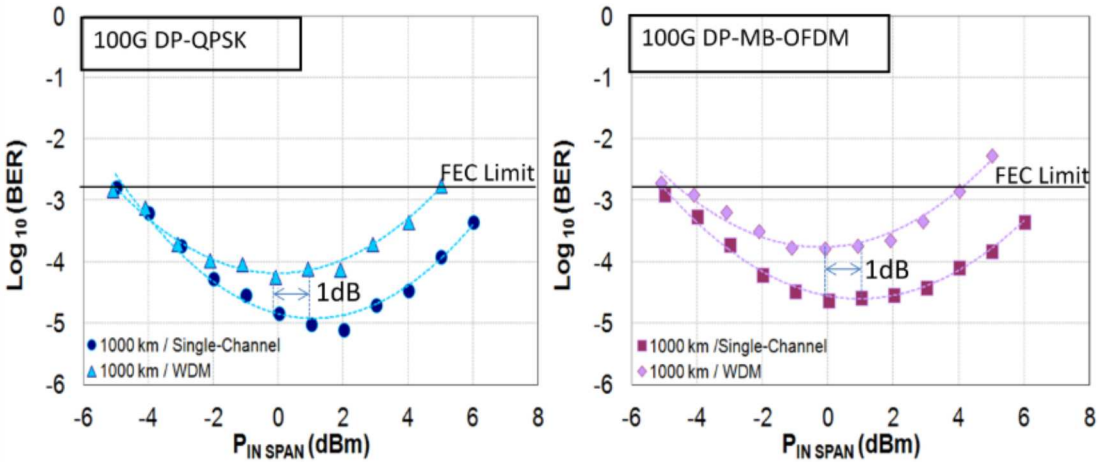

Figure 21 : BER en fonction de la puissance d'entrée par canal ($P_{IN\ SPAN}$) du DP-QPSK (à gauche) et du DP-MB-OFDM (à droite) après transmission sur 1000 km de fibres G.652 sans gestion de dispersion mesurés dans deux configurations différentes : "Single-Channel" et "WDM".

Les courbes montrent que la configuration « Single Channel » a de meilleures performances que « WDM » ; la différence d'une décade entre « Single Channel » et « WDM » et la différence de 1dB de puissance injectée montrent que, dans une transmission DCF-free, la configuration WDM est impactée par la modulation de phase croisée (XPM) et son corollaire la modulation de polarisation croisée (XPolM).
Dans le cadre de comparaison entre le 100 Gbps DP-MB-OFDM et 100 Gbps DP-QPSK, on trouve que moins d'une demi-décade existe entre les deux courbes au point de puissance optimum injectée montrant ainsi que les deux formats 100 Gbps DP-MB-OFDM et 100 Gbps DP-QPSK ont quasiment les mêmes performances.

Transmission de DP-OFDM et DP-QPSK sur une ligne avec gestion de la dispersion

Une autre configuration étudiée ici, notée par "10G WDM" sur la Figure 24, correspond au cas où les canaux à 100 Gbps sont déployés dans un système de transmission WDM avec des canaux 10 Gbps NRZ-OOK. Deux canaux NRZ-OOK sont éteints et sont remplacés par les deux canaux cohérents à 100 Gbps.
Les signaux DP-MB-OFDM et DP-QPSK transmis respectivement sur les longueurs d'onde 1552,93 nm et 1548,11 nm sont combinés avec un multiplex de 78 longueurs d'onde espacées de 50 GHz et modulées à 10,7 Gbps avec NRZ-OOK. Les canaux NRZ-OOK sont alimentés par des laser diodes (LD) avec de longueurs d'onde allant de 1529,16 nm à 1560,61 nm. Ces 78 canaux pairs et impairs sont d'abord codés avec un code RS (255, 239), multiplexés séparément, indépendamment modulés avec des séquences PRBS 2^{31}-1, puis couplés avec les deux canaux à 100 Gbps.
Dans la ligne de transmission, les modules de gestion de la dispersion chromatique ont été insérés après chaque span et un module de pré-compensation a été inséré en début de ligne alors qu'un module de post-compensation a été inséré à la fin de la ligne de transmission. L'égalisateur de gain est placé au milieu de la ligne.
Du coté récepteur, les signaux à 100 Gbps sont détectés par des détecteurs cohérents alors qu'un signal à 10 Gbps situé tout près d'un canal à 100 Gbps est détecté avec une détection directe.

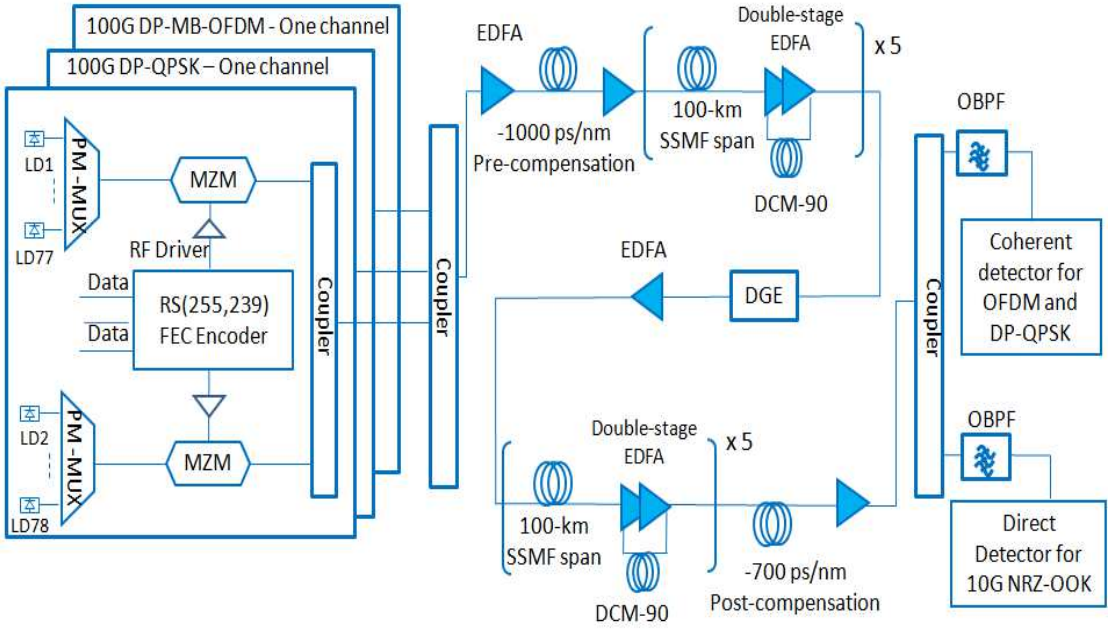

Figure 22 : Montage expérimental des émetteurs de DP-MB-OFDM, DP-QPSK et NRZ-OOK, de la ligne de transmission avec gestion de la dispersion et des détecteurs cohérent et direct.

L'alternance entre les fibres SSMF et DCM génère un profil de dispersion cumulée appelé "carte de dispersion" du système comme indiqué dans la Figure 23.

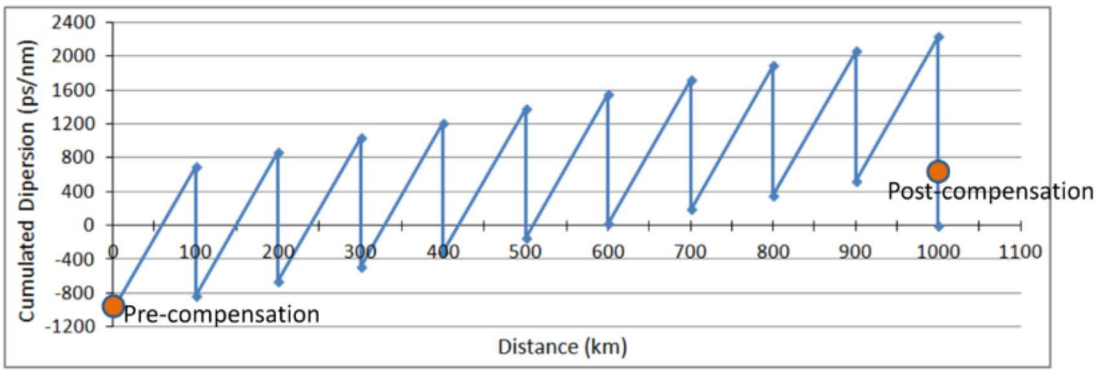

Figure 23 : Evolution de la dispersion chromatique à 1550 nm le long de la ligne.

Résultats expérimentaux

La Figure 24 ci-dessous montre bien qu'aucun des canaux à 100 Gbps transmis, avec les canaux à 10 Gbps, sur 1000 km de fibre G.652 avec gestion de la dispersion ne peut fonctionner vu que les performances sont au-dessus de la limite FEC. Les effets non-linéaires tels que le mélange à quatre ondes (FWM), XPM et XPolM induits par les canaux 10 Gbps NRZ-OOK dégradent considérablement la qualité de transmission des signaux cohérents à 100 Gbps.

Afin de limiter l'impact de FWM, XPM et son corollaire, un premier schéma a été testé, et consiste à insérer une bande de garde de 100 GHz et 150 GHz, correspondant à l'extinction d'un et de deux canaux à 10 Gbps de chaque côté des canaux à 100 Gbps (configurations

« GB = 100 GHz » et « GB = 150 GHz»). Le BER vs $P_{IN\ SPAN}$ est tracé pour les deux systèmes sur la Figure 24.
Ce schéma améliore légèrement le BER des canaux à 100 Gbps, mais pas suffisamment pour être en-dessous de la limite FEC. Notez également que l'élargissement de la bande de garde de 100 GHz à 150 GHz n'améliore pas les performances de transmission.

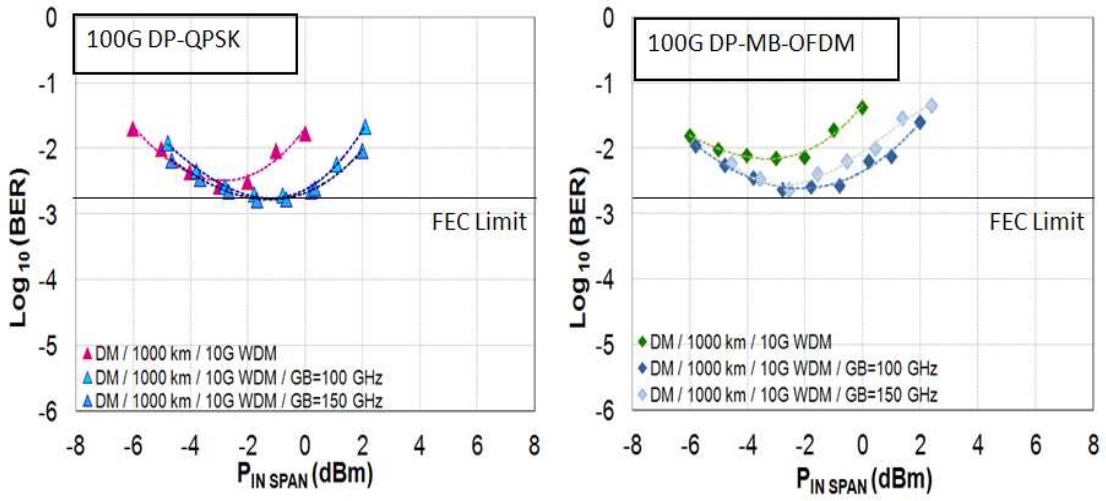

Figure 24 : BER en fonction de la puissance d'entrée par canal du DP-QPSK (à gauche) et du DP-MB-OFDM (à droite) après transmission sur 1000 km de fibres G.652 avec gestion de dispersion dans une configuration "WDM" avec et sans insertion de bande de garde.

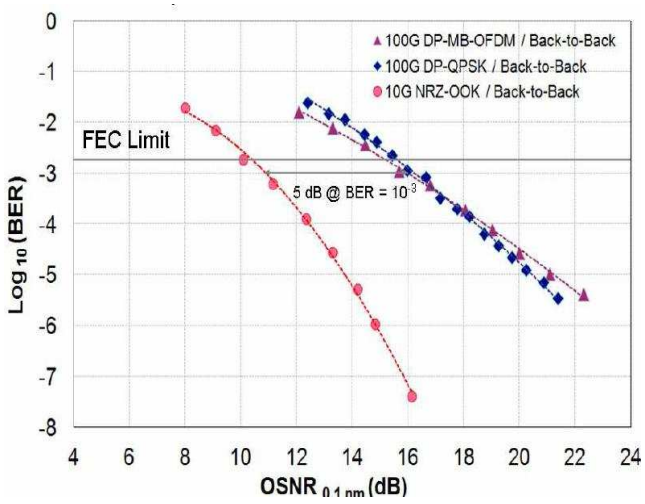

Figure 25 : BER en fonction d'OSNR mesuré en back-to-back avec 100 Gbps DP-MB-OFDM, 100 Gbps DP-QPSK et 10 Gbps NRZ-OOK.

Une autre possibilité pour réduire l'impact des effets non-linéaires entre les canaux 10 Gbps NRZ-OOK et ceux à 100 Gbps est la réduction de la puissance des canaux à 10 Gbps. Afin de vérifier la faisabilité de cette deuxième solution, nous avons tracé dans la Figure 25 le BER en fonction de l'OSNR mesurée en configuration back-to-back pour les trois différents formats de modulation utilisés dans le système WDM: 100 Gbps DP-MB-OFDM, 100 Gbps DP-QPSK et 10 Gbps NRZ-OOK.
Les formats 100 Gbps DP-QPSK et 100 Gbps DP-MB-OFDM ont les mêmes performances en back-to-back. Par contre, le signal NRZ-OOK à 10 Gbps présente, près de la limite FEC, un avantage en OSNR de 5 dB par rapport aux signaux 100 Gbps DP-QPSK et 100 Gbps

DP-MB-OFDM. Cet avantage en OSNR de 5 dB peut être utilisé pour réduire l'impact des effets non-linéaires dans la fibre.

Afin d'améliorer les performances des systèmes à 100 Gbps, une différence de puissance de 5 dB est mise en place entre les canaux à 100 Gbps et 10 Gbps à la transmission. Cette configuration dite « No GB/P (100G)-P (10G)=5dB » représente une transmission des canaux de 10 Gbps avec les canaux à 100 Gbps sans une bande de garde entre les canaux mais avec une différence de 5dB entre la puissance injectée pour les canaux à 100 Gbps et celle pour 10 Gbps.

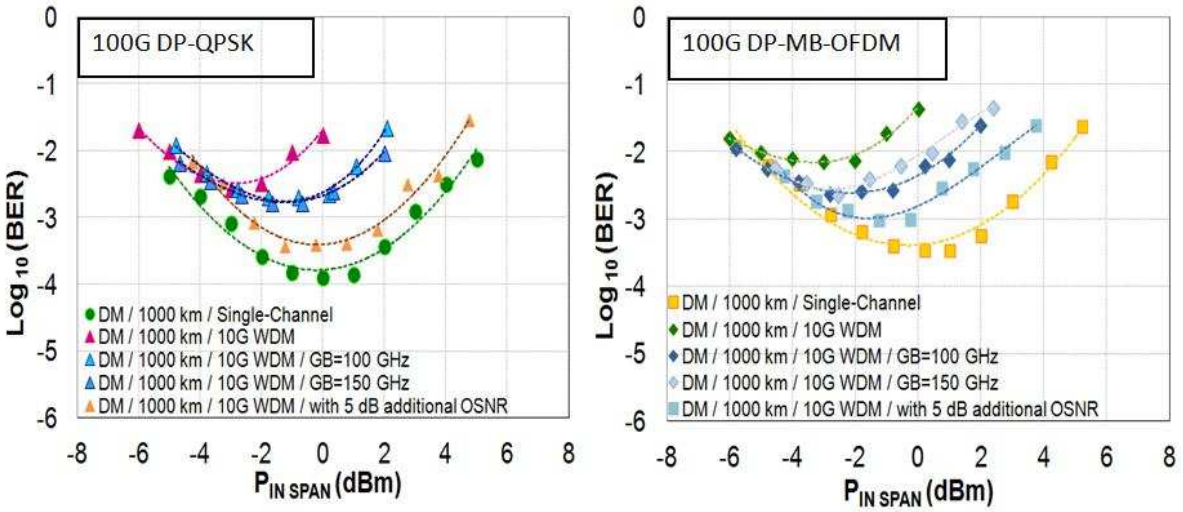

Figure 26 : BER en fonction de la puissance d'entrée par canal du DP-QPSK (à gauche) et du DP-MB-OFDM (à droite) après transmission sur 1000 km de fibres G.652 avec gestion de dispersion obtenus avec toutes les configurations étudiées.

Cette solution améliore le BER des signaux 100 Gbps DP-QPSK et DP-MB-OFDM de manière significative: près d'une décade est gagnée par rapport à la configuration antérieure où une bande de garde était introduite. En même temps, la puissance d'entrée optimale par canal est renforcée, par rapport à la configuration "No Garde-Band", de 3 dB pour DP-QPSK et de 2 dB pour DP-MB-OFDM soulignant la réduction de l'impact des effets non-linéaires causés par les interactions entre les canaux 10 Gbps NRZ-OOK et ceux à 100 Gbps.

Notez qu'aucune erreur n'a été détectée pour les deux canaux à 10 Gbps les plus proches des canaux à 100 Gbps DP-MB-OFDM et DP-QPSK (à la puissance d'entrée optimale par canal sur les courbes de la Figure 26). La Figure 26 montre également que dans les différentes configurations étudiées le 100 Gbps DP-QPSK a une performance légèrement supérieure à celle du 100 Gbps DP-MB-OFDM.

Conclusion

Nous avons présenté la mise en œuvre d'un émetteur / récepteur multi-bandes OFDM à double polarisation (DP-MB-OFDM) fonctionnant à 100 Gbps pour une transmission WDM longue distance. Le débit de 100 Gbps, contenu dans 50 GHz de bande passante, est obtenu par multiplexage de quatre sous-bandes OFDM indépendantes portant chacune un quart du débit total.
Nous avons démontré expérimentalement que le format DP-MB-OFDM est une solution crédible pour une transmission WDM DCF-free à 100 Gbps.
Sur l'infrastructure de fibre actuelle, la transmission sur 1000 km de fibre G.652 des canaux 100 Gbps DP-QPSK et DP-MB-OFDM est possible, à condition de diminuer la puissance des canaux 10 Gbps NRZ-OOK de 5 dB par rapport aux canaux cohérents à 100 Gbps. Dans cette configuration, les formats 100 Gbps DP-MB-OFDM et 100 Gbps DP-QPSK ont une performance à peu près semblable. Même si la performance de l'OFDM est légèrement plus dégradée que celle du 100 Gbps DP-QPSK, ces résultats sont très encourageants si l'on considère la prochaine génération de systèmes WDM visant les débits de 1Tbps ou 400 Gbps et basée sur la technologie OFDM.

Bibliographie

[Fuj07] Fujitsu. (2007) http://www.fujitsu.com/global/news/pr/archives/month/2007/20070327-02.html.

[Jan07] S. L. Jansen, I. Morita, N. Takeda, and H. Tanaka, "20-Gb/s OFDM transmission over 4,160-km SSMF enabled by RF-Pilot tone phase noise compensation," in *Optical Fiber Communication Conference and Exposition and The National Fiber Optic Engineers Conference*, 2007.

[Jan08] S. L. Jansen, I. Morita, T. C. W. Schenk, N. Takeda, and H. Tanaka, "Coherent Optical 25.8-Gb/s OFDM Transmission Over 4160-km SSMF," *Journal of lightwave technology*, 2008.

[Jan09] S. L. Jansen, I. Morita, T. Schenk, and H. Tanaka, "121.9-Gb/s PDM-OFDM transmission With 2-b/s/Hz spectral efficiency over 1000 km of SSMF," *Journal of lightwae technology*, vol. 27, 2009.

[Liu08] X. Liu and F. Buchali, "Intra-symbol frequency-domain averaging based channel estimation for coherent optical OFDM," *Optics express*, vol. 16, no. 26, pp. 21944-21957, Dec. 2008.

[LiY06] Y. Li and G. L. Stüber, *Orthogonal frequency division multiplexing for wireless communications*. Springer, 2006.

[Pet07] D. Petrovic, W. Rave, and G. Fettweis, "Effects of phase noise on OFDM systems with and without PLL: characterization and compensation," *IEEE transactions on communications*, vol. 55, 2007.

[Sak07] T. Sakamoto, T. Kawanishi, and M. Izutsu, "Asymptotic formalism for ultraflat optical frequency comb generation using a Mach–Zehnder modulator," *optics letters*, vol. 32, 2007.

[Shi07] W. Shieh, X. Yi, and Y. Tang, "Transmission experiment of multi-gigabit coherent optical OFDM systems," 2007.

List of Abbreviations

A

ADC	Analog to Digital Convertor
ASE	Amplified Spontaneous Emission
ASIC	Application Specific Integrated Circuit
AWG	Arbitrary Waveform Generator
AWGN	Additive White Gaussian Noise

B

BER	Bit Error Rate
BERT	BER tester
BPF	Band Pass Filter
BPSK	Binary Phase-Shift Keying

C

CD	Chromatic Dispersion
CDR	Clock and Data Recovery
CFO	Carrier Frequency Offset
CMA	Constant Modulus Algorithm
CMZM	Complex Mach-Zehnder modulator
CO	Coherent Optical
CPE	Common Phase Error

D

DAC	Digital to Analog Convertor
DCF	Dispersion Compensation Fiber
DCM	Dispersion Compensation Module
DD-OFDM	Direct Detection-OFDM
DFT	Discrete Fourier Transverse
DGD	Differential Group Delay
DGE	Dynamic Gain Equalizer
DLI	Delay Line Interferometers
DM	Dispersion Managed
DP-MB-OFDM	Dual Polarization Multi-band OFDM
DPO	Digital Phosphore Oscilloscope
DP-QPSK	Dual Polarization QPSK
DSL	Digital Subscriber Loop
DSP	Digital Signal Processing

E

ECL	External Cavity Laser
EDC	Electronic Dispersion Compensation
EDFA	Erbium-Doped Fiber Amplifier
EFEC	Enhanced FEC
ENOB	Effective Number Of Bits

F

FEC	Forward Error Correction
FFT	Fast Fourier Transform
FIR	Finite Impulse Response
FOPMD	First Order of PMD
FPGA	Field Programmable Gate Arrays
FWM	Four Wave Mixing

G

GVD	Group Velocity Dispersion

I

I	in-phase
ICI	InterCarrier Interference
IDFT	Inverse DFT
IFFT	Inverse FFT
ISFA	Intra-Symbol Frequency Averaging
ISI	InterSymbol Interference
ITU	International Telecommunication Union

L

LD	Laser Diode
LEAF	Large Effective Area Fiber
LO	Local Oscillator
LPF	Low Pass Filter
LS	Least-Square
LTE	Long Term Evolution

M

MB	Multi-Band
MIMO	Multiple Input Multiple Output
MLSE	Maximum Likelihood Sequence Estimation
MZM	Mach-Zehnder Modulator

N

NGI CO-OFDM	No-Guard Interval CO-OFDM
NRZ	Non Return to Zero
N-WDM	Nyquist-Wavelength-Division Multiplexing

O

OBM-OFDM	Orthogonal-Band-Multiplexed OFDM
OBPF	Optical BPF
OEO	Optical-to-Electrical-to-Optical
OFDM	Orthogonal Frequency Division Multiplexing
OOK	On-Off Keying
OSA	Optical Spectrum Analyzer
OSNR	Optical Signal to Noise Ratio

P

PAPR	Peak to Average Power Ratio
PBC	Polarization Beam Combiner
PBS	Polarization Beam Splitter
PCD	Polarization dependent Chromatic Dispersion
PDM	Polarization Division Multiplexing
PM	Polarization-Maintaining
PMD	Polarization Mode Dispersion
PRBS	Pseudo Random Bit Sequence
PS	Polarization Scrambler
PSCF	Pure Silica Core Fiber
PSK	Phase Shift Keying
PSP	Principle State of Polarization

Q

Q	in-Quadrature
QAM	Quadrature Amplitude Modulation
QN-WDM	Quasi-Nyquist Wavelength-Division Multiplexing
QPSK	Quaternary Phase Shift Keying

R

RFP	RF Pilot
RGI CO-OFDM	Reduced Guard Interval CO-OFDM
ROADM	Reconfigurable Optical Add Drop Multiplexer
RS	Reed-Solomon
RZ	Return-to-Zero

S

SDM	Spatial Division Multiplexing
SNR	Signal to Noise Ratio
SOP	State Of Polarization
SOPMD	Second Order PMD
SPM	Self-Phase Modulation
SSMF	Standard Single Mode Fiber

T

TDA	Time Domain Averaging
TDE	Time-Domain-Equalization

V

VOA	Variable Optical Attenuator

W

WDM	Wavelength-Division Multiplexing

X

XPM	Cross Phase Modulation
XPolM	Cross Polarization Modulation

Z

ZF	Zero-Forcing

List of Figures

Figure 2-1: Evolution of experimentally achieved single channel bit (green circles), and aggregate per-fiber capacities (triangles) using wavelength-division multiplexing (WDM) [Ess10]. 56
Figure 2-2: Typical gain bandwidth of the EDFA located in the C band. 57
Figure 2-3: WDM transmission system [Fal11]. 58
Figure 2-4: 40 Gbps coherent DP-QPSK transceiver card [Sun08]. 59
Figure 2-5: Attenuation in dB/km Vs wavelength in nm for a typical SSMF and a fiber without the water absorption peak [Ess10]. 62
Figure 2-6: Effect of PMD in a short fiber. 64
Figure 2-7: Modeling a long fiber as a concatenation of birefringent segments. 64
Figure 2-8: The variation of the SOP on an arc of circle on the Poincaré sphere [She04]. .. 65
Figure 2-9: Principle of EDFA operation [htt07]. 66
Figure 2-10: Example of a typical transmission line comprising several EDFA amplifiers. 67
Figure 2-11: The basic principle of the transmitter set-up [Nee00]. 73
Figure 2-12: OFDM transmitter and receiver set-up. 74
Figure 2-13: OFDM spectrum. 74
Figure 2-14 : The time domain (left fig.) and spectra (right fig.) of 4 subcarriers within an OFDM symbol. 75
Figure 2-15: The left side of this figure represents the subcarriers of an OFDM symbol on the transmitted side while the right side the subcarriers is affected by CD. The impact of CD on an OFDM symbol in the case where the cyclic prefix is not implemented is represented on the first row and when the cyclic prefix is implemented, it is represented on the second row. 77
Figure 2-16: Phase diversity coherent receiver. 79
Figure 2-17: The basic transmitter design architectures based on the use of a MZM (first row) and CMZM (second row) and the corresponding OFDM spectra before and after optical up-conversion. 80
Figure 2-18: Concatenation of several orthogonal sub bands [Shi10]. 80
Figure 2-19: Comb generator (left fig) and recirculating frequency shift loop (right fig). ... 81
Figure 2-20: Typical diagram of an all optical-OFDM system [Ell08]. 83
Figure 2-21: Tx and Rx design with the DSP for a no-guard interval CO-OFDM [San09]. 84
Figure 3-1: Proposed Multi-Band OFDM configuration for carrying 100 Gbps in a 50 GHz WDM channel (X and Y are the two polarization axis). 95
Figure 3-2: Spectrum of an OFDM band with a baseband bandwidth equal to 4 GHz sampled at 8 GHz (first row) and 12 GHz,(second row) shown before and after filtering through a 4 GHz filter. 95
Figure 3-3: IFFT inputs as it is defined in Matlab; the unused subcarriers in the middle represent the highest and lowest frequencies set to zero for oversampling. 96
Figure 3-4: Transmitter set-up for the generation and processing of one OFDM sub-band. 100
Figure 3-5: OFDM coherent receiver set-up. 101
Figure 3-6: End-to-end signal processing model of the transmission link. 102
Figure 3-7: Signal processing architecture of the 2x2 baseband electrical OFDM receiver. 104
Figure 3-8: The 4 typical scenarios arising in OFDM timing synchronization. Cases a and b show two 105

Figure 3-9: Receive constellations before (left fig) and after (right fig) channel equalization, when the FFT window starts within the ISI-free region inside the cyclic prefix (scenario b). 4QAM was used for transmission. 106
Figure 3-10: Receive constellations before (left fig) and after (right fig) channel equalization when the DFT windows starts one sample outside the cyclic prefix (scenarios c or d). 106
Figure 3-11: Receive constellations before (left fig) and after (right fig) channel equalization in the presence of a very large timing offset. 107
Figure 3-12: Generic structure of the training symbol in the time-domain. 107
Figure 3-13: Comparison of the Shi & Serpedin and Minn & Barghava timing metrics for a training symbol made of L=4 repetitions. 109
Figure 3-14: Minn & Barghava timing metric for a training symbol made of L=8 repetitions. 109
Figure 3-15: BER vs OSNR for the two synchronization methods. 110
Figure 3-16: Constellation at the DFT output in the presence of a normalized CFO $\epsilon = 1$ (left fig: before CPE/ right fig: after CPE). A 4-QAM constellation is used at the transmitter.. 111
Figure 3-17: Constellation at the DFT output in the presence of a normalized CFO $\epsilon = 0.02$ (left fig: before CPE/ right fig: after CPE). A 4-QAM constellation is used at the transmitter. 112
Figure 3-18: Constellation at the DFT output in the presence of a normalized CFO $\epsilon = 0.32$ (left fig: before CPE/ right fig: after CPE). A 4-QAM constellation is used at the transmitter. 112
Figure 3-19: SNR penalty as a function of the frequency offset for 256-subcarrier QPSK modulated OFDM systems [Shi10]. 113
Figure 3-20: Power spectral density vs. sub-carrier index of the transmitted and received OFDM signal (here, the CFO = -21 Δf is measured). 116
Figure 3-21: Particular structure of the two training symbols used for channel estimation in the DP case. 118
Figure 3-22: BER vs OSNR for the time-domain averaging method for several values of the training symbol repetition factor *l*. 120
Figure 3-23: BER vs OSNR for the intra-symbol frequency averaging method based on a total of 2m+1 subcarriers, for several values of m. 121
Figure 3-24: BER vs OSNR for the combination of ISFA (m=2) and TDA with a varying number *l* of training symbol repetitions. 122
Figure 3-25: Principle of insertion (left figure) and extraction (right figure) of the RF pilot tone in the RF pilot method for compensating phase noise [JanM08]. 124
Figure 4-1: Experimental set-up of the OFDM transmitter and receiver. 132
Figure 4-2: Experimental set-up of the basic electrical back-to-back experiment. 133
Figure 4-3: OFDM spectrum before filtering. 133
Figure 4-4: The rare peaks of the OFDM exceeding the clipping level are clipped to this value. 134
Figure 4-5: OFDM baseband electrical spectra without (left fig) and with pre-emphasis and low pass filtering (right fig). 135
Figure 4-6: 4-QAM constellation (left fig.); BER vs SNR obtained after digital demodulation of the electrical OFDM signal (right fig.). 135
Figure 4-7: Experimental set-up of the electrical experiment. 136
Figure 4-8: 4-QAM constellation diagram observed by testing different attenuator values at the RF driver inputs, with a peak-to-peak input voltage equal to 450 mVpp. The input driver voltage is measured after the insertion of the attenuator. 137
Figure 4-9: BER vs SNR of the generated electrical OFDM signals and the theoretical case. 138

Figure 4-10: Constellation diagram obtained with 8-QAM and 16-QAM modulations. 138
Figure 4-11: Experimental set-up of the homodyne optical OFDM single-band signal. 139
Figure 4-12: CMZM structure. 140
Figure 4-13: DQPSK waveform after direct detection. Here, the CMZM biases are adjusted precisely. 140
Figure 4-14: OFDM spectrum after CMZM. The CMZM biases are adjusted precisely. 141
Figure 4-15: Spectra of the OFDM signal for different Tx IQ imbalance issues. a) represents the upper and lower bands of the OFDM signal when the DC component is removed. The other cases represent the upper-band of the OFDM signal: we identify in b) the ideal settings, in c) a phase/gain mismatch, in d) a time mismatch; and in e) the presence of the DC component. 144
Figure 4-16: BER vs OSNR for optical single-band back-to-back OFDM signal, also we have reproduced the sensitivity curve of the reference [JanM08]. 145
Figure 4-17: Experimental set-up of the CO DP-OFDM system. 146
Figure 4-18: Structure of the training symbols used for channel estimation. The transmitted OFDM signal on polarization X is delayed by one OFDM symbol with respect to the signal on polarization Y due to the PDM unit. 147
Figure 4-19: BER vs. OSNR for single and dual polarization OFDM signal. 148
Figure 4-20: Receiver set-up for experimental validation with heterodyne detection. 148
Figure 4-21: Temporal fluctuation of the normalized CFO, including the integer and fractional parts. 149
Figure 4-22: BER vs. OSNR (in 0.1 nm) for the CO DP-OFDM system with/without CFO. 150
Figure 4-23: Transmitter set-up for the 128 Gbps DP-MB-OFDM signal. The corresponding spectrum is shown in the inset. 151
Figure 4-24: Transmittance of one arm of DLI. 151
Figure 4-25: Spectrum of the 10 GHz-spaced optical carriers at the MZM output. 152
Figure 4-26: BER versus OSNR (in 0.1 nm) measured in back-to-back for DP-MB-OFDM, DP-QPSK, and NRZ-OOK signals. 153
Figure 4-27: Experimental set-up. In inset, the Poincare sphere at the output of the scrambler is represented when the input signal is singly polarized. 154
Figure 4-28: Left fig: BER vs. SOP variation speed when FOPMD=125 ps – Right fig: BER vs. FOPMD when SOP variation speed is equal to 70°/ms. 155
Figure 4-29: BER vs. OSNR (in 0.1 nm) with SOP variation speed equal to 70°/ms for various configurations of FOPMD and SOPMD. 155
Figure 4-30: Experimental set-up of the dual polarization OFDM sub-band affected by PMD and CD. 156
Figure 4-31: BER vs. OSNR (in 0.1 nm) with and without CFO for various configurations of CD, FOPMD and SOPMD. 156
Figure 5-1: BER vs. P_{inspan} (left fig) and BER vs. received OSNR $_{0.5\ nm}$ (left fig) after 1000 km of transmission over the DCF-free G.652 fiber line in "Single-Channel" and after the back-to-back design. 163
Figure 5-2: DP-QPSK transmitter and receiver set-up. 164
Figure 5-3: Spectrum of the forty 100 Gbps channels including the two channels under measurement, i.e. the 100 Gbps DP-QPSK and 100 Gbps DP-MB-OFDM channels. 165
Figure 5-4: Set-up of the 100 Gbps DP-MB-OFDM and DP-QPSK transmitters, 1000 km DCF-free transmission line and coherent receiver. 165
Figure 5-5: BER vs. span input power per channel for 100 Gbps DP-MB-OFDM (right fig) and DP-QPSK (left fig) after 1000 km of transmission over DCF-free G.652 fiber line in "Single-Channel" and "WDM" configurations. 166

Figure 5-6: BER vs. received OSNR $_{0.5\ nm}$ for 100 Gbps DP-MB-OFDM (right fig) and DP-QPSK (left fig) after 1000 km of transmission over the DCF-free G.652 fiber line in "Single-Channel" and "WDM" configurations and after the back-to-back design. 167
Figure 5-7: Set-up of the 100 Gbps DP-MB-OFDM and DP-QPSK transmitters, 1000 km DCF transmission line and coherent receiver. 168
Figure 5-8: Evolution of the chromatic dispersion at 1550 nm. 169
Figure 5-9: BER vs. span input power per channel for 100 Gbps DP-MB-OFDM (right fig) and DP-QPSK (left fig) after 1000 km of transmission over the DCF and DCF free G.652 fiber line in "Single-Channel" configuration. 170
Figure 5-10: Waveform evolution of a phase-modulated signal along a transmission over DCF-free line (top fig) and over dispersion-managed line (bottom fig) [Jan12]. 171
Figure 5-11: BER vs. span input power per channel for 100 Gbps DP-MB-OFDM (right fig) and DP-QPSK (left fig) after 1000 km of transmission over the DCF and DCF free G.652 fiber line in "WDM" configuration and over DCF fiber line in "Single-Channel" configuration. 172
Figure 5-12: BER vs. received OSNR $_{0.5\ nm}$ for 100 Gbps DP-MB-OFDM (right fig) and DP-QPSK (left fig) after 1000 km of transmission over DCF G.652 fiber line in "Single-Channel" and "WDM" configurations and after the back-to-back design. 173
Figure 5-13:Set-up of the 100 Gbps DP MB-OFDM, 100 Gbps DP-QPSK, 10.7 Gbps NRZ-OOK transmitters, 10×100 km G.652 fiber transmission line, coherent receiver and direct detector with RS (Reed-Solomon). 174
Figure 5-14: BER vs. span input power per channel for 100 Gbps DP-MB-OFDM (right fig) and DP-QPSK (left fig) after 1000 km of transmission over the DCF legacy fiber infrastructure in "WDM" configuration with and without adding a guard band between the 10 G and 100 G channels. 175
Figure 5-15: BER versus OSNR (in 0.1 nm) measured in back-to-back for the 124 Gbps DP-MB-OFDM, 112 Gbps DP-QPSK, and 10.7 Gbps NRZ-OOK signals. 175
Figure 5-16: BER versus span input power per channel after the dispersion-managed 10×100-km G.652 fiber line for the 112 Gbps DP-QPSK and the 124 Gbps DP-MB-OFDM signals for the various configurations under study. 176

1 Introduction

Chapter 1

Introduction

Optical fiber communication systems are playing an important role in our lives. We are able to communicate almost instantaneously between any two points on the globe. A few terabits of information can be transmitted through one thin optical fiber. The network providing this capability is based on optical fibers criss-crossing the earth: under the seas, over land, and across mountains. Submarine, the undersea network, allows intercontinental connection with links reaching distances of more than 2000 km (~6000 km for transatlantic cables and ~10000 km for transpacific ones) and supporting high data rates. Currently carrying a total data rate of 96x10 Gbps, the undersea network is expected, however, to be upgraded in the future to 96x40 Gbps by using return-to-zero quaternary phase shift keying (RZ-QPSK) modulation in place of the return-to-zero on-off keying (RZ-OOK) modulation currently in use. Conversely, terrestrial telecommunication networks are basically divided into three major types: core, metro and access networks. They differ in their geographical coverage range. The core networks cover typical distances of up to a few hundred of kilometers and are used for connecting cities or countries with data rate of ~1 Tbps (96x10 Gbps). The metro connects the access and core networks and covers distances of several tens of kilometers. At the end of the global network is the access network which provides connectivity to the users. However, the demand for more broadband services such as TV on demand, social networks, network gaming, grid/cloud computing & storage, home working … and other potential future services, is expected to gain further importance and to put an additional burden on the transport networks. It will force the access network to support and provide these services to the end users. Consequently, for mobile transmission, the fourth generation of mobile communications (LTE) starts to be deployed, while for the optical access network, fiber-to-the-home (FTTH) technology becomes more and more popular (4000 new customers each week adopt FTTH by Orange). The fourth generation of mobile communication is expected to provide 1 Gbps in downlink applications by using OFDM modulation whereas FTTH is capable of delivering up to 2.5 Gbps to the user, based on non-return-to-zero NRZ modulation and it is expected to reach 10 Gbps in the coming years. The dramatic upgrade in network capacity can only be provided by the introduction of efficient transport technologies into the existing long-distance transport networks.

In the past, the explosive demand for network bandwidth has been provided using wavelength-division multiplexing (WDM) technologies, combined with erbium-doped fiber amplifier (EDFA). EDFA has a huge gain bandwidth and permits the amplification of a multiplex of optical signals having a wavelength in the [1530 nm-1565 nm] spectral region. EDFAs have allowed transcontinental communications, and, additionally multiplied the capacity of a single fiber.

Furthermore, during recent decades, the quest for further capacity has required the deployment of 10 Gbps NRZ-OOK channels operating on a 50 GHz channel grid and transmitted over typical distances of 1000-2000 km over the existing legacy fiber infrastructure. The maximum capacity transported by 10 Gbps WDM long-haul transmission systems in the C-band (1530-1565 nm) is ~1Tbps, corresponding to a spectral efficiency of 0.2 bit/s/Hz. Chromatic dispersion (CD) which severely impairs system performance (as it induces intersymbol interference (ISI)), can be overcome by the insertion of dispersion compensation fiber (DCF) modules. However, besides CD, NRZ-OOK transmission over optical fiber also suffers from polarization mode dispersion (PMD) impairments, especially in the context of high data rate long-haul transmission. Consequently, upgrading the

10 Gbps WDM transmission systems from 10 Gbps to 40 Gbps by simply increasing the symbol rate of the OOK modulation format is not a viable solution.

The technological breakthrough that allowed the increase of data rate up to 40 and 100 Gbps was the revival of coherent optical detection, made possible by the advent of very-high-data-rate digital circuits. Coherent detection allows the use of any kind of high order modulation, and further provides the opportunity to double links capacity through the use of polarization division multiplexing. Within the coherent receiver, digital signal processing algorithms are used to compensate, in the electrical domain, for transmission impairments such as CD and PMD.

Nowadays, the need for increasing the global capacity of WDM long-haul transmission has found an answer in the implementation of coherent dual-polarization quaternary phase shift keying (CO DP-QPSK) transponders which operate at 100 Gbps. Within the ITU WDM grid, certain channels at 10 Gbps are upgraded to 100 Gbps using the CO DP-QPSK technique. The aim is to transport 100 Gbps WDM channels on the 50 GHz ITU grid, enabling 2 bits/s/Hz spectral efficiency and the reach of a maximum capacity of ~10 Tbps over long haul transmission systems. The CO DP-QPSK is a modulation format resistant to transmission impairments such as CD and PMD. However, coherent dual-polarization multi-band OFDM (CO DP-MB-OFDM) has also been suggested in the past few years for 100 Gbps application, and remains currently a very interesting candidate for WDM transmission at 400 Gbps and 1 Tbps.

OFDM is intrinsically resistant to CD and PMD and involves in particular a simple signal equalization technique to recover the transmitted data at the receiver side. OFDM also has other interesting advantages, due to its very well-defined narrow spectrum and to its individually modulated sub-carriers. In particular, optical aggregation/disaggregation can be realized at the sub-band level. Such a thin spectrum granularity allows the users to access and manipulate very small portions of the transmitted spectrum. Moreover, OFDM technology is suitable for direct and coherent detection and thus can be adapted to various networks (access, metropolitan and core networks). Direct detection benefits from a simpler and cheaper receiver as it only requires a single photodiode, but with lower sensitivity and spectral efficiency. Coherent detection, on the other hand, has a higher sensitivity and spectral efficiency, but it comes with additional cost and complexity. Direct detection is generally preferred for access applications, while coherent detection is more suitable for core and metro long-haul transmission applications.

In the future, the demand for a further increase of data traffic in optical networks is expected to be amplified. This prompts the need for the next generation of optical transmission, enabling 400 GbE or up to 1 TbE per channel. Multi carrier transmission techniques are very likely to be used at such data rate. Two candidates today appear to have found general approval: Nyquist-WDM (N-WDM) and MB-OFDM technologies. However, a debate exists concerning the ability of OFDM to manage fiber nonlinearities in long-haul WDM transmission, due to its supposed higher sensitivity to nonlinear effects. The target of this thesis is to answer this question by implementing an experimental performance comparison of DP-MB-OFDM and DP-QPSK at 100 Gbps for a transmission over 1000-km DCF-free and dispersion-managed G.652 fiber line.

Report structure

This report is divided into five chapters:

Chapter 2 gives a general overview on the capacity evolution of optical fiber transmission. It then discusses the main physical impairments encountered by the signal during the propagation along the fiber. It finally introduces the principles of OFDM, and the generation of high bit rate OFDM signals for long-haul optical transmissions.

Chapter 3 first describes the design of the OFDM modulation format considered in this work. The dimensioning process leads to four polarization multiplexed OFDM sub-bands. Each sub-band carries a date rate of 25 Gbps within an 8 GHz bandwidth. The digital signal processing architecture of the digital transmitter and receiver is also introduced.

Chapter 4 describes the basic experimental steps that we have followed in order to realize, for the first time in France, a coherent DP-MB-OFDM system operating at 100 Gbps. In particular, several experiments have been carried out to characterize either the electrical or optical components and to validate the corresponding digital signal processing algorithms. The impact of CD and PMD on the system performance has also been investigated.

Chapter 5 addresses transmissions experiments over DCF-free fiber line as well as transmissions over legacy transport infrastructure, mixing G.652 fiber and 10 Gbps WDM systems. Several performance comparisons of DP-MB-OFDM and DP-QPSK at 100 Gbps have been carried out. To the best of our knowledge, it is the first time that such experimental performance comparisons are realized.

Chapter 6 gives a general conclusion about the results of this work, and also opens up a few perspectives for further research.

2 OFDM for optical communication systems

Chapter 2

OFDM for optical communication systems

Orthogonal Frequency Division Multiplexing (OFDM) has received considerable attention in the recent past as it provides a simple and effective mean for combating frequency selective fading channels [Sca00]; thus it has been widely employed in numerous digital standards for a broad range of applications such as digital audio/video broadcasting and wireline/wireless communication systems. The resilience of OFDM to severe channel conditions can be further enhanced by means of an adaptive bit loading algorithm. The carriers undergoing strong signal attenuation are disabled or carry low bit rate; conversely, the bit rate is maximized over the carriers benefiting from favorable transmission conditions [Yan08]. Bit loading has been first used with success in digital subscriber loop (DSL).

Recently some research work has considered OFDM as an attractive transmission technology to increase the data rate in fiber optics communication systems. Although the optical fiber channel is not frequency selective, it is very dispersive due to the presence of polarization mode dispersion (PMD) and chromatic dispersion (CD). By inserting a cyclic prefix at the beginning of each transmitted block of data, the OFDM modulation format can be made naturally robust against channel dispersion. The cyclic prefix can be designed for propagation across distances as long as 2000 km or even beyond, over the installed standard single mode fiber (SSMF) transport networks.

This chapter gives an overview of the optical communication domain and the OFDM technique. We begin the chapter by reviewing the evolution of optical fiber transmission capacity from 2.5 to 100 Gbps. Later on, we present the optical fiber impairments that occur in long-haul transmission and degrade the system performance. They can be divided into two main categories; the first category is known as the linear effects; among which we find CD and PMD. The second category comprises the non linear distortions induced by Kerr effect, such as self-phase modulation (SPM), cross phase modulation (XPM), four-wave mixing (FWM) and cross polarization modulation (XPolM). In the last section of this chapter, OFDM for optical long-haul high data rate transmission is described. We also summarize the latest OFDM transmission records attained in either offline or real-time OFDM experiments.

2.1 Capacity evolution of optical transmission

The ever increasing demand for information and communication requires capacity evolution from the metro and core networks. During the last decade, the quest for further capacity in the wavelength division multiplexing (WDM) system has implied the deployment of 10 Gbps Non-Return-to-Zero On/Off Keying (NRZ-OOK) channels operating on a 50 GHz channel grid. The maximum capacity transported by 10 Gbps WDM long-haul transmission systems is ~1Tbps in the C-band (1530-1565 nm) corresponding to a spectral efficiency of 0.2 bit/s/Hz. Increasing further the spectral efficiency can be done either by broadening the amplifier gain bandwidth which is much lower than the total usable fiber bandwidth [Ess10], or by increasing the data rate carried by each channel. The top of Figure 2-1 represents the capacity evolution of single channel as well as WDM systems over almost 2 decades achieved in various record research experiments [Ess10]. Also shown in the bottom of this figure is the spectral efficiency attained by such systems. Around the nineteen"s the data rate carried by a single channel was 10 Gbps. It was attained thanks to CD compensation and the

implementation of forward error correction codes (FEC). Then the WDM technology developed in the mid-1990s has rapidly boosted the total capacity. Later, around 2008 the implementation of the coherent detector has enabled a data rate of 100 Gbps in a single channel. Coherent detection is considered as a technological breakthrough that allows high data-rate long-haul transmission. This technology is also expected to play a crucial role for any technique considered in the future in order to further raise capacity. The bottom plot of Figure 2-1 shows the evolution of the spectral efficiency, it attained 2 bits/s/Hz around 2000 and increased up to 10 bits/s/Hz in 2010. This is brought by the use of advanced modulation formats that have quickly replaced the NRZ-OOK systems in the long-haul transport.

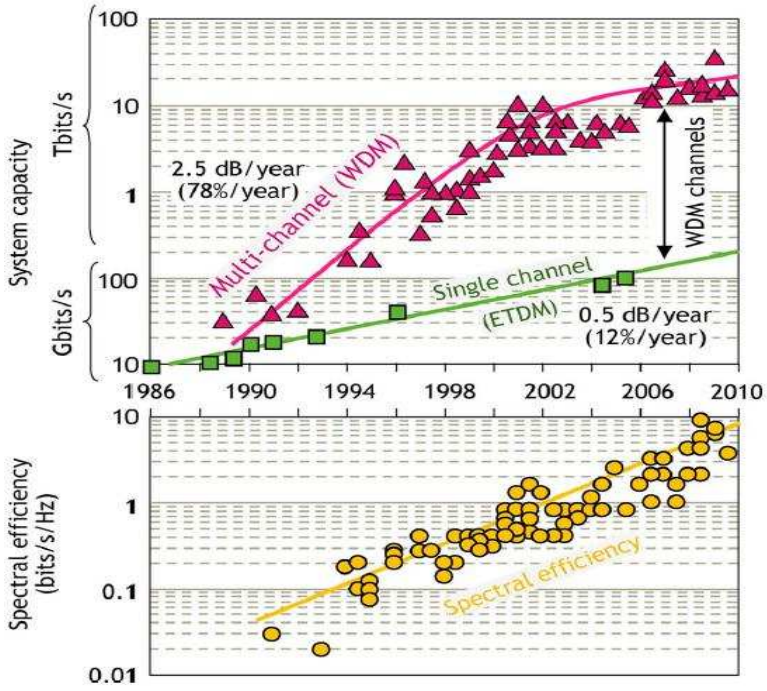

Figure 2-1: Evolution of experimentally achieved single channel bit (green circles), and aggregate per-fiber capacities (triangles) using wavelength-division multiplexing (WDM) [Ess10].

We review quickly in this section the evolution of optical channel capacity from 2.5 to 100 Gbps and open the prospect for data rate beyond 100 Gbps.

2.1.1 What has permitted the EDFA invention?

The first major milestone in the evolution of optical fiber transmission systems was the invention of the erbium-doped fiber amplifiers (EDFA) at the end of the 80"s. It replaces the expensive optical-to-electrical-to-optical (OEO) regenerators and it is able to amplify a multiplex of optical signals having their wavelength inside the amplificator bandwidth. This permits the increase of the system capacity by aggregating several wavelengths simultaneously without increasing the data rate carried by a wavelength. Multiplexing data over several wavelengths is called WDM.

Currently EDFA is the most practical way to amplify 50 GHz or 100 GHz optical channels within the ITU-T grid in the C-band. It is characterized by its low power consumption and its gain bandwidth located in the [1530 nm-1562 nm] spectral region (C-band) (Figure 2-2) that lines up with the low loss attenuation window of SSMF (minimal at 1550 nm) [Ram02]. However, a peak appeared around 1530 nm due to the high excitation levels. Thus gain

flattening is required and it can be obtained through a filter designed to have an inverse profile of the gain spectrum.
EDFA can be also designed to have its gain bandwidth in the Long, or L-band, from approximately 1570 nm to 1610 nm. Usually, its gain is optimized in one of these bands.

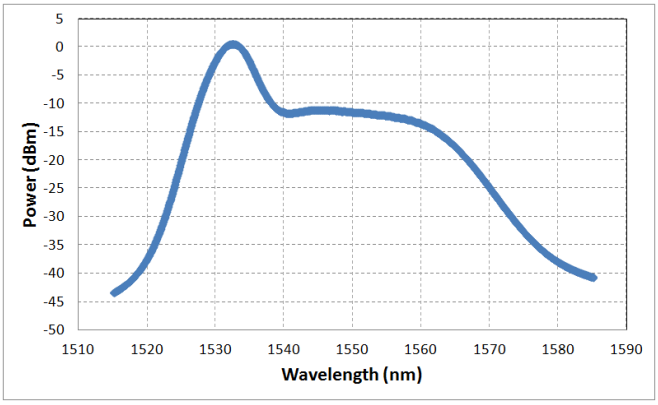

Figure 2-2: Typical gain bandwidth of the EDFA located in the C band.

2.1.2 From 2.5 to 10 Gbps based on OOK format

WDM systems were deployed in the mid nineties with a wavelength data rate of 2.5 Gbps and with a total of 40 channels per fiber for a transmission over 600 km of SSMF. This capacity was made possible by the compensation of fiber loss thanks to the EDFA, and by the negligible impact of CD and PMD at such a low data rate. However, as EDFA amplificators were progressively added on fiber links, the transmission distance □□ □□ was increased up to the point where accumulated chromatic dispersion (□□□□ □□□ became a major impairment for increasing further the bit rate. The relation between the maximum transmission length □□ □□ before being affected by chromatic dispersion and the data rate □, in case of NRZ-OOK format, is calculated by [Cha08]:

$$\square^{\square}\square_{\square\,\square\square} \square \frac{\square}{\square\square\square\,\square\square^{\square}} \qquad \text{Eq. 2-1}$$

where □□is the chromatic dispersion expressed in ps/(nm.km) and □ is the wavelength at 1550 nm. Due to this equation, the theoretical □□ □□ attained by 10 Gbps NRZ-OOK channel over SSMF, having a CD coefficient of 17 ps/(nm.km), is around 61 km. This length is divided by 16 when the channel capacity is upgraded to 40 Gbps. Thus, CD sets a limit on the system capacity and must be overcome to reach several thousand kilometers at a bit rate as high as 10 Gbps per channel.
Fortunately, new techniques have enabled the transition from 2.5 to 10 Gbps. The deployment of the inline dispersion compensation fiber (DCF) and the implementation of forward error correction codes (FEC) have allowed the channel data rate to reach 10 Gbps [Ram02]. The inline dispersion compensation consists in compensating the chromatic dispersion by inserting a fiber that exhibits a dispersion of opposite sign with respect to the already installed fiber, while the FEC consists in adding additional redundant information to the signal in order to correct transmission errors at the receiver. 10 Gbps transponders were equipped with (255,239) Reed-Solomon (RS) FEC codes which provide about 6 dB gain in optical to signal noise ratio (OSNR).

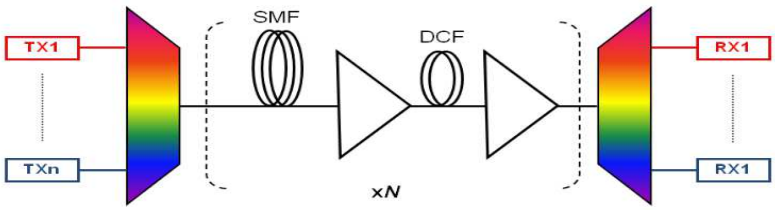

Figure 2-3: WDM transmission system [Fal11].

In order to further increase the transmission distance, Enhanced-FEC (EFEC) with 8.5 dB gain in OSNR have replaced RS codes. On the receiver side, EDC (Electronic Dispersion Compensation) was also implemented, either in the form of a linear equalizer or a more complex MLSE (Maximum Likelihood sequence estimator) [Pin11]. All these systems however still relied on the same modulation format, NRZ-OOK, a form of intensity modulation coupled with direct detection at the receiver.

2.1.3 Toward 40 Gbps technologies

In this subsection, we present the capacity transition from 10 to 40 Gbps. The upgrading to 40 Gbps based on the NRZ-OOK, which is the modulation format already used for the 10 Gbps systems, was not possible as we will see in the first part of this subsection. It was the implementation of coherent optical technology that made possible the jump to data rate of 40 Gbps. The coherent 40 Gbps system architecture is introduced in the second part of this subsection.

2.1.3.1 10 to 40 Gbps based on OOK format

The rapid advances in optical, electronic, and optoelectronic device technologies, permitted at this level to increase the capacity up to 40 Gbps [Winz12]. In particular, chromatic dispersion can be overcome by the insertion of inline DCF module and as such, does not set a hard limit for increasing the date rate. On the other hand, PMD, which did not affect 10 Gbps NRZ-OOK links is no longer negligible when raising to symbol rate to 40 Gbps. Indeed, the maximum allowable PMD on the link is given by [Ten06]:

□□ □ □ $\frac{\square_{\square}}{\square\square}$ **Eq. 2-2**

where $\square_{\square}$ is the bit period.
For polarization preserving fiber the PMD increases linearly with the fiber length □ [Agr97]; however because of random coupling between the two modes, induced by random perturbations of birefringence, PMD is proportional to the square root of the fiber length □ and it is then given by [Ten06].

□□ □ □ □□ $\square_{\square\square\square\square}\square\square$ **Eq. 2-3**

where □□ $\square_{\square\square\square\square}$ is the PMD coefficient which is specified by the manufacturer for commercially available fibers.
Accordingly, upgrading OOK systems from 10 to 40 Gbps decreases the maximum cumulated PMD tolerated by 10 Gbps systems by a factor of 4. The tolerance accepted by

the NRZ-OOK WDM system is 10 ps at 10 Gbps while 2.5 ps is the limit at 40 Gbps, thereby reducing the transmission length. Moreover, chromatic dispersion tolerance is divided by a factor of 16 at 40 Gbps with respect to 10 Gbps and the required optical signal-to-noise ratio (OSNR) has to be improved by 6 dB at 40 Gbps to maintain the same performance with respect to 10 Gbps system at fixed BER [Pin11,Kam10]. Besides, the coexistence between the 10 Gbps and 40 Gbps NRZ-OOK channels into a same WDM transmission system leads to strong nonlinear distortions. Furthermore the 40 Gbps NRZ-OOK was not compliant with the configurable optical add drop multiplexers (ROADM) which are usually designed for systems working with 50 GHz channel spacing at 10 Gbps [Pin11].

2.1.3.2 The coherent detection revival

The technological breakthrough that allowed the increasing of data rate was the introduction of coherent optical technology by Nortel in 2008 [Sun08]. Two things helped the implementation of this technology [Kik08]. The first is the ability to detect the signal amplitude and phase, thereby opening the way to the use of multilevel modulation formats in optical communication systems. By doing so, one can achieve spectral efficiencies much greater than intensity modulation with direct detection which is limited to ~1 bit/s/Hz (0.8 bit/s/Hz in practice). Second, coherent detection can be efficiently combined with digital signal processing (DSP) algorithms able to fully compensate for CD and PMD directly in the electrical domain, at baseband. Thus coherent technology avoids the need for inline dispersion compensation fiber (DCF) in the transmission line, which reduces in turn the impact of nonlinearities and improves the received OSNR. It has been shown in [Pin12] that transmission over DCF free fiber line has a better resistance to nonlinear effects.

Figure 2-4: 40 Gbps coherent DP-QPSK transceiver card [Sun08].

Various transmission techniques have been studied for 40 Gbps DWDM transmission systems. Coherent dual-polarization quaternary phase shift keying (DP-QPSK), coherent dual-polarization binary phase-shift keying (DP-BPSK), and two sub-carriers, coherent dual-polarization binary phase shift keying (2□ DP-BPSK) have been suggested by equipment suppliers for 40 Gbps long-haul WDM transmission [Pink11].

In existing legacy networks, optimized for 10 Gbps NRZ-OOK transmission, chromatic dispersion is compensated through the insertion of the inline DCF module after each amplifier, 40 Gbps transponders satisfy the required conditions to cross reconfigurable optical add drop multiplexers (ROADM) and also have the same reach than classical 10 Gbps NRZ-OOK transponders.

2.1.4 100 Gbps coherent DP-QPSK systems

40 Gbps systems arrived on the market in mid 2000 but due to the growing requirement for additional capacity, an upgrade to higher data rate was already in order. This time capacity upgrading did not follow the traditional approach which consists in defining next generation systems having four times the capacity of the previous generation. Indeed Optical Transport Network (OTN), the successor to SONET/SDH, defined by the ITU-T, will be based upon 100 Gbps Ethernet, leading to the standardization of 100 Gbps links instead of 160 Gbps(4x40 Gbps) [Gor10]. As traffic growth today is largely dominated by IP data [Shi07], 100 Gbps Ethernet is considered by many as the next-generation transport standard for IP networks [Bor07, Winz10]. In addition, 100 Gbps technology is cost effective since it permits to reuse the already installed equipments (Mux/Demux, ROADM, EDFA, DCF modules), contrarily to the 160 Gbps technology.
The coherent 100 Gbps technology appeared in 2010. It relies on the DP-QPSK modulation format already in use for 40 Gbps WDM systems. The convergence to 100 Gbps DP-QPSK was largely facilitated by the maturity reached by 40 Gbps technology and by the bandwidth compatibility of the electric and optical devices with the 100 Gbps data rate requirements. 100 Gbps channels are compliant with 50 GHz channel spacing and 50 GHz-based ROADM cascade. They operate on the 50 GHz ITU-T grid and are robust to the PMD level tolerated by existing 10 Gbps WDM systems. However, based on the same FEC codes already in use in 40 Gbps 100 Gbps PM-QPSK cannot reach the 2000 km maximum transmission distance achieved by 40 Gbps PM-QPSK, and are limited to about 1200 km only. But with the advent of soft-decision FEC that will provide extra OSNR margins to the system, the maximum reach of 100 Gbps PM-QPSK is expected to be enhanced.

2.1.5 Beyond 100 Gbps

Nowadays the implementation of coherent DP-QPSK channels operating at 100 Gbps and enabling 2 bit/s/Hz spectral efficiency has been privileged for long haul transmission. But in parallel, experimental studies of 100 Gbps OFDM were successfully carried out in a number of research works [Jan09]. The OFDM signal spectrum is approximately rectangular, allowing the juxtaposition of several OFDM bands without inter-band interference. This spectral property is particularly attractive when considering the use of super-channels, which consists in juxtaposing in the frequency domain a set of very compact bands. Thus OFDM seems to be a convincing solution for high bit rate transmission beyond 100 Gbps (400 Gbps and 1 Tbps). In order to assess the performance of OFDM in the context of high data rate date long haul transmission, we will experimentally focus on optical OFDM in this thesis.
Another competitor for optical data transmission beyond 100 Gbps is the Nyquist wavelength-division multiplexing (N-WDM) that consists in applying an electrical or optical Nyquist filter to the single carrier signal in order to obtain a rectangular spectrum.

However in order to pave the road to high data rate long haul transmission, several technological evolutions are still required. In particular, the speed of the electrical devices and the DSP processing rate must be improved. RF drivers, trans-impedance amplifiers, IQ modulators, photo-receivers and the digital to analog and analog to digital converters must be made more effective. Also efficient algorithms to compensate for the nonlinear effect must be implemented.

2.2 Main physical impairments in long-haul optical fiber transmission

Long-haul high-data-rate transmission over optical fiber suffers from several impairments. Depending on the transmission wavelength, fiber loss reduces the signal launched power, calling for the periodic insertion of EDFA in the link. In turn, EDFA generates amplified spontaneous noise (ASE) that resembles white noise. Besides ASE, several other propagation impairments exist. Chromatic dispersion (CD) and polarization mode dispersion (PMD) cause intersymbol interference (ISI) and are two important limiting factors for long haul high bit rate transmission system. CD and PMD are classified as linear impairments. But there exists also nonlinear distortions in optical fiber, mostly induced by the Kerr effect. Among the nonlinear effects that deserve attention, Self phase modulation (SPM), Cross-phase modulation (XPM), Cross-polarization modulation (XPolM) and Four-wave mixing (FWM) usually are the most prevalent.
In this section, we briefly review the physical causes as well as the impact of linear and nonlinear effects on the transmitted optical signal.

2.2.1 Attenuation

Attenuation refers to the loss of optical power observed during light propagation along the fiber. The attenuation is given by:

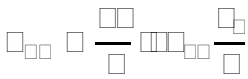

Eq. 2-4

when considering an input power P_{in} injected into a fiber of length L and detected at the fiber end with a received power P_{out}.
The attenuation in optical fiber is caused by several factors such as Rayleigh scattering, absorption and bending losses [Agr97]. Fiber scattering is due to the interaction of light with density fluctuations within a fiber. The related loss decreases when the wavelength increases, reducing the loss of higher wavelength (Figure 2-5 reproduced from [Ess10]). Besides the Rayleigh scattering loss, the presence of impurities in the optical fiber may absorb light. OH^- is the most important impurity that affects fiber loss. It is responsible for the peaks observed in 1380 nm, 1250 nm and 950 nm. Today, G.652 fibers do not have an OH- peak at 1380 nm, which decreases the level of losses from ~ 0.5 dB/km to ~0.3 dB/km [Fal11] and allows thus a transmission in the entire region located between 1300 and 1700 nm. In this region, the fiber loss is less than 0.35 dB/Km. Practically, the transmission bandwidth is limited by the bandwidth of amplification.

Another type of absorption contributing to fiber loss is caused by the property of silica. Pure silica leads to two intrinsic absorption regions which are the ultraviolet and the infrared above 2000 nm regions.
By accounting for the contribution of all the intrinsic losses, we can see from the Figure 2-5 that around 1550 nm the loss attains its minimum value of about ~0.2 dB/km in standard G.652 and G.655 fibers; as a consequence the distance between two consecutive amplifiers can be between 50 km and 100 km depending on the total transmission length. For long-haul terrestrial transmission system, the distances between EDFAs are typically 80-100 km for a total transmission length between 1500 and 3000 km.
The total loss must include the bending losses and the losses due to the connection of two fiber pieces.

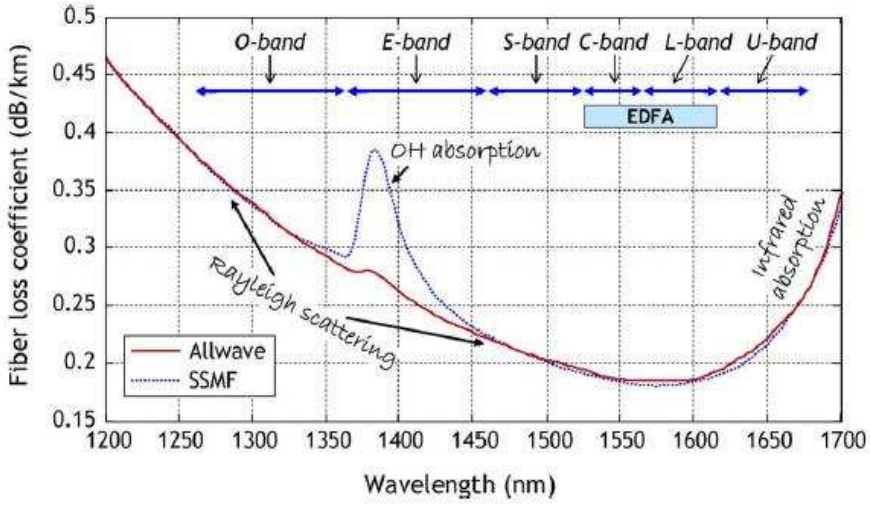

Figure 2-5: Attenuation in dB/km Vs wavelength in nm for a typical SSMF and a fiber without the water absorption peak [Ess10].

2.2.2 Chromatic Dispersion

Chromatic dispersion is the phenomenon by which different spectral components of a pulse propagate along the fiber with different velocities. It induces pulse broadening and leads to significant ISI that degrades system performance.
The effect of fiber dispersion is best described by expanding the mode-propagation constant β into a Taylor series around the center frequency ω_0:

$$\beta(\omega) = \beta_0 + \beta_1(\omega - \omega_0) + \frac{1}{2}\beta_2(\omega - \omega_0)^2 + \frac{1}{6}\beta_3(\omega - \omega_0)^3 + \cdots \qquad \text{Eq. 2-5}$$

Where

$$\beta_m = \left(\frac{d^m \beta}{d\omega^m}\right)_{\omega = \omega_0} \qquad \text{Eq. 2-6}$$

The first derivative is the inverse of the group velocity $v_g = \frac{d\omega}{d\beta}$ and the second derivative, β_2, is responsible for the pulse broadening and called group velocity dispersion (GVD) parameter.

□□ is the result of the contribution of the material dispersion and waveguide dispersion. Material dispersion occurs because the refractive index □□□□of silica, the material used to make optical fiber, is frequency dependent□□□□ [Agr97]. Since different spectral components are associated with the optical pulse, and since the light velocity is determined by □□□□□□, the different spectral components of a pulse travel at different velocities. We recall that waveguide dispersion occurs when the speed of a wave in a waveguide (such as an optical fiber) depends on its frequency for geometric reasons.

The wavelength corresponding to □□ □ □is □□ and called zero dispersion wavelength. However, □ is the dispersion parameter in the units of ps/(km.nm) that is commonly used to indicate the amount of dispersion in fiber rather than GVD. □ is related to □□ by

$$\square \square \square \frac{\square\square\square}{\square^{\square}} \square_{\square} \qquad \text{Eq. 2-7}$$

For wavelengths such as□□ □ □□, □□ □ □ (or □ □ □□, the fiber is said to have normal dispersion. In this case, the highest frequency (lowest wavelength) components of an optical pulse travel slower than the lower (higher) components. On the contrary, for □□ □□, □□ □ □ (or □ □ □□, the fiber is said to have anomalous dispersion and the high frequency components travel faster than the low frequency components [Agr89].

We should notice that the amount of CD, PMD as well as the attenuation at a specific wavelength depends on the fiber characteristics. In Table 2-1 we report the value of the linear properties of several well-known commercially available fibers, namely SSMF which is the major deployed fiber, large effective area fiber (LEAF) (corning), teralight (Draca), truewave (OFS) and the pure silica core fiber (PSCF) (corning vascade Ex2000 fiber). The CD and attenuation values are given for the reference wavelength 1550 nm.

Fiber Type	ITU standard	CD @1550 nm (ps/nm/km)	PMD_{coeff} ($ps/km^{1/2}$)	α @1550 nm (dB/km)	Effective area (μm^2)
SSMF	G.652	+16/17	< 0.08	0.19	80
LEAF	G.655	4.2	< 0.04	0.21	72
Teralight	G.655	8	< 0.04	0.21	62
Truewave	G.655	6	< 0.04	0.21	55
PCSF	G.654	20	< 0.04	0.16	80-115

Table 2-1: Values of CD, PMD, attenuation and effective area for different fiber types.

2.2.3 Polarization mode dispersion

During last few years, PMD has been recognized as the major impairment factor limiting high data rate transmission. The origin is found firstly in the manufacturing process and lastly in the deployment conditions; in an ideal environment, the core fiber is an isotropic material due to its perfect cylindrical geometry. Thus, when a pulse propagates across the fiber; its polarization in the x direction would not couple with the polarization in the y direction and both polarizations would travel at the same velocity.
However, in practice, the fiber is not as perfect as we desire, as a consequence of the manufacturing process and resulting in an elliptical core instead of circular core. Besides, due to the fiber condition deployment and the temperature variation, the distortions of the core may be enhanced [Spa06]. The core asymmetry means that the refraction index is not the same in both polarization states resulting in a slow and fast axis. Subsequently, the two

polarization modes travel along the fiber at different velocities. This property is referred as modal birefringence.
As shown in Figure 2-6, considering a uniform birefringence along a short fiber and for a given state of polarization (SOP) denoted in the figure by x and y, the x and y polarization travel through the fiber at different velocities due to the difference in the refractive indices n_x and n_y.
The birefringence in a short fiber can be expressed as the difference between the propagation constants of the slow and fast axis:

$$\beta = \frac{\omega}{c}(n_x - n_y); \quad \text{with } \omega = 2\pi f \qquad \text{Eq. 2-8}$$

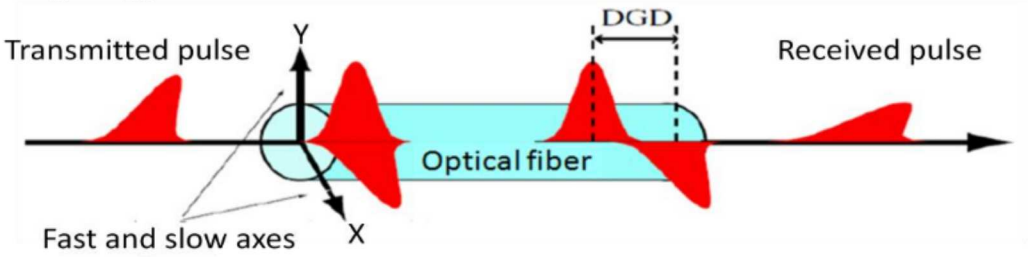

Figure 2-6: Effect of PMD in a short fiber.

Birefringence induces a delay $\Delta\tau$, between the two modes referred to as differential group delay (DGD) and broadens the transmitted signal which is the result of the two polarization components (Figure 2-6). The DGD can be calculated by [Agr97]:

$$\Delta\tau = \frac{\partial \beta}{\partial \omega}\Delta\omega = \frac{\partial \beta}{\partial \omega}\frac{2\pi c}{\lambda^2}\Delta\lambda \qquad \text{Eq. 2-9}$$

The PMD is the average of the DGD and causes ISI.

For a long fiber, birefringence is no longer uniform, and the fiber can be modeled as a concatenation of birefringence segments whose birefringence axes change randomly. For each segment, the birefringence and the orientation of the birefringence axis stay constant but different from the other juxtaposed segments (Figure 2-7). When the pulse is launched in a segment it is decomposed to the slow and fast axes of this segment. As the next segment is characterized by a different birefringence, the pulse crossing the first segment is again decomposed to the slow and fast axes corresponding to the next segment. Along the optical fiber, the random axes cause polarization mode coupling and make PMD a random variable. The statistical nature of PMD makes compensation very difficult in optical domain.

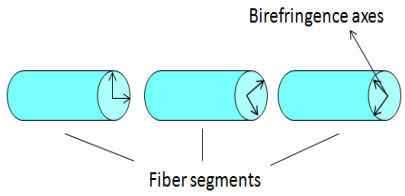

Figure 2-7: Modeling a long fiber as a concatenation of birefringent segments.

The first PMD order is represented by [Fra98]:

□□□ □□ □□□□□ Eq. 2-10

□□□ □is the PMD vector in the Stokes space, □□ is the group delay difference between the principle state of polarizations PSPs (DGD) given the magnitude of the vector □and □□is a unit vector that points in the direction of the slow principle axis of the PSPs. In short fiber, the PSPs simply correspond to the birefringence axes; it is defined such that for a special input SOP the output SOP is independent of frequency to first order. In stokes space, the slow PSP axis is denoted by □.

For a given fixed input SOP for different frequencies, PMD will manifest as a change of the output SOP □with frequency according to the relation [She04]:

$$\frac{\square\square\square\square}{\square\square} \square \square\square\square\square\square\square\square \quad \text{Eq. 2-11}$$

□□□ □is the PMD vector at frequency □. As can be seen from equation 2-11, the PMD describes how the output □□changes around the PSP as the frequency varies, given the fixed input SOP (see Figure 2-8) [She04].

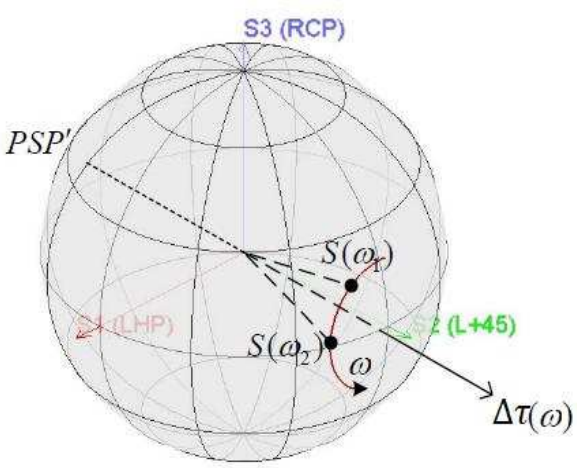

Figure 2-8: The variation of the SOP on an arc of circle on the Poincaré sphere [She04].

Then, the measure of the DGD □□is the rate of rotation of the output SOP around the PSP and is expressed as:

□ □ □□□□□ Eq. 2-12

□ is the amount of rotation about the PSP. If □□□ □is aligned with □□□ □then the output SOP is frequency independent.

Second-order PMD is described by the frequency derivative of □and is given by [Spa06]:

□□□ □ □□□ □□□□ □□□□□ Eq. 2-13

The subscript □ indicates differentiation with respect to □. The first component is parallel to the vector □□as the first PMD vector, and causes a dependency of the DGD with the frequency. It is known as PCD (polarization dependent chromatic dispersion) and it is

viewed as the chromatic dispersion variation dependent on the polarization. The second component describes the rotation of PSP with frequency.

2.2.4 Optical amplification

As we have seen in subsection 2.1.2, the optical amplifier was the first major invention that allowed a significant increase in the maximum transmission distance. It avoids the OEO conversion and permits the deployment of WDM system. Currently the EDFA is the most used optical amplifier for terrestrial transmission systems. The principle of EDFA is based on exciting the Erbium ions to higher energy levels. Two pumps at 980 and 1480 nm will excite erbium Er^{3+} ions. When the number of atoms in the higher energy level is greater than the number of atoms in the lower energy state, a phenomenon called population inversion results, which is essential for signal amplification [Des91]. As a result, the optical signal passing through the amplifier causes the Er3+ ions to return to a lower energy level and to emit a photon. The photon will induce the emission of new photons. This process is called stimulated emission and generates photons having the same energy, same wavelength, and being in phase with each other.
However the signal will act as a pump and will excite the ions. After relaxation, photons are emitted in the wavelength band 1520-1570 nm with a random phase. This is called spontaneous emission. This process is accompanied by the generation of amplified spontaneous emission (ASE). Indeed, the photon with a random phase propagates with the signal and in turn can be amplified by stimulated emission. This noise is known as ASE noise and is cumulated by passing through each amplifier. The ASE noise reduces transmission distance. It is quantified by the optical signal to noise ratio (OSNR).

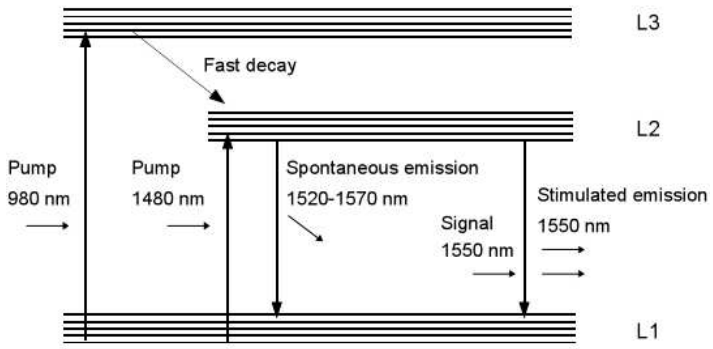

Figure 2-9: Principle of EDFA operation [htt07].

The OSNR is defined as:

$$\text{OSNR} = \frac{P_{signal}}{P_{ASE}} \cdot \frac{B_{ref}}{B_{noise}} \qquad \text{Eq. 2-14}$$

where B_{ref} is the reference optical bandwidth. The factor 2 is due to the random distribution of the noise on the two polarizations. P_{ASE} denotes the power spectral density of ASE in one polarization, and is given by

$$P_{ASE} = n_{sp} \cdot h\nu \cdot (G - 1) \qquad \text{Eq. 2-15}$$

where $\square_{\square\square}$ is the spontaneous emission factor, $\square$ is Planck"s constant, $\square$ is the frequency of the light ($\square\square$ is the photon energy) and $\square$ is the EDFA gain.

Generally, an EDFA is characterized by its gain $\square\square$ and noise figure $\square\square$. The noise figure permits us to quantify the noise added to the signal after amplification; it is expressed by [Ban00]:

$$\square\square\ \square = \frac{\square}{\square}\ \square\square = \frac{\square\square\square\square_{\square\square\square}}{\square\square}\ \square\ \square\square \qquad \text{Eq. 2-16}$$

Terrestrial long-haul optical fiber transmission links are usually made of several spans separated by amplifiers. It is schematically represented in Figure 2-10.

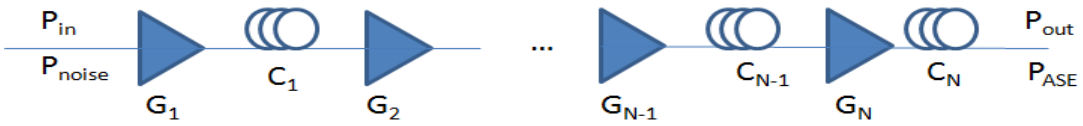

Figure 2-10: Example of a typical transmission line comprising several EDFA amplifiers.

The $\square\square\square\square$ at the end of the system (receiver side) is then expressed by [Fri03]

$$\square\square\square\square\square_{\square\square\square\square} = \square_{\square\square\square\square} + \square\ \frac{\square_{\square\square\square\square}}{\square_{\square\square\square\square}} \qquad \text{Eq. 2-17}$$

where:

$$\square_{\square\square\square\square} = \square\square\ \square_{\square}\square_{\square}\square\ \square\square_{\square\square} \qquad \text{Eq. 2-18}$$

$$\square\square_{\square\square\square\square}\ \square_{\square\square\square\square} = \square\ \square\ \square\ \square\ \square_{\square\square\square}\square_{\square}\square\ \square\square\square\square\square_{\square\square\square}\ \square\square\square_{\square\square\square\square} \qquad \text{Eq. 2-19}$$

$\square_{\square}$ is the loss introduced during the propagation along a span between two amplifiers; $\square\square_{\square\square\square\square}$ is the power spectral density of the noise inserted in the first amplifier.
As the signal passes through multiple spans and amplifiers, there is an amplification of the ASE power; and $\square_{\square\square\square\square}$ is expressed as the ASE power generated and or amplified by each amplifier (first term of Eq.2-19) and as the sum of the power noise injected in the first amplifier (second term of Eq. 2-19)

If the injected power, at the output of the amplifier, in the span is the same, it means $\square_{\square\square\square} = \square_{\square}\ \square$ and the amplifiers have the same gain and noise figure, while the noise before the first amplifier is neglected the $\square\square\square\square_{\square\square\square\square}$ is then expressed by

$$\square\square\square\square\square_{\square\square\square\square} = \square\ \frac{\square\square\square_{\square\square}}{\square\ \square\square\square\square\square_{\square\square\square}\ \square\square\square_{\square\square\square\square}} \qquad \text{Eq. 2-20}$$

With [illegible] and [illegible] then,

$$[illegible]$$ Eq. 2-21

2.2.5 Nonlinear effects in optical fiber

Modern optical communication system are now using advanced modulation format in combination with coherent detection. High spectral efficiency can then be achieved while DSP is used to overcome and even cancel the detrimental effect of PMD and CD. But CD and PMD are not the only distortions encountered in an optical fiber. Instantaneous variations of signal power within the channel may cause changes in the refractive index, which may lead in turn to a signal phase change. This effect is known as SPM. The fiber refractive index also depends on the power variations of the other co-propagating channels inside the fiber. This is called XPM. Furthermore, the co-propagating channels can interact to create signals at new frequencies, resulting in FWM. In addition, the SOP of a transmitted signal is affected by the SOP of the other co-propagating channels leading to XPolM.

SPM, XPM, XPolM and FWM are all special instances of a more general physical phenomenon called the Kerr effect, which finds its roots in the dependence of the fiber refractive index on the signal power [Agr89]. The refractive index inside the fiber is expressed by:

$$[illegible]$$ Eq. 2-22

where [illegible] is the linear part of the refractive index, [illegible] is the nonlinear-index coefficient, [illegible] is the optical power, [illegible] is the effective core area and I is the optical intensity. The value of [illegible] is approximately 1.5 whereas [illegible] is around [illegible] . We can induce from the equation above that either high optical power and/or small [illegible] increase the impact of Kerr effect.

The propagation of an optical pulse within a single-mode fiber obeys the nonlinear Schroëdinger equation, which can be written as [Agr89]:

$$[illegible]$$ Eq. 2-23

In the above equation, [illegible] is the complex field envelope, [illegible] is the distance, and [illegible] is the nonlinear coefficient that is expressed by:

$$[illegible]$$ Eq. 2-24

where [illegible] is the effective transmission distance, given by:

$$[illegible]$$ Eq. 2-25

We note above that L_{eff} takes into account the fiber attenuation α.
We mention that the influence of Kerr effect is the strongest in the first part of the fiber of length L_{eff} after the EDFA since that, after this transmission length, the signal power is reduced due to the presence of fiber attenuation.

Another general class of nonlinear effects is simulated inelastic scattering. The two important effects related to this class are Stimulated Brillouin Scattering (SBS) and Stimulated Raman Scattering (SRS) [Agr89] but these two effects will not receive further attention in the present work.

In the following of this subsection, we develop in more details the physical origin as well as the impact of SPM, XPM, XPolM and FWM.

2.2.5.1 Self-phase modulation

The refractive index is intensity dependent and leads to a nonlinear phase shift expressed by:

$$\phi_{NL}(t) = \gamma L_{eff} P(t) \qquad \text{Eq. 2-26}$$

We note that the nonlinear phase depends on the effective transmission distance, and also on the optical power $P(t)$ of the signal, meaning that the transmitted pulse modifies its own phase. SPM causes a phase change without changing the envelope of the pulse. It induces an instantaneous frequency deviation (frequency chirp) given by:

$$\delta\omega(t) = -\frac{\partial \phi_{NL}}{\partial t} = -\gamma L_{eff} \frac{\partial P(t)}{\partial t} \qquad \text{Eq. 2-27}$$

The chirp $\delta\omega$ increases in magnitude with the transmission distance. Thus new frequency components are continuously generated as the pulse propagates down the fiber.

The SPM induced chirp is independent of the sign of the dispersion. However the combined effect of CD and SPM induces two different phenomena depending on the sign of the dispersion. In the normal dispersion regime, SPM enhances the effect of dispersion which results in a significant broadening of the spectral pulse [Agr89]. On the contrary, in the anomalous dispersion regime, the effect of CD is reduced and the pulse is compressed. When the effect of SPM balances the effect of CD, the pulse shape can be preserved during the propagation down the fiber, leading to a particular form of signal propagation called Soliton. However, in practice, fiber attenuation reduces the signal power along the fiber, decreasing in turn the effect of SPM. Conversely the CD value remains stable, thus preventing ideal Soliton propagation.

2.2.5.2 Cross-phase modulation

Another consequent effect of the dependency of the fiber refractive index on the time varying signal intensity is XPM. It occurs when two or more optical signals carried by different wavelengths co-propagate inside the fiber. When the signals are overlapped, the combined intensity of all transmitted channels induces a nonlinear phase shift given by:

Eq. 2-28

The first term of the equation is the SPM, while the second term denotes the contribution of XPM. Thus a propagating optical signal not only modifies its own phase, but also the phase of other neighboring co-propagating signals. The factor 2 in front of the second term implies that XPM has two times more impact than SPM on the considered signal. XPM causes spectral broadening, timing jitter and amplitude distortion in time domain.

The presence of CD reduces the impact of XPM. Signals at different wavelengths travel at different velocities, limiting the interaction time between channels. If the channels are separated far apart from each other, the XPM effects are relatively weak because the two signals walk off from each other quickly. On the other hand, XPM is all the more significant that the channel spacing is narrow.

2.2.5.3 Cross-polarization modulation

Polarization division multiplexing is seen today as an attractive technique to increase spectral efficiency by doubling the data rate carried by a wavelength. The signal is transmitted in both orthogonal SOP's of each co-propagating wavelength channel. However, the SOP of a transmitted signal can be affected by the SOP of the other co-propagating channels which evolve randomly throughout the fiber due to PMD [Win10]. This effect, known as XPolM, leads to a signal depolarization. The effect of XPolM is described by the following equation:

Eq. 2-29

with

$\vec{s}_k$ denotes the Stokes vector of channel k, $\vec{s}_{sum}$ comprises the sum of all Stokes vector of all wavelength channels in the WDM system and $\vec{s}_k$ is the stoke vector of channel k, for which we analyze the nonlinear polarization shift induced by the co-propagating channels. The effect of XPolM takes the form of a rotation of the state of polarization of channel k around the instantaneous sum of the Stokes vectors of the co-propagating channels $\vec{s}_{sum}$. This cross polarization modulation dramatically influences polarization de-multiplexing at the receiver and dominates over the normal XPM penalty in multi-channel polarization division multiplexing transmission. It induces crosstalk and can be modeled as an additive Gaussian noise source [Win10].
We should note that when the signals are either in the collinear or orthogonal polarization states, the polarization of the signals is not affected.

2.2.5.4 Four wave mixing

In WDM system, the intensity dependence of the refractive index causes nonlinear phase shift and in addition gives rise to signals at new frequencies. This last phenomenon is the FWM that leads to transfer energy to another created signal.

For the WDM system with carrier frequencies □□, □□ and □□, the FWM generates new signals carried by □□□ that are expressed by:

□□□ □ □□ □ □□ □ □□ Eq. 2-30

The number of FWM generated signals is given by:

□ □ $\frac{□^{□}□□ □ □□}{□}$ Eq. 2-31

with N being the number of channels carrying data inside the WDM system.
If the generated signals fall into other WDM channels, the system performance will be seriously degraded due to the cross talk among channels.

FWM depends on the channel spacing and fiber dispersion. Decreasing the channel spacing or decreasing the fiber dispersion increases the FWM effect. For G.652 SSMF where the 50-GHz channels are sufficiently spaced apart from each other, the effect of FWM is negligible. On the other hand, in a G.655 LEAF where CD is low, the effect of FWM can be significant for a similar channel spacing.
SSMF is today the most commonly deployed fiber. The insertion of inline DCF modules in SSMF fiber link has made possible high transmission distance for the 10 Gbps NRZ-OOK signal, which is intrinsically robust to nonlinear effects. On the other hand, in DCF-free SSMF fiber link, CD reduces the impact of the nonlinear effects as the signals walk off from each other quickly, making the SSMF fiber a favorable medium for high bit rate (100 Gbps and beyond) long-haul transmission for DP-QPSK or DP-OFDM signal which are robust against CD and PMD.

2.3 OFDM for optical transmission

In response to the demand for increasing data rate across dispersive optical transmission systems, and taking advantage of the availability of transmitter and receiver equipment able to process electrical signals at very high data rate, OFDM technique has been the subject of a number of research works in the field of optical communication systems. The first coherent optical (CO) OFDM transmission experiment was reported for 1000 km SSMF transmission at 8 Gbps by Shieh et al. [Shi07], quickly followed by another CO-OFDM transmission experiment over 4160 km of SSMF at 20 Gbps realized by Jansen et al. [Jan07]. In 2009, 100 Gbps CO-OFDM transmission over 1000 km of SSMF was described [Jan09]. Currently, CO-OFDM is considered as an attractive competitor to the DP-QPSK single-carrier transmission format currently in use at 100 Gbps for next generation high bit rate long-haul optical transmission systems.

In this section we begin by presenting the generic principal of the OFDM technique, with an emphasis on the orthogonality concept and the crucial role of the cyclic prefix. Then we introduce the principles of CO-OFDM for long-haul optical transmission. Since hardware constraints limit today the generation of a single-band high bit rate OFDM signal, we discuss the attractive concept of multi-band OFDM (MB-OFDM). We then review the offline as well as real-time experimental records attained with the OFDM technique. Finally,

the last two subsections provide a quick overview of two closely related concepts, namely all-optical OFDM and no guard interval coherent optical OFDM.

2.3.1 Generic principles of OFDM

The basic principle of OFDM is to split a high rate data stream into a number of lower rate data streams that are transmitted simultaneously over a number of subcarriers. Each subcarrier is individually modulated by using Quadrature Amplitude Modulation (QAM) or Phase Shift Keying (PSK) and characterized by a sinc spectrum allowing overlapping in the frequency domain. Then, a cyclic prefix is added at the beginning of each OFDM symbol to avoid ISI and to maintain the orthogonality among the subcarriers. When a sufficiently high number of subcarriers is considered, the OFDM spectrum has approximately a rectangular shape which enables high spectral efficiency.
The OFDM principles, the transceiver architecture, the orthogonality concept and the role of the cyclic prefix will be detailed hereafter.

2.3.1.1 OFDM principles

Let N_{sc} denote the number of subcarriers, T_s the OFDM symbol duration, $g(t)$ the impulse response of the pulse shaping filter, and $c_{k,n}$ be the complex information symbol transmitted on the subcarrier k in the OFDM symbol n. The complex baseband OFDM signal in the electrical domain is then expressed by:

$$s(t) = \sum_{n=-\infty}^{+\infty} \sum_{k=0}^{N_{sc}-1} c_{k,n}\, g(t - nT_s)\, e^{j2\pi k \Delta f (t - nT_s)} \qquad \text{Eq. 2-32}$$

$$\Delta f = \frac{1}{T_s} \qquad \text{Eq. 2-33}$$

More explicitly, $c_{k,n}$ is carried by the frequency f_k related to the subcarrier k, and the N_{sc} modulated subcarriers are added together. The resulting signal is filtered by a rectangular time-limited filter $g(t)$ in order to obtain an OFDM symbol. For the sake of simplicity, and since the OFDM signal $s(t)$ is constituted of the concatenation of all the OFDM symbols, we will omit the time index n in the following and the transmitted signal will be restrained to the generation of one OFDM symbol. In this case $s(t)$ reduces to [LiY10]:

$$s(t) = \sum_{k=0}^{N_{sc}-1} c_k\, g(t)\, e^{j2\pi k \Delta f t} \qquad \text{Eq. 2-34}$$

In order to satisfy the orthogonality condition (discussed later) the subcarriers must be spaced apart by a quantity inversely proportional value to the OFDM symbol duration. As we shall see later, this condition permits the separation of the subcarriers without any interference between them. The subcarrier frequencies are defined through the following relation:

[illegible] Eq. 2-35

Here [illegible] is the useful OFDM symbol duration which does not includes the duration of the cyclic prefix (the cyclic prefix will be introduced later on in this section).

The block diagram of the OFDM modulator is represented in Figure 2-11.

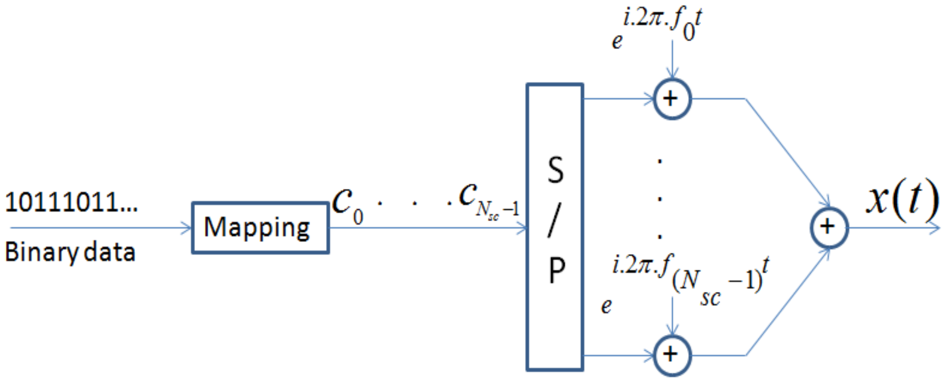

Figure 2-11: The basic principle of the transmitter set-up [Nee00].

When the number of subcarriers is large enough, the OFDM signal [illegible] is approximately band-limited to the frequency interval [illegible]. Then, according to the Shannon-Nyquist sampling theorem, [illegible] can be perfectly reconstructed by the sequence of its samples [illegible] obtained at the sampling rate [illegible]:

[illegible] Eq. 2-36

Inspection of equation 2-36 reveals that the time-domain samples [illegible] with [illegible] can be obtained by computing the length-[illegible] inverse Discrete Fourier Transform (IDFT) of the frequency-domain modulated symbols [illegible] for [illegible] till [illegible]. In practice, [illegible] is usually chosen as a power of 2 so that a computationally-efficient Fast Fourier Transform (FFT) is used in place of the IDFT. The continuous-time OFDM signal [illegible] is finally obtained by supplying the sequence of time-domain samples to a digital to analog convertor (DAC). By doing so we replace the bank of analog modulators in Figure 2-11 by a simple and efficient digital signal processing operation (IFFT) performed in discrete-time, followed by a digital-to-analog signal conversion.

The demodulation process that consists in getting back the frequency-domain complex information symbols [illegible] from the time-domain samples [illegible] is performed in a very simple and similar manner by computing the FFT of the discrete-time received signal [illegible].

2.3.1.2 Transmitter and receiver structures

The OFDM transmitter set-up is shown in Figure 2-12. The binary data are mapped onto M-QAM symbols, parallelized and then sent to the IFFT. After applying the IFFT to the symbols [illegible], we obtain a complex OFDM symbol. We split it into real (I) and imaginary (Q) components. The two components are then transferred simultaneously to two digital to analog convertors (DACs). At the output of the DAC, we get an analog signal mixed with an aliasing signal. Subsequently, low pass filters (LPF) are used to eliminate the aliasing replicas and isolate the signal of interest. Finally, the I(t) and Q(t) are modulated respectively by $\cos(2\pi f_{IF} t)$ and $-\sin(2\pi f_{IF} t)$ and combined together. The generated signal is thus carried by the intermediate frequency f_{IF}, which is here the central frequency, and is written as:

[illegible] **Eq. 2-37**

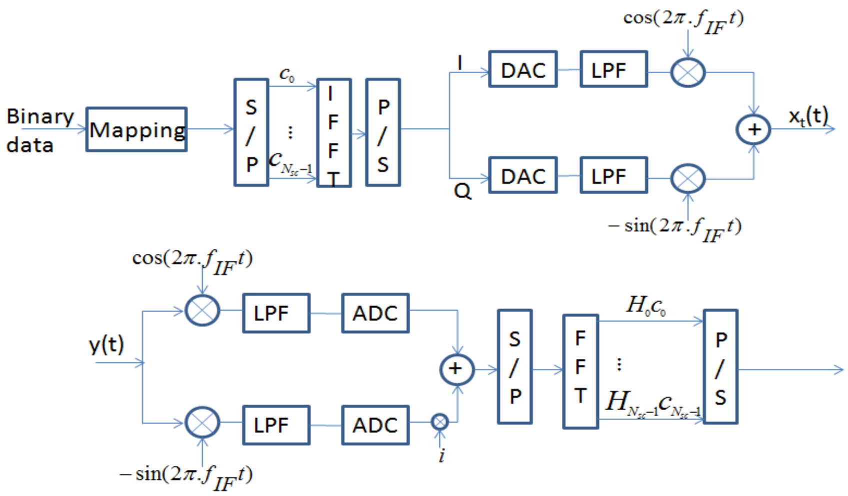

Figure 2-12: OFDM transmitter and receiver set-up.

The corresponding spectrum of $x_t(t)$ is represented in Figure 2-13.

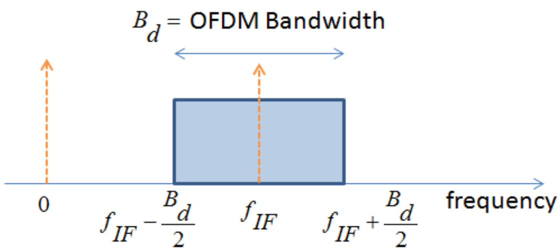

Figure 2-13: OFDM spectrum.

The OFDM receiver, also shown in Figure 2-12, realizes the inverse steps to down-convert and demodulates the received signal $y(t)$. First, $y(t)$ is split into two parallel arms through the use of 1:2 coupler. One arm is multiplied by $\cos(2\pi f_{IF} t)$ and the second by $-\sin(2\pi f_{IF} t)$. Two low pass filters are used on the parallel arms to remove the high frequencies. We obtain [illegible] on one arm and [illegible] on the second arm, where [illegible] is the impulse response of the continuous-time baseband channel. These two signals feed two analog to digital convertors (ADCs), and then they are combined together through

a multiplexer (Figure 2-12). At this level an FFT is applied, yielding the discrete-time quantities □□□□ where □□ is the complex channel coefficient for the subcarrier □. An equalizer (see Chapter 3) is applied in order to retrieve the information symbol □□, which is finally demapped so as to recover the binary transmitted sequence.

2.3.1.3 OFDM orthogonality concept

One of the most important property of the OFDM signal is the orthogonality between the sub-carriers. This orthogonality in the frequency-domain is achieved by imposing a subcarrier spacing equal to□□□ □ $\frac{□}{□□}$ □ $\frac{□□}{□□□}$. By doing so, it is possible to demodulate each subcarrier without any interference from the other subcarriers [LiY06]. The spectrum of an OFDM signal made of 4 subcarriers is shown in the right hand side of Figure 2-14. We can notice that each subcarrier has a sinc spectrum. But more importantly, at the maximum peak value (center frequency) of each subcarrier spectrum, all other subcarrier spectra are zero. This explains the absence of intercarrier interference (ICI). In the time domain, orthogonality between subcarriers translates into an integer number of cycles for each subcarrier within the symbol duration (left hand side of the Figure 2-14).

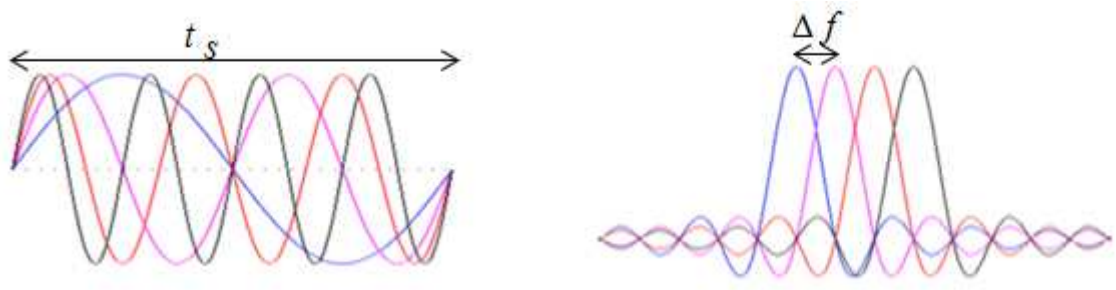

Figure 2-14 : The time domain (left fig.) and spectra (right fig.) of 4 subcarriers within an OFDM symbol.

Unfortunately, the orthogonality property breaks down in the presence of channel dispersion. As we shall see now, this problem can be solved by adding a cyclic prefix to each transmitted OFDM symbol.

2.3.1.4 Avoiding ISI: Cyclic prefix concept

The OFDM symbol duration is usually much longer than the channel delay spread, which limits the impact of ISI to a small part in each OFDM symbol. To completely avoid the effects of ISI, a guard interval needs to be inserted between successive OFDM symbols. Its duration, □□, is chosen to be longer than the maximum delay spread of the channel. In order to maintain the orthogonality between subcarriers and thus avoiding ICI, the guard interval between two OFDM symbols is formed by cyclic extension of the next OFDM symbol, and is thus called cyclic prefix. By doing so, the integer number of cycles within the FFT time window is preserved, and so is the orthogonality between subcarriers. In context of optical transmissions, the cyclic prefix offers robustness against CD and PMD provided □□ is chosen to be bigger than the CD maximum duration □□ □□□□ and the maximum DGD related to a fiber, □□ □□□□□, so that we must have: □□ □ □□ □□□□ □ □□ □□□□□

We illustrate below the impact of CD on the OFDM signal, first without adding a cyclic prefix and second with the insertion of a cyclic prefix at the beginning of each OFDM symbol.

In the first row on the left hand side of Figure 2-15, we have plotted the time domain representation of three different subcarriers within an OFDM symbol. The first subcarrier has the lowest frequency while the last subcarrier has the highest frequency. On the right hand side, the three subcarriers are represented at the receiver after undergoing chromatic dispersion. The CD induces propagation of the subcarriers at different velocities. Therefore, the first subcarrier is delayed with respect to the last one by the time □□□□. Consequently, the DFT window matches the duration of the first subcarrier while, due to the CD, the other waveform subcarriers are not completely inside the DFT window; a small part of the neighboring symbol waveform falls inside the DFT window of the corresponding symbol. Consequently interference between symbols occurs and furthermore, the orthogonality condition that consists in having a complete number of cycles inside the DFT window is broken, leading to interference between subcarriers.

In the second part of Figure 2-15, we present the impact of CD on the OFDM symbol in the presence of a cyclic prefix. The cyclic prefix is formed by cyclic extension of the OFDM subcarrier waveforms within the guard interval, whose duration is chosen greater than or equal than the maximum delay □□□□ induced by CD. The drawing clearly shows how the cyclic prefix absorbs the time-domain overlapping of neighboring OFDM symbols caused by channel dispersion. As such, an additional phase shift is induced on each subcarrier. This phase shift is dealt with through channel estimation.
Thanks to the time-domain structure cyclic prefix, the DFT window remains free of intersymbol interference and a complete number of cycles is preserved inside the DFT time window, so that orthogonality is maintained in the frequency-domain, avoiding intercarrier interference during the demodulation process.

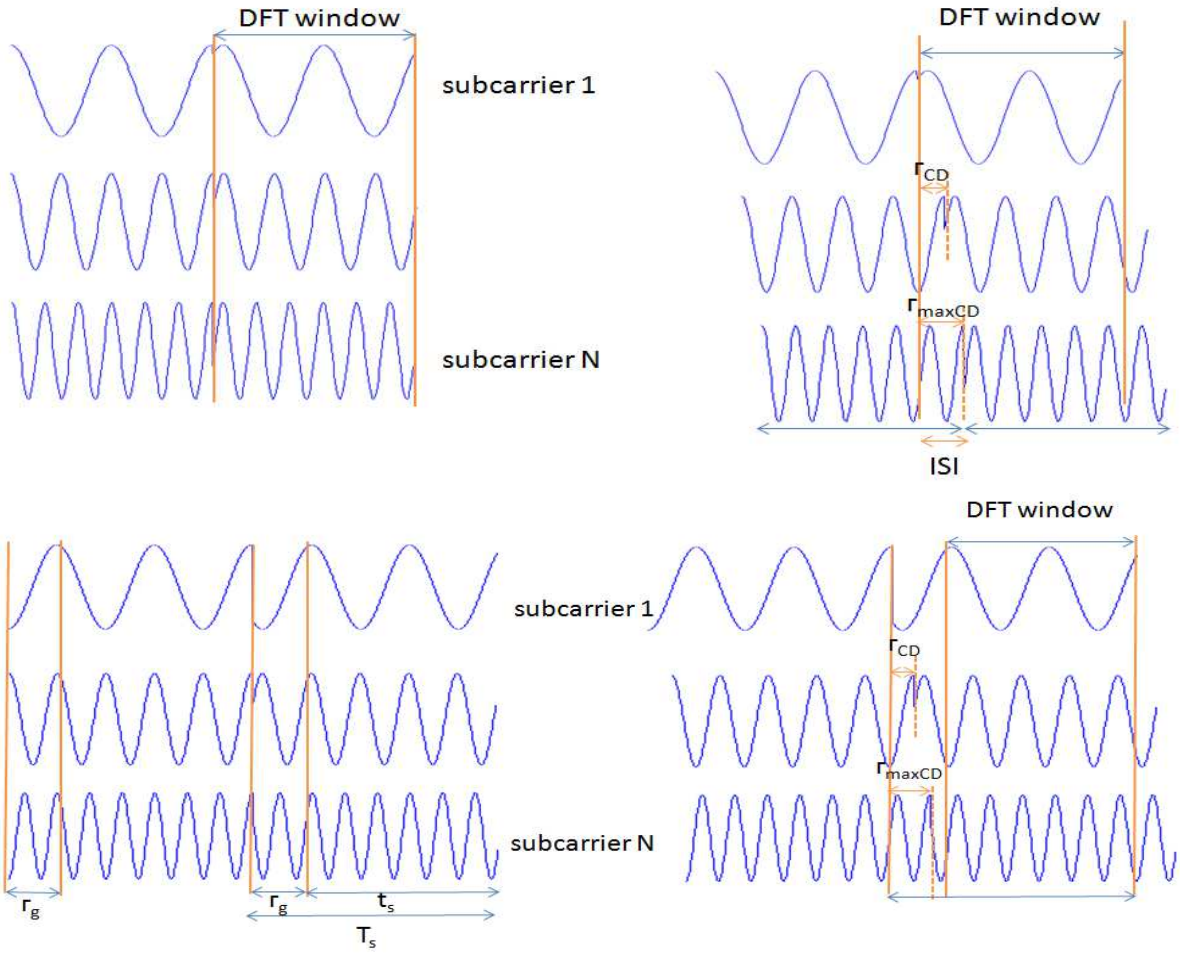

Figure 2-15: The left side of this figure represents the subcarriers of an OFDM symbol on the transmitted side while the right side the subcarriers is affected by CD. The impact of CD on an OFDM symbol in the case where the cyclic prefix is not implemented is represented on the first row and when the cyclic prefix is implemented, it is represented on the second row.

2.3.2 OFDM for long haul coherent optical transmission

Having introduced the generic principles of OFDM, we now present in this section how the OFDM concepts have been adapted to the peculiarities of long-haul fiber optics transmissions. In particular, we justify the choice of coherent detection for long-haul transmission, and also describe the two possible transmitter architectures that can be used in such scenarios.

2.3.2.1 Appropriate detection technique for long-haul transmission

Two different detection techniques can be used with OFDM modulation. We briefly review the two approaches.

In the first technique, called direct detection (DD), a photo-detector converts the optical signal into the electrical domain by producing a current proportional to the square of the received optical field amplitude□□. The photocurrent is expressed by

□□ □ □ □□ **Eq. 2-38**

where [illegible] is the responsivity of the photo-detector.
This detection technique requires that the transmitted OFDM signal satisfies two mandatory conditions to ensure signal detection without distortion: firstly, the optical carrier must be transmitted with the signal; and secondly, the OFDM signal spectrum must be separated from the optical carrier by a guard band equal to the signal bandwidth [Low09, Fen09]. Because of this guard band, only half of the required bandwidth is allocated to the signal; consequently the spectral efficiency is not optimized. In addition, half the power is "wasted" for the optical carrier, which explains the worse sensitivity of DD-OFDM [higher bit-error rate at a given OSNR] with respect to the case where the carrier is not transmitted [Jan12]. Yet direct detection is well regarded when targeting low cost systems, as required for example in access and/or metro applications.

In contrast, coherent detection has higher complexity than direct detection [Fen09, Kam08]. The phase diversity coherent receiver requires a local oscillator, an hybrid 90° as well as balanced photo-detector in order to convert the signal into the electrical domain. The signal and LO are split into two paths. A phase difference of 90° is added to one LO path; then each part of the signal is combined with one part of LO (Figure 2-16).

The photocurrents [illegible] and [illegible] obtained at the output of the two photo-detectors constituting one balanced photo-detector, and [illegible] and [illegible] found at the output of the other two photo-detectors of the other balanced photo-detector are expressed by, respectively [Kam08]:

[illegible] **Eq. 2-39**

Thus the signals at the output of the balanced photo-detector are given by:

[illegible] **Eq. 2-40**

[illegible] **Eq. 2-41**

[illegible] and [illegible] are the in-phase and quadrature tributaries of the down-converted received OFDM signal and [illegible] is the received signal.

We note that the signal detected by a phase diversity coherent receiver needs to be precisely aligned with the Eigen axis of the coherent receiver, as the signal polarization evolves with time. This condition is no longer needed with phase and polarization diversity coherent receiver. Such a receiver consists in separating the two polarization components of a polarization multiplexed signal as well as the in-phase and quadrature tributaries of a signal, similarly to the phase diversity coherent receiver.

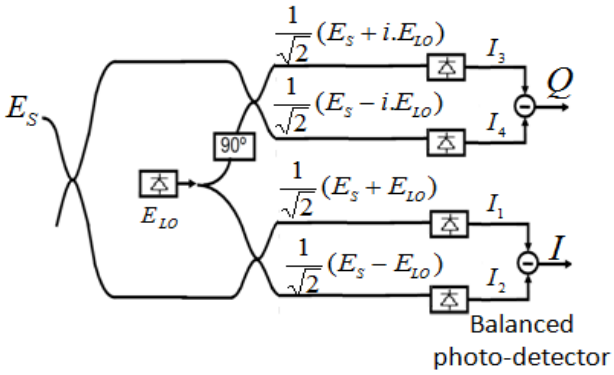

Figure 2-16: Phase diversity coherent receiver.

Coherent detection cancels the unwanted mixing in the signal bandwidth (Eq. 2-40, 41) and conserves all the information on the complex amplitude of the transmitted optical signal after detection. Also this detection type does not require sending the optical carrier with the signal, nor the presence of a guard band between the useful signal and the optical carrier. So CO-OFDM is more spectrally efficient than DD-OFDM and achieves better sensitivity [lower bit-error rate at a given OSNR]. All these advantages explain why coherent detection is the preferred choice for high-capacity long-haul optical transmission systems.

2.3.2.2 Typical OFDM transmitters structures

The transmitter architecture presented in the beginning of this section gives a general overview of the generation of an OFDM signal for all kinds of application. In practice however, up-conversion of the baseband electrical signal into the optical domain can be carried out in two different ways: either by using a simple Mach-Zehnder modulator (MZM), or a complex MZM (CMZM) made of two MZMs. Also, once the discrete-time I and Q tributaries are converted into analog signals via the DACs, signal up-conversion can be implemented through two different designs [Shi08]. This yields different possible designs for realizing a coherent optical OFDM modulator, each design having its pros and cons. We briefly review and comment on the two most common OFDM transmitter designs.
The first one is represented on Figure 2-17.a. The I an Q signals are electrically mixed, and the signal is first carried by an intermediate RF frequency. Then a MZM is used to convert the electrical OFDM signal at into the optical domain. The up-conversion generates an undesired image sideband which is finally removed by an optical band pass filter (OBPF).
The second transmitter, shown on Figure 2-17.b, was essentially motived by the commercial availability of advanced CMZM [Fuj07]. In this approach, the up-conversion is carried out by optically combining the I and Q signals through a CMZM. Thus the CMZM eliminates the need for an intermediate electrical stage as well as for the OBPF (no image sideband is produced here). For all these reasons, this is currently the preferred design for most coherent detectors.

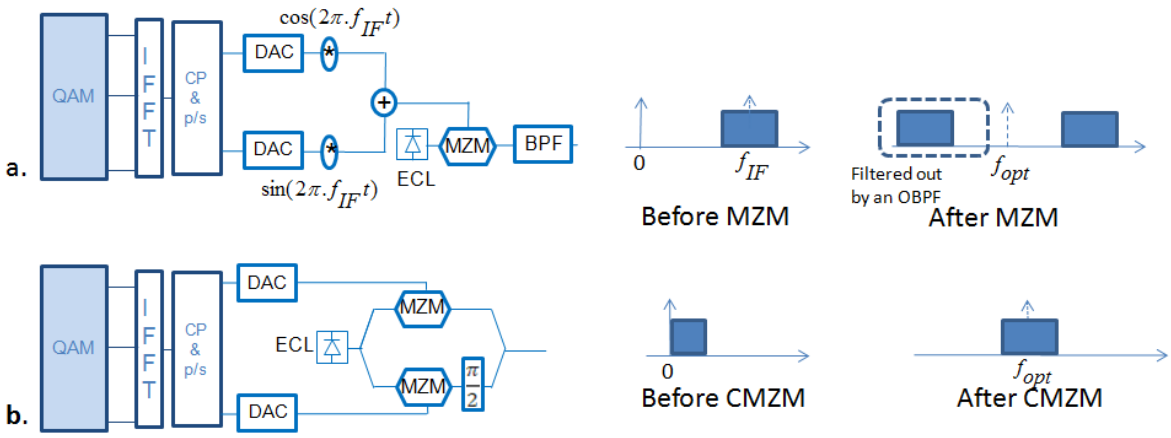

Figure 2-17: The basic transmitter design architectures based on the use of a MZM (first row) and CMZM (second row) and the corresponding OFDM spectra before and after optical up-conversion.

2.3.3 Multi-band optical OFDM approach

Long-haul transmission of high data rate is conditioned to the availability of high performance analog to digital (ADC) and digital to analog (DAC) convertors. The generation of one single-band 40Gbps/100Gbps OFDM requires one pair of DAC with considerably high bandwidths and sampling rates. Given the characteristics of commercially available DAC and ADC, the generation of high bit rate single-band OFDM signal is currently not feasible. Conversely, the multi-band OFDM (MB-OFDM) approach decreases considerably the pressure put on the bandwidth and sampling speed of DAC/ADC and is more suitable for long-haul transmission applications. The MB approach consists in splitting the global data rate into several OFDM sub-bands generated by several transmitters at different wavelengths. Each OFDM sub-band has then lower bandwidth and lower data rate. Afterwards, the sub-bands are combined together and transmitted. At the receiver each band is detected separately; a filter with bandwidth slightly larger than the bandwidth of each band can be used to select the desired band. Figure 2-18 shows a particular instance of MB-OFDM where the complete OFDM spectrum is divided into N orthogonal bands. The orthogonality condition between sub-bands implies that the guard band between two adjacent OFDM sub-bands must be a multiple of subcarrier spacing (□□). This scheme permits the multiplexing and de-multiplexing of OFDM bands without inter-band interference and permits one to achieve high spectral efficiency since the guard band can be a zero or very small. This concept is referred to as orthogonal-band-multiplexed OFDM (OBM-OFDM) [Shi10].

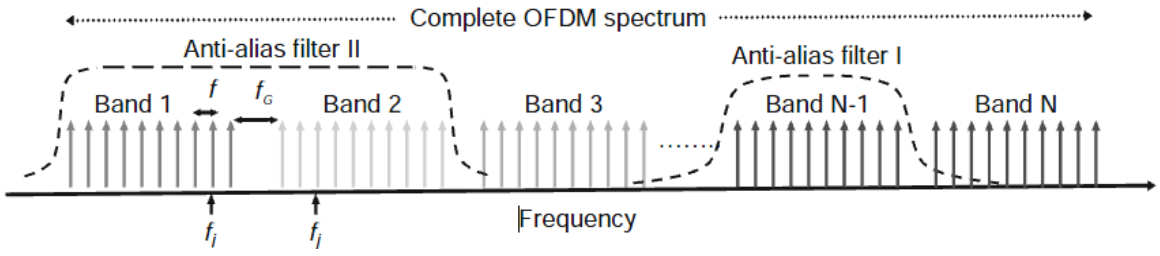

Figure 2-18: Concatenation of several orthogonal sub bands [Shi10].

Different methods can be used to generate several OFDM sub bands on distinct optical carriers, and without necessarily enforcing the orthogonality constraint. Basically the implementation technique requires a whole transmitter corresponding to the desired number of sub-bands and relies on the use of a comb generator that produces the optical tones. The tones are split to feed an optical modulator driving the two tributaries of the OFDM signal where the CMZM is used (Figure 2-19). A scheme permitting the generation of multiple tones or directly multiple OFDM bands on a recirculating frequency shifter loop detailed in [MaY10] deserves to be highlighted here. The generation of multiple tones necessitates having a continuous wave laser coupler, a CMZM tunable band pass filter and amplifiers. The dual arms of the CMZM are driven by the same RF tones except that they are phase shifted by 90°. Then the first produced tone is shifted with respect to the optical wavelength by a value equal to the RF frequency, while the second tone by twice the value of RF frequency and so forth. The number of tones is controlled by the bandwidth of the optical band pass filter in the loop. The existence of amplifiers inside the loop is required to compensate for the losses. Also the delay of the recirculating loop can be adjusted to an integer number of the OFDM symbol periods in order to generate orthogonal bands [MaY10] (right hand side of Figure 2-19).

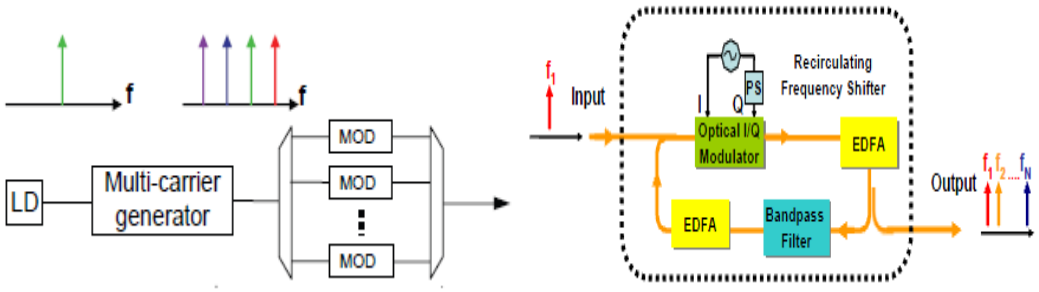

Figure 2-19: Comb generator (left fig) and recirculating frequency shift loop (right fig).

The comb generator is an attractive experimental solution that alleviates hardware constraints while increasing the total data rate.

2.3.4 Optical OFDM experiments: state of the art

Optical OFDM has gained substantial interest because of its high spectral efficiency and its intrinsic robustness against CD and PMD. The OFDM performance technique and all the developed algorithms have been evaluated in a number of research works with offline processing at the transmitter and at the receiver. But the fast progress in optical OFDM also has prompted real-time development. Experiments have been carried out to validate the developed techniques and algorithms with real-time transceivers.

Real-time OFDM consists in implementing the DSP at high speed using field programmable gate arrays (FPGA) or application specific integrated circuits (ASIC). The FPGA offers cost-effectiveness and flexibility for experimental work with respect to the ASIC. In any case, the processing speed of the processor is much smaller than the ADC sampling speed; thus payload needs to be de-multiplexed into multiple channels [Yan12]. Optical OFDM experiment records with "offline" and "real-time" implementation are summarized in the table below, which do not claim to be fully comprehensive.

Transmission of coherent offline OFDM over standard single mode fiber						
Author (year)	data rate (Gbps)	QAM order	sub-bands number	DP	Distance (km)	Amplification scheme
Jansen (2008) [JanM08]	20.2	4	2	No	4160	EDFA
Takahashi (2009) [Tak09]	404	16	8	Yes	640	Raman/EDFA
Takahashi (2009) [Tak09]	448	32	8	Yes	240	Raman/EDFA
Ma (2009) [MaY09]	1080	4	36	Yes	600	EDFA
Yang (2011) [Yan11]	1080	16	50	Yes	1040	EDFA
Qian (2012) [Qia12]	101700	128	370x4	Yes	165	Raman

Real-time OFDM							
Author (year)	data rate (Gbps)	QAM order	sub-bands number	DP	FFT size	Distance (km)	Tx/Rx
Yang (2009) [Yan09]	54	4	15	No	128	0	Rx (CO)
Benlachtar (2009) [Ben09]	8.36	4	1	No	128	1600	Tx
Giddings (2010) [Gid10]	11.25	64	1	No	32	25	Tx&Rx (DD)
Schmorgrow (2011) [Sch11]	84.4	16	1	No	128	400	Tx
Inan (2011) [Ina11]	23.9	4	1	No	1024	0	Tx
Buchali (2009) [Buc09]	109	4	9	No	256	400	Tx

Table 2-2: Optical OFDM experiment records with "offline" and "real-time" implementation.

2.3.5 All-optical OFDM solution

The excellent transmission performance of optical-OFDM is due in large part to the progress of high-speed digital signal processing. High-speed electronic processing, however, has the drawback of high power consumption, which increases with the processing speed [Kan11]. In addition even if the processing speed is improved, it will still be limited by the electronic DACs. Moreover the linearity of E/O conversion could also affect the quality of the OFDM signal [Hua09].

Thus, an attractive and alternative approach could be to perform the signal processing all-optically, preferably using passive devices. In particular, an all-optical DFT, which is the critical operation for channelizing orthogonally multiplexed subcarriers, can be implemented by combining two optical passive devices: the delay lines and the optical phase shifters, required to adjust the optical phases of the delay lines.

Figure 2-20 shows the transmitter and receiver diagram for generating an all optical OFDM, described in detail in [Ell08]. At the transmitter, a comb generator generates seven comb lines, spaced at precisely the symbol rate in order to satisfy the orthogonality condition. This comb is launched into the data encoding block, where each line was demultiplexed and independently encoded. Time delays and optical phase delays were optimized and then a

passive combination of the seven modulated sub-channels gave the total capacity. At the receiver, each individual sub-channel was then measured after optical demultiplexing, using an asymmetric Mach-Zehnder dis-interleaver, and band-pass filtering.

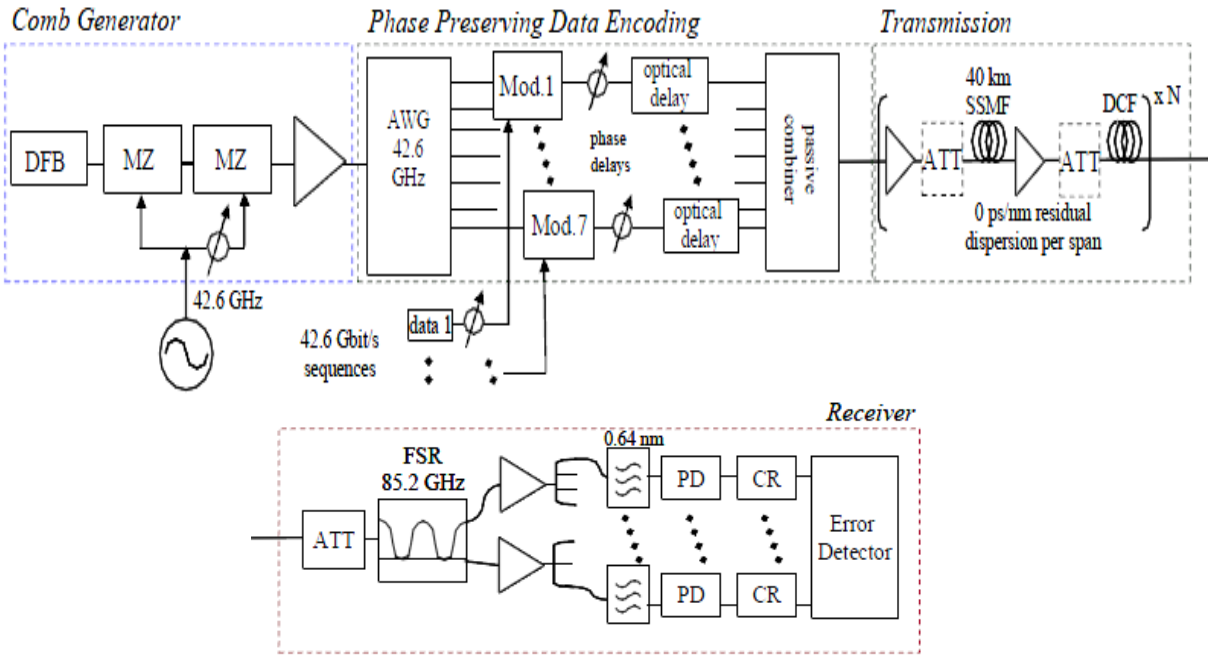

Figure 2-20: Typical diagram of an all optical-OFDM system [Ell08].

2.3.6 No guard interval coherent optical OFDM

Another related and worth-mentioning approach is no-guard interval CO-OFDM (NGI-CO-OFDM), illustrated in Figure 2-21. The subcarriers are optically generated from a unique laser source through a comb generator. The subcarrier spacing equals the symbol rate of data modulation so the multiplexed signal is orthogonal [San09]. NGI-CO-OFDM has the advantage of reducing overhead, compared to classical CO-OFDM, since the cyclic prefix is not generated. Besides, this scheme can re-use the conventional transmitter setup already deployed for single-carrier transmission [Shi10].

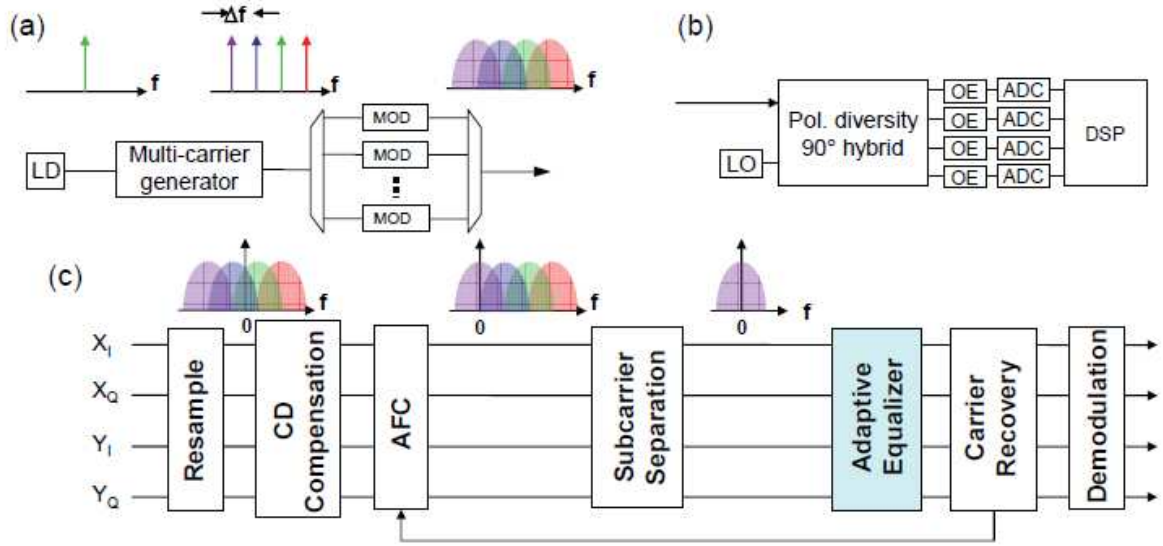

Figure 2-21: Tx and Rx design with the DSP for a no-guard interval CO-OFDM [San09].

The subcarriers generated by a comb generator are split to feed each, an optical modulator. Then the modulated subcarriers are combined and polarization multiplexed. On the receiver side, the signals are detected by a polarization diversity coherent receiver. The signals are converted back to the digital domain with a real-time oscilloscope (DPO). Then the "offline" DSP is performed separately for each signal.

2.4 Conclusion

Optical transmission suffers from several impairments especially in the context of high data rate long haul transmission. Chromatic dispersion (CD) and polarization mode dispersion (PMD) are two important linear factors limiting high data rate long haul transmission. However the use of advanced modulation formats such as orthogonal frequency division multiplexing (OFDM) overcome these two effects but do not remedy the detrimental impact of the nonlinear effects. The presence of nonlinear effects is due to the dependence of the fiber refractive index on the transmitted signal power. It is responsible for self phase modulation (SPM), cross-phase modulation (XPM), cross-polarization modulation (XPolM) and four-wave mixing (FWM).

Fiber impairments have not prevented the capacity to increase in wavelength division multiplexing transmission systems. For high bit rate long haul transmission the coherent multi-band OFDM was proposed to overcome the linear transmission impairments while enabling high bit rate. The need for a multi-band approach is prompted here by the limited sampling frequency and bandwidth of the DAC and ADC, which prevent the generation of high bit rate single-band OFDM signal. At the receiver side, we have seen that coherent detection is the most suitable technique long haul high date rate transmission scenarios, owing to its better sensitivity and high spectral efficiency.

Several types of OFDM systems have been investigated for optical fiber transmission. We can distinguish between the typical offline OFDM, all-optical OFDM and real-time OFDM. All the schemes try to increase the data rate more and more. In this thesis, we experimentally study offline OFDM. Our main objective is to assess the performance of the 100 Gbps coherent multi-band OFDM system in WDM transmission over 1000 km of G.652 fiber line. The corresponding OFDM format as well as the related digital signal processing algorithms are described in the next chapter.

Bibliography

[Agr89] G. P. Agrawal, *Nonlinear Fiber Optics*. AT&T Bell Laboratories, 1989.

[Agr97] G. P. Agrawal, *Fiber-Optic communication systems*, 2nd ed. John Wiley&Sons, INC., 1997.

[Ban00] D. M. Baney, P. Gallion, and R. S. Tucker, "Theory and measurement techniques for the noise figure of optical amplifiers," *Optical Fiber Technology*, 2000.

[Ben09] Y. Benlachtar, P. M. Watts, R. Bouziane, P. Milder, R. Koutsoyannis, J. C. Hoe, M. Puschel, M. Glick, and R. I. Killey, "21.4 GS/s real-time DSP-based optical OFDM signal generation and transmission over 1600 km of uncompensated fibre," in *ECOC*, 2009.

[Bor07] D. V. D. Borne, T. Duthel, C. R. S. Fludger, E. D. Schmidt, T. Wuth, C. Schulien, E. Gottwald, G. D. Khoe, and H. De Waardt, "Coherent equalization versus direct detection for 111 Gb/s ethernet transport," in *EEE/LEOS Summer Topical Meetings*, 2007.

[Buc09] F. Buchali, R. Dischler, A. Klekamp, M. Bernhard, and D. Efinge, "Realisation of a real-time 12.1 Gb/s optical OFDM transmitter and its application in a 109 Gb/s transmission system with coherent reception," in *ECOC*, 2009.

[Cha08] G. Chauvel, "Dispersion in optical fibers," *White paper*, no. Anritsu Corporation, 2008.

[Des91] E. Desurvire, "Modeling erbium-doped fiber amplifiers," *Journal of Lightwave Technology*, 1991.

[Ell08] A. D. Ellis, F.C.G.Gunning, B.Cuenot, T.C.Healy, and E.Pincemin, "Towards 1TbE using coherent WDM," in *Opto-Electronics and Communications Conference, 2008 and the 2008 Australian Conference on Optical Fibre Technology*, 2008.

[Ess10] R.-J. Essiambre, G. Kramer, P. Winzer, G. J. Foschini, and B. Goebel, "Capacity limits of optical fiber networks," *Journal of Lightwave Techonology*, vol. 28, 2010.

[Fal11] A. R. E. Falou, "Etude et analyse des dispositifs de compensations des distorsions dans les systèmes de transmission WDM longue portée à 10 et / ou 40 Gbit/s," 2011.

[Fen09] K.-M. Feng, R.-T. Shiu, Y.-W. Huang, and W.-R. Peng, "Sensitivity improvement using amplified optical self-coherent detection in an optical OFDM system," in *LEOS Annual Meeting Conference Proceedings*, 2009.

[Fra98] C. Francia, F. Bruyère, D. Penninckx, and M. Chbat, "PMD second-order effects on pulse propagation in single-mode optical fibers," *IEEE photonics technology letters*, vol. 10, no. 12, pp. 1739-1741, Dec. 1998.

[Fri03] Y. Frignac, "Contribution à l'ingénierie des systèmes de transmission terrestres sur fibre optique utilisant le multiplexage en longueur d'onde de canaux modulés au débit de 40 Gbps," ENST, 2003.

[Fuj07] Fujitsu. (2007) http://www.fujitsu.com/global/news/pr/archives/month/2007/20070327-02.html.

[Gid10] R. P. Giddings, X. Q. Jin, E. Hugues-Salas, E. Giacoumidis, and J. M. Tang, "Experimental demonstration of record high 11.25Gb/s real-time end-to-end optical OFDM transceivers for PONs," in *Future Network and Mobile Summit*,

2010.

[Gor10] S. Gorshe, "A Tutorial on ITU-T G.709 Optical Transport Networks (OTN)," *Optical Transport Networks Technology*, 2010.

[htt07] (2007) http://www.iet.ntnu.no/courses/tfe4165/laboppgaver/edfalab_exercise.pdf.

[Hua09] Y.-K. Huang, D. Qian, J. Yu, and T. Wang, "150 Gb/s PolMUX-8PSK all-optical OFDM using digital coherent detection with modified CMA algorithm," in *LEOS Annual Meeting Conference Proceedings*, 2009.

[Ina11] B. Inan, O. Karakaya, P. Kainzmaier, S. Adhikari, S. Calabro, V. Sleiffer, N. Hanik, and S. L. Jansen, "Realization of a 23.9 Gb/s real time optical-OFDM transmitter with a 1024 point IFFT," in *OFC*, 2011.

[Jan07] S. L. Jansen, I. Morita, N. Takeda, and H. Tanaka, "20-Gb/s OFDM transmission over 4,160-km SSMF enabled by RF-Pilot tone phase noise compensation," in *Optical Fiber Communication Conference and Exposition and The National Fiber Optic Engineers Conference*, 2007.

[Jan09] S. L. Jansen, I. Morita, T. Schenk, and H. Tanaka, "121.9-Gb/s PDM-OFDM transmission With 2-b/s/Hz spectral efficiency over 1000 km of SSMF," *Journal of lightwae technology*, vol. 27, 2009.

[Jan12] S. L. Jansen, "Multi-Carrier approaches for next-generation transmission: why, where and how?," in *OFC tutorial*, 2012.

[JanM08] S. L. Jansen, I. Morita, T. C. W. Schenk, N. Takeda, and H. Tanaka, "Coherent Optical 25.8-Gb/s OFDM Transmission Over 4160-km SSMF," *Journal of lightwave technology*, 2008.

[Kam08] I. P. Kaminow, T. Li, and A. E. Willner, *Optical Fiber Telecommunications V B*, chapter 3, Elsevier, Ed. 2008.

[Kam10] V. Kamalov, B. Koley, X. Zhao, and C. F. Lam, "Field verification of 40 G QPSK upgrade in a legacy 10 G networks," in *OFC*, 2010.

[Kan11] I. Kang, M. Rasras, X. Liu, S. Chandrasekhar, M. Cappuzzo, L. T. Gomez, Y. F. Chen, L. Buhl, S. Cabot, and J. Jaques, "All-optical OFDM transmission of 7 x 5-Gb/s data over 84-km standard single-mode fiber without dispersion compensation and time gating using a photonic-integrated optical DFT device," *Optics express*, 2011.

[Kik08] K. Kikuchi, "History of coherent optical communication and challenges for the future," in *IEEE/LEOS Summer Topical Meetings*, 2008.

[LiY06] Y. Li and G. L. Stüber, *Orthogonal frequency division multiplexing for wireless communications*. Springer, 2006.

[Low09] A. J. Lowery, "Amplified-spontaneous noise limit of optical OFDM lightwave systems," *Optics Express*, 2009.

[MaY09] Y. Ma, Q. Yang, Y. Tang, S. Chen, and W. Shieh, "1-Tb/s per Channel Coherent Optical OFDM Transmission with Subwavelength Bandwidth Access," in *OFC*, 2009.

[MaY10] Y. Ma, Q. Yang, Y. Tang, S. Chen, and W. Shieh, "1-Tb/s single-channel coherent optical OFDM transmission with orthogonal-band multiplexing and subwavelength bandwidth access," *Journal of Lightwave Technology*, 2010.

[Nee00] R. V. Nee and R. Prasad, *OFDM for wireless multimedia communications*. Artech house, 2000.

[Pin11] E. Pincemin, P. Gavignet, and Y. Loussouarn, "40/100 Gbps WDM transmission:

perspectives & evolutions," 2011.

[Pin12] E. Pincemin, J. Karaki, M. Selmi, D. Grot, T. Guillossou, C. Gosset, Y. Jaouën, and P. Ciblat, "100 Gbps DP-QPSK Performance over DCF-Free and Legacy System Infrastructure," in *IPC*, 2012.

[PinK11] E. Pincemin, J. Karaki, Y. Loussouarn, H. Poignant, C. Betoule, G. Thouenon, and R. L. Bidan, "Challenges of 40/100 Gbps and beyond deployments over long-haul transport networks," *Optical Fiber Technology*, 2011.

[Qia12] D. Qian, M.-F. Huang, E. Ip, Y.-K. Huang, Y. Shao, J. Hu, and T. Wang, "High capacity/spectral efficiency 101.7-Tb/s WDM transmission using PDM-128QAM-OFDM over 165-km SSMF within C- and L-bands," *Journal of Lightwave Technology*, 2012.

[Ram02] R. Ramaawami, "Optical fiber communication: from transmission to networking," *IEEE communications magazine*, pp. 138-147, 2002.

[San09] A. Sano, E. Yamada, H. Masuda, E. Yamazaki, T. Kobayashi, E. Yoshida, Y. Miyamoto, R. Kudo, K. Ishihara, and Y. Takatori, "No-guard-interval coherent optical OFDM for 100-Gb/s/ch long-haul WDM transmission," *Journal of Lightwave Technology*, 2009.

[Sca00] A. Scaglione, S. Barbarossa, and G. B. Giannakis, "Robust OFDM transmissions over frequency-selective channels with multiplicative time-selective effects," in *Acoustics, Speech, and Signal Processing*, 2000.

[Sch11] R. Schmogrow, D. Hillerkuss, P. A. Milder, R. J. Koutsoyannis, Y. Benlachtar, P. M. Watts, P. Bayvel, R. I. Killey, C. Koos, W. Freude, and J. Leuthold, "85.4 Gbit/s real-time OFDM signal generation with transmission over 400 km and preamble-less reception," in *OFC*, 2011.

[She04] P. Shen, N. J. Gomes, P. A. Davies, and W. P. Shillue. (2004) PMD effects on the analogue signal transmission.

[Shi07] W. Shieh, X. Yi, and Y. Tang, "Transmission experiment of multi-gigabit coherent optical OFDM systems," 2007.

[Shi08] W. Shieh, H. Bao, and T. Tang, "Coherent optical OFDM: theory and design," *Optics Express*, 2008.

[Shi10] W. Shieh and I. Djordjevic, *OFDM for optical communications*. Elsevier, 2010.

[ShiY07] W. Shieh, X. Yi, and Y. Tang, "Transmission experiment of multi-gigabit coherent optical OFDM systems over 1000 km SSMF fiber," *Electron. Lett.*, 2007.

[Spa06] P. Spalevic, M. Petrovic, S. Stanojcic, I. Petrovic, and B. Milosevic, "Statistical characteristics of the first and second order PMD of PAPER," *Electronics*, 2006.

[Sun08] H. Sun, K.-T. Wu, and K. Roberts, "Real-time measurements of a 40 Gb/s coherent system," *Optics Express*, 2008.

[Tak09] H. Takahashi, "Coherent OFDM transmission with high spectral efficiency," in *ECOC*, 2009.

[Ten06] S. Ten and M. Edwards, "An introduction to the fundamentals of PMD in fibers," *White paper*, no. Corning Incorporated, 2006.

[Win10] M. Winter, D. Kroushkov, and K. Petermann, "Cross-polarization modulation in polarization division multiplexed transmission systems," *Photonics Technology Letters*, 2010.

[Winz10] P. J. Winzer, "Challenges and evolution of optical transport networks," in *ECOC*,

2010.

[Winz12] P. J. Winzer, "High-Spectral-Efficiency Optical Modulation Formats," *Journal of Lightwave Technology*, 2012.

[Yan08] Q. Yang, W. Shieh, and Y. Ya, "Bit and power loading for coherent optical OFDM," in *IEEE Photonics Technology Letters*, 2008.

[Yan09] K. Yang, N. Kaneda, X. Liu, S. Chandrasekhar, W. Shieh, and Y. K. Chen, "Real-time coherent optical OFDM receiver at 2.5-GS/s for receiving a 54-Gb/s multi-band signal," in *OFC*, 2009.

[Yan11] Q. Yang, Z. He, W. Liu, Z. Yang, S. Yu, W. Shieh, and I. B. Djordjevic, "1-Tb/s large girth LDPC-coded coherent optical OFDM transmission over 1040-km standard single-mode fiber," in *OFC*, 2011.

[Yan12] Q. Yang, T. Zeng, X. Xiao, and W. Shieh, "Real-time optical OFDM experiments," in *Conference on Optical Internet*, 2012.

3 Dimensioning & signal processing architecture of the 100 Gbps OFDM format

Chapter 3

Dimensioning & signal processing architecture of the 100 Gbps OFDM format

The previous chapter has provided a generic overview on the generation of high bit rate OFDM signals for long-haul optical transmissions. The aim of this chapter is to describe the specification of a 100 Gbps OFDM signal allowing the transmission of 2 bits/s/Hz in a 50 GHz channel over 1000 km of G.652 fiber line. This chapter is organized as follows. In a first step, we describe the targets and constraints considered in this thesis, and discuss the design choices consequently adopted. Once the key parameters of the OFDM signal have been defined, the transmitter architecture is introduced. We finally discuss the important issue of the digital OFDM receiver design. In particular, the main transmission impairments are characterized, and appropriate signal processing algorithms are introduced in order to guarantee demodulation of the transmitted data with sufficiently low error probability.

3.1 OFDM parameters design

The main objective of this thesis is to transport a 100 Gbps OFDM channel within a 50 GHz ITU grid, enabling 2 bits/s/Hz spectral efficiency for the purpose of assessing its performance in WDM transmission over 1000 km of G.652 fiber line. CD and PMD which are the main impairments in such a link for 10 Gbps NRZ-OOK system, are overcome in the OFDM technique thanks to the combined use of a cyclic prefix (defined to be longer than the maximum channel dispersion) and per-tone equalization in the frequency-domain. Besides the cyclic prefix, several other key parameters of the OFDM transmission format like FFT size, total data rate and various overheads must be well-defined so as to achieve the target spectral efficiency of 2 bits/s/Hz while guaranteeing high system performance. However the implementation of an OFDM transmitter/receiver for high-bit-rate long-haul transmission is constrained by several hardware limitations. In this section, we first describe the specifications, targets and material constraints considered in this thesis, and discuss the design choices consequently adopted. The design methodology is then explained and afterwards applied to the transmission scenario of interest in order to obtain the parameters of the OFDM system that will be used for the rest of the thesis

3.1.1 Transmission targets, hardware constraints and design choices

The target of this work is to assess the performance of 100 Gbps optical OFDM transmission over 1000 km of G.652 fiber, in the presence of □□□□□□□□□□□□□□□□ of chromatic dispersion and □□□□□ of PMD. This requires the use of ADC and DAC with high performances. However, these two devices are, up to now, largely imperfect in terms of sampling frequency □□, bandwidth (□□□□□□□□□□□□□□□□ and vertical resolution, which represents the possible output voltage levels and is characterized by the effective number of bits□□□□□□□□. For the DAC, we considered □□ □ □□□□□□□□□□□□□□□□ □ □□□□□ and □□□□ □ □□□□□□ while for the ADC, the constraints on □□and □□□□ are more relaxed. In addition, up and down-conversion of the optical OFDM signal are achieved using lasers which introduce phase noise impairments all the more severe that the laser has a large line-width, encouraging the use of high-quality lasers with line-width of the order of 100 kHz or even below.

To deal with the transmission goals and material constraints presented above, or simply to reduce the implementation complexity of the system, several design choices have been made in this work. They are discussed below.

The first design choice results from the transmission target: as 100 Gbps has to be transmitted over 1000 km with high spectral efficiency, coherent detection is used since, as discussed in Chapter 2, it offers a higher noise margin and higher spectral efficiency than direct detection.

A second important design choice is the outcome of our decision to reduce the number of RF components at the transmitter side. As shown in Chapter 2, two different approaches can be used to perform up-conversion of the baseband digital signal into the optical domain. One is based on the use of MZM while the other uses CMZM. CMZM have been retained in this thesis, as this solution permits direct up-conversion of the OFDM signal into the optical domain without the need for an intermediate electrical stage. In addition and as seen in Chapter 2, it eliminates the need for an optical BPF.

Having presented the hardware design choices implied either by the transmission specifications or by our desire to reduce the implementation complexity, we now present additional design choices induced by hardware constraints.

To a first approximation, the nominal data rate □ can be related to the OFDM signal bandwidth □□ by (see e.g. [Jan09] and [Shi08]):

□ □ □□□□□□□□□□□□□□□□ **Eq. 3-1**

where □ is the size of the constellation and□□ □ □ for single polarization transmission, or □ □ □ for polarization multiplexed transmission. Based on this relation, Table 3-1 gives the minimum OFDM bandwidth required in single and dual polarization configuration (DP), to achieve the transmission target of 100 Gbps with QPSK (M=4) and 16-QAM (M=16) signal sets.

QPSK order	□□ for p=1	□□ for p=2
M=4	50 GHz	25 GHz
M=16	25 GHz	12.5 GHz

Table 3-1: Minimum OFDM bandwidth, B_d, required in single (p=1) and dual polarization (p=2) to achieve 100 Gbps with QPSK (M=4) and 16-QAM (M=16).

We note that the most favorable case, corresponding to 16-QAM with □ □ □, uses a minimum bandwidth of 12.5 GHz. This is not compatible with our hardware constraints since the DAC limitations implies that the total signal bandwidth must be less than the DAC maximum sampling frequency □□ □ □□□□□□. *This precludes a single-band approach*. Thus we have considered instead a multi-band (MB) OFDM system. In addition to relaxing the pressure on the DAC/ADC specifications (cf Chapter 2), MB-OFDM also offers interesting advantages in term of flexibility at the network level [Blo11]. In this work, the following MB setup has been retained: the 50 GHz WDM channel is divided into 4 sub-bands of width 8 GHz, each sub-band carrying 25 Gbps using coherent optical dual polarization OFDM (CO DP-OFDM) (or, equivalently, 12.5 Gbps per polarization). A guard interval of 2 GHz is used

to separate consecutives sub-bands. The proposed MB setup is illustrated in Figure 3-1. Note that a total bandwidth of 8 GHz (per sub-band) is now compatible with the DAC maximum sampling frequency.

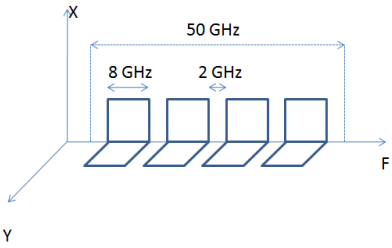

Figure 3-1: Proposed Multi-Band OFDM configuration for carrying 100 Gbps in a 50 GHz WDM channel (X and Y are the two polarization axis).

The last design choice follows from the imperfect rectangular shape of frequency response of the anti-aliasing low pass filter at the DAC output. According to the sampling theorem, an OFDM signal having a bandwidth of 4 GHz at baseband ideally requires a minimum sampling frequency of 8 GHz (first row of Figure 3-2). If this minimum sampling frequency is used, there is no guard band separating the original spectrum and its periodic replica, so that if the DAC LPF does not have an ideal rectangular shape, aliasing arises and creates signal distortion [Tra08]. It is thus preferable to sample the signal at a frequency higher than 8 GHz (second row of Figure 3-2). Here, we propose to operate the DAC at a sampling frequency of 12 GHz, which is the highest sampling frequency supported by our AWG, in order to guarantee an efficient separation of the useful signal from the aliasing products.

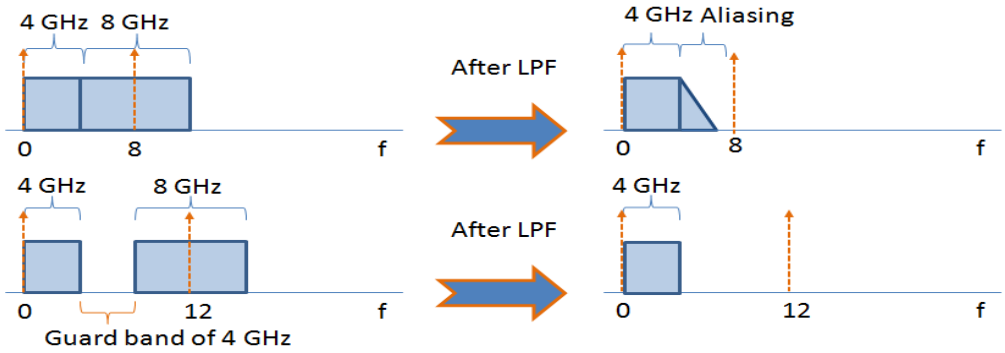

Figure 3-2: Spectrum of an OFDM band with a baseband bandwidth equal to 4 GHz sampled at 8 GHz (first row) and 12 GHz,(second row) shown before and after filtering through a 4 GHz filter.

In an OFDM signal, the guard band between the baseband signal and the aliasing products can be generated directly in the digital transmitter, before the IFFT operation, by setting to zero the highest subcarriers (□□). The remaining subcarriers denoted by □□□□□□□□□ will define the total useful bandwidth of the OFDM signal, □□. The input of the IFFT is represented is illustrated in Figure 3-3.

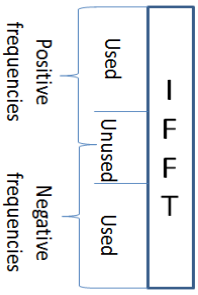

Figure 3-3: IFFT inputs as it is defined in Matlab; the unused subcarriers in the middle represent the highest and lowest frequencies set to zero for oversampling.

In the next subsection, we show how to design a DP-OFDM transmission format that can transmit 25 Gbps in a maximum of 8 GHz in each sub-band.

3.1.2 OFDM sub-band design methodology and results

The purpose of this subsection is to determine the key parameters of the OFDM format namely the FFT size, cyclic prefix, modulation order and various overheads. The parameters are chosen so as to meet the transmission targets and the design constraints, which consists in generating 4 polarization multiplexed OFDM sub-bands, each carrying a data rate of 25 Gbps within a total bandwidth no larger than 8 GHz. As explained in the previous Section, a sampling frequency of 12 GHz is used in the DAC.

The first step consists in determining the minimum cyclic prefix size $\square_{\square}$ (in number of samples) or duration $\square_{\square}$ (in seconds) required to avoid ISI between successive OFDM symbols. We must have $\square_{\square} \square \frac{\square_{\square}}{\square_{\square}} \square \square_{\square\,\square\square}$ with $\square_{\square\,\square\square} \square \square_{\square\,\square\square\square\square} \square \square_{\square\,\square\square\square\square\square}$ [JanM08], then

$$\square_{\square} \square \square\square\square \square_{\square} \square \frac{\square}{\square_{\square\square\square}\square} \square \square\square\square\square_{\square\,\square\square} \qquad \textbf{Eq. 3-2}$$

where $\square$ is the CD, $\square$ is fiber length, $\square_{\square}$ is the required OFDM bandwidth, $\square_{\square\square\square}$ the optical carrier frequency and $\square$ is the speed of light. The first term of this equation gives the delay spread caused by CD; while the second term $\square\square\square_{\square\,\square\square}$ is the maximum DGD related to a fiber. It is usually equal to 3.5 times the PMD [Ten06]. Then the cyclic prefix duration must be at least equal or greater than $\square_{\square}$.

For a target reach $\square \square \square\square\square\square\square\square\square$, dispersion parameter $\square \square \square\square\square^{\square\square}_{\square\square\square\square\square\square\square}$, $\square\square \square \square \square\square\square\square\square$, optical carrier $\square_{\square\square\square} \square \square\square\square\square\square\square\square$ and maximum OFDM bandwidth $\square_{\square} \square \square\square\square\square$, we obtain

$$\square_{\square} \square \square\square\square\square\square\square \qquad \textbf{Eq. 3-3}$$

or, equivalently, $\square_{\square} \square \square\square\square\square\square\square\square$. In the following, we choose $\square_{\square} \square \square\square\square\square\square\square\square$

Once the size of the cyclic prefix is chosen, the second step consists in determining the FFT size N_{FFT}. Here we require that the cyclic prefix overhead, given by $\alpha_{overhead} = \frac{N_{CP}}{N_{FFT}} = \frac{N_{CP}}{N_{FFT} + N_{CP}}$, is less than a prescribed maximum value $\alpha_{overhead,max}$. This yields:

$$N_{FFT} = \frac{N_{CP}}{\alpha_{overhead,max}} \qquad \text{Eq. 3-4}$$

For $\alpha_{overhead,max} = 1/16$ and $N_{CP} = 15$, we obtain $N_{FFT} = 240$. By rounding up this value to the nearest power of two, the FFT size N_{FFT} is then obtained, yielding $N_{FFT} = 256$ in this case, which corresponds to a cyclic prefix overhead $\alpha_{overhead} = \frac{16}{256} = 6.25\%$.

From the FFT size, we can now calculate the OFDM time duration T_u and the subcarrier spacing Δf and the total symbol duration T_s:

$$T_u = \frac{N_{FFT}}{f_s} = \frac{256}{32} = 8\ \text{ns} \qquad \text{Eq. 3-5}$$

$$\Delta f = \frac{1}{T_u} = 125\ \text{MHz} \qquad \text{Eq. 3-6}$$

$$T_s = \frac{N_{FFT} + N_{CP}}{f_s} = 9\ \text{ns} \qquad \text{Eq. 3-7}$$

Note that the cyclic prefix overhead may be further reduced by considering larger FFT sizes. On this other hand, increasing the number of subcarriers increases in turn the OFDM symbol duration (at fixed sampling rate) and thus the sensibility to phase noise.

At this level, it remains to determine the modulation order M and the various OFDM overheads so as to satisfy the target data rate and bandwidth constraints.

We assume that the OFDM transmission is organized into frames, each frame being formed of N_{TS} training symbols followed by N_{OFDM} OFDM symbols. Within the N_{FFT} subcarriers composing each OFDM symbol, we assume that only N_{used} subcarriers are used for transmission, the remaining $N_{FFT} - N_{used}$ being set to 0 so as to create a guard interval, as explained in Section 3.1.1. We further assume that among the N_{used} subcarriers, N_{pilot} pilot tones are dedicated to common phase error (CPE) estimation. Each data subcarrier carries $b = \frac{k}{n}$ information bits, where k denotes the message length and n is the codeword length at the FEC output. Finally, taking into account the extra overhead introduced by the Ethernet protocol, we assume that only a fraction $\frac{k'}{k}$ of the information bits really convey information. Then, considering all possible overheads in the transmission, the information rate carried out by one polarization can be expressed as:

$$R_{info} = \frac{N_{used}\left(1 - \frac{N_{pilot}}{N_{used}}\right) b \frac{k'}{k}}{T_s} \qquad \text{Eq. 3-8}$$

and the total used and unused subcarriers are determined by:

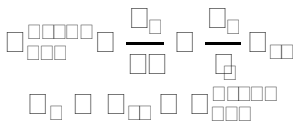

Eq. 3-9

The raw data rate of 12.5 Gbps in which no overheads is accounted, may be expressed as:

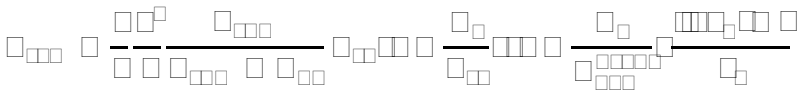

Eq. 3-10

or, equivalently

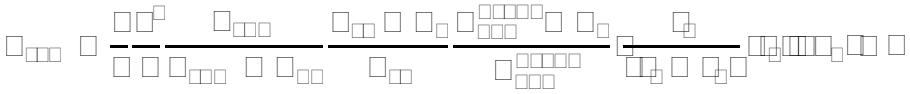

Eq. 3-11

yielding the following more compact expression:

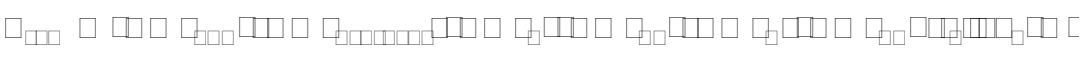

Eq. 3-12

where we have introduced the oversampling overhead 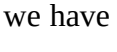 which, from Eq.-2.9, may be equivalently defined as 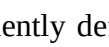 , the FEC overhead if we consider the (255, 239) RS code over GF(256) [Aza11], the cyclic prefix overhead  , the pilot tone overhead (for phase noise compensation) 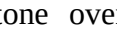 , the training symbol overhead (for channel estimation purpose) 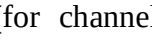 , and the Ethernet protocol overhead  .

We will see in Section 3.3 as well as in the next chapter that 5 training symbols provide a good trade-off between performance and overhead. In addition, the experimental results presented in the next chapter will validate the assumption that the optical channel can be considered as approximately time-invariant during at least 100 successive OFDM symbols. Thus the training symbol overhead has been set to: . We also propose here to use the full OFDM bandwidth 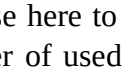 . Accordingly, from Eq. 3.9, the number of used subcarriers has to be set to 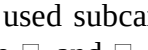 . Then our remaining degrees of freedom are  and . Under the previous assumptions, we now look for the smallest value of which guarantees a data rate at least as high as the target data rate, assuming that all non zero carriers convey information (no pilot tone). Then the remaining extra data rate, if any, is finally allocated to the pilot tones.

Here we consider QPSK transmission on each subcarrier (). This choice is compatible with the ADC ENOB constraint of 5 bits, and results in a data rate of 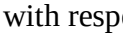 Gbps which is in excess with respect to our target of Gbps.

We conclude that QPSK is sufficient and propose to allocate the extra bandwidth to pilot tones, yielding □□ □ □ pilot tones. As we will see later in this chapter, 5 pilot subcarriers turn out to be sufficient to compensate for the common phase error caused by phase noise.

Table 3-2 below summarizes the main parameters of the proposed MB-OFDM format.

Data rate	100 Gbps
Number of sub-bands	4 sub-bands
Data rate with FEC overhead (7%) and protocol overhead (4%)	111.28 Gbps
Overall data rate	128 Gbps
Data-rate carried by each dual-polarization sub-band	32 Gbps
Modulation used	4-QAM
B_d	8 GHz
B_d in baseband	4 GHz
Sampling frequency f_S	12 GSa/s
Cumulated chromatic dispersion D.L	17000 ps/nm
N_g	18 samples
FFT size N_{sc}	256 points
effective subcarriers used	170 sub-carriers
N_0	85 sub-carriers
Pilot tones (□□)	5 sub-carriers
Symbol duration without cyclic prefix t_s	21.33 ns
N_{TS}	5 symbols
N_{sym}	100 symbols
Symbol duration with cyclic prefix T_S	22.83 ns
Subcarrier spacing Δf	46.9 MHz
Guard band between consecutive sub-bands	2 GHz
Channel spacing	50 GHz

Table 3-2: Main parameters of the proposed OFDM format.

3.2 Transmitter / receiver set up

Having defined the parameters of the OFDM signal, we will now describe the transmitter and receiver architecture in charge of generating and processing the coherent DP-OFDM signal within each sub-band. We also introduce the model of the transmitted signal.

3.2.1 25 Gbps Transmitter set up

Figure 3-4 shows the block diagram of a generic DP-OFDM transmitter system. It is basically constituted of two OFDM transmitters operating in parallel, each generating a baseband OFDM signal (one per polarization). The two electrical signals are then up-converted and mapped, into the optical domain, onto the two principal states of polarization of the laser source.

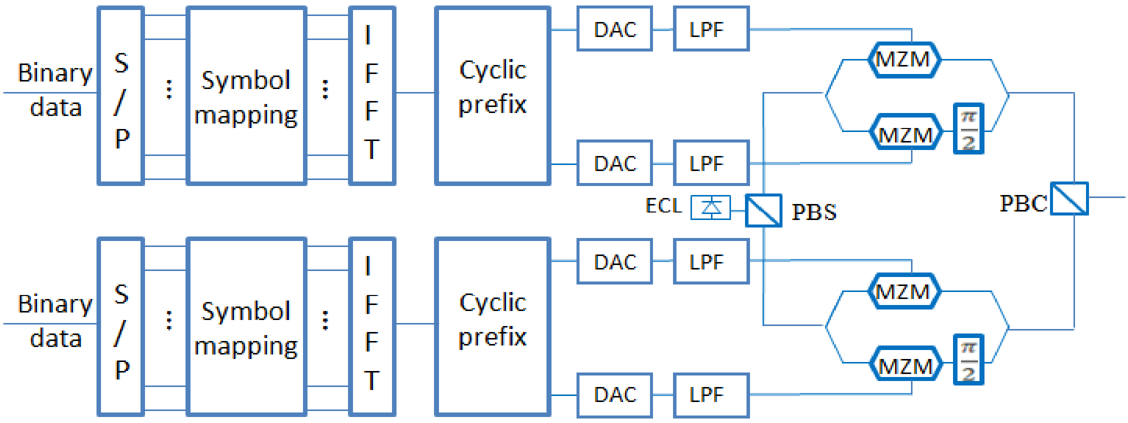

Figure 3-4: Transmitter set-up for the generation and processing of one OFDM sub-band.

Within each baseband electrical OFDM transmitter, the input digital data stream is split into sub-streams of [illegible] bits, where [illegible] is the size of the modulation alphabet. [illegible] consecutive sub-streams are mapped onto [illegible] complex information symbol [illegible] through a serial to parallel conversion followed by a symbol mapper. These [illegible] complex symbols define an OFDM symbol, and are simultaneously modulated onto [illegible] orthogonal subcarriers by applying an IFFT of size [illegible], thereby generating the time domain OFDM signal. A cyclic prefix formed by the copy of the last [illegible] samples of the block is finally appended at the beginning of each OFDM symbol to absorb channel dispersion, yielding the following expression for the [illegible] time-domain samples defining OFDM symbol [illegible] on polarization [illegible]:

$$[illegible] \qquad \text{Eq. 3-13}$$

Note that owing to the presence of the cyclic prefix, [illegible] for [illegible].

This discrete-time signal is split into real (I) and imaginary (Q) parts and sent to two DACs operating at a sampling frequency [illegible], where [illegible] is the useful OFDM symbol duration (cyclic prefix excluded). At the DAC output, the aliasing products are removed by an anti-aliasing filter. Assuming ideal DACs with pulse shaping function [illegible], the baseband analog signal can be conveniently expressed in vector form as:

$$[illegible] \qquad \text{Eq. 3-14}$$

where [illegible] is the duration of the cyclic prefix, [illegible] is the total duration of an OFDM symbol, [illegible], and

$$[illegible]$$

The baseband OFDM electrical signal at the output of each transmitter is directly up-converted into the optical domain by using an optical IQ modulator which is composed of a pair of Mach–Zehnder modulators (MZMs) with a 90 degree phase shift. Let [illegible] and [illegible]

denote the angular frequency and the instantaneous phase of the laser source, respectively. Then the two optical OFDM signals are multiplexed together onto the x and y PSPs of the laser through a polarization beam combiner, and the transmitted optical OFDM signal can be written as:

Eq. 3-15

3.2.2 Receiver set up

As discussed in Section 3.1, a dual-polarization receiver based on coherent heterodyne detection is considered here. The filtered signal and the local oscillator are split into orthogonal polarization components through two polarization beam splitters (PBS). For each polarization, a 90° hybrid mixes the incoming signal with the local oscillator (LO). The I and Q outputs of the two 90° hybrids are sent to four balanced photo-diodes and sampled by four ADCs for subsequent offline processing.

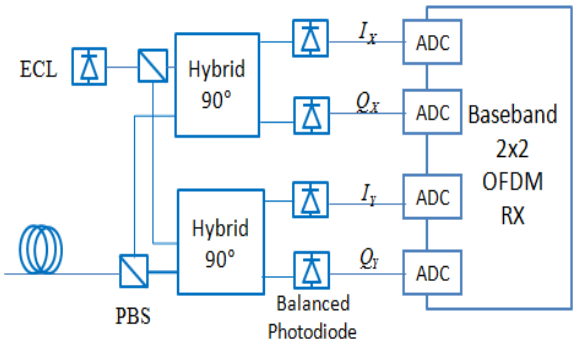

Figure 3-5: OFDM coherent receiver set-up.

The final 2x2 baseband OFDM receiver module has the crucial task of performing the OFDM demodulation and correcting directly into the electrical domain the various impairments encountered during the transmission, so as to recover as reliably as possible the transmitted data bits. The design of this fundamental block is the subject of the next section.

3.3 OFDM digital receiver design

During the transmission, the DP-OFDM signal faces a number of distortions which, if left uncompensated, can lead to severe performance degradations or even link failures. These distortions may originate from optoelectronic devices imperfections (eg laser phase noise at the transmitter and receiver LO), or from the propagation itself along the fiber. In particular, we have seen in Chapter 2 that in the linear regime, the optical fiber introduces chromatic dispersion as well as polarization mode dispersion which cause in turn intersymbol interference. Finally, the receiver also has to cope with several synchronization issues. In particular, since heterodyne detection is considered here, there exists a frequency and phase mismatch between the transmitter and receiver ECL. In addition, the propagation delay is also a priori unknown to the receiver. All these impairments need to be taken into account by the baseband OFDM receiver in order to achieve reliable communication. This is usually realized by cascading dedicated and often sophisticated signal processing functions.

In this Section, we first provide an overview and signal processing models for the prevalent impairments considered in this thesis, and introduce the general architecture of the OFDM digital receiver. Then we successively characterize each impairment and introduce appropriate algorithms to compensate for it.

3.3.1 Transmission impairments and signal processing model

The end to end signal processing model relating the discrete-time signals at the DACs inputs to the discrete-time signals at the ADCs output is presented in Figure 3-6 below.

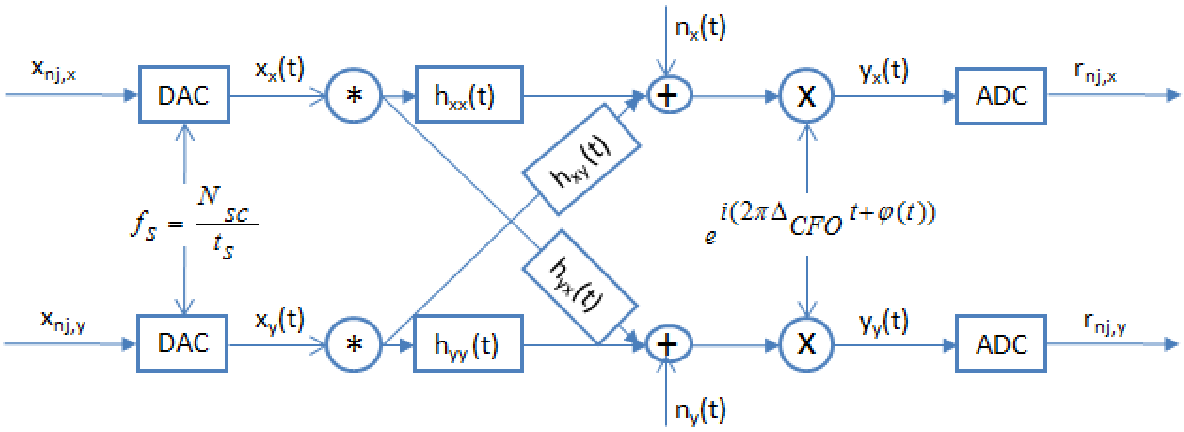

Figure 3-6: End-to-end signal processing model of the transmission link.

We assume here that the optical fiber can be modeled by a linear system whose 2x2 impulse response is denoted:

$$\underline{h}(t) = \begin{bmatrix} h_{xx}(t) & h_{xy}(t) \\ h_{yx}(t) & h_{yy}(t) \end{bmatrix} \qquad \text{Eq. 3-16}$$

In order to simplify the exposition, we first ignore the presence of phase noise. After down-conversion, the received signal, in the electrical domain, on the two polarizations can be written in vector form as [Mor07]:

[illegible] Eq. 3-17

Where [illegible] is the (unknown) propagation delay, [illegible] is the relative frequency offset between the transmitter and receiver ECLs, and [illegible] is a circularly symmetric complex gaussian vector modeling the ASE noise [Sin08]. Static phase offsets have been implicitly taken into account into the channel impulse response [illegible]. It is interesting to note here that the frequency offset impacts both polarizations in exactly the same way. We assume here that the channel impulse response can be considered time-invariant over several successive OFDM symbols.

The received electrical signal is finally sampled by the ADCs, at rate $f_s = \frac{1}{T_s}$, and the received sample in vector form at discrete time $t = k\frac{T_s}{N}$ is given by [Mor07]:

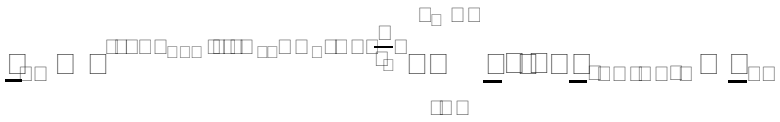

Eq. 3-18

for $k = 0, \ldots, N-1$
In the previous expression, $h_{pq}[\ell]$ for $p, q = 1, 2$ denotes the impulse response of the discrete time channel relating the transmit polarization p to the receive polarization q, while $n_{0,q}$ is the integer part of the timing offset.

For each received symbol m, the OFDM demodulator discards the cyclic prefix and passes the remaining N time-domain samples $r_{q,n}$, $n = 0, \ldots, N-1$ to a DFT unit. For properly designed OFDM systems, the cyclic prefix length N_g is bigger than the maximum channel impulse response span L, $N_g \geq L$, in order to avoid interference between successive symbols. Then, assuming perfect time ($n_{0,q} = 0$) and frequency $\Delta f_{q,p} = 0$ synchronization, the DFT output on subcarrier k for symbol m is the following 2x2 MIMO system:

Eq. 3-19

with $H_{pq}[k,m] = \sum_{\ell=0}^{L-1} h_{pq}[\ell,m] e^{-j2\pi k\ell/N}$ the channel frequency response and $n = 0, \ldots, N-1$.

Equivalently, the previous expression can be written in more compact form as:

Eq. 3-20

In the presence of phase noise, an additional phase noise term $\theta_{q,n}$ must be considered at the receiver input, which accounts for the phase noise introduced by the transmit as well as the receive lasers. In this case, the received electrical signal becomes:

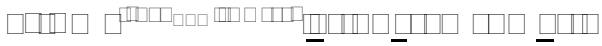

Eq. 3-21

and the ADC output now reads :

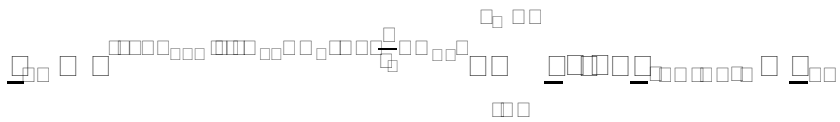

Eq. 3-22

with $k = 0, \ldots, N-1$

In order to properly retrieve the transmitted data, the OFDM baseband receiver has to go through several steps of digital signal processing. The first step consists in locating the OFDM frame starting point by estimating the time offset n_0 and properly aligning the DFT window with each OFDM symbol. Then the carrier frequency offset $\Delta f_{q,p}$ is estimated and corrected. Afterwards, the cyclic prefix is removed and an FFT is applied to convert the

signal back into the frequency domain. Channel estimation is then performed, followed by channel equalization which aims at separating the two polarization components and compensating for the channel gain/phase offset on each subcarrier. Finally, the residual phase error common to all subcarriers in each OFDM symbol is corrected, and the resulting symbols are demodulated to produce a decision on the transmitted bits. This yields the general signal processing architecture shown in Figure 3-7 for the OFDM baseband receiver.

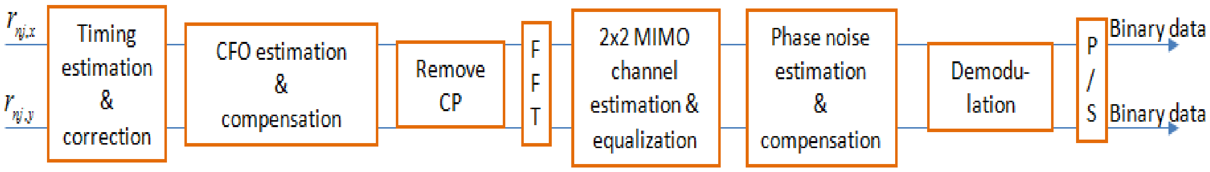

Figure 3-7: Signal processing architecture of the 2x2 baseband electrical OFDM receiver.

In the following we will describe in more details each of the prevalent impairments, and introduce dedicated DSP algorithms to cope with them.

3.3.2 Timing Synchronization

In this Section, we study the impact of the timing offset [illegible] on the performance of the OFDM demodulator. We show that timing synchronization is critical in the sense that an incorrect estimation of the start of the OFDM symbol may result in both intersymbol interference (ISI) and intercarrier interference (ICI), leading to severe performance degradation. Then we present and compare several timing synchronization algorithms proposed in the literature.

3.3.2.1 Impact of a timing offset

In order to simplify the discussion, perfect frequency synchronization as well as the absence of phase noise are assumed in the following. In the sole presence of an integer[1] timing offset [illegible], expressed in units of the sampling period [illegible], the received signal can be written as follows :

[illegible] **Eq. 3-23**

As depicted in Figure 3-8, four typical scenarios need to be considered here.

[1] A small fractional timing offset needs not to be considered here, since, as we shall see later, it causes a phase shift which may be considered as part of the channel action, and thus will be automatically corrected by the channel equalizer.

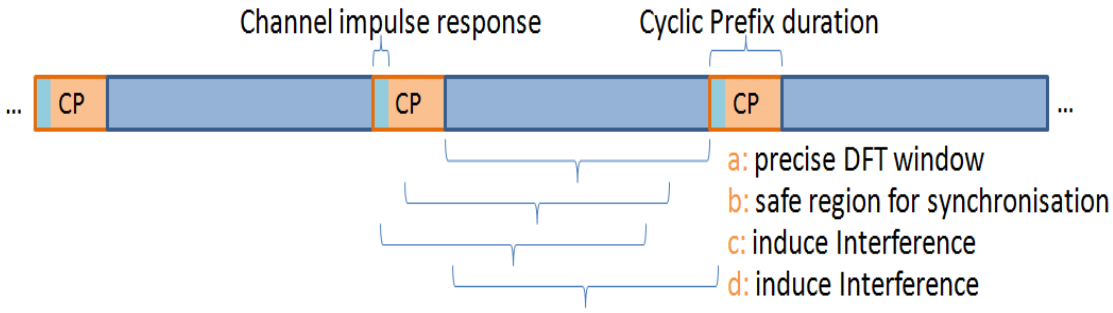

Figure 3-8: The 4 typical scenarios arising in OFDM timing synchronization. Cases a and b show two acceptable timing instants for synchronization. Cases c and d cause interference.

In the ideal case for which □ □ □(perfect synchronization, Case a in Figure 3-8), the signal is recovered without any interference and the DFT output is given by:

□□□ □ □□ □□□□ □ □□□ **Eq. 3-24**

In the second scenario (Case b in Figure 3-8), the DFT window starts within the safe region of the cyclic prefix which is not affected by samples from the previous OFDM symbol. This corresponds to the case □ □ □□□□ □ □□ □ □□□□□ □□ □□□□. The DFT output then reads [Min03]:

□□□ □ □□ □□□□□ □□□ **Eq. 3-25**

In this case, the timing offset generates a phase shift increasing linearly with the offset □and the subcarrier index□□. This impairment needs not to be taken into account since it will be automatically corrected by the channel equalizer (the linear phase shift may be absorbed into the definition of the channel transfer function). Note also that scenario a is a particular case of scenario b. In both scenarios, the orthogonality between subcarriers is maintained and the transformed signal is free of interference. This scenario is illustrated in Figure 3-9 which depicts the received constellations before (left figure) and after (right figure) channel equalization. 4-QAM modulation and an ideal, noise-free channel were considered. The left figure shows in particular the linear phase shift arising when the FFT window starts within the cyclic prefix. After simple channel equalization, the rotation is corrected and the symbols are ISI free.

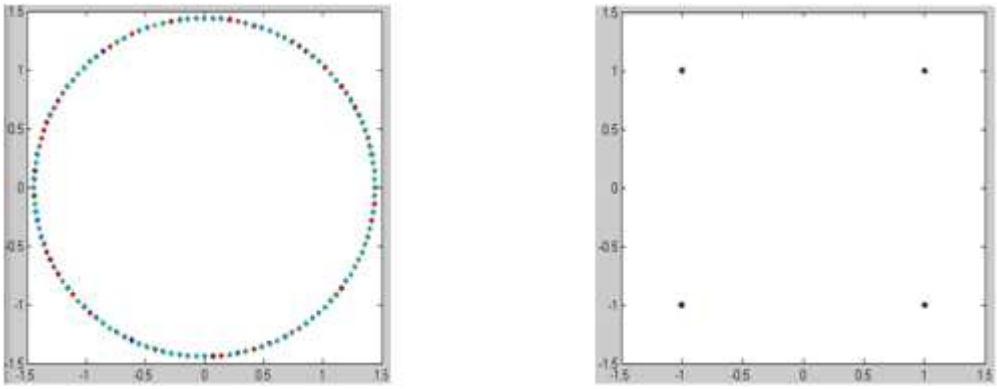

Figure 3-9: Receive constellations before (left fig) and after (right fig) channel equalization, when the FFT window starts within the ISI-free region inside the cyclic prefix (scenario b). 4QAM was used for transmission.

Consider finally scenarios c or d in which the DFT window starts either in the part of the cyclic prefix affected by the channel, or outside the cyclic prefix. In both cases, the DFT window contains not only part of the OFDM symbol of interest, but is also affected by samples from the previous or the next OFDM symbol, thereby causing interference. In such situations, the DFT output can be written as [Min03]:

Eq. 3-26

In addition to the linear phase shift, the symbol of interest on subcarrier is attenuated by a coefficient which is a function of . The term accounts for both ICI and ISI. Such a scenario is illustrated in Figure 3-10, where the synchronization begins at , one sample outside the cyclic prefix (again, 4-QAM transmission over an ideal noise free channel was considered). As shown on the left hand side of this figure, the phase rotation proportional to the subcarrier index still exists. We also note the presence of interference which broadens the constellation points. As can be seen on the right figure, channel equalization cannot compensate for the interference. The broadening of the constellation points is all the more important that the time offset extends far from the correct location.

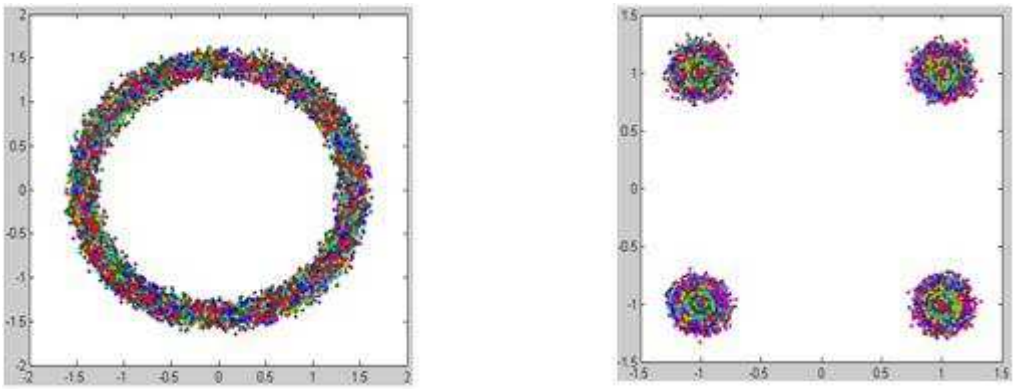

Figure 3-10: Receive constellations before (left fig) and after (right fig) channel equalization when the DFT windows starts one sample outside the cyclic prefix (scenarios c or d).

As shown in Figure 3-11, the transmitted data can never been recovered correctly in the presence of very large timing offsets.

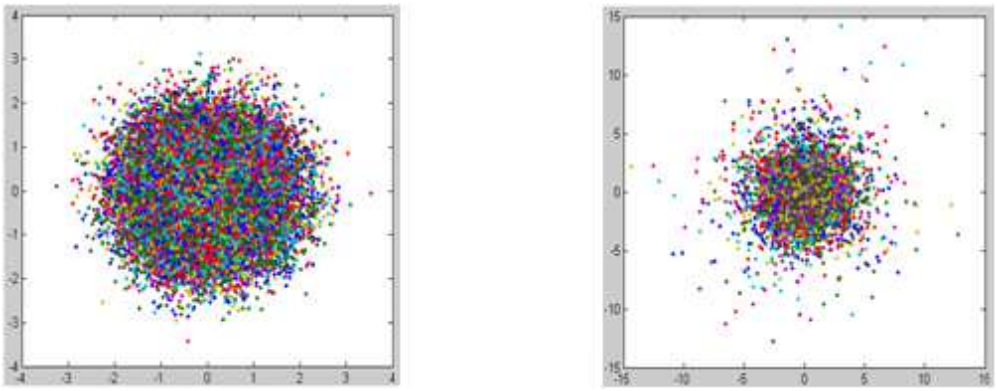

Figure 3-11: Receive constellations before (left fig) and after (right fig) channel equalization in the presence of a very large timing offset.

3.3.2.2 Timing synchronization algorithms

The purpose of timing offset estimation is to locate accurately the start of OFDM symbols within the received signal, in order to avoid ISI and ICI. We have shown in the previous section that this task is mandatory for correct demodulation of the received signal.

Many timing synchronization algorithms have been proposed in the literature. In this work, we will focus on a particular family of timing algorithms based on OFDM training symbols formed by the □-fold repetition of a pre-determined basic pattern B of length $\frac{□□}{□}$, possibly with alternation of signs. The general structure of the training symbol, denoted later by TS1, is shown in Figure 3-12.

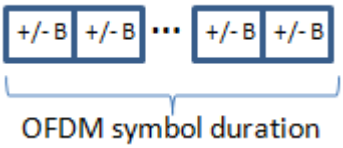

Figure 3-12: Generic structure of the training symbol in the time-domain.

Accordingly, the received signal is correlated with itself (auto-correlation) over sliding windows of length $\frac{□□}{□}$ in order to find the repeated patterns and thus to locate the start of the training symbol TS1. This is done by maximizing a metric of the form:

□ □□□□ □ □□□ $\frac{□□ □□□□}{□□□□}$ □ **Eq. 3-27**

where □ is an appropriate autocorrelation metric, □ is an energy normalization metric, and *p* ranges over the admissible time indices. We now present several classical algorithms which belong to this general family.

The first estimator of this form was proposed by Schmidl and Cox [Sch97]. It is based on a training symbol whose two halves are identical in the time domain. Hence □□ □ and TS1 has the structure [+B +B]. The timing metric is known to exhibit a plateau due to the presence of the cyclic prefix, which introduces uncertainty in the estimation and does not guarantee that the DFT starts within the safe region [Ren05]. For this reason this estimator has not been further considered in this work.

Latter, a more robust timing algorithm was proposed by Minn and Barghava [Min03]. Their method extends the Schmidl and Cox original approach by allowing more than 2 repetitions of the basic pattern, and introducing sign inversion between certain repetitions. These two modifications were shown to improve timing offset estimation by ruling out the plateau problem and yielding timing metrics with steeper roll-off. In [Min03], Minn and Barghava focused on the cases □□ 4, 8 and 16, and found that the best performance were obtained with training symbols of the form [+B +B +B–B], [+B +B –B –B +B –B –B –B], and [+B –B –B +B +B +B –B –B +B –B +B +B –B +B –B –B], respectively.

In [Kai04], Shi and Serpedin refined the results obtained by Minn & Barghava. Considering the particular case □□ □, they obtained a more advanced timing metric derived from the maximum likelihood criterion. They also showed that for L=4, the training symbol structure [+B +B –B +B] (the –B can be located anywhere) leads to the lowest false detection and the highest correct acquisition probability.

Table 3-3 summarizes in a unified manner the similarities and differences between the three abovementioned algorithms. The following notation is used in the table:

□ □□□□ □□ □ □□ □□□□□□□□□□ □ □□□ □ □□□ □□ □ □□

Eq. 3-28

	Schmidl and Cox	Minn and Barghava	Shi and Serpedin
TS1	[+B +B]	[+B +B +B–B]	[+B +B –B +B]
Timing metric (□ is a time index)	□ □□□ □ □ □□□	□ □□□ □ □□	□ □□□ □ □□□
Sum of the pairs of products	□□□□ □	□□□ □ □	□□□ □ □ □ □
Received energy	□□□ □ □	□ □ □	□ □

Table 3-3: Timing metric of three different estimators: Schmidl and Cox, Minn and Barghava and Shi and Serpedin (only the case L=4 is considered for the last two algorithms).

In this work, we have investigated by simulation the performance of the Minn and Barghava and Shi & Serpedin algorithms. Figure 3-13 compares the timing metric of these two estimators for a training symbol made of □□ □ repetitions. None of them exhibits a plateau. However we notice that both estimators present high sidelobe peaks, which are more

important in the case of the Minn & Bhargava estimator than in the Shi & Serpedin one. We conclude that, for a given number of repetitions □(eg *L*=4), the Shi & Serpedin estimator is more reliable than the estimator of Minn & Bhargava. This was to be expected since Shi & Serpedin consider all possible combinations of patterns auto-correlations in the derivation of its timing metric. The metric of Minn & Bhargava is essentially a simplified version of the Shi & Serpedin metric.

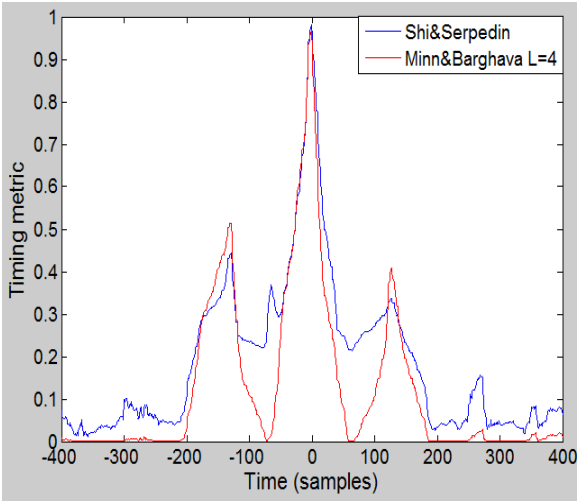

Figure 3-13: Comparison of the Shi & Serpedin and Minn & Barghava timing metrics for a training symbol made of L=4 repetitions.

Figure 3-14 shows the timing metric for the Minn & Barghava algorithm in the case of a training symbol made of □□ □ repetitions. We observe that the metric trajectory has a steeper roll-off with much lower side-lobe peaks than in the □□ □ case. Unfortunately the optimal TS1 structure for the □□ □ case under the maximum likelihood criterion was not given explicitly by Shi & Serpedin, precluding a comparison in similar conditions here.

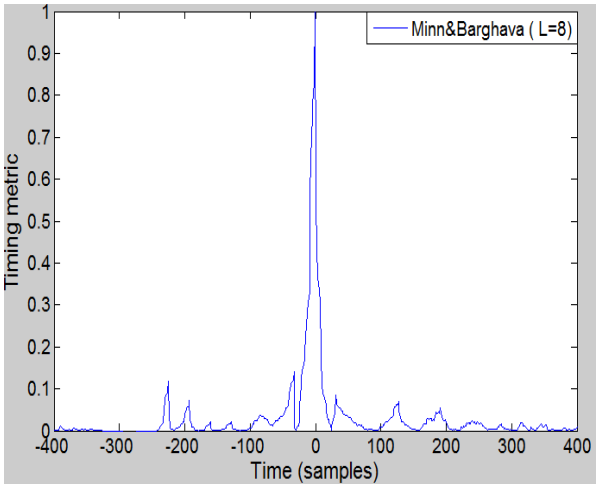

Figure 3-14: Minn & Barghava timing metric for a training symbol made of L=8 repetitions.

We finally compare by simulation the performance of the Shi & Serpedin algorithm with □□ □ to the performance of the Minn & Barghava estimator with □□ □, after 1000 km of transmission over G.652 SSMF fiber (only chromatic dispersion has been considered). The bit error rate (BER) has been evaluated as a function of optical signal-to-noise-ratio (OSNR)

in a resolution of 0.1 nm for a single-band OFDM signal. The sensitivity curve of the two different synchronization methods are represented in Figure 3-15 and compared to the theoretical performance of QPSK under ISI free transmission. We conclude that although the Minn & Barghava metric is not theoretically optimal, a TS made of [illegible] repetitions provides better performance and increased robustness than a TS made of [illegible] repetitions but with an optimal metric. Note that this comparison is fair in the sense that both approaches approximately have the same complexity (both involve 6 or 7 autocorrelations, although not of the same size).

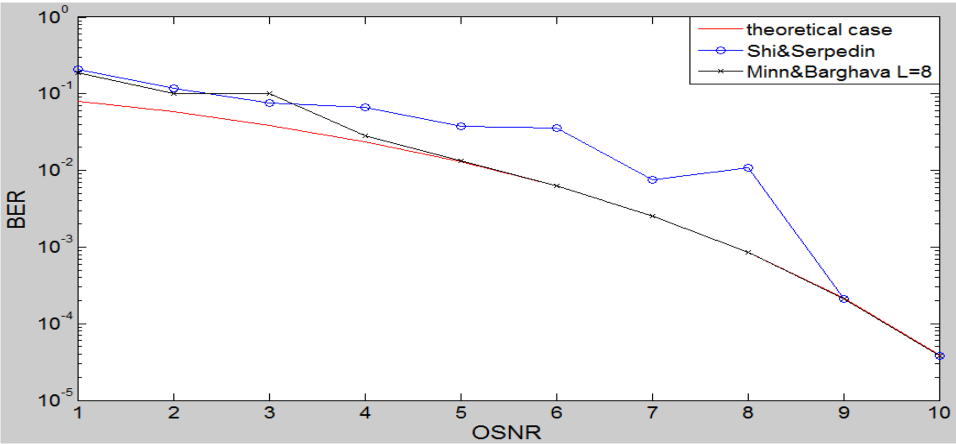

Figure 3-15: BER vs OSNR for the two synchronization methods.

3.3.3 Frequency synchronization

Once the correct timing is acquired, the next step consists in compensating for the relative carrier frequency offset [illegible] between the transmit and receive lasers. We first characterize the impact of the CFO on the system performance, and show that it is mandatory to correct, at least partially, the CFO before applying the FFT. Then we discuss CFO estimation and compensation. In particular, an original algorithm is introduced and validated for the estimation of the integer part of the CFO.

3.3.3.1 Impact of CFO

For the sake of clarity, we ignore the presence of the noise in the following exposition. The received signal, solely affected by a frequency offset [illegible], can be expressed in the time domain as follows:

[illegible] **Eq. 3-29**

where [illegible] is the normalized carrier frequency offset with respect to subcarrier spacing [illegible].

At the DFT output, we obtain:

Eq. 3-30

Here, φ_0 is a phase offset common to all subcarriers in symbol l. As we shall see later in section 3.3.5, such a constant phase shift will be automatically corrected by the common phase error (CPE) correction that follows channel equalization.

Two cases can be distinguished here. We first consider the particular situation that arises when ε has integer value, or, equivalently, when Δf_{offset} is an exact integer multiple of the subcarrier spacing Δf. In such a case, the signal at the DFT output simplifies into:

Eq. 3-31

where $((k-\varepsilon))_N$ denotes the value of $k-\varepsilon$ reduced to the interval $[0, N-1]$. We observe that orthogonality is maintained, but the frequency multiplex appears shifted at the DFT output, in such a way that the information detected on the k^{th} subcarrier corresponds to the information transmitted on the $((k-\varepsilon))_N^{th}$ subcarrier. This situation is illustrated in Figure 3-16 below, where we show the constellation obtained at the DFT output in the presence of normalized CFO $\varepsilon = 1$, for several successive OFDM symbols. A 4-QAM constellation was used at the transmitter. No ICI is observed on the left figure, but we note the impact of rotation $e^{j\varphi_l}$ which is a function of l and $\frac{\varepsilon}{N}$, and which increases linearly with the symbol index l. The right figure presents the constellation obtained after correction of the phase shift φ_0 by the CPE. An ideal 4-QAM constellation is retrieved.

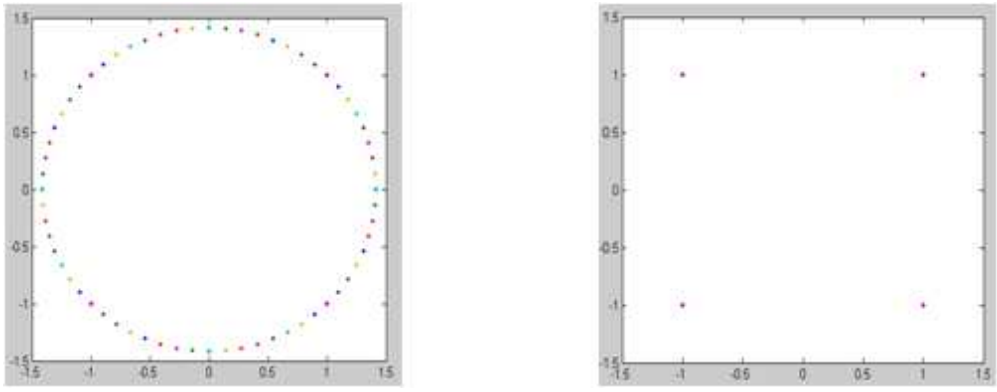

Figure 3-16: Constellation at the DFT output in the presence of a normalized CFO $\epsilon = 1$ (left fig: before CPE/ right fig: after CPE). A 4-QAM constellation is used at the transmitter.

In the more general case of a real-valued normalized CFO ε, the received OFDM symbol at the DFT output can be expressed as:

Eq. 3-32

Apart from the phase shift already discussed above, we see that the CFO results in a complex attenuation common to all the subcarriers and OFDM symbols, and in ICI. The first term will be automatically compensated for by the channel equalizer, while the latter will results in an irreducible performance loss.

In order to illustrate how fast ICI evolves as a function of , we show in Figure 3-17 and Figure 3-18 the constellations obtained at the DFT output for normalized CFO values and , respectively. In both cases, 4-QAM modulation was used at the transmitter. For , the 4-QAM constellation cannot be distinguished even after CPE correction.

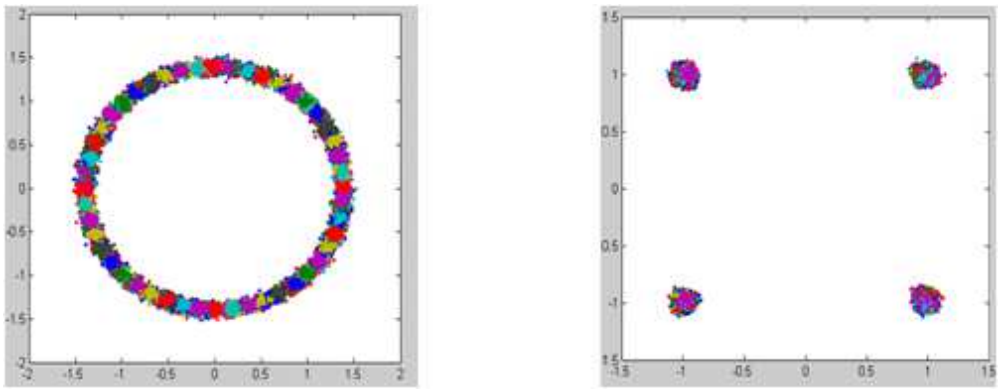

Figure 3-17: Constellation at the DFT output in the presence of a normalized CFO ε = 0.02 (left fig: before CPE/ right fig: after CPE). A 4-QAM constellation is used at the transmitter.

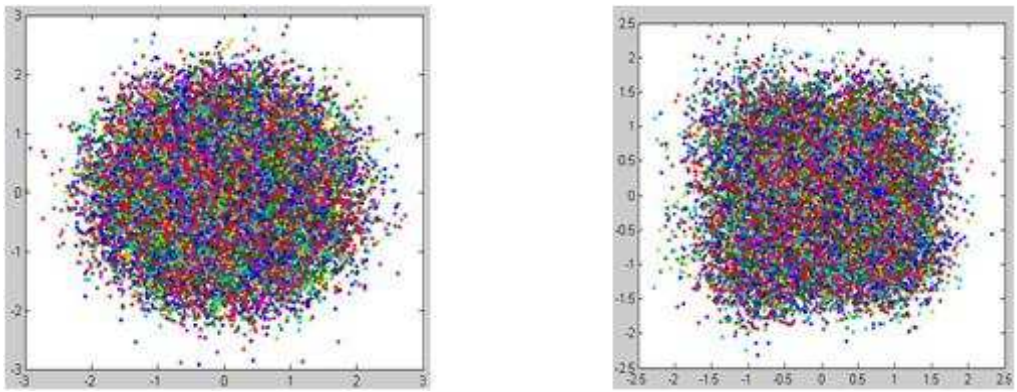

Figure 3-18: Constellation at the DFT output in the presence of a normalized CFO ε = 0.32 (left fig: before CPE/ right fig: after CPE). A 4-QAM constellation is used at the transmitter.

Finally in order to assess more precisely the impact of the CFO on the system performance, we show in Figure 3-19 (reproduced from [Shi10]) the evolution of the SNR penalty as a function of , for a QPSK modulated OFDM system with subcarriers and at a target bit error rate of 10^{-3}. We observe that results in a 2 dB penalty, while as much as 8 dB penalty is obtained for . We conclude that the residual CFO should be kept

below 0.07 in order to maintain the penalty below 1 dB. Note that, in the presence of a CFO, BER performance curves typically exhibit a flattening at high SNRs, so that much higher penalties may be measured at BER below10^{-3}.

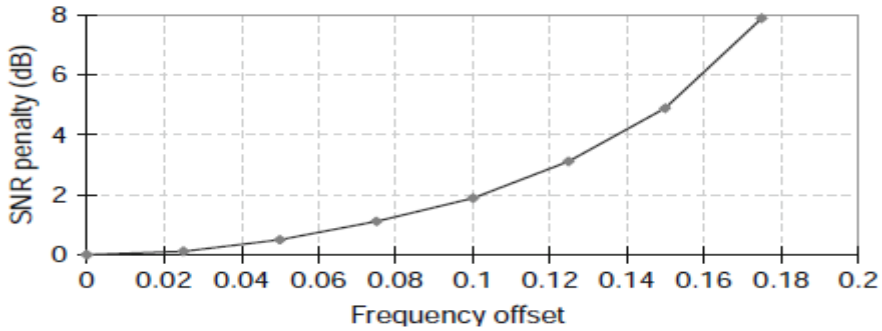

Figure 3-19: SNR penalty as a function of the frequency offset for 256-subcarrier QPSK modulated OFDM systems [Shi10].

3.3.3.2 CFO estimation and correction

We have shown that an accurate CFO estimation is mandatory in order to guarantee correct performance. One problem is that the CFO encountered in practice is quite large. Another problem is that the CFO evolves with time, due to the wavelength instabilities of the ECL used at the transmitter and receiver. Since, as we shall see later, frequency estimation algorithms usually have limited estimation range, the usual approach is to decompose the CFO into a fractional part and an integer part [LiY06]:

Eq. 3-33

Estimation and correction of is then performed in two steps:

1. Estimation of the fractional part in time domain (before the DFT unit) and correction of the fractional CFO
2. Estimation of the integer part in the frequency domain, and correction of the integer CFO

We now describe specific algorithms for realizing each of those two steps.

3.3.3.2.1 Estimation of the fractional part of the CFO

There exist many methods for estimating a frequency offset in the literature. The algorithms consider in this work exploit the repetitive structure introduced in the training symbol used for timing acquisition.

Consider, for the ease of exposition, a transmission over an ideal ISI free noiseless channel. By construction of the TS1, we know that:

Eq. 3-34

where denotes the number of repetitions of the basic pattern within TS1.

From Eq. 3-34 and since we have assumed, for simplicity, that □□ □ □(ISI free channel), the received samples corresponding to TS1 satisfy [LiY06]:

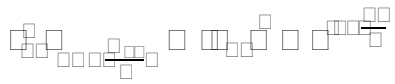

Eq. 3-35

An estimate of the normalized CFO □□is then given by:

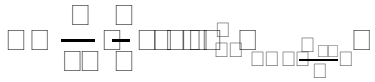

Eq. 3-36

In order to improve the accuracy of the previous estimate in the presence of noise, the estimation can be averaged over the $\frac{\square\square}{\square}$ samples constituting the basic pattern of the training symbol, yielding:

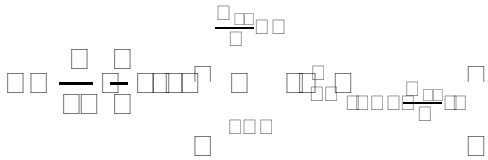

Eq. 3-37

Since □□□ □□□□□□□□ □, the acquisition range is limited to □ $\frac{\square}{\square\square}$ □ □□ $\frac{\square}{\square\square}$

We can conclude that the estimation range of □can be improved by:

1. Considering a training symbol composed of a higher number □ of repetition of the basic pattern
2. Considering only correlations between consecutive sub-symbols (*ie* focusing on d=1)

Let us specialize the previous result to the particular case of the Minn & Barghava and Shi & Serpedin timing synchronization algorithms discussed earlier. For the Minn & Barghava algorithm with □□ □, TS1 has the structure [+B +B +B -B]. Hence

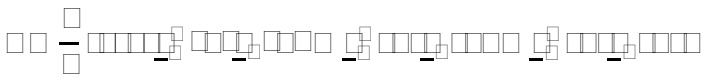

Eq. 3-38

where vectors □□□□are defined as in Eq. 3.28, and where □denotes here the start of the training symbol in the received sequence, as estimated by the timing synchronization algorithm.

Similarly, for Shi & Serpedin timing algorithm, TS1 has the structure [+B +B -B +B] and

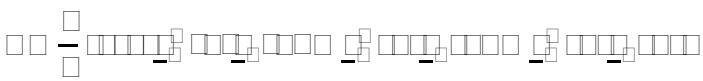

Eq. 3-39

In both cases, □□ □ and the estimation covers the range □□□ □□ □□. Thus we may decompose □as :

□□ □□ □with □□□ □ □□ □□and □□ □□with □ an integer.

The previous algorithm will then estimate the fractional part□, and thus compensate for it in the time domain as follows:

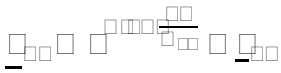

Eq. 3-40

By doing so; the corrected symbol presented at the DFT input is now solely affected by a residual integer CFO . We now consider the problem of estimating .

3.3.3.2.2 Estimation of the integer part of the CFO

Upon correction of the fractional CFO , and capitalizing on the results established in section 3.3.3.2 the signal at the DFT output reads:

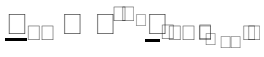

Eq. 3-41

Thus estimating is tantamount to estimate the integer shift affecting the modulated subcarriers at the DFT output.

We propose here a simple method to estimate this frequency shift. Our method exploits the presence of null subcarriers on both sides of the spectrum, and attempts to locate the edges of the signal spectrum at the DFT output. It operates in two steps, as follows:

1. Average the received signal power on each subcarrier over successive OFDM symbols:

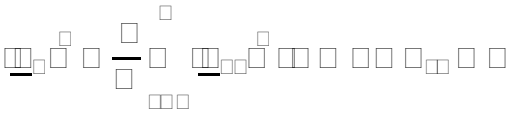

Eq. 3-42

2. Cross-correlate this average power spectrum with an appropriate frequency mask in order to detect the edges of the signal spectrum, and deduce the corresponding frequency shift from the location of the edges.

Step 2 performs a maximization of the form (search for a correlation peak):

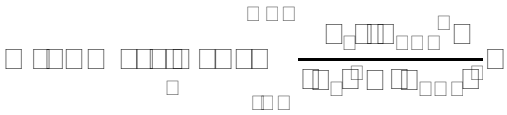

Eq. 3-43

where is the considered frequency mask, of length . Since we aim at locating the spectrum edges, the following simple mask of length has been retained in our experiments:

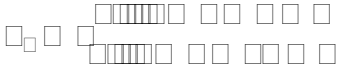

Eq. 3-44

where is an integer less than half the number of null subcarriers ().

Once the edge location has been obtained, the integer part of the CFO is finally given by:

$$[illegible]$$ **Eq. 3-45**

In our simulation and experiments, the parameter [illegible] was set to 7. (Here, the notation of subcarriers corresponds to the position of [illegible] at the IFFT input as defined in matlab (see Figure 3-3)).

Compensation of the integer part of the CFO is usually carried out in time domain, in front of the DFT module, jointly with the correction of the fractional part of the CFO. Another approach consists in performing the compensation directly in the frequency domain, after the FFT, by shifting the spectrum circularly by −[illegible] positions.

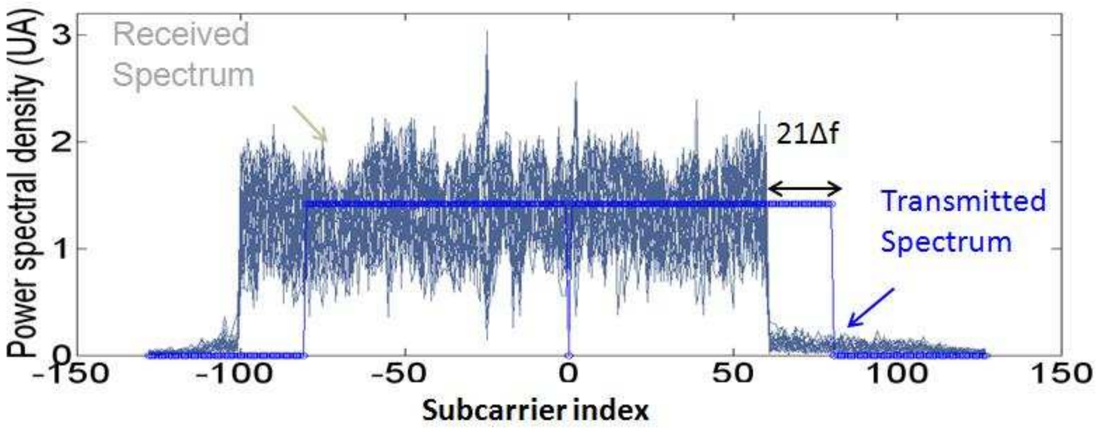

Figure 3-20: Power spectral density vs. sub-carrier index of the transmitted and received OFDM signal (here, the CFO = -21 Δf is measured).

3.3.4 Channel equalization

Ignoring phase noise and assuming perfect timing and frequency synchronization, the signal at the DFT output for OFDM symbol [illegible] can be expressed as:

$$[illegible]$$

The next step is thus the separation of the two polarizations and the compensation for the channel distortion (phase rotation and attenuation) on each subcarrier. For the sake of clarity, we first introduce channel equalization in the single polarization case, extend it to the dual polarization (DP) case, and finally discuss and compare several approaches to improve performance at this stage.

3.3.4.1 Channel equalization for single polarization OFDM transmission

In our system, channel estimation is based on training symbols periodically inserted in the flow of OFDM data symbols at a rate that depends on the channel coherence time. As we shall see in the next chapter, experiments have shown that the optical channel can be safely considered as time-invariant during the transmission of [illegible] successive OFDM

symbols. Once the channel estimate is obtained, equalization is performed in order to compensate for signal distortion.

In the single polarization case, the received signal simplifies into:

$$\square_{\square\square} \square \square_{\square} \square \square_{\square\square} \square \square_{\square\square} \qquad \textbf{Eq. 3-46}$$

Since the modulated symbols $\square_{\square}$ composing the training symbol are known to the receiver, the channel frequency response on each subcarrier can be estimated according to the least-square (LS) criterion, by solving the following optimization problem [Chi07]:

$$\square_{\square} \square \square\square\square\square \square\square\square_{\square} \square \square_{\square} \square_{\square}^{\square} \qquad \textbf{Eq. 3-47}$$

The solution is given by:

$$\square_{\square} \square \frac{\square_{\square}}{\square_{\square}} \square\square\square \square \square\square \square_{\square\square} \square \square \qquad \textbf{Eq. 3-48}$$

The channel estimate computed from the training symbol is then used to equalize several (100 in our case) successive OFDM data symbols. The role of channel equalization is to compensate for the distortion (gain/phase) experienced by the subcarriers. Zero-Forcing (ZF) equalization is a common and simple approach to channel equalization which does not require any other knowledge than the channel frequency response. It has the additional advantage of being optimal for optical channels since their frequency response has unit magnitude ($\square\square_{\square}\square\square \square\square$, thereby avoiding the classical problem of noise enhancement. The output of the ZF equalizer is:

$$\square_{\square} \square \frac{\square_{\square}}{\square_{\square}} \qquad \textbf{Eq. 3-49}$$

In practice, the channel estimate $\square_{\square}$ is used in place of the true channel frequency response $\square_{\square}$.

Note that in addition to compensate for channel gain and phase distortion on each subcarrier, channel equalization also addresses implicitly the linear phase shift caused by small timing errors (they are automatically considered as part of the channel frequency response calculated from the training symbol, and thus corrected by the subsequent ZF equalizer).

3.3.4.2 Extension to CO DP-OFDM transmission

In a DP configuration, the received signal on each subcarrier $\square$ is a MIMO 2x2 linear system:

$$\begin{matrix} \square_{\square\square\square\square} & \square_{\square\square\square\square} & \square_{\square\square\square\square} & \square_{\square\square\square} \\ \square_{\square\square\square\square} & \square_{\square\square\square\square} & \square_{\square\square\square\square} & \square_{\square\square\square} \end{matrix} \begin{matrix} \square\square \\ \square\square \end{matrix} \begin{matrix} \square_{\square\square\square} \\ \square_{\square\square\square} \end{matrix} \square$$

The signal received on each polarization is a linear combination (mixing) of the two polarization-multiplexed transmitted signals. Specifically, for a given subcarrier $\square$, $\square_{\square\square}\square\square\square$ and $\square_{\square\square}\square\square\square$ represent the energy transferred from the transmit polarization x towards the

receive polarizations x and y, respectively. Similarly, [illegible] and [illegible] represent the energy transferred from transmit polarization y towards receive polarizations x and y, respectively.

For convenience, the above equations can be represented in matrix notation as follows:

[illegible]

where [illegible] represents the [illegible] channel matrix describing the polarization effects and [illegible] is the 2x1 vector of transmitted data symbol on subcarrier [illegible].

2x2 MIMO least-square channel estimation can be carried out in a similar way than in the single polarization case, at the notable difference that 2 training symbols instead of 1 must now be used (on each polarization), otherwise an underdetermined linear system arises. In addition, a 2x2 matrix inversion is also required. A special structure for the training symbols can be used to alleviate the computational complexity. In particular, as originally suggested by [Jan08] and depicted in Figure 3-21, we can choose to transmit only on one of the two polarizations in each time slot, and alternate between the active polarizations between the two training symbols.

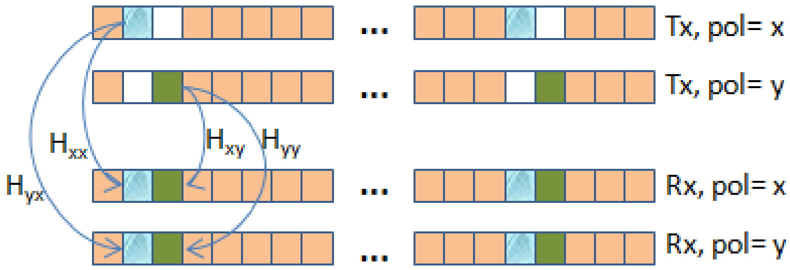

Figure 3-21: Particular structure of the two training symbols used for channel estimation in the DP case.

Then the following system arises:

[illegible] **Eq. 3-50**

In this case, 2x2 LS channel estimation reduces to 4 scalar LS channel estimation problems, whose solutions are given respectively by:

[illegible] **Eq. 3-51**

In this way we replace the costly 2x2 matrix inversion by 4 scalar divisions.

Once the 2x2 channel estimate is obtained, it is used to equalize several OFDM data symbols. The output of the 2x2 MIMO ZF equalizer is then given by:

Eq. 3-52

where $\mathbf{H}_k^{-1}$ is the inverse of the 2x2 channel frequency response (or, in practice, its estimate) for subcarrier k. Note that for an optical transmission impaired by CD and PMD, the 2x2 channel matrix is unitary and verifies $\mathbf{H}_k \mathbf{H}_k^{\dagger} = \mathbf{I}_2$. Then the matrix inversion can be advantageously replaced by a simple Hermitian transpose.

3.3.4.2.1 Improving channel estimation

In our previous description, only one training symbol (two in the DP case) is used to compute the channel estimate. The presence of noise will affect the quality of the channel estimation, and degrade in turn the performance of the equalizer. A general approach (but not unique) to improve channel estimation is to compute several estimates and average them. Two different methods have been considered and compared in this work. The first one sends more than one training symbols, and performs averaging in the time-domain. The second method does not require additional training symbols, but performs instead averaging in the frequency-domain by assuming that the channel is approximately constant over neighboring subcarriers. We finally discuss the combination of these two different techniques.

3.3.4.2.2 Time domain averaging

Time domain averaging (TDA) (see eg [Jan07]) consists in sending periodically a group of N_{TDA} training symbols (or N_{TDA} in the DP case), computing a different channel estimate $\hat{\mathbf{H}}_{k,n}$ for each training symbol n ($1 \le n \le N_{TDA}$) in the group and each subcarrier k (using *eg* the LS methods described in the previous subsection), and then averaging these N_{TDA} channel estimates, yielding:

Eq. 3-53

We have simulated the performance of this method by considering DCF-free single polarization transmission over 1000 km with 17000 ps/nm of cumulated CD and a variable number N_{TDA} ($N_{TDA} \ge 1$) of training symbol repetition. The results are shown in Figure 3-22 (BER vs OSNR). We first observe an OSNR penalty of 3 dB with respect to the theoretical performance (ideal channel estimation) when a single training symbol is used ($N_{TDA} = 1$). Increasing N_{TDA} beyond 1 improves the performance. The OSNR penalty reduces to approximately 0.75 dB for $N_{TDA} = 4$. No further improvement is observed beyond this value. We recall here that using more than one training symbol increases the transmission overhead.

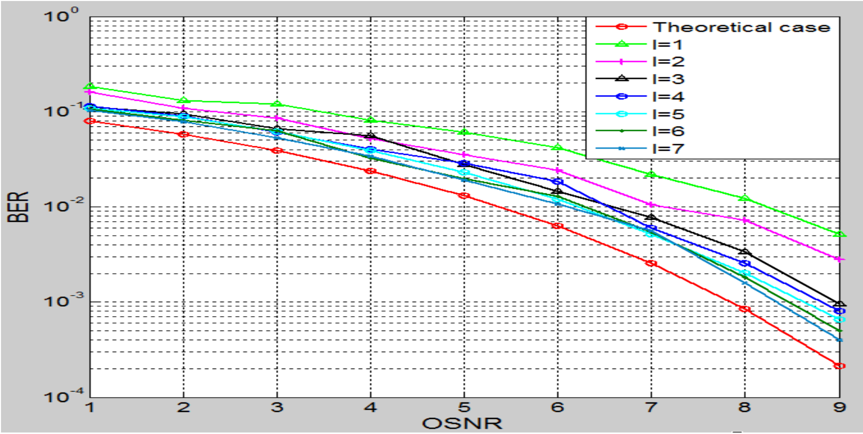

Figure 3-22: BER vs OSNR for the time-domain averaging method for several values of the training symbol repetition factor *l*.

3.3.4.2.3 Frequency domain averaging

In order to reduce transmission overheads while maintaining a high channel estimation accuracy, another method called intra-symbol frequency averaging (ISFA) was proposed in [Liu08]. It relies on the implicit assumption that the channel frequency response $\underline{H}_k$ is approximately constant over several neighboring subcarriers. Then based on a single training symbol (or 2 in the DP case), an improved estimate on subcarrier k can be obtained by averaging the channel estimate obtained on the $2m+1$ subcarriers in the range $[k-m, k+m]$:

$$\underline{\hat{H}}_k = \frac{1}{2m+1}\sum_{i=k-m}^{k+m} \underline{\hat{H}}_i = \frac{1}{2m+1}\sum_{i=k-m}^{k+m} \begin{pmatrix} \hat{H}_{xx}(i) & \hat{H}_{xy}(i) \\ \hat{H}_{yx}(i) & \hat{H}_{yy}(i) \end{pmatrix} \qquad \text{Eq. 3-54}$$

In an optical transmission context, the previous assumption requires that the accumulated CD be not too large and the subcarrier spacing be small enough to hold approximately true.

The performance of the ISFA method has been evaluated by simulation in the same transmission conditions than for the TDA method. The variable parameter is now the number m of neighboring subcarriers considered on the left and right, respectively, of the subcarrier of interest. Note that classical LS channel estimation described in subsections 3.3.4.1 and 3.3.4.2 corresponds to the case $m = 0$. The results are shown in Figure 3-23. We first note that the OSNR penalty is reduced from 3 dB to 1 dB by simply averaging over 3 subcarriers ($m = 1$). No significant improvement is observed for $m = 2$ and $m = 3$. The performance quickly deteriorates as we increase *m* beyond 3. This is due that owing to CD, subcarriers far apart from each other experience different phase rotations and thus the channel can no longer be considered as constant in such frequency ranges.

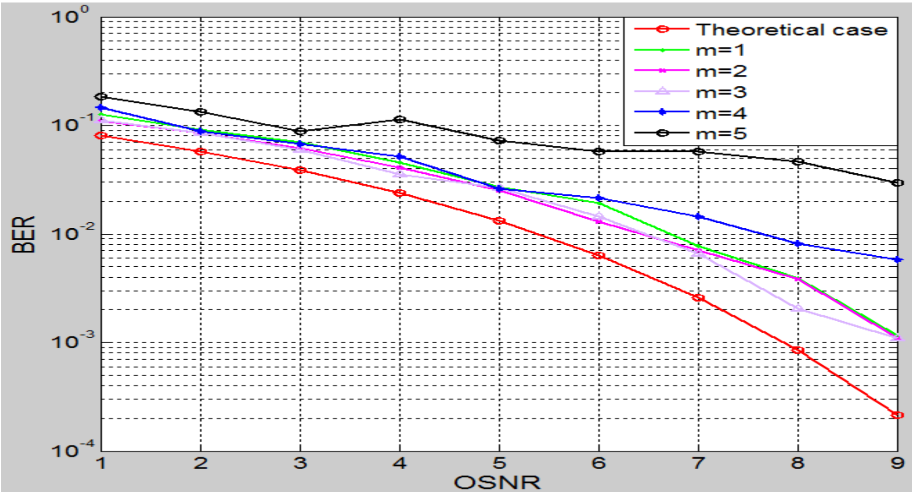

Figure 3-23: BER vs OSNR for the intra-symbol frequency averaging method based on a total of 2m+1 subcarriers, for several values of m.

3.3.4.2.4 Combination of TD and FD averaging

We have shown that TDA yields the best performance (OSNR penalty reduced to 0.75 dB with respect to ideal channel estimation) but at the cost of a significantly increased overhead (5 training symbols required). On the other hand, ISFA reduces the OSNR penalty to about 1 dB, without any overhead since a single training symbol is used. These two approaches are in fact complementary. Thus we propose to combine them, in order to get the best possible performance with minimum overhead.

The channel estimate obtained by combining TDA based on [illegible] training symbols ([illegible] in the DP case) with ISFA based on [illegible] subcarriers is given by:

[illegible] **Eq. 3-55**

The performance of the combined approach has been investigated in the same transmission conditions than previously. The results are shown in Figure 3-24. Parameter [illegible] was set to 2, while parameter l varies from [illegible] to [illegible]. We observe that the OSNR penalty is reduced to 0.6 dB for [illegible]. No performance is observed beyond this value.

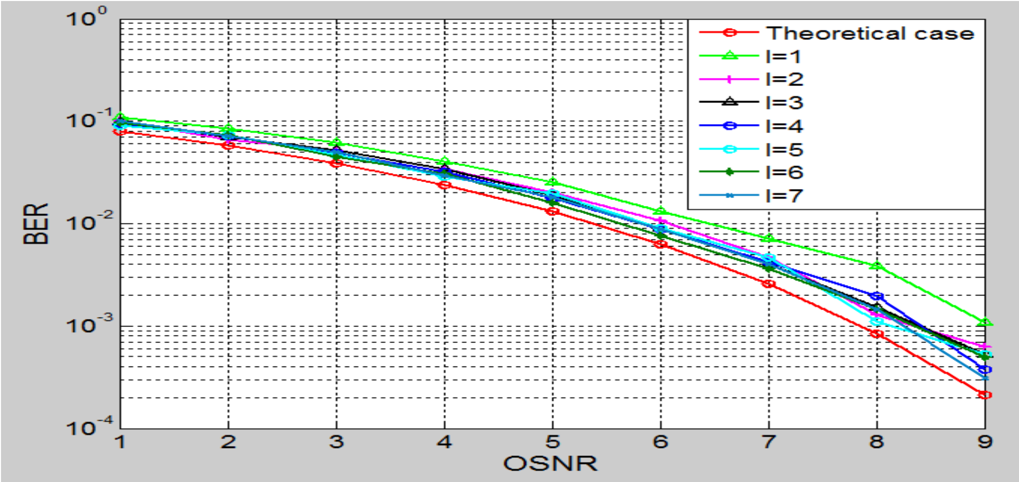

Figure 3-24: BER vs OSNR for the combination of ISFA (m=2) and TDA with a varying number *l* of training symbol repetitions.

These results suggest that periodically inserting [illegible] training symbols (4 in the DP case) every [illegible] OFDM data symbols is sufficient for the channel estimation performance point of view.

3.3.5 Phase noise compensation

Up to now, we have ignored the presence of phase noise in order to simplify the description of the algorithms. However, in practice, lasers phase noise is a major impairment limiting the performance of OFDM systems.

In this final Section, we first discuss the modeling and the impact of phase noise. We then discuss several ways to compensate for it, at least partially.

3.3.5.1 Impact of phase noise

Assuming perfect time and frequency synchronization but ignoring noise for the sake of clarity, the time-domain signal at the DFT input may be expressed as follows:

[illegible] **Eq. 3-56**

In the frequency domain, at the DFT output we get:

[illegible] **Eq. 3-57**

By decomposing the phase noise term affecting OFDM symbol j into a mean rotation [illegible] and a random fluctuation [illegible] around the mean

$$[illegible]$$ **Eq. 3-58**

the previous expression may be rewritten as follows

$$[illegible]$$ **Eq. 3-59**

We observe that phase noise has two different kinds of effect on the OFDM signal. At the DFT output, the modulated subcarriers are affected by an attenuation [illegible] and a phase shift [illegible] which are common to all subcarriers in symbol [illegible], but vary from symbol to symbol. We also note the presence of ICI. If we assume that the phase noise trajectory slowly evolves around its mean along the OFDM symbol duration and neglect the small fluctuations [illegible], then [illegible] so that, besides ICI, only the common phase error (CPE) term [illegible] has to be considered and corrected [Pet07].

3.3.5.2 Phase noise compensation

Essentially two methods have been proposed in the literature in order to compensate for the laser phase noise. The first one, first developed for wireless OFDM systems, is commonly called common phase error (CPE) estimation. It uses pilot-tones (known data on certain subcarriers) to estimate and correct the phase rotation common to all subcarriers in an OFDM symbol at the FFT output, but does not address the ICI [Xin07]. The other one was proposed in [JanM08] and is commonly referred to as the RF pilot (RFP) method. As shown in Figure 3-25, at the output of the two DACs embedded inside an AWG, a DC offset is inserted in the I and Q tributaries of the OFDM signal before the IQ modulator. As a result an RF pilot appears at the null frequency. As the DC offset is up-converted simultaneously with the OFDM signal, the RF pilot will be in the middle of the optical OFDM signal spectrum. This pilot tone will experience the same phase noise than the whole OFDM signal. At the receiver, a low-pass filter is used to extract this RF pilot tone, which is then used in turn to compensate for the phase noise affecting the received signal, by simple conjugation and signal multiplication (right side of Figure 3-25). This method does not only compensate for the CPE but can also address the fast temporal fluctuations of the phase (as well as a residual carrier frequency offset), thereby significantly reducing ICI at the FFT output.

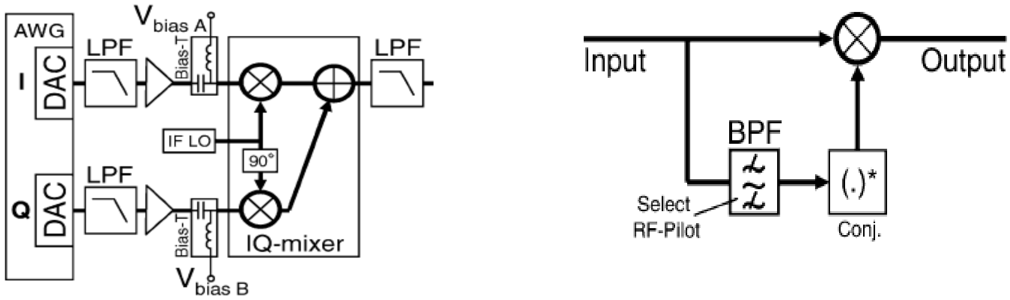

Figure 3-25: Principle of insertion (left figure) and extraction (right figure) of the RF pilot tone in the RF pilot method for compensating phase noise [JanM08].

Due to time and hardware constraints, only pilot-tone-based CPE estimation has been considered in this work. Thus, only the common phase shift [illegible] is considered and addressed by our digital baseband receiver.

Once synchronization, FFT, channel estimation and channel equalization have been performed, the pilot subcarriers dedicated to the phase noise estimation are extracted from the equalizer output for each OFDM symbol [illegible]. Then, the phase difference between the received pilot tones and the transmitted ones is calculated. The CPE [illegible] affecting symbol [illegible] is finally obtained by averaging the phase difference over the pilot tones:

[illegible] **Eq. 3-60**

where [illegible] is the set of pilot tones subcarrier indices, of size [illegible], [illegible] is the equalizer output for the pilot tone of index [illegible], and [illegible] is the known transmitted symbol on this pilot tone.

The CPE is finally corrected by multiplying each OFDM symbol by the conjugate of the complex exponential function of the corresponding CPE.

[illegible] **Eq. 3-61**

In our experiments, we have verified that [illegible] pilot tones were sufficient to correctly address phase noise issues.

3.4 Conclusion

In this chapter, we have specified an OFDM system allowing the transmission of 100 Gbps over 1000 km over G.652 fiber line in a 50 GHz ITU grid. Bandwidth as well as DAC sampling speed constraints have required us to resort to a Multi-Band approach, and thus to split the data rate between four polarization-multiplexed OFDM sub-bands. Then by accounting for the various transmission overheads the data rate carried by each sub-band, of width 8 GHz, is increased up to 32 Gbps. The IFFT size is set to 256, from which 170 subcarriers are modulated by the 4-QAM modulation while the highest frequencies are set to zero, in order to provide a 2-GHz guard band between the OFDM baseband signal and the aliasing products at the DAC output. Among the non-zero subcarriers, five pilot tones are dedicated for common phase error correction. In addition a first training symbol formed by repeating several times a basic pattern during the symbol duration is inserted at the beginning of the signal for the synchronization operation and two training symbols are repeated each 100 OFDM symbols for channel estimation. A cyclic prefix of 18 samples, defined in order to make the OFDM symbols resistant to intersymbol interference (ISI) generated by the chromatic dispersion accumulated over 1000 km of G.652 standard single mode fiber (SSMF), is added at the beginning of each OFDM symbol.

We have also introduced in this chapter appropriate digital signal processing (DSP) algorithms allowing recovery of the transmitted data with low error probability. Four main steps are involved: timing synchronization using the algorithm developed by Minn & Bhargava, two-steps frequency synchronization, improved channel estimation combining time and frequency-domain averaging, followed by 2x2 MIMO zero-forcing equalization, and finally compensation of the common phase noise generated by the ECLs using pilot sub-carriers.

Having defined the parameters of the OFDM signal and specified the DSP algorithms required at the transmitter and receiver side, the next step is now to implement and validate the proposed 100 Gbps DP-MB-OFDM transmission system in experimental conditions. This is the purpose of the next chapter.

Bibliography

[Aza11] A. A. Azad, M. Huq, and I. R. Rokon, "Efficient hardware implementation of Reed Solomon encoder and decoder in FPGA using Verilog," in *ICAEPE*, 2011.

[Blo11] S. Blouza, J. Karaki, N. Brochier, E. L. Rouzic, E. Pincemin, and B. Cousin, "Multi-Band OFDM networking concepts," *Eurocon*, 2011.

[Chi07] T.-D. Chiueh and P.-Y. Tsai, *OFDM basebandreceiver design for wireless communications*. Wiley, 2007.

[Jan07] S. L. Jansen, I. Morita, N. Takeda, and H. Tanaka, "20-Gb/s OFDM transmission over 4,160-km SSMF enabled by RF-Pilot tone phase noise compensation," in *Optical Fiber Communication Conference and Exposition and The National Fiber Optic Engineers Conference*, 2007.

[Jan08] S. L. Jansen, I. Morita, T. C. W. Schenk, and H. Tanaka, "Long-haul transmission of 16x52.5 Gbits/s polarization-division-multiplexed OFDM enabled by MIMO processing," in , vol. 7, Feb. 2008, pp. 173-182.

[Jan09] S. L. Jansen, I. Morita, T. Schenk, and H. Tanaka, "121.9-Gb/s PDM-OFDM transmission With 2-b/s/Hz spectral efficiency over 1000 km of SSMF," *Journal of lightwae technology*, vol. 27, 2009.

[JanM08] S. L. Jansen, I. Morita, T. C. W. Schenk, N. Takeda, and H. Tanaka, "Coherent Optical 25.8-Gb/s OFDM Transmission Over 4160-km SSMF," *Journal of lightwave technology*, 2008.

[Kai04] S. Kai and S. Erchin, "Coarse frame and carrier synchronisation of OFDM Systems: a new metric and comparison," *IEEE transactions on wireless communications*, vol. 3, no. 4, pp. 1271-1284, Jul. 2004.

[Liu08] X. Liu and F. Buchali, "Intra-symbol frequency-domain averaging based channel estimation for coherent optical OFDM," *Optics express*, vol. 16, no. 26, pp. 21944-21957, Dec. 2008.

[LiY06] Y. Li and G. L. Stüber, *Orthogonal frequency division multiplexing for wireless communications*. Springer, 2006.

[Min03] H. Minn, V. K. Bhargava, and K. B. Letaief, "A robust timing and frequency synchronization for OFDM systems," *IEEE transactions on wireless communications*, vol. 2, no. 4, pp. 8022-839, Jul. 2003.

[Mor07] M. Morelli, C. .-C. J. Kuo, and M.-O. Pun, "Synchronization techniques for Orthogonal Frequency Division Multiple Access (OFDMA): A tutorial review," *Proceedings of the IEEE*, 2007.

[Pet07] D. Petrovic, W. Rave, and G. Fettweis, "Effects of phase noise on OFDM systems with and without PLL: characterization and compensation," *IEEE transactions on communications*, vol. 55, 2007.

[Ren05] G. Ren, Y. Chang, H. Zhang, and H. Zhang, "Synchronisation method based a new consstant envelop preamble for OFDM systems," *IEEE transactions on broadcasting*, vol. 51, no. 1, pp. 139-143, Mar. 2005.

[Sch97] T. M. Schmidl and D. C. Cox, "Robust frequency and timing synchronisation for OFDM," *IEEE transactions on communicaions*, vol. 45, no. 12, pp. 1613-1621, Dec. 1997.

[Shi08] W. Shieh, H. Bao, and T. Tang, "Coherent optical OFDM: theory and design," *Optics Express*, 2008.

[Shi10] W. Shieh and I. Djordjevic, *OFDM for optical communications*. Elsevier, 2010.

[Sin08] A. C. Singer, N. R. Shanbhag, and H.-M. Bae, "Electronic dispersion compensation," *IEEE Signal Processing Magazine*, vol. 25, 2008.

[Ten06] S. Ten and M. Edwards, "An introduction to the fundamentals of PMD in fibers," *White paper*, no. Corning Incorporated, 2006

[Tra08] I. Trachanas, M. Gaida, and N. J. Fliege, "On SNR degradation in OFDM systems with aliasing and a frequency offset," in *ISCCSP*, 2008.

[Xin07] X. Yi, W. Shieh, and Y. Tang, "Phase estimation for coherent optical OFDM," *IEEE photonics technology letters*, vol. 19, no. 12, pp. 919-921, Jun. 2007.

4 Experimental implementation of 100 Gbps MB-OFDM transmitter with polarization diversity coherent receiver

Chapter 4

Experimental implementation of 100 Gbps MB-OFDM transmitter with polarization diversity coherent receiver

As discussed in the previous chapter, current ADC/DAC limitations led us to distribute the total data rate of 100 Gbps into four polarization multiplexed OFDM sub-bands. Each sub-band will actually transport 32 Gbps rather than 25 Gbps, to account for the various transmission overheads (pilot tones, cyclic prefix, training symbols, as well as FEC and protocol overhead). The OFDM signal in each sub-band has a bandwidth of 8 GHz and operates at a sampling frequency set to 12 GHz in order to facilitate aliasing elimination at the DAC output. 256-points FFT/IFFT are used, among which only 170 subcarriers carry information, using 4-QAM modulation. Coherent detection has been retained in order to the transmission target of transporting a spectral efficiency of 2 bits/s/Hz over 1000 km of SSMF.

The aim of this chapter is to describe the experimental implementation of the 100 Gbps coherent OFDM system. Several experiments have been carried out to validate the components used and to overcome the system impairments. First, the proposed methodology is exposed in Section 1. Then, the following sections detail the successive steps required for successfully building the polarization multiplexed OFDM system carried out in each sub-band. In Section 2, the electrical back-to back arrangement is detailed. After that, Section 3 describes the test-bed permitting the up-conversion into the optical domain and the homodyne detection of the optical OFDM single sub-band signal. We propose in particular a simple method to fine-tune the optical IQ modulator while avoiding IQ-imbalance on the transmitter. Later on in Section 4 we generate and detect a polarization-multiplexed OFDM signal. Heterodyne detection, for which a carrier frequency mismatch exists between the transmitter and receiver lasers and has thus to be compensated for, is also investigated. Having achieved the description of the experimental implementation of the 25 Gbps OFDM system and validated the results through a comparison with theoretical performance, we present in Section 5 the experimental set-up of the 100 Gbps OFDM system. The system performance is then compared to the performance of 100 Gbps DP-QPSK system. Finally the impact of CD and PMD on the OFDM system performance is investigated.

4.1 Proposed methodology

The CO-OFDM system has a complex transmitter and receiver architecture, the latter comprising a coherent detector and advanced digital signal processing. Thus its implementation requires an optimization of the various electrical and optical components, as well as the validation of the developed algorithms.
We will describe in this section the successive steps carried out to build a dual polarization (DP) CO-OFDM system operating at an effective data rate of 25 Gbps.

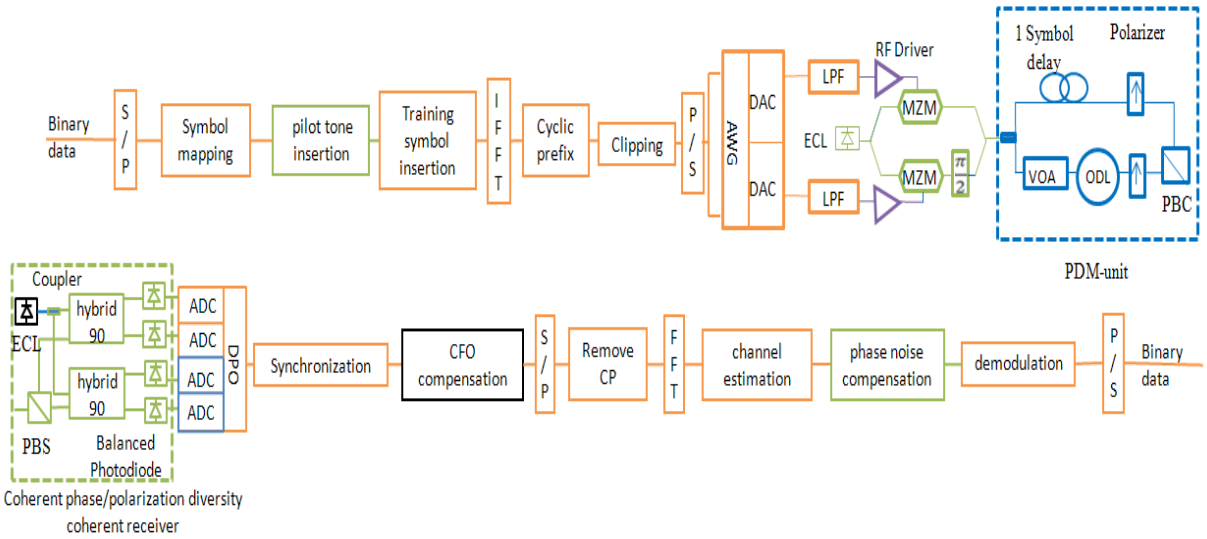

Figure 4-1: Experimental set-up of the OFDM transmitter and receiver.

Figure 4-1 shows the experimental set-up of the proposed Tx/Rx OFDM system. Several colors are used on this figure to identify the different implementation steps successively carried out to evaluate and validate the transmitter and receiver architecture.

The first experiment carried out was the electrical back-to-back validation, completed in two steps. The blocks of the first step are identified by the orange color and consist in connecting the filtered outputs of the AWG to the ADCs embedded inside the real-time digital oscilloscope (DPO). The next step in the electrical back-to-back experiment was the insertion of RF drivers. At this level an optimization of the attenuator values at the RF drivers inputs was required in order for these devices to work in their linear regime.

The second experiment consists in up-converting the electrical OFDM signal into the optical domain, and, on the receiver side, in establishing homodyne coherent detection. The extra steps required in addition to the back-to-back electrical validation are represented in green in Figure 4-1. Up-conversion onto the optical domain is realized by impressing the filtered electrical I and Q signals at the output of the DACs onto an optical carrier using a CMZM. The same laser feeds both the CMZM and the coherent detector. However this laser induces phase noise and thus a common phase error affects all subcarriers within each OFDM symbol. The compensation of this phase shift is achieved by the CPE correction algorithm introduced in Chapter 3, Section 3.3.5.

The third experiment, figured in blue, has allowed the generation of a polarization multiplexed OFDM signal by the insertion, at the output of the CMZM, of the Polarization Division Multiplexing (PDM) unit. Now detection of the two polarization multiplexed OFDM bands requires the use of the 4 ADCs embedded inside the DPO. On the DSP side, channel estimation and equalization based on ZF-MIMO processing have been developed in order to separate the two polarizations.

Until now, detection was based on homodyne detection. In the final step, heterodyne detection is established by using two different lasers for the CMZM and the coherent receiver. The additional blocks required for this experiment are represented in black in Figure 4-1. The transition from homodyne to heterodyne detection induces in particular a carrier frequency offset (CFO) that must be compensated for by appropriate synchronization algorithms.

4.2 Electrical back-to-back arrangement

The first experiment to carry out was the electrical back-to-back setup. We first describe in this section the preliminary experiment that consists in connecting the filtered output of the two DACs to the two ADCs. Signal pre-emphasis was found to be necessary in order to correct the frequency response of the DACs, as well as clipping of the OFDM signal. Then we present the complete back-to-back experiment. In particular we connect RF drivers at the DAC outputs, and optimize the drivers settings so that the RF drivers operate in their linear regime.

4.2.1 Preliminary experiment

The preliminary experiment, shown in Figure 4-2, consists in combining together the AWG, anti-aliasing RF filters and real-time digital oscilloscope (DPO).

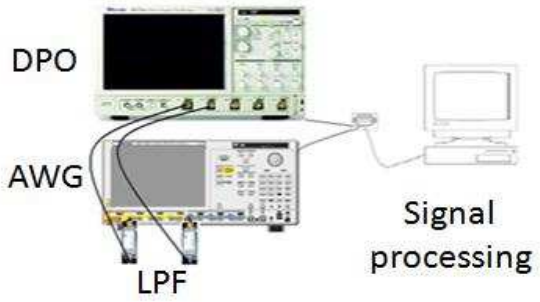

Figure 4-2: Experimental set-up of the basic electrical back-to-back experiment.

The OFDM signal generated offline is split into real (I) and imaginary (Q) parts and sent to two DACs embedded inside the Tektronix AWG 7122B arbitrary waveform generator. The latter is set to operate at a sampling rate of 12 GSa/s to generate OFDM baseband signal. The in-phase (I) and in-quadrature (Q) components of the OFDM waveform have a bandwidth of ~4 GHz. The output of one of the DACs is shown in Figure 4-3. The aliasing products are removed by an anti-aliasing filter. The two filtered I and Q signals are then connected to two different input channels (i.e. ADC) of the DPO. The DPO is used at a sampling rate of 50 GHz. After detection, the data is processed offline. Note here that the AWG continuously transmits the signals to the DPO, thus requiring a timing synchronization process to be implemented in the digital OFDM receiver (cf Chapter 3).

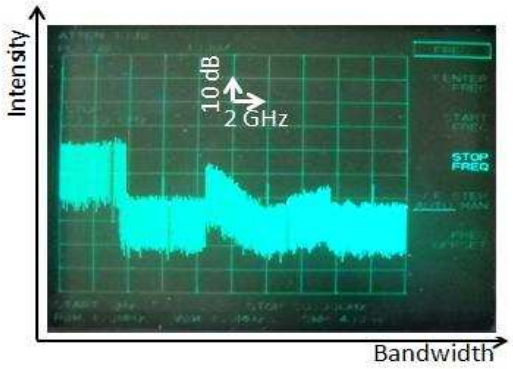

Figure 4-3: OFDM spectrum before filtering.

4.2.1.1 Clipping and Pre-emphasis

The OFDM signal waveform generated offline can exhibit very high amplitude fluctuations in the time domain. Such signal peaks induce in turn an inefficient use of the global dynamic range of the DACs. Since the DAC has limited resolution, limiting the signal amplitude variations within a pre-determined range is an important step that has to be carried out before digital-to-analog conversion of the discrete-time signal. The data at the output of the IFFT whose values exceed a pre-determined maximum level are thus clipped to this maximum level (Figure 4-4) [LiY06]. Note that clipping introduces distortion and thus may cause severe degradation of the system performance if signal peaks occur frequently.

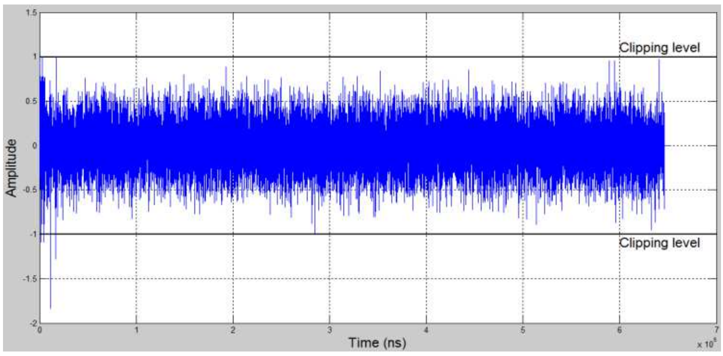

Figure 4-4: The rare peaks of the OFDM exceeding the clipping level are clipped to this value.

Besides the limited DAC resolution, the frequency response of the DAC has a sinus cardinal ($sinc$) envelope [Yan06] whereas for an ideal DAC, the output is a train of impulses in the time domain and thus the corresponding spectrum has a rectangular shape. Practical, DACs hold the voltage constant during a period of $T_s (f_s = 1/T_s)$. The input signal, x, is expressed at the output of the DAC by x_{DAC} which is given by:

$$x_{DAC}(t) = \sum_{n} x(nT_s) \cdot rect\left(\frac{t - \frac{T_s}{2} - nT_s}{T_s}\right) \qquad \text{Eq. 4-1}$$

In the frequency domain this effect translates into a multiplication of the signal spectrum by a $sinc$ function, yielding:

$$X_{DAC}(f) = \frac{1}{T_s} \sum_{k} X(f - kf_s) \cdot e^{-j\pi f T_s} sinc(fT_s) \qquad \text{Eq. 4-2}$$

We note that the summation includes all periodic replicas of the signal centered at frequencies kf_s where k is an integer factor [Opp99]. After filtering, the replicas with $k \neq 0$ are removed. However, the frequency response of the signal of interest is not flat; instead, due to the $sinc$ term, it is attenuated especially at high frequencies. The electrical spectrum of I channel before pre-emphasis is shown in Figure 4-5. An intensity difference of about 8 dB is observed between the first and last subcarrier of the OFDM signal. Such an attenuation in the frequency response is unacceptable and calls for corrections techniques in order to obtain a flat frequency response. Fortunately, several techniques are available to cope with the non-ideal frequency response of the DAC. The most common techniques are pre-equalization filtering, and post-equalization filtering. The filter coefficients are chosen

from the inverse of the □□□□□ function. Here we chose to take advantage of the pre-emphasis function provided by the AWG to equalize the power of the various OFDM subcarriers. The OFDM baseband signal with pre-emphasis is shown in Figure 4-5. The pre-emphasis is tuned in such a way that the intensity after the IQ mixer is equal for all the subcarriers.

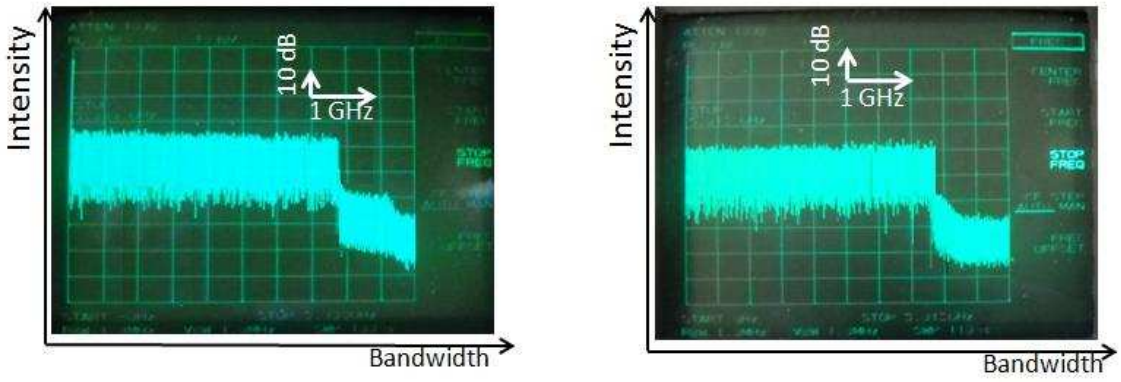

Figure 4-5: OFDM baseband electrical spectra without (left fig) and with pre-emphasis and low pass filtering (right fig).

4.2.1.2 Results

Figure 4-6 below shows the 4-QAM constellation retrieved offline with our signal processing algorithms. In order to verify the system performance in back-to-back configuration, the OFDM signal was impaired by additive white Gaussian noise (AWGN). The noise was simulated in discrete-time at the transmitter side and added to the OFDM signal, before sending the OFDM tributaries to the two DACs.
The Bit Error Rate (BER) has been plotted as a function of SNR in Figure 4-6. To validate the good operation of our OFDM system, the results are compared to the theoretical performance of 4-QAM given by: □□□ □ □□□ □□□□□□□□ □□□□. The theoretical curve and the curve resulting from the preliminary back-to-back experiment are superimposed, thereby validating the basic RF chain. This also allows us to conclude that, for 4-QAM constellation, the ENOB limitation of our DAC/ADC does not affect the system performance, at least down to a BER of 10^{-5}.

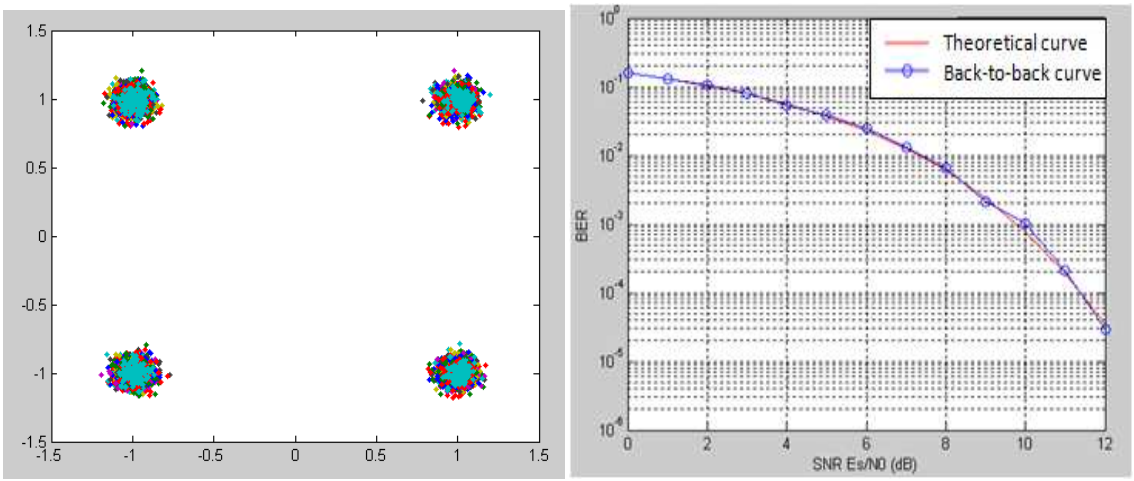

Figure 4-6: 4-QAM constellation (left fig.); BER vs SNR obtained after digital demodulation of the electrical OFDM signal (right fig.).

4.2.2 Complete experiment

In the preliminary back-to-back experiment reported before, the DAC outputs were filtered by 4 GHz bandwidth low pass filters (LPF) and then directly connected to the ADCs. But in fact, the DACs outputs cannot be directly connected to the IQ modulator since the modulator must be fed by an RF driver. In addition, the IQ modulator has a push-pull structure and is dual-drive: it requires consequently differential signal inputs, which are provided by an appropriated RF driver, having itself differential inputs and outputs. In order to feed accordingly the two RF drivers (one for the I component and another one for the Q component) and the IQ modulator, it is necessary to insert a component which generates the signal and its complementary counterpart: this device is called "fanout". In this experiment we have completed the initial electrical back-to-back experiment by adding the fanouts and the RF drivers at the outputs of the AWG. In order to maintain good system performance, the fanouts and RF drivers inputs have to be carefully optimized so as to guarantee linear regime operation of these two key components. The method retained to perform this optimization will be described in detail hereafter.

We first have connected each of the filtered I and Q signals to the previously described fanouts. Then, by connecting the fanouts outputs to the ADCs, a new back-to-back characterization of the RF chain can be obtained. In particular, we are able to tune precisely the response of the fanouts that we want to be as linear as possible. To do so, we insert a manually variable attenuator between the AWG and the fanout (see Figure 4-7). Through the examination of the 4-QAM constellation quality as well as through BER measurements at a given SNR value, we determine the attenuation value that gives the best performance and makes the fanout behavior linear. In our setting, the optimal attenuation was found to be 16 dB, corresponding to an output differential peak-to-peak voltage of 450 mVpp.

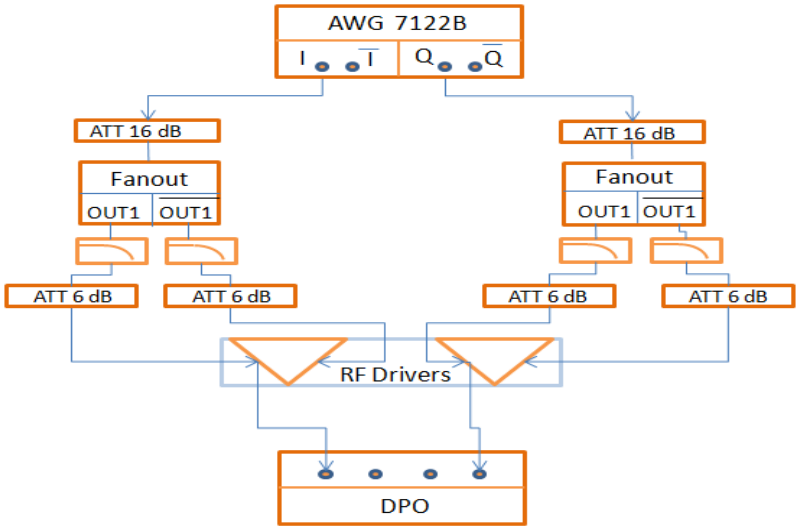

Figure 4-7: Experimental set-up of the electrical experiment.

In a second step, we have connected the outputs of the fanouts to the RF drivers (see Figure 4-7 above). The RF driver outputs are then connected to the DPO. In order to optimize the input levels of the RF drivers, we use the same procedure than for the fanout, by inserting variable attenuators between the fanout outputs and the RF drivers inputs. We present in Figure 4-8 the 4-QAM constellation diagram for several tested attenuator values. For an attenuator value of 0 dB, a constellation of poor quality is obtained after signal processing,

proving that the RF drivers operate outside the linear regime. At the opposite, an attenuation value of 20 dB results in a high quality constellation diagram. However, a 20 dB attenuation value corresponds to an output peak-to-peak voltage of 270 mVpp, which is too small to drive correctly the IQ modulator and results in an inefficient use of the total linear range of the modulator. Other attenuator values have been tried out in order to find the best trade-off between good linearity of the RF driver response and a sufficiently high output voltage delivered by the driver. With attenuators of 6, 10, 13 and 16 dB, we obtain approximately the same performance than those obtained with the 20 dB attenuator. An attenuation value of 6 dB was therefore finally retained in the following of this work, corresponding to an output single-ended peak-to-peak voltage of 1.1 Vpp and output differential peak-to-peak voltage of 2.2 Vpp.

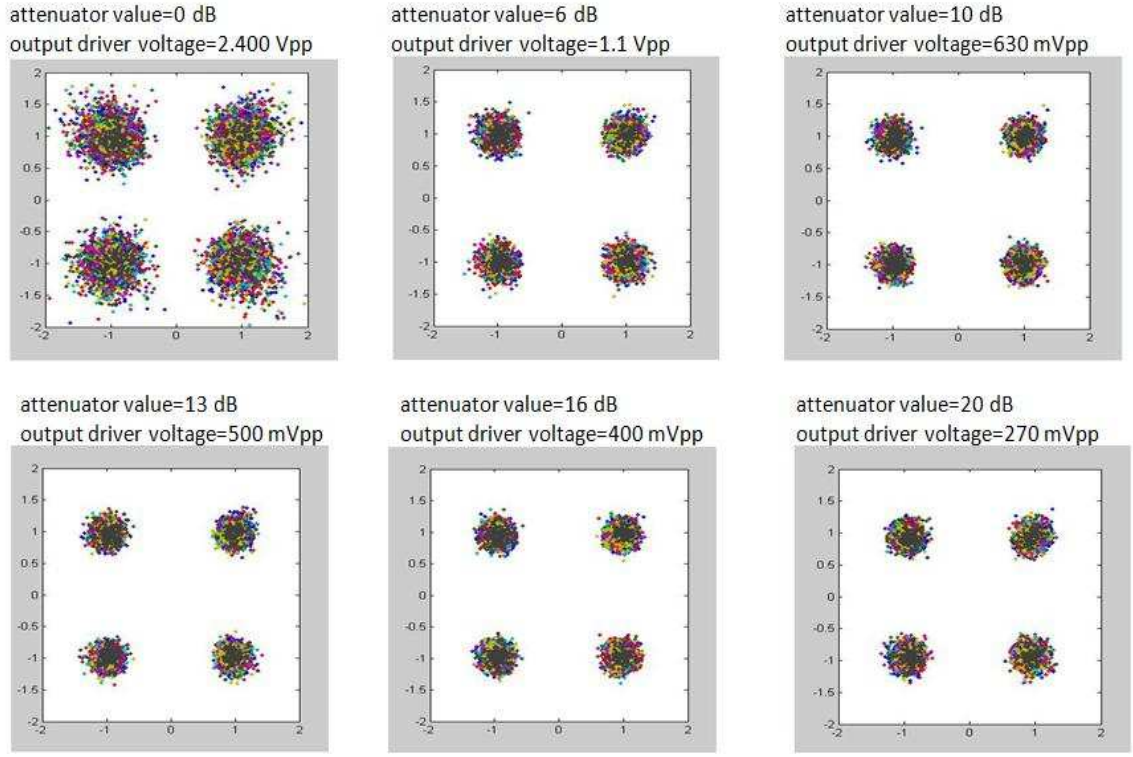

Figure 4-8: 4-QAM constellation diagram observed by testing different attenuator values at the RF driver inputs, with a peak-to-peak input voltage equal to 450 mVpp. The input driver voltage is measured after the insertion of the attenuator.

In order to verify the system performance of this back-to-back experiment including the complete RF chain, we have plotted the BER as a function of SNR on the AWGN channel using 4-QAM modulation (Figure 4-9). To validate the good operation of our OFDM system in back-to-back, we compare the results with the theoretical performance given by: □□□ □ □□□ □□□□□□□□ □□□□. The curves resulting from the preliminary back-to-back experiment (DAC filtered by 4 GHz bandwidth LPF) and from the complete back-to-back experiment (which includes the fanouts and RF drivers) are superimposed on the theoretical curve, showing that no penalty is induced by any of the electrical components inserted into the RF chain.

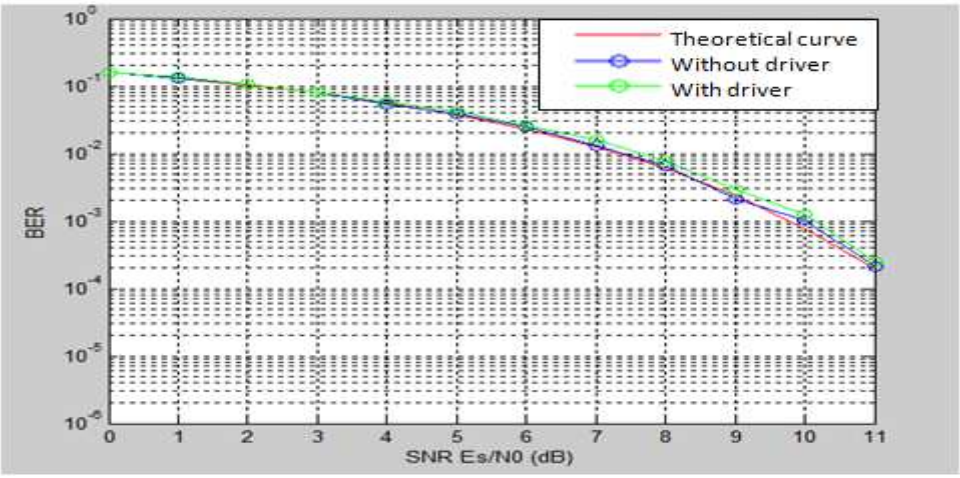

Figure 4-9: BER vs SNR of the generated electrical OFDM signals and the theoretical case.

Wondering about the capability of our DAC / ADC to generate and detect higher order M-QAM constellation, we have replaced the QPSK modulation by 8-QAM and 16-QAM modulations and upgraded our digital receiver algorithms to detect such constellations. The results are given in Figure 4-10 below. Inspection of these constellations suggests that the signal quality is good enough to envisage a possible experimental implementation, at least for 8-QAM which was shown to be sufficiently robust to the accumulation of phase noise into the optical transmission line [Jan09]. This extension will be studied in forthcoming 400 Gbps experiments which are beyond the scope of this thesis.

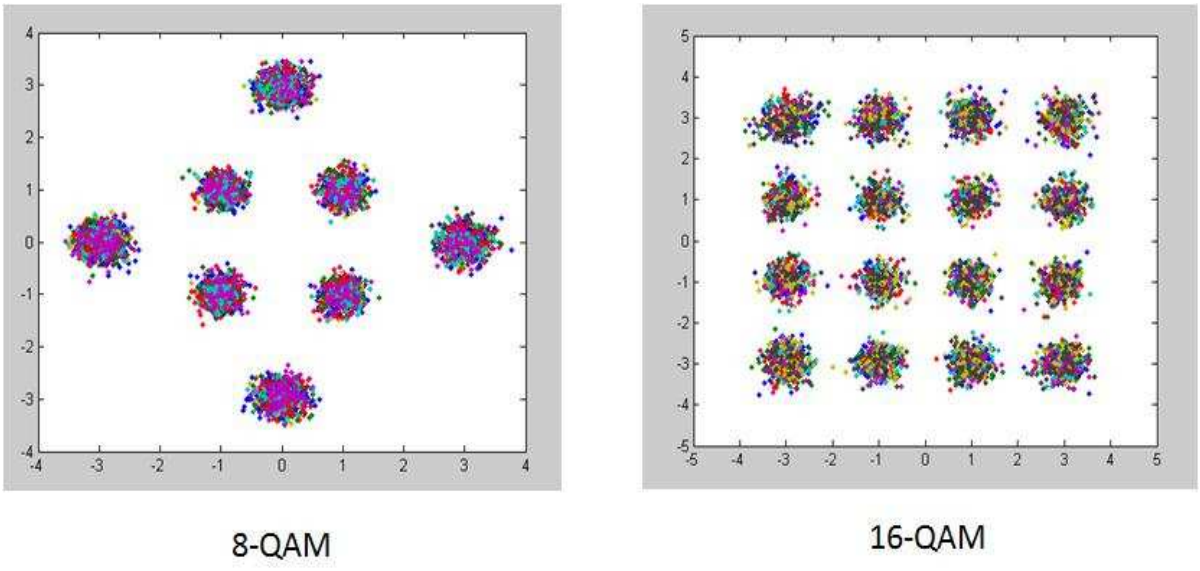

Figure 4-10: Constellation diagram obtained with 8-QAM and 16-QAM modulations.

4.3 Single polarization Tx/Rx design and validation

The electrical back-to-back experiment has been carried out and characterized. We have inserted all the RF components and we have optimized their input level to obtain a linear operation of the RF chain. The next step, described in this section, consists in up-converting the electrical OFDM signal into the optical domain by inserting an IQ modulator, and, at the

other end, down-converting the optical signal by using a polarization/phase diversity coherent receiver. However, several imperfect transmitter adjustments such as phase, gain and/or time delay mismatch between the I and Q paths can occur, leading to IQ imbalance problems. Thus we propose and describe a new and simple method to adjust the transmitter so as to avoid Tx IQ imbalance problems. Lastly we present the experimental results.

4.3.1 Experimental set-up

Figure 4-11 represents the experimental set-up of our coherent single-band OFDM transmitter/receiver. At the transmitter, the I and Q signals generated by two DACs are filtered, amplified through two RF drivers working in their linear regime, and mixed together thanks to a Fujitsu FTM7960EX optical IQ modulator. The laser used to feed both the transmitter and the receiver is an external cavity lasers (ECL) having a line-width of ~100 kHz, in order to limit as much as possible the intrinsic phase noise. At the receiver side, the polarization diversity coherent receiver, constituted of two 90° hybrids, allows the separation of the in-phase (I) from the quadrature-phase (Q) component. Their outputs are connected to four balanced photo-receivers, which are themselves coupled to the four 50 GSa/s ADCs of the DPO. Homodyne detection is considered here, so that the same laser feeds in parallel the IQ modulator and the coherent detector through the use of a 1:2 coupler.

The offline digital receiver performs first timing synchronization, followed by FFT demodulation, channel estimation, and zero-forcing equalization. Pilot tones are finally used to compensate for the common phase error caused by phase noise.

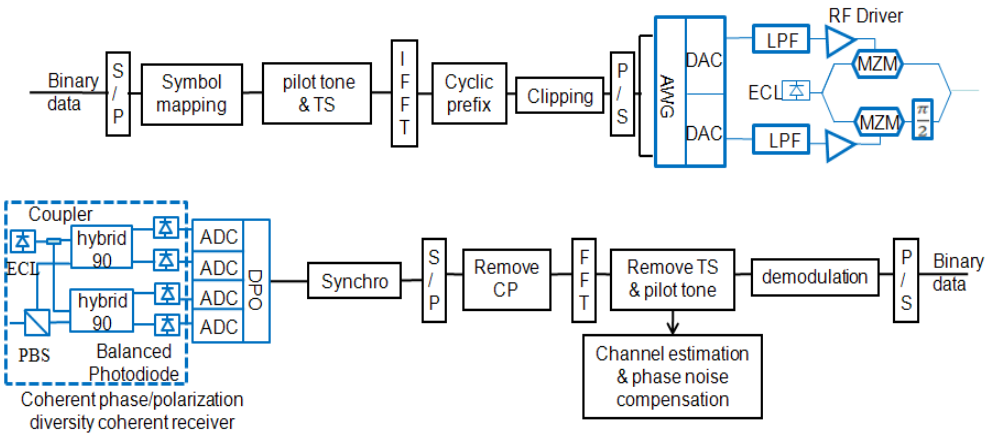

Figure 4-11: Experimental set-up of the homodyne optical OFDM single-band signal.

4.3.2 Transmitter adjustments

One of the most complex steps of this experimental implementation is the fine-tuning of the optical IQ modulator, or equivalently of the complex Mach-Zehnder modulator (CMZM). The CMZM is constituted of a Mach-Zehnder super-structure comprising two Mach-Zehnder modulators (MZM) in parallel, and a □/2 phase shifter which is inserted for instance in the lower arm of the CMZM super-structure. The CMZM has thus three bias voltages that need to be finely adjusted. They are called Bias 1, Bias 2 and Bias 3 in Figure 4-12 below,

respectively. The optimal bias for MZM1 and MZM2 corresponds to the null transmission point, whereas the optimal bias for MZM3 is the quadrature point.

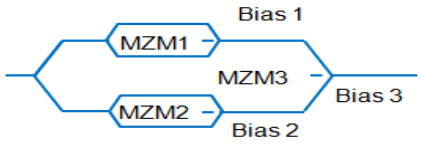

Figure 4-12: CMZM structure.

The three biases of the CMZM can be set as follow:

1. Apply and adjust all the bias voltages to get maximum optical power without RF signal.
2. Adjust bias voltage Bias 1 to get 25% of the maximum power.
3. Adjust bias voltage Bias 2 to get minimum power.
4. Apply PRBS signals to the RF input of MZM1 and MZM2, then adjust Bias 3 to get, with intensity detection, the optimum waveform for dual quadrature phase shift keying (DQPSK) as shown in Figure 4-13. At this level, the relative phase between the two arms of the CMZM is set to 90° but the bias voltages of MZM1 and MZM2 are not precisely adjusted at the null transmission point.
5. Generate an OFDM signal, visualize its optical spectrum at the output of the CMZM on an optical spectrum analyzer (OSA) and optimize Bias 1 & Bias 2 to fully suppress the DC component of optical spectrum observed in the middle of the spectrum when one of the two bias voltages is inaccurately adjusted (Figure 4-14).

The CMZM is a thermal-sensitive component. Small temperature variations can modify the three optimum bias voltages. To deal with possible deviations, the last two steps must be repeated on a daily basis.

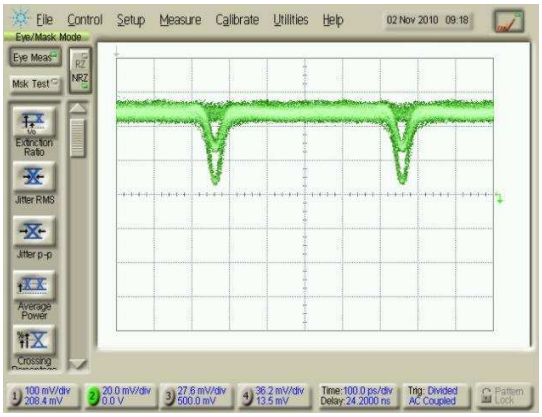

Figure 4-13: DQPSK waveform after direct detection. Here, the CMZM biases are adjusted precisely.

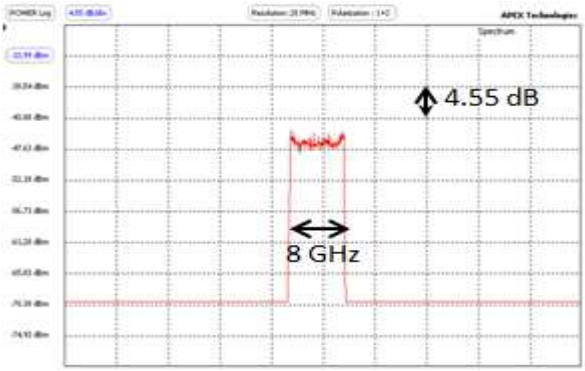

Figure 4-14: OFDM spectrum after CMZM. The CMZM biases are adjusted precisely.

The method described above for fine-tuning the IQ modulator is complex and requires daily modifications of the transmitter/receiver architecture (substitution of the OFDM transmitter by a PRBS generator, and replacement of the coherent detector by a direct detection receiver). In addition, it does not address all possible transmitter imperfections so that the problem of IQ imbalance at the transmitter is not removed. IQ imbalance degrades system performance since it generates a mirror image of the subcarrier *kth* on the *-kth* subcarrier and vice versa [Sch08]. Several methods exist in the literature to mitigate Tx IQ imbalance [Ami10, Cao11]. Hereafter we propose a new, simple and original method to avoid IQ imbalance in the transmitter. Our approach is solely based on the observation of the OFDM signal spectrum. As a by-product, this method permits also to suppress the DC component which does not induce IQ imbalance but consumes a large portion of the signal power, thereby also degrading performance [Tan07].

The optical signal at the output of the CMZM is represented by the following equation [Shi10]:

Eq. 4-3

where $\square_{\square}$ and $\square_{\square}$ stand for the I and Q tributary voltages of the signal at the input of the CMZM, $\square_{\square\square}$ is the DC bias voltage of the modulator and $\square_{\square\square}$ is the frequency of the ECL feeding the CMZM.

To fully suppress the DC component from the signal spectrum, the bias voltage Bias 1 & Bias 2 of the MZMs must be finely-tuned on the $\square_{\square}$ value ($\square_{\square}$ is the half-wave switching voltage of each MZM). For instance, we have represented in Figure 4-15e, the OFDM signal spectrum corresponding to the case where one of the two bias voltages is not correctly adjusted. We note here that DC component removal can be carried out experimentally whether both the positive and negative frequencies carry data, or if just the lower or upper band carries data. Once the bias voltages of MZM1 and MZM2 have been properly tuned at the null transmission point, we obtain the spectrum illustrated in Figure 4-15a.

At the optimal null bias condition $\square_{\square\square} \square \square_{\square}$, and as V_I and V_Q are small, we can write:

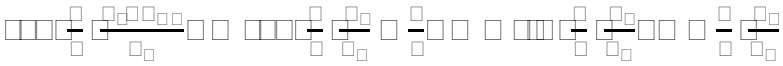

Then Eq. 4- 3 becomes:

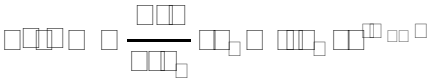

Eq. 4-4

This equation shows that the baseband signal (is linearly up-converted to the center frequency [Shi10].
The baseband OFDM signal can be expanded as follows:

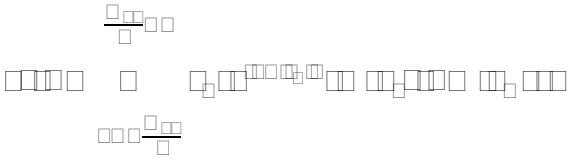

Eq. 4-5

Note that, for notational convenience, the subcarriers are numbered differently from the previous chapters, and we have
Then,

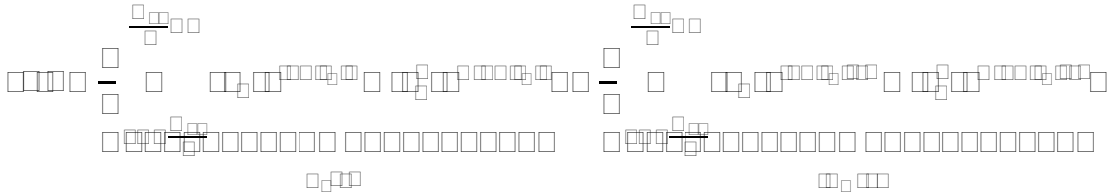

Several stages in the transmitter structure can be the source of an IQ mismatch, e.g., a gain difference between the I and Q arms, a deviation from the phase-shift between the two paths, and/or a time delay mismatch between the I and Q tributaries of the OFDM signals.
A gain mismatch between the I and Q paths may come from different attenuations values in the I & Q RF chain, or by a gain difference between the I & Q tributaries at the RF drivers level. Imperfections in the transmitter structure may result in I and Q electrical paths with different length, each path being composed of an RF cable, attenuators, LPF and driver. A small difference of length between any of those electrical components will result in a time delay between the I and Q signals. Finally, an inaccurate tuning of voltage bias 3 can cause deviation from the optimal point.
By sake of simplicity and given that the up-conversion process is linear (Eq. 4-5), a model of the OFDM baseband signal affected by IQ imbalance is:

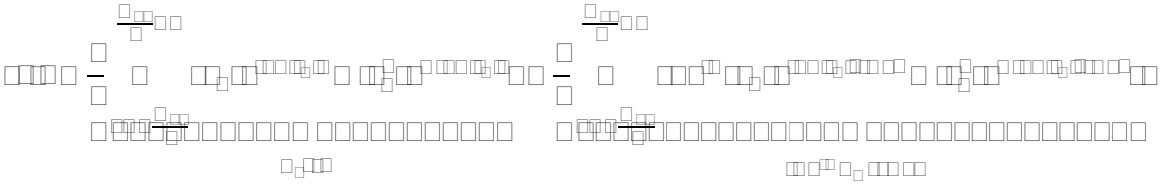

where , and model the Tx time, gain and phase mismatch, respectively. Rearranging the terms, we obtain:

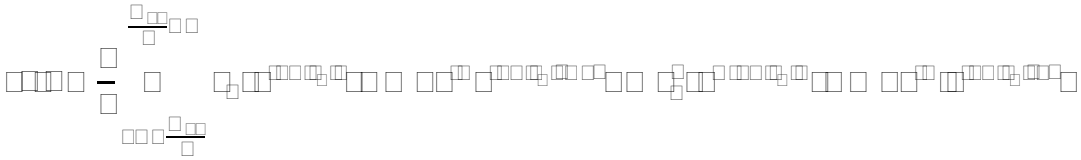

or, equivalently,

Eq. 4-6

where the coefficient $\square_{\square\square}$ and $\square_{\square\square}$ are defined as follow:

Eq. 4-7

The received symbol $\square_{\square}$ at the FFT output on subcarrier $\square$ is then given by:

Eq. 4-8

It can be concluded from the Eq. 4-8 that, in the presence of IQ imbalance, the *kth* subcarrier is given by the transmitted information symbol on the *kth* subcarrier multiplied by a complex factor $\square_{\square\square}$, plus the complex conjugate of the symbol transmitted on the *-kth* subcarrier multiplied by another complex factor $\square_{\square\square}$. In case of perfect matching (i.e. $\square$ $\square_{\square\square}$ $\square$ $\square_{\square\square}$), $\square_{\square\square}$ $\square$ $\square$ and $\square_{\square\square}$ $\square$ $\square$.

We have chosen to solve the IQ imbalance imperfections in an experimental manner, without the need for additional signal processing. Our method is based on observing the *upper band* of the OFDM signal on a high resolution (20 MHz or 0.16 pm) optical spectrum analyzer (OSA).

In case of a path mismatch between the I and Q components of the OFDM signal, the impact of the IQ imbalance appears very clearly on the OFDM spectrum. More precisely, a mirror image of the subcarrier $\square$ will be observed on the *-kth* subcarrier since $\square_{\square\square}$ is not zero (Eq. 4-8). The OFDM spectrum obtained after the CMZM is represented in Figure 4-15d.

A simple remedy to path length mismatch is the insertion of a delay line in each of the I and Q electrical paths. Then, by a simple observation of the OFDM spectrum, we can finely tune the delay lines in order to minimize the power level of the lower side-band.

To cope with phase deviations from the optimal $\square$ setting, we can also inspect the upper band of the optical spectrum of OFDM signal after the CMZM, and adjusting the phase voltage Bias 3 so as to maximize the power difference between the upper and lower band over the optical spectrum (Figure 4-15c).

Finally, the spectrum of the OFDM signal in the presence of a gain mismatch between I and Q paths is similar to the spectrum obtained with a phase mismatch (Figure 4-15c). This particular case of imbalance can thus be solved by finely controlling the I and Q voltages at the output of the driver.

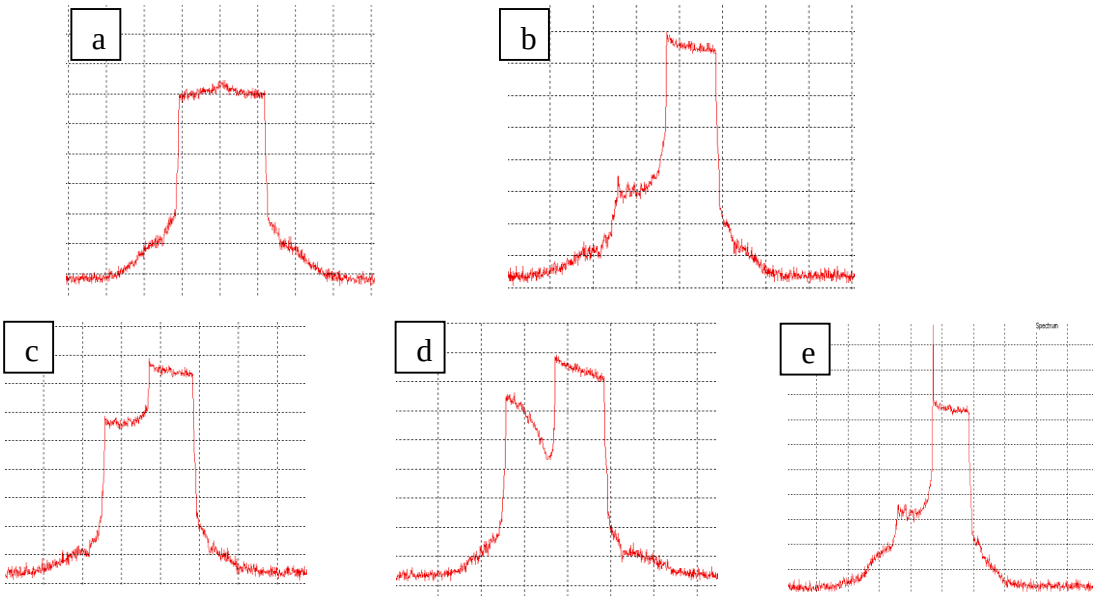

Figure 4-15: Spectra of the OFDM signal for different Tx IQ imbalance issues. a) represents the upper and lower bands of the OFDM signal when the DC component is removed. The other cases represent the upper-band of the OFDM signal: we identify in b) the ideal settings, in c) a phase/gain mismatch, in d) a time mismatch; and in e) the presence of the DC component.

To summarize, IQ imbalance is the result of either a phase, power or delay mismatch between the I and Q tributaries of the OFDM signals. To counteract the impact of the IQ imbalance in the transmitter, we just need to observe the OFDM spectrum at the output of the CMZM. Fine tuning of the bias voltages (Bias 1 and Bias 2) of the two MZMs embedded into the CMZM can be used to remove the carrier that may appear in the middle of the signal spectrum, while fine tuning of the phase (through the bias voltage Bias 3), of the gain (through the use of attenuators) and/or of the delay (by inserting appropriate delay lines) imbalance between the I and Q paths can be achieved by visual inspection of the optical power contained in the lower side-band.

4.3.3 Experimental results

The BER has been measured as a function of OSNR in a 0.1 nm reference bandwidth for the finely adjusted OFDM system. The measured back-to-back sensitivity of this single-band OFDM signal is compared to the back-to-back measurement obtained in [JanM08]. In this reference, the authors have generated two OFDM sub-band signals, each carrying a raw data rate of 10 Gbps. Quite similar digital signal processing algorithms have been implemented, exception made for phase noise compensation. Reference [JanM08] indeed implemented the RF-pilot tone method whereas pilot-tone-based CPE correction with 5 pilot tones has been carried out in our experiments. The two performance curves are shown in Figure 4-16. We measured a BER□□ □□□□ at an OSNR value of 6.5 dB, whereas in the considered reference, the required OSNR is above 8.7 dB. Generally, at low OSNR our system has better performance compared to the reference system, and approximately the same performance at high OSNR. Thus, even though pilot-tone method is not able to cope with the ICI caused by the fast temporal fluctuations of the phase and besides the fact that only 5 pilot tones are used here, the system performance is satisfactory. Generally, when external cavity lasers with line-width around 100 KHz are used and linear or quasi-linear conversion from optical to electrical domain and vice versa is achieved, the pilot-tone approach is an efficient

method to compensate for the impairments caused by phase noise at reasonable complexity. Note however that RF pilot can be used to handle any phase distortions affecting the OFDM signal, carrier-frequency offsets included [JanM08].

For reference purpose, we have also plotted the theoretical performance of 4-QAM modulation at the same data rate. The theoretical BER is given by: □□□ □ □□□□ □□□□□□□□□□□□. In order to compare the sensitivity curve of the single polarization with the theoretical curve, the electrical SNR must be related to the OSNR by the following relation [Ess10]:

$$\text{SNR} = \frac{B_o}{m \cdot B_e} \cdot \text{OSNR} \qquad \text{Eq. 4-9}$$

where m is equal to 1 in the case of single polarization transmission, or 2 in the case of polarization division multiplexing. Here we have $B_o = 0.1$ nm, B_e is the symbol rate and $\text{OSNR}_{0.1\text{nm}}$ is the signal to noise ratio measured in one polarization.
When we compare the sensitivity curve of the single polarization with the theoretical curve, we observe a larger penalty at high OSNRs. At a BER of 10^{-3} corresponding to an OSNR of 6.5 dB, the OSNR penalty with respect to the theoretical curve is 2 dB, while the penalty increases to 5 dB at a BER of 10^{-5} (the corresponding OSNR is 12.5 dB). This is due to the significant impact of ASE on the system performance at low OSNRs, whereas, at high OSNRs, the impact of ASE is reduced and consequently the system is limited by the residual phase error.

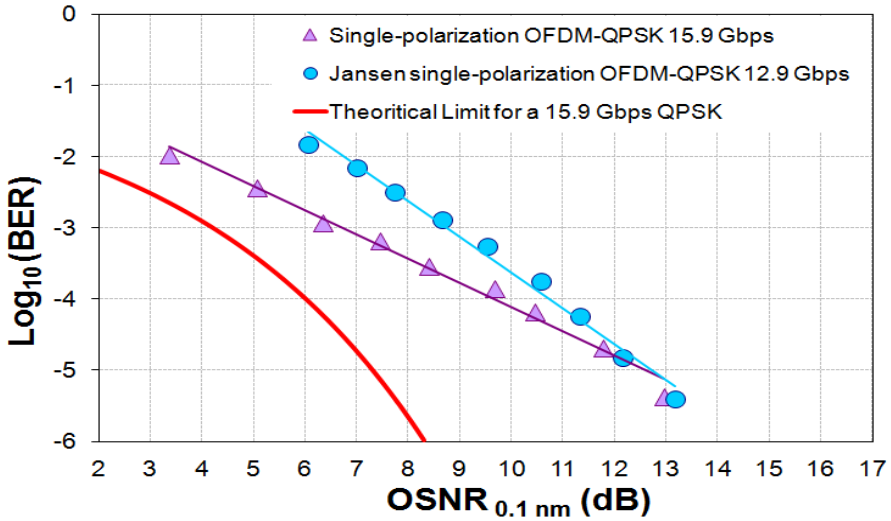

Figure 4-16: BER vs OSNR for optical single-band back-to-back OFDM signal, also we have reproduced the sensitivity curve of the reference [JanM08].

4.4 Dual polarization Tx/Rx design and validation

The implementation of a single-band OFDM Tx/Rx able to transport a total data rate of ~16 Gbps in a bandwidth of 8 GHz has been successfully carried out in the previous section. But in order to achieve a total transmission rate of 100 Gbps, the total data rate must be increased to 32 Gbps in the same bandwidth. This corresponds to an information rate of 25 Gbps, overheads excluded. This increase in data rate will be realized by means of

polarization-division multiplexing of two 16 Gbps OFDM signals in each sub-band. At the receiver side the separation of the two polarization tributaries is achieved by a zero-forcing MIMO equalizer.
In this section we describe the design and the validation of the polarization division multiplexing OFDM system. The performance is evaluated for two different detection scenarios: the first one is homodyne detection, in which the CMZM and the coherent detector share the same laser; the second scenario corresponds to the more realistic case of heterodyne detection, in which two different lasers are used in the transmitter and receiver, respectively. In the latter case, a carrier frequency offset (CFO) arises and must be compensated in order to avoid ICI and thus degradation of the system performance. This task is usually accomplished by means of appropriate frequency synchronization algorithms in the digital receiver.

4.4.1 Experimental validation with homodyne detection

In order to double the spectral efficiency, polarization-division-multiplexing is implemented based on homodyne detection in a first step. Two different transmitters generate two OFDM signals of equal bandwidth, and a polarization beam combiner is used to combine the two polarization components into one DP-OFDM signal. Since this approach requires several pairs of DACs and CMZMs, it is very expensive to implement in a research laboratory. A simple method to emulate a CO DP-OFDM system at reduced cost is depicted in Figure 4-17 below.

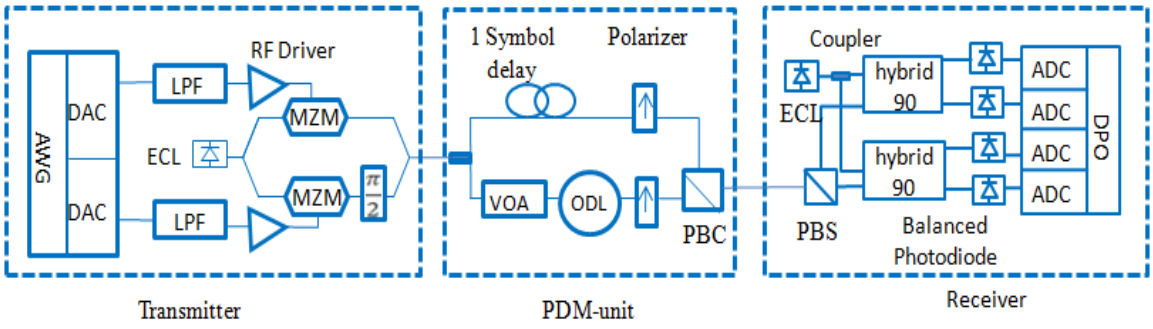

Figure 4-17: Experimental set-up of the CO DP-OFDM system.

In this approach, a single OFDM transmitter is used, instead of two, and connected to a particular polarization-division-multiplexing (PDM) unit made of a 3 dB coupler (which splits the signal into two equal components), a delay line, a variable optical attenuator (VOA), two polarizers and a polarization beam combiner (PBC). The VOA located in the lower arm of the PDM unit is used to adjust the optical power in the two arms so that the two polarization multiplexed tributaries have equal power. The delay line is realized using ~5 meters of fiber and is used to delay the OFDM signal carried by the X polarization by one OFDM symbol period with respect to the OFDM signal carried by the Y polarization. Fine tuning of the delay line is done through the variable optical delay line (ODL) located in the lower arm. This one-symbol-period delay is required in order to distinguish between the training symbols on the two polarizations since they will be received one after the other [Jan08]. As we have seen in section 3.3.4.2 of Chapter 3, two non-zero training symbols distributed among four time slots were shown to be sufficient for obtaining accurate channel estimates. Because of the use of the PDM unit, the OFDM preamble will now include five

training symbols instead of four, organized according to the structure [0 TS 0 TS 0] on each polarization. As illustrated in Figure 4-18, the one-symbol-period delay inserted between the X and Y polarizations will guarantee that the training symbols sent in each polarization will not overlap in time at the receiver side.

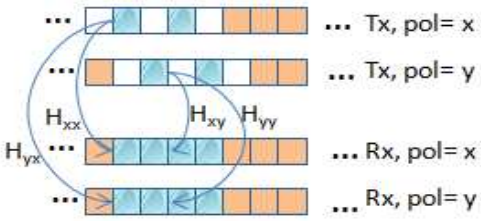

Figure 4-18: Structure of the training symbols used for channel estimation. The transmitted OFDM signal on polarization X is delayed by one OFDM symbol with respect to the signal on polarization Y due to the PDM unit.

In practice, the signal state of polarization (SOP) does not remain constant over long distances in the fiber. This leads to a power exchange between the two polarizations of the propagating DP-OFDM signal, but the orthogonality between the two polarization multiplexed bands is maintained. We have been able to reproduce such a dynamic behavior in our laboratory experiments by inserting a fully random Polarization Scrambler (PS) after the PDM unit. Then the signal is optically amplified, filtered and sent to the oscilloscope (DPO).
The digital OFDM receiver performs timing synchronization, channel estimation based on combining time and frequency-domain averaging methods, 2x2 MIMO zero-forcing equalization and CPE correction using pilot tones.

The BER for the DP-OFDM signal has been plotted as a function of the OSNR measured in a resolution of 0.1 nm in Figure 4-19. In order to validate and assess the performance of the MIMO channel estimation and equalization process for the DP-OFDM signal, we compare its sensitivity curve with the one previously obtained with the single polarization transmission experiment. Recall that a 3 dB difference should, in theory, be measured between the curves corresponding to the single and dual polarization OFDM signals.
An OSNR difference ranging from 2.7 dB to 3.5 dB is measured between the two performance curves in Figure 4-19. Hence we conclude that the proposed MIMO channel estimation and ZF-equalization algorithms does not introduce any additional OSNR penalty.

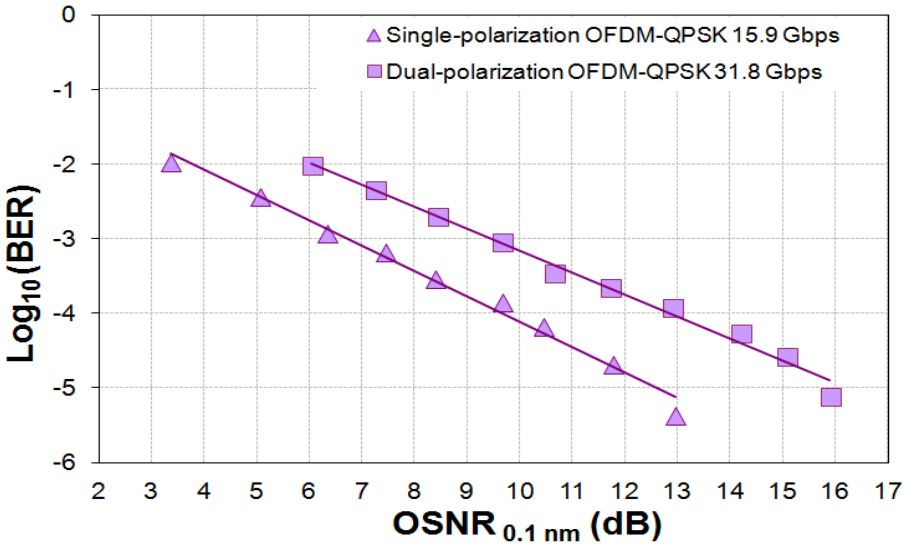

Figure 4-19: BER vs. OSNR for single and dual polarization OFDM signal.

4.4.2 Experimental validation with heterodyne detection

Having validated the performance of CO DP-OFDM transmission in the simplified case of homodyne detection, we now consider the more realistic situation of heterodyne detection, in which two different laser sources are used to drive the CMZM and the coherent detector, respectively. A frequency mismatch between the wavelengths of the transmitter laser and local oscillator will then occur, inducing intercarrier interference (ICI) and performance degradation of the system. The corresponding receiver set-up is depicted in Figure 4-20 below. A frequency-synchronization algorithm has been inserted between timing synchronization and FFT demodulation, in order to estimate and compensate for the carrier frequency offset.

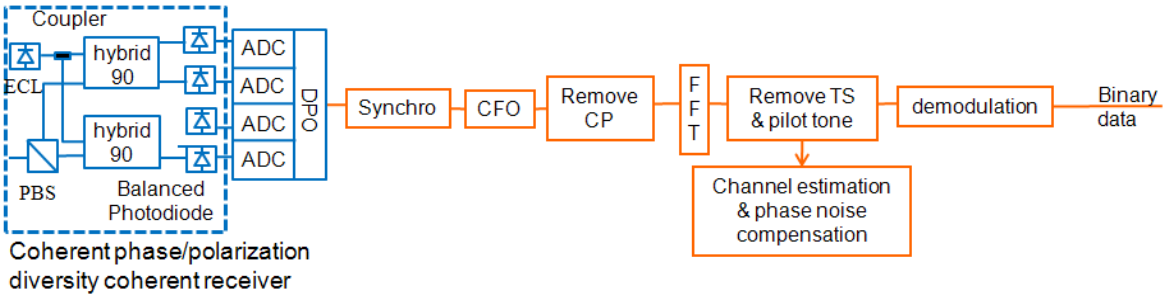

Figure 4-20: Receiver set-up for experimental validation with heterodyne detection.

In order to quantify the speed of variation of the CFO over time, we have plotted with blue colors in Figure 4-21 the fluctuation of the normalized CFO □(see Chapter 3 Section 3.3.3 for the definition of □) during an observation period of 50 minutes. The integer part and fractional part of □are represented in red and green, respectively. From the first to the last measurements, obtained 50 minutes apart, we measure a frequency deviation of 8.□f (□□□□ □ □□□ □ □□□□□□□□□□).

Within the digital receiver, estimation and compensation of the CFO are thus performed in two steps; first we estimate a frequency offset in the range of ±2□f (□f being the sub-carrier

spacing), by following the Minn & Barghava approach (Chapter 3, Section 3.3.3.2) and exploiting the particular time-domain structure of the training symbol used for timing synchronization (As 8 repetitions of a basic sub-symbol with a sign inversion between certain repetitions were considered, after timing synchronization, we have altered the sign of the sub-symbols preceded by a negative sign, and then we have concatenated each two consecutives sub-symbols together in order to estimate the CFO fractional part accurately). Once the fractional part of CFO has been estimated and corrected, we estimate the remaining integer part of the CFO by measuring the frequency shift experienced by the last filled OFDM sub-carriers, and then compensate for it [Kar11].

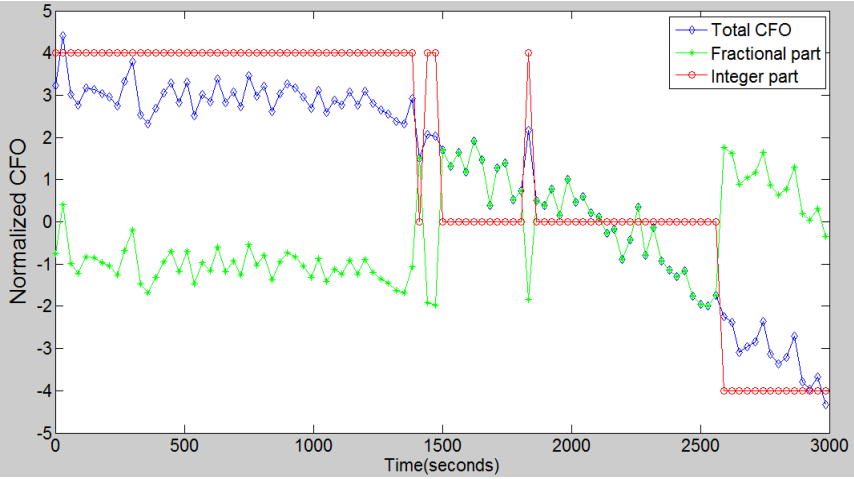

Figure 4-21: Temporal fluctuation of the normalized CFO, including the integer and fractional parts.

Figure 4-22 compares the evolution of BER as a function of the OSNR measured in a 0.1 nm reference bandwidth, for the homodyne and heterodyne detection experiments. In both cases, the generated DP-OFDM signal feeds the polarization scrambler (PS), the amplifier, the filter and then the DPO. For homodyne detection, CFO estimation is not required and the corresponding sensitivity curve (pink square in Figure 4-22) is used as reference, whereas the CFO estimation algorithm is switched on for heterodyne detection. We do not observe any relevant differences between the two performance curves. This validates the efficiency of our CFO synchronization method.

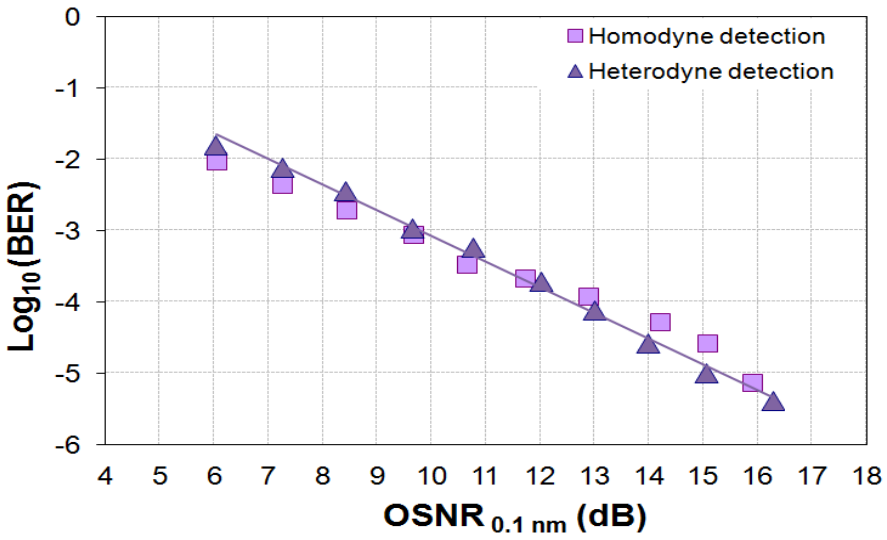

Figure 4-22: BER vs. OSNR (in 0.1 nm) for the CO DP-OFDM system with/without CFO.

4.5 100 Gbps transmitter set-up and validation

After completed the experimental generation of one polarization multiplexed OFDM sub-band carrying an information data rate of 25 Gbps, we describe in this section the transmitter set-up for generating the 100 Gbps multi-band (MB) OFDM signal. The system is validated by comparing its performance with a reference 100 Gbps DP-QPSK system. The comparison is fair in the sense that both systems transport the same effective data rate of 100 Gbps. Note however that the two transmission formats have different overheads, and thus different total data rate, namely 111 Gbps for the DP-QPSK system, compared to ~128 Gbps for the DP-MB-OFDM system.

4.5.1 Multi-band approach for 100 Gbps OFDM signal generation

Figure 4-23 shows the experimental transmitter set-up used to generate the 100 Gbps DP-MB-OFDM signal. A comb of optical carriers spaced by 10 GHz (shown in Figure 4-25) is generated by driving a dual-arm Mach-Zehnder modulator (MZM) with a large amplitude 10 GHz RF frequency according to the recommendations of reference [Sak07].
Thus, higher order side band frequency components with respect to the continuous light are generated. These components are used as a frequency comb because the signal has a constant frequency spacing. However, the spectral flattening is established by finely adjusting the voltage bias of the MZM.

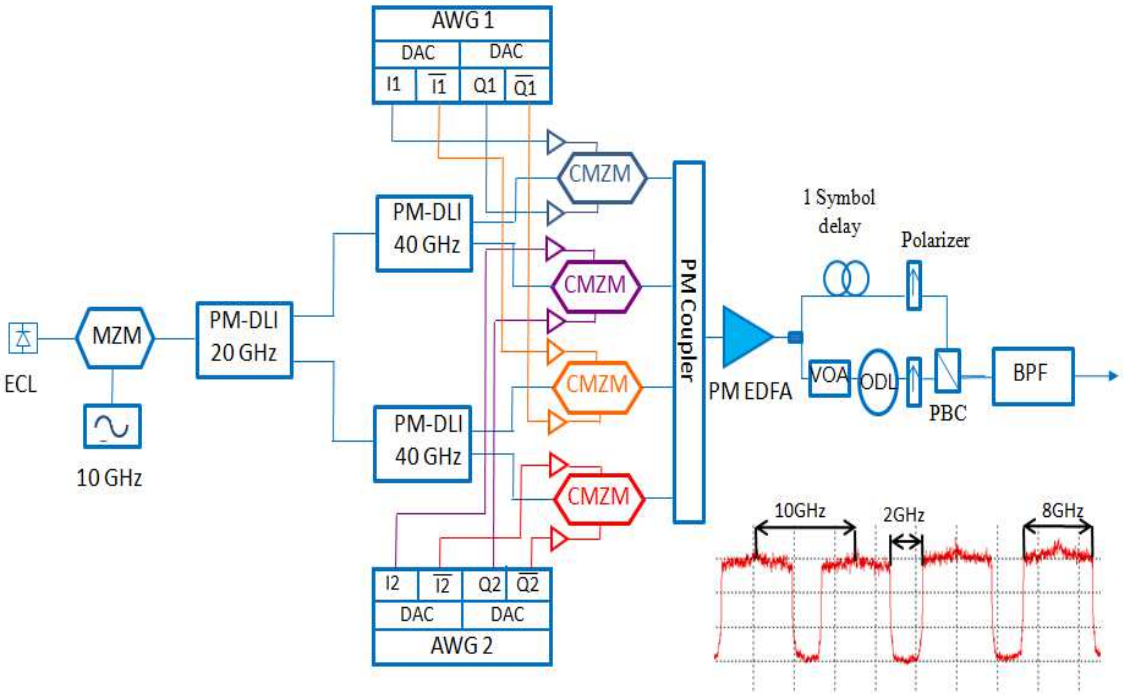

Figure 4-23: Transmitter set-up for the 128 Gbps DP-MB-OFDM signal. The corresponding spectrum is shown in the inset.

As we can see on Figure 4-25, the frequency components around the center frequency have approximately the same intensity and all the frequency components are equally spaced. We mention here that the central frequency corresponds to the frequency generated by the ECL while the other frequencies are dependent on the harmonic order of the MZM. In order to separate the different carriers, polarization-maintaining delay line interferometers (PM-DLI) have been used. The incoming comb of optical carriers is split into two tributaries. The first arm selects the even frequencies, multiples of its designed frequency, while the second arm selects the odd frequencies, also multiples of its designed frequency (Figure 4-24).

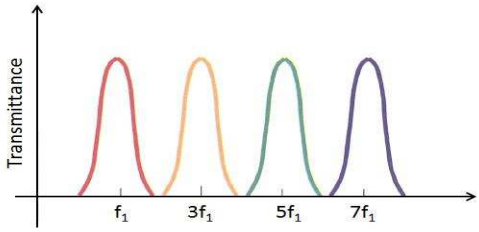

Figure 4-24: Transmittance of one arm of DLI.

Hence a combination of 20 GHz and 40 GHz polarization-maintaining delay line interferometers (PM-DLI) allows to split the initial comb of 10 GHz-spaced sub-carriers into four combs of sub-carriers spaced by 40 GHz. Each comb is individually modulated by a complex-MZM (CMZM), and the four resulting modulated optical signals are combined together through the use of a 4:1 polarization maintaining coupler (Note that an OBPF is inserted to select only 4 subcarriers). Regarding now the generation of the OFDM baseband signals, we take advantage of the fact that our AWGs can provide both a complex I/Q signal and its complement. Hence, overall, two AWGs (instead of 4) are sufficient to build the 4 complex tributaries corresponding to the four sub-bands of our 100 Gbps multi-band OFDM

signal. In order to ensure that the data transported in neighboring sub-bands are decorrelated, AWG 1 generates data for the first and third sub-bands while AWG 2 generates data for the second and fourth sub-bands. A polarization-maintaining Erbium-doped fiber amplifier (PM EDFA) compensates for the losses introduced by the MZM, DLIs, CMZMs and coupler and feeds a polarization-multiplexing module. Then a square flat-top optical band-pass filter (BPF) of ~ 40 GHz bandwidth is used to select the four optical carriers at the transmitter output. The spectrum of our 100 Gbps DP-MB-OFDM signal at the transmitter output is shown in the inset of Figure 4-23.

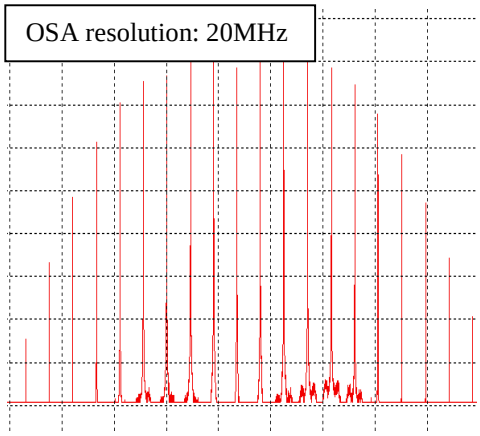

Figure 4-25: Spectrum of the 10 GHz-spaced optical carriers at the MZM output.

4.5.2 Performance comparison with 100 Gbps DP-QPSK system

In order to validate the proposed DP-MB-OFDM system, we have compared its performance in back-to-back configuration with the reference performance of the 100 Gbps DP-QPSK single-carrier system standardized for 100 Gbps long-haul optical transmissions. In particular, if the OFDM system is found to be inferior to the single carrier approach in back-to-back configuration, this precludes the need to further consider CO-OFDM for optical transmission.

We have plotted in Figure 4-26 the BER of 100 Gbps DP-MB-OFDM and 100 Gbps DP-QPSK as a function of OSNR in a 0.1 nm reference bandwidth, in back-to-back configuration. For reference purpose, the performance of 10 Gbps NRZ-OOK is also shown. The transmitter and receiver set-ups of the 100 Gbps DP-QPSK and 10 Gbps NRZ-OOK systems are developed in chapter 5 in paragraphs 5.2.1 and 5.4 respectively. Note that these three formats operate within a bandwidth of 50 GHz. We observe that the OFDM and QPSK systems have approximately the same OSNR performance. This confirms the fact that OFDM is indeed robust to CD and PMD, and suggests that DP-MB-OFDM may be an alternative solution to DP-QPSK for high bit rate transmission provided it also exhibit performance similar to DP-QPSK in the presence of nonlinear effects. Such investigations will be the subject of the next chapter.

Comparison of performance between the 100 Gbps signals and the 10 Gbps signal shows an OSNR difference of about 5 dB at a BER of 10^{-3}, in favor of the NRZ-OOK signal. Hence raising the data rate by a factor of 10 increases the OSNR by a factor of ~4. We conclude that the 100 Gbps CO-OFDM and 100 Gbps CO-QPSK systems present a good tradeoff between increased data rate and OSNR requirements.

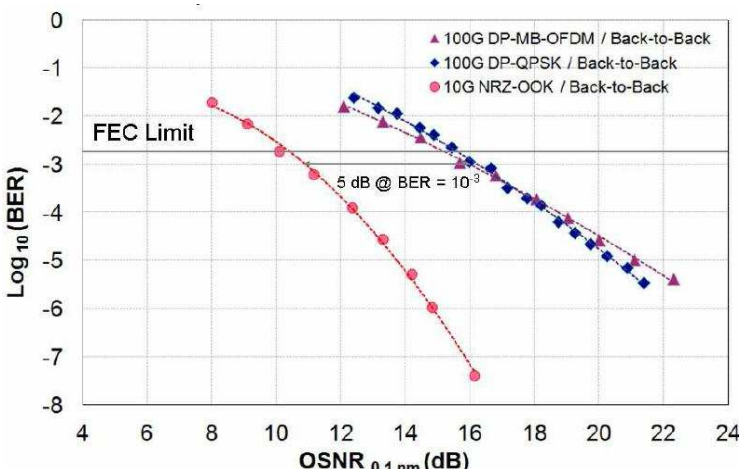

Figure 4-26: BER versus OSNR (in 0.1 nm) measured in back-to-back for DP-MB-OFDM, DP-QPSK, and NRZ-OOK signals.

4.6 Impact of Linear impairments impact

In this section, we investigate the impact of first and second-order PMD on the performance of the 100 Gbps polarization-multiplexed multi-band coherent OFDM system with homodyne detection. The signal polarization is randomly scrambled at the rate 70°/ms before the PMD emulator, for more relevant "field" conditions. Then we investigate the performance of CO-OFDM under first and second order PMD, as well as CD, and with heterodyne detection. This study focuses on the performance of one 25 Gbps OFDM sub-band, chosen in the middle of the MB-OFDM multiplex.

4.6.1 First and second PMD impact on the OFDM system performance

In theory, the presence of the cyclic prefix allows to the CO-OFDM receiver to mitigate PMD without the need for additional signal processing in the digital receiver. Many simulation results as well as experimental measurements carried out in static conditions by considering the worst state of polarization (SOP) case at the PMD generator input indeed confirm the intrinsic robustness of CO-OFDM against first-order PMD (FOPMD). But these measurements have not been done in realistic conditions. As explained in the previous section, the SOP varies with time during system operation, with variation speeds as fast as 72°/ms measured in the "field" [Sal09]. In order to investigate the robustness of the proposed coherent DP-OFDM signal in such realistic transmission conditions, experiments have been carried out by inserting a "General Photonics" PMD emulator able to generate first-order PMD (FOPMD) up to 180 ps as well as second-order PMD (SOPMD) up to ~8220 ps^2. The corresponding experimental setup is depicted in Figure 4-27.

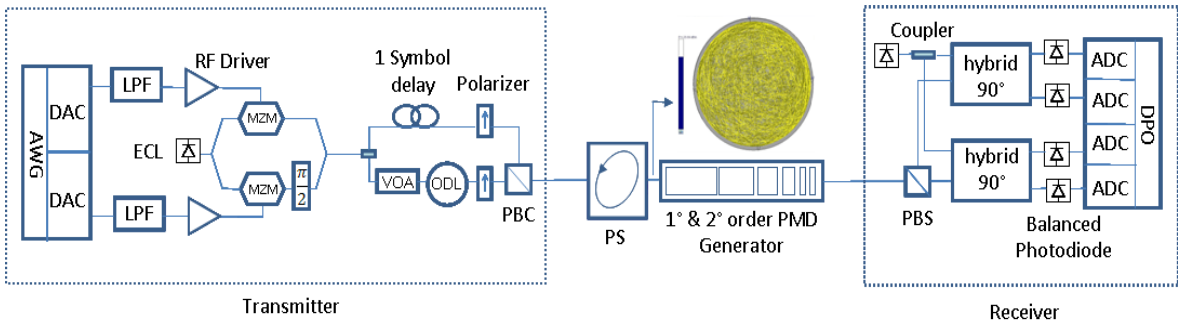

Figure 4-27: Experimental set-up. In inset, the Poincare sphere at the output of the scrambler is represented when the input signal is singly polarized.

The first order PMD, which is the average of the DGD, induces a phase rotation on each OFDM subcarrier that can be compensated directly through appropriate MIMO processing.
The second-order PMD effects are represented by frequency dependent terms; the first term, known as PDC (polarization dependent chromatic dispersion) as accounts for the polarization-dependent variations of the chromatic dispersion variation. The second term is a result of the rotation of the PSP with frequency (see chapter 2). Then, the impact of first order or second order PMD on the CO-OFDM performance is a subcarrier polarization rotation that can be easily treated through channel estimation and then does not induce any impairment on the coherent OFDM signal.

In the experimental setup of Figure 4-27, our coherent DP-OFDM transmitter generates one polarization-multiplexed OFDM sub-band and is connected to the random polarization scrambler (PS) able to emulate SOP variation speed up to 70°/ms. The resulting optical signal is processed by the "General Photonics" PMD emulator, and finally sent to the coherent receiver.

Several experiments have been done. The first experiment consists in evaluating the influence of the speed of SOP variation on the OFDM system performance in the presence of FOPMD. The FOPMD was set to 125 ps, while the SOP variation speed varied between 0°/ms and 70°/ms thanks to our PS. Note that the signal SOP at the PS output is totally random, as shown in the inset of Figure 4-27, where the SOP of a single-polarized signal recorded over one minute is represented. By sake of simplicity, we have done the measurements for a pre-determined value of the OSNR (equal to 9.7 dB) corresponding to a BER=10^{-3} in the back-to-back case. As shown in Figure 4-28, the increase of SOP variation speed up to 70°/ms has no impact on the OFDM system performance. Compared to the OFDM frame structure which is constituted of 105 OFDM symbols of duration 22.75 ns, a SOP variation speed of 70°/ms represents a minor change of ~0.17° per OFDM frame. Thus the channel can be safely considered as time invariant along the OFDM frame duration. Note also that the BER is evaluated over more than hundred frames.
The second experiment aims at measuring the impact of FOPMD on the DP-OFDM signal under the abovementioned realistic field conditions. So the SOP variation speed is fixed to 70°/ms while the FOPMD is varied between 0 ps and 180 ps, at a fixed OSNR of 9.7 dB. Once again, we observe in Figure 4-28 that the increase of FOPMD up to 180 ps does not impact the OFDM system performance. That is due to the presence of the cyclic prefix whose duration was chosen to be larger than the maximum delay introduced by the various sources of dispersion in the fiber (CD and PMD, cf chapter 3).

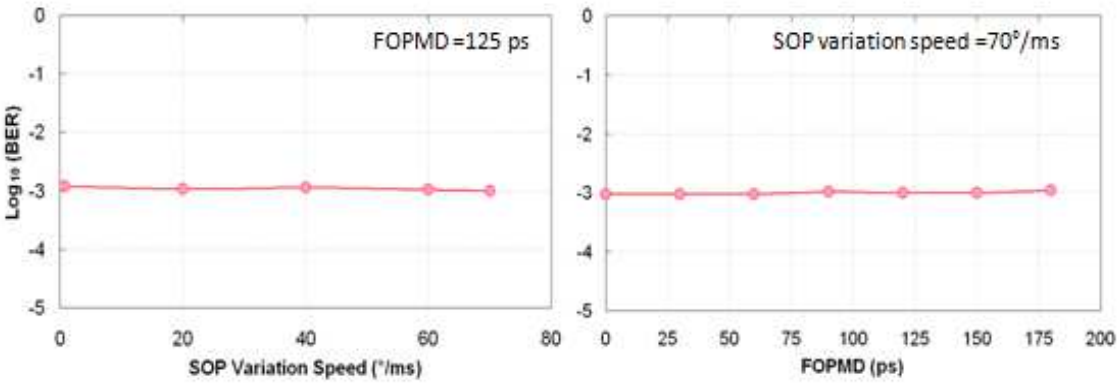

Figure 4-28: Left fig: BER vs. SOP variation speed when FOPMD=125 ps – Right fig: BER vs. FOPMD when SOP variation speed is equal to 70°/ms.

Finally, the third experiment represents the sensitivities curves for four different configurations of FOPMD / SOPMD, namely: 0 ps / 0 ps², 180 ps / 0 ps², 112.6 ps / 6052 ps², and 128.4 ps / 8220.6 ps². The SOP variation speed is still fixed to 70°/ms. Figure 4-29 shows the BER evolution as a function of OSNR. All the sensitivity curves experience an OSNR penalty with respect to the 0 ps/ 0 ps² case which is lower than ~0.5 dB, proving that neither the high FOPMD values nor the high combined FOPMD and SOPMD values have a real impact on the performance of the CO-DP-OFDM system.

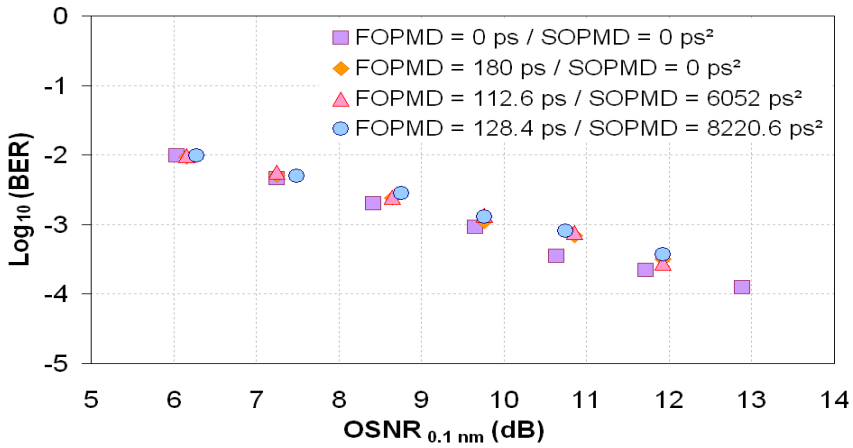

Figure 4-29: BER vs. OSNR (in 0.1 nm) with SOP variation speed equal to 70°/ms for various configurations of FOPMD and SOPMD.

4.6.2 Impact of PMD and CD on the system performance

In this last heterodyne back-to-back characterization experiment, we have inserted to the random polarization scrambler (PS) followed by a PMD emulator and a fixed fibre Bragg grating-based CD emulator (Teraxion ClearSpectrum DCMEX) of 10000ps/nm. Our purpose here was to assess the impact of CD and PMD on the OFDM signal in the absence of nonlinearities. The corresponding experimental set-up is shown in Figure 4-30.

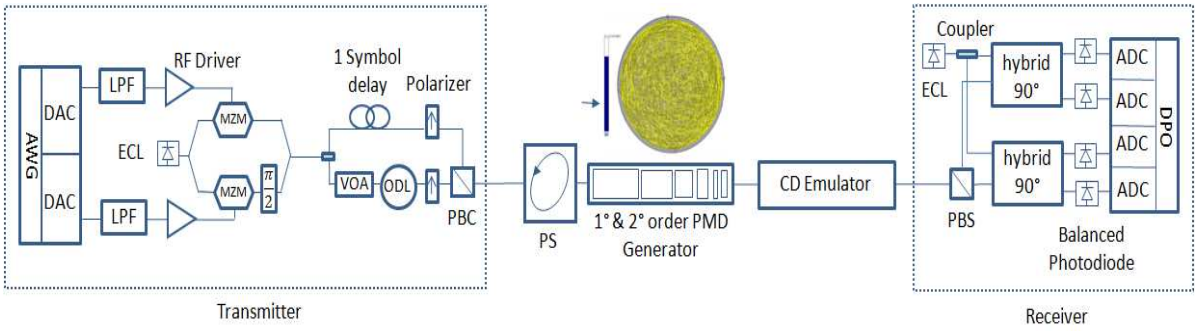

Figure 4-30: Experimental set-up of the dual polarization OFDM sub-band affected by PMD and CD.

The BER as a function of the OSNR measured in a 0.1 nm reference bandwidth is evaluated for various configurations. The CO-OFDM system was stressed out using successively: -10000 ps/nm of CD only, -10000 ps/nm of CD and 180 ps of FOPMD, -10000 ps/nm of CD, 128 ps of FOPMD and 8220 ps² of SOPMD. The results are shown in Figure 4-31. No OSNR penalty is measured in all these configurations at BERs higher than 10^{-4}. At lower BERs, however, an error floor appears around 10^{-5}, showing that high values of CD and PMD do impact the system performance. Note that the presence of CD and PMD does not impact our CFO estimation algorithm as this error floor around 10^{-5} has also been observed in the case of homodyne detection.
The CD emulator is suspected to be the cause of this error floor. Indeed, as we will see in the next chapter, the floor does not appear after signal transmission along 1000 km of SSMF, and better performance is obtained around BER of ~10^{-5}; however we are not able to know if an error floor still exists below this BER limit since the system performance is then limited by intra-channel nonlinearities.

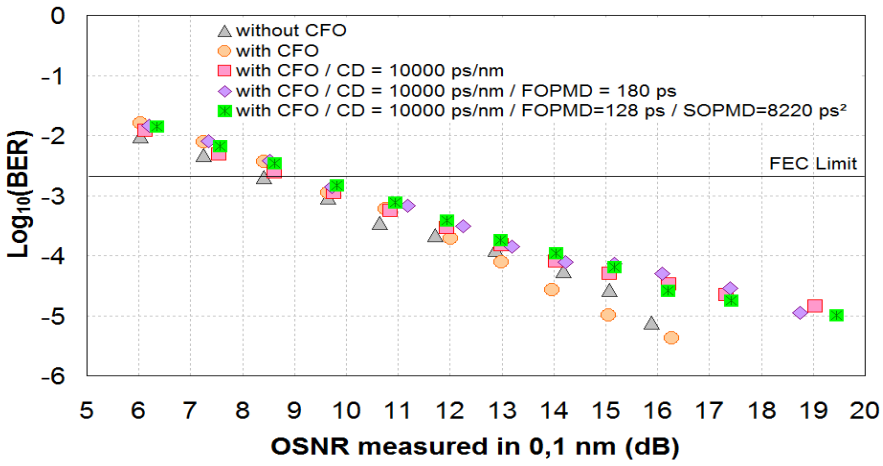

Figure 4-31: BER vs. OSNR (in 0.1 nm) with and without CFO for various configurations of CD, FOPMD and SOPMD.

4.7 Conclusion

In this chapter, we have detailed the successive experimental implementation steps that we have followed to successfully demonstrate a CO DP-MB-OFDM system operating at 100 Gbps.
Briefly, the transmitter set-up is constituted of an AWG with two DACs operating at 12 GSa/s for I and Q signals generation, followed by anti-aliasing low pass filters, fanouts, drivers and an optical IQ mixer. At the output of the optical modulator, the optical OFDM signal feeds a PDM unit. The raw data rate of the generated DP-OFDM signal is 25 Gbps. In order to obtain a total data rate of 100 Gbps in a 50 GHz bandwith, a multi-band OFDM signal composed of 4 polarization multiplexed 25 Gbps DP-OFDM sub-bands is generated, by means of a comb generator comprising a MZM driven by an RF frequency with high amplitude, followed by the combination of 20 GHz and 40 GHz polarization-maintaining delay line interferometers (PM-DLI). We obtain 4 combs of sub-carriers that feed 4 optical modulators each driven by the I and Q components of the 4 OFDM signals. The signals at the outputs of CMZMs are finally polarization multiplexed and filtered.
At the receiver side, one sub-band OFDM signal is detected by a polarization diversity coherent receiver using a ~100 kHz bandwidth external cavity laser as local oscillator. The signal is converted back to the digital domain using a 50 GSa/s real-time oscilloscope (DPO). "offline" digital signal processing (DSP) is then performed to retrieve the transmitted data.

The system performance and the developed digital signal processing have been validated. The impact of CD and PMD on the system performance has also been investigated and was shown to be negligible (no penalty) for BERs greater than or equal to 10^{-4}.

This chapter did not consider the impact of nonlinear effects on the system performance. This is the subject of the next chapter, which investigates the performance of the proposed OFDM format in a WDM transmission context over 1000 km of G.652 fiber line.

Bibliography

[Ami10] A. A. Amin, S. L. Jansen, H. Takahash, I. Morita, and H. Tanaka, "A hybrid IQ imbalance compensation method for optical OFDM transmission," *Optics express*, vol. 18, 2010.

[Cao11] S. Cao, C. Yu, and P.-Y. Kam, "Decision-Aided Joint Compensation of channel distortion and transmitter IQ imbalance for coherent optical OFDM," in *IEEE MWP*, 2011.

[Ess10] R.-J. Essiambre, G. Kramer, P. Winzer, G. J. Foschini, and B. Goebel, "Capacity limits of optical fiber networks," *Journal of Lightwave Techonology*, vol. 28, 2010.

[Jan08] S. L. Jansen, I. Morita, T. C. W. Schenk, and H. Tanaka, "Long-haul transmission of 16x52.5 Gbits/s polarization-division-multiplexed OFDM enabled by MIMO processing," in , vol. 7, Feb. 2008, pp. 173-182.

[Jan09] S. L. Jansen, I. Morita, T. Schenk, and H. Tanaka, "121.9-Gb/s PDM-OFDM transmission With 2-b/s/Hz spectral efficiency over 1000 km of SSMF," *Journal of lightwae technology*, vol. 27, 2009.

[JanM08] S. L. Jansen, I. Morita, T. C. W. Schenk, N. Takeda, and H. Tanaka, "Coherent Optical 25.8-Gb/s OFDM Transmission Over 4160-km SSMF," *Journal of lightwave technology*, 2008.

[Kar11] J. Karaki, E. Pincemin, Y. Jaouën, and R. L. Bidan, "Frequency offset estimation robustness of a Polarization-Multiplexed Coherent OFDM system stressed by 180-ps instantaneous PMD and 10000-ps/nm chromatic dispersion," in *CEO US*, 2011.

[LiY06] Y. Li and G. L. Stüber, *Orthogonal frequency division multiplexing for wireless communications*. Springer, 2006.

[Min03] H. Minn, V. K. Bhargava, and K. B. Letaief, "A robust timing and frequency synchronization for OFDM systems," *IEEE transactions on wireless communications*, vol. 2, no. 4, pp. 8022-839, Jul. 2003.

[Opp99] A. V. Oppenheim, R. W. Schafer, and J. R. Buck, *Discrete-time signal processing*. New Jersey: Prentice Hall, 1999.

[Sak07] T. Sakamoto, T. Kawanishi, and M. Izutsu, "Asymptotic formalism for ultraflat optical frequency comb generation using a Mach–Zehnder modulator," *optics letters*, vol. 32, 2007.

[Sal09] S. Salaun, F. Neddam, J. Poirrier, B. Raguenes, and M. Moignard, "Fast SOP Variation Measurement on WDM Systems, Are the OPMDC Fast Enough?," in *ECOC*, 2009.

[Sch08] T. Schenk, *RF imperfections in high-rate wireless systems*. Springer, 2008.

[Shi10] W. Shieh and I. Djordjevic, *OFDM for optical communications*. Elsevier, 2010.

[Tan07] Y. Tang, W. Shieh, X. Yi, and R. Evans, "Optimum design for RF-to-optical up-converter in coherent optical OFDM systems," *IEEE photonics technology letters*, vol. 19, no. 7, pp. 483-485, Apr. 2007.

[Yan06] K. Yang. (2006) Flatten DAC frequency response.

5 100 Gbps Transmission Experiments

Chapter 5

100 Gbps Transmission Experiments

The maximum capacity transported by 10 Gbps WDM long-haul transmission systems operating on a 50 GHz channel grid is ~ 1 Tbps on the C-band, corresponding to a spectral efficiency of 0.2 bit/s/Hz. Today Coherent Dual-Polarization Quadrature Phase Shift Keying (DP-QPSK) is the industrial solution for 100 Gbps long-haul WDM transport [Alc]. Two strategies are envisaged to deploy the 100 Gbps technology. The first strategy consists in upgrading legacy system infrastructure at 100 Gbps through the insertion of DP-QPSK channels into the existing dispersion-managed 10 Gbps NRZ-based WDM system. The second strategy consists in implementing 100 Gbps DP-QPSK WDM system for DCF-free transmission, so that all 10 Gbps channels will be replaced by 100 Gbps DP-QPSK channels. In both strategies, the aim is to transport 100 Gbps WDM channels on a 50 GHz ITU grid, enabling 2 bit/s/Hz spectral efficiency.
Coherent DP-QPSK is a transmission technique resistant to linear transmission impairments such as CD and PMD. On the other hand coherent dual-polarization multi-band OFDM (DP-MB-OFDM) has been also proposed in the past few years for 100 Gbps application, and remains today a very interesting candidate for WDM transmission at 400 Gbps and 1 Tbps. However, a debate exists about whether OFDM can be as efficient as single-carrier QPSK modulation for long-haul WDM transmission, due to its supposed higher sensitivity to fiber nonlinearities.

In this chapter we start our investigations by comparing the performance of 100 Gbps coherent DP-MB-OFDM and 100 Gbps coherent DP-QPSK signals for 10x100 km transmission over G.652 fiber without insertion of any dispersion compensation fiber module (DCM). This type of line configuration is better known under the name of DCF-free configuration. Two different schemes are thus studied: the first one corresponds to the "Single-Channel" configuration in which only two well-spaced channels carry 100 Gbps data traffic (one supporting DP-MB-OFDM modulation and the other one DP-QPSK format), while the other wavelengths do not transport any traffic; the second one corresponds to the "WDM" configuration in which the two previous channels are coupled with 50-GHz spaced wavelengths modulated with 100 Gbps DP-QPSK modulation. We demonstrate that DP-MB-OFDM is as robust as DP-QPSK for 100 Gbps transmission in the "Single-Channel" and "WDM" configurations: this result brings a clear response to the usual point of view predicting that OFDM is intrinsically more sensitive to fiber nonlinearities. It constitutes an original and new input to the debate over the respective performance of OFDM and single-carrier modulation techniques for long-haul WDM transmission.

A second original contribution of our work has consisted in comparing the relative performance of 100 Gbps coherent DP-MB-OFDM and 100 Gbps coherent DP-QPSK formats for transmission over a G.652 fiber-based dispersion-managed (DM) line. In a first step, only 100 Gbps channels carrying either DP-MB-OFDM or DP-QPSK have been implemented over this DM transmission line. This configuration provides a reference for experiments which have been made in a second step. These experiments correspond to the case of legacy transport infrastructure, constituted exclusively of G.652 fiber and 10 Gbps NRZ-OOK WDM system. In this scheme, 100 Gbps channels are introduced by switching-off 10 Gbps wavelengths. This cost-effective configuration enables to carry out a smooth and progressive up-grade of already deployed 10 Gbps WDM links. Through the simultaneous propagation of two well-spaced 100 Gbps coherent DP-MB-OFDM and

100 Gbps coherent DP-QPSK channels in a 78x10 Gbps NRZ-OOK WDM transmission system we compare the respective performance of these two modulation techniques over a 10x100-km DM G.652 fiber-based line. We show that both 100 Gbps DP-MB-OFDM and 100 Gbps DP-QPSK are not able to operate under the FEC threshold even in the presence of a guard-band between the 10 Gbps and 100 Gbps channels. However, by reducing the power of 10 Gbps NRZ-OOK channels with respect to that of the 100 Gbps signals, 100 Gbps DP-MB-OFDM and DP-QPSK channels recover some performance and can be considered error-free (after FEC) after 1000-km propagation. Furthermore, even for this particular configuration quite detrimental for fiber nonlinear effects, we show that 100 Gbps coherent DP-MB-OFDM is not so disadvantaged when compared to 100 Gbps coherent DP-QPSK modulation. This result is also new and original, and provides some constructive answers to skeptical people who believe that OFDM is highly more sensitive to fiber nonlinearities than single-carrier DP-QPSK modulation.

5.1 Representation of the performance curves

The performance assessment of 100 Gbps coherent DP-MB-OFDM and 100 Gbps coherent DP-QPSK signals for 10x100 km transmission over G.652 fiber are carried out by plotting their sensitivity curves in two different mode of representation. One of them is the representation of the BER as a function of the input power per span per channel denoted by $P_{IN\ SPAN}$. $P_{IN\ SPAN}$ is the output power of any amplifier inserted at the beginning of a span so that the same power $P_{IN\ SPAN}$ is launched into all the spans. A second representation mode consists in plotting the BER as a function of the received OSNR measured in a 0.5 nm reference bandwidth, using the fact that an increase of 1 dBm in $P_{IN\ SPAN}$ increases the received OSNR by ~1 dB. This type of representation permits the superimposition of the sensitivity curves obtained after transmission with the one measured in back-to-back, thereby deducing the transmission OSNR penalty which is defined as the OSNR difference measured between the back-to-back and the sensitivity curves at the optimum BER obtained after transmission.

We show in Figure 5-1 the two modes of representation for the 100 Gbps coherent DP-MB-OFDM signal after transmission over 10x100 km of G.652 without the insertion of the DCM module. The BER in function of $P_{IN\ SPAN}$ is plotted in the left hand side of Figure 5-1. The $P_{IN\ SPAN}$ is incremented by 1 dB at each measurement. The optimum input power obtained after transmission is 1 dBm given the lowest BER of ~$2.5x10^{-5}$.

The BER as a function of received OSNR measured in 0.5 nm is plotted in the right side of Figure 5-1. The sensitivity curve after the transmission matches the sensitivity curve of the back-to-back one at low OSNRs (below 13 dB) revealing that the system performance is just limited by the accumulated amplified spontaneous (ASE) noise generated by the amplifiers. A better performance is obtained around the BER of ~$2.5x10^{-5}$ corresponding to an optimum OSNR of 15 dB and resulting in an OSNR penalty of 2 dB. However for an OSNR higher than 15 dB, the system performance is limited by intra-channel nonlinear effects.

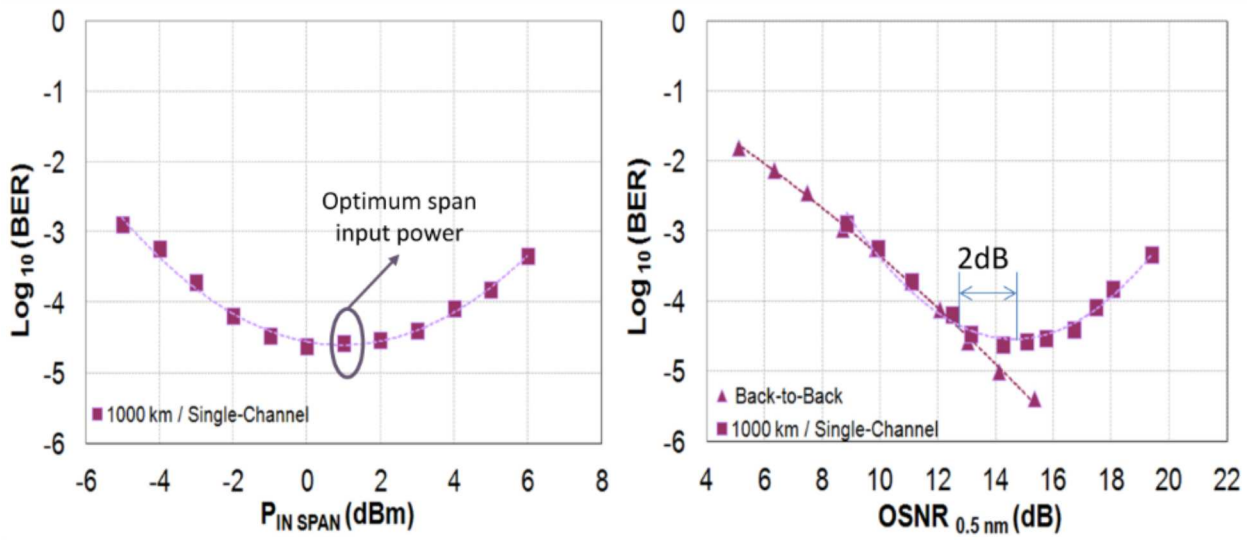

Figure 5-1: BER vs. P_{inspan} (left fig) and BER vs. received $OSNR_{0.5\ nm}$ (left fig) after 1000 km of transmission over the DCF-free G.652 fiber line in "Single-Channel" and after the back-to-back design.

5.2 Mixed 100 Gbps DP-MB-OFDM and 100 Gbps DP-QPSK transmission over DCF-free fiber line

The DP-MB-OFDM and DP-QPSK signals operating both at 100 Gbps are now simultaneously transmitted over our 10x100 km G.652 fiber line. Note that in this section, the transmission line adopts the DCF-free configuration, i.e. no in-line chromatic dispersion compensation module (DCM) is used or, equivalently, dispersion management is not implemented. Performance comparison between the two modulation techniques (100 Gbps coherent DP-MB-OFDM and 100 Gbps coherent DP-QPSK) is carried out here for the two following configurations: the first one is the "**Single-Channel**" configuration, in which each of the two widely spaced channels (the first one carrying the 100 Gbps coherent DP-MB-OFDM channel, and the other one the 100 Gbps coherent DP-QPSK signal) are transmitted over the transmission line while the other wavelengths do not transport any signal; the second configuration is the "**WDM**" one, for which the two previous channels are coupled with 50 GHz-spaced wavelengths carrying 100 Gbps coherent DP-QPSK signals. Before investigating the transmission performances of the OFDM and QPSK systems, we will begin by introducing the DP-QPSK experimental set-up.

5.2.1 100 Gbps DP-QPSK transceiver description

The DP-QPSK transmitter structure is described in Figure 5-2. A CMZM which includes two MZM modulators in its two parallel arms is fed by an external cavity laser (ECL). Subsequently, the light is split into two tributaries and then sent to the two MZM modulators. Each MZM modulator is driven by a 2^{15}-1 pseudo random binary bit sequence (PRBS) and then generates an optical signal with two phase levels $\{0, \pi\}$. However, as the phase of the signal passing through one arm of CMZM is shifted by $\pi/2$ with respect to the second arm, the output of the CMZM produces four phase levels, $\{0, \pi/2, \pi, 3\pi/2\}$, which is equivalent to the generation of the four QPSK symbols. After that, the dual-polarization QPSK signal is generated by connecting the output of the CMZM to a polarization-multiplexing module. A 10-ns timing delay is introduced between the two replicas of the

QPSK signal into the polarization-multiplexing module in order to de-correlate the two polarization multiplexed QPSK signals.

The targeted 100 GbE raw data rate is ~104 Gbps. After including 7% overhead for Forward Error Correction (FEC), the global data rate of DP-QPSK channels is increased up to 112 Gbps. In that case, the total data rate carried by each polarization is equal to 56 Gbps and corresponds to the data rate generated at the output of the CMZM. Consequently, each MZM modulator must operate at a symbol rate of 28 Gbaud and subsequently must be fed by a 2^{15}-1 PRBS at 28 Gbps. The significant reduction of the symbol rate offered by the DP-QPSK modulation format in comparison with two levels formats without polarization multiplexing makes the 28 Gbaud DP-QPSK signal compliant with the 50 GHz channel spacing (or, equivalently with the 50 GHz ITU grid).

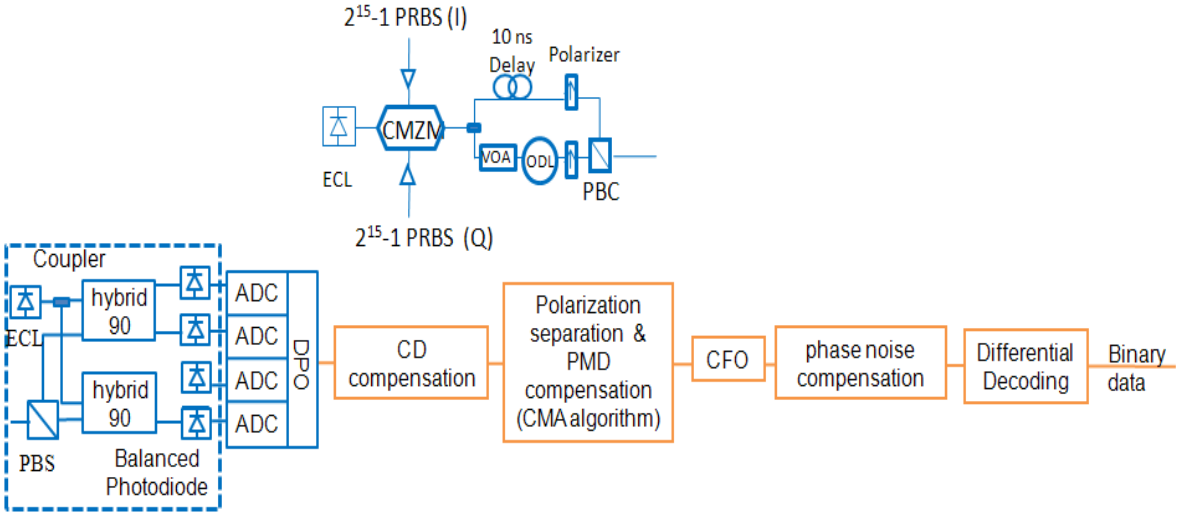

Figure 5-2: DP-QPSK transmitter and receiver set-up.

At the receiver side, the signal is selected by a square flat-top optical band-pass filter (OBPF) of 0.4 nm bandwidth, and detected by a polarization diversity coherent receiver using a ~100 kHz line-width ECL as a local oscillator (LO). The signals are converted back to the digital domain by the use of a 50 GSa/s real-time oscilloscope (DPO). "Offline" digital signal processing (DSP) is then performed. It is based on blind equalization and more particularly on the constant modulus algorithm (CMA) which carries out polarization separation and residual chromatic dispersion (CD) compensation [Sav08]. The ~17000 ps/nm CD accumulated in the line is compensated for through the well-known time-domain-equalization (TDE) method described in [Sav08] which permits to determine the coefficients of the two finite impulse response (FIR) filters for the polarization X and Y. Frequency offset compensation and carrier phase estimation are done by the methods described in [LyG06]. Differential decoding is used to avoid cycle slips issues.

5.2.2 100 Gbps Transmission performance

Our previously described 100 Gbps DP-MB-OFDM transmitter operating at 1552.93 nm is introduced into a multiplex of forty 50-GHz-spaced wavelengths modulated at 100 Gbps by the DP-QPSK format (Figure 5-3). Only one 100 Gbps DP-QPSK channel is fed by an ECL at 1548.11 nm, while the thirty-nine other channels are fed by standard laser diodes (LD). The 100 Gbps DP-QPSK odd and even channels are separately multiplexed, independently

modulated, combined with the 100 Gbps DP-MB-OFDM transmitter through a coupler. The transmission line is constituted of 10 spans of 100 km of G.652 standard single-mode fiber (SSMF) separated by EDFAs with 20 dB gain and a 5.5 dB noise figure. In the middle of our transmission line, a dynamic gain equalizer (DGE) is inserted in order to flatten the multiplex power after 1000 km. No dispersion compensation fiber (DCF) is introduced between the SSMF spans, resulting in optimal propagation conditions for the channels.

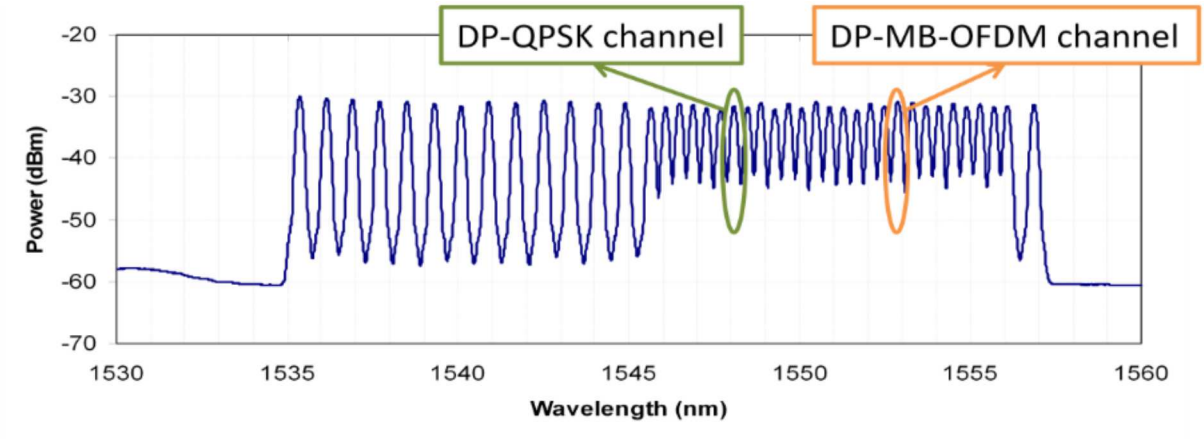

Figure 5-3: Spectrum of the forty-one 100 Gbps channels including the two channels under measurement, i.e. the 100 Gbps DP-QPSK and 100 Gbps DP-MB-OFDM channels.

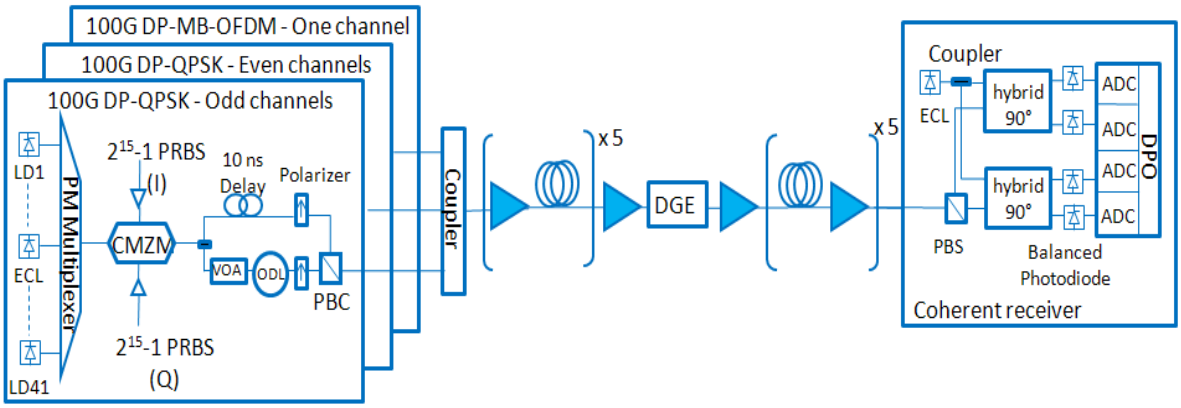

Figure 5-4: Set-up of the 100 Gbps DP-MB-OFDM and DP-QPSK transmitters, 1000 km DCF-free transmission line and coherent receiver.

At the receiver side, the signals are detected by a polarization diversity coherent receiver using a ~100 kHz line-width ECL as LO. The signals are converted back to the digital domain with a 50 GSa/s real-time oscilloscope (DPO). In the DP-MB-OFDM detection case, the LO wavelength is tuned to the centre of the OFDM sub-bands under measurement. Then, digital signal processing is performed as described previously for each of the two modulation formats (i.e. DP-QPSK and DP-MB-OFDM).

5.2.2.1 Experimental Results: BER Vs PIN SPAN

Two different configurations have been evaluated here. In the first one referred to as "Single-Channel" configuration in Figure 5-5, the wavelengths were not modulated except for the channel at 1552.93 nm which carries the 100 Gbps DP-MB-OFDM signal and for the

channel at 1548.11 nm which transports the 100 Gbps DP-QPSK signal. The second configuration, called "WDM" in Figure 5-5, corresponds to the WDM propagation of mixed 100 Gbps DP-MB-OFDM and 100 Gbps DP-QPSK channels as described in the previous paragraph.

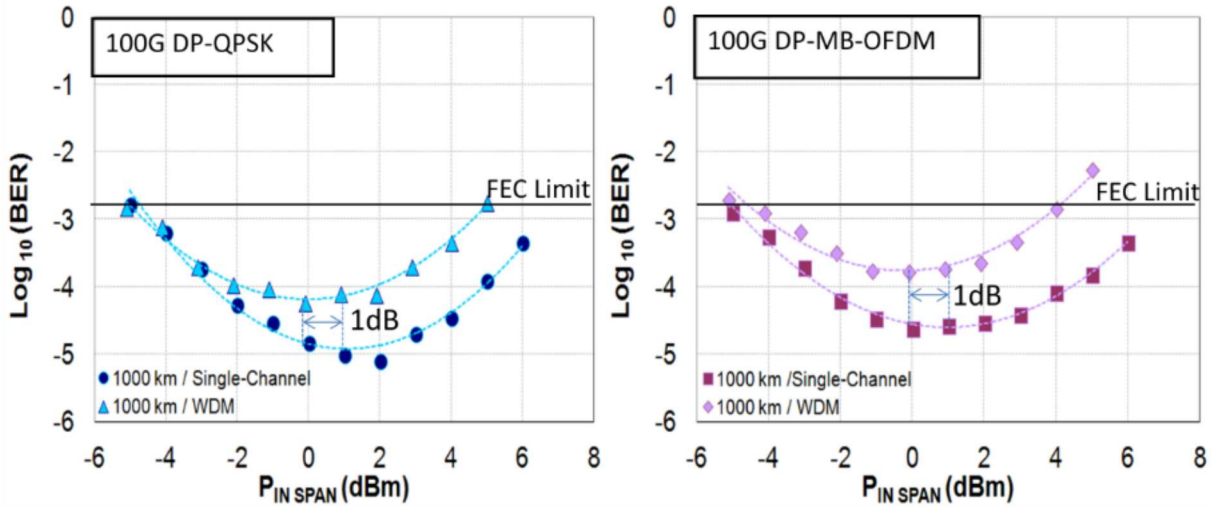

Figure 5-5: BER vs. span input power per channel for 100 Gbps DP-MB-OFDM (right fig) and DP-QPSK (left fig) after 1000 km of transmission over DCF-free G.652 fiber line in "Single-Channel" and "WDM" configurations.

Figure 5-5 summarizes our experimental results. On the left and right hand sides of Figure 5-5 the BER is plotted as a function of the $P_{IN\ SPAN}$ for the two 100 Gbps DP-QPSK and 100 Gbps DP-MB-OFDM channels, respectively. When we compare the "Single-Channel" configuration to the "WDM" one, we notice that the "Single-Channel" configuration is better than the "WDM" one by approximately one decade in BER and ~1 dB in $P_{IN\ SPAN}$ for the two formats under study. It clearly signifies that the XPM and its corollary XPolM exacerbated by the "WDM" scheme badly impact the WDM transmission even in its DCF-free configuration. The peak-to-average-power-ratio (PAPR) of 100 Gbps DP-MB-OFDM and 100 Gbps DP-QPSK increases regularly over a DCF-free transmission line. In the "Single-Channel" configuration, only the SPM excited at the locations of the high peaks impacts the transmission performance, while in the "WDM" configuration, the inter-play between the high-peaks in the neighboring channels through XPM and XPolM adds an extra-penalty to the WDM system performance.

When we compare now the two modulation formats between them, we notice that in the "Single-Channel" configuration, after 1000 km transmission, the 100 Gbps DP-QPSK channel (BER~$1x10^{-5}$ at $P_{IN\ SPAN}$ ~ 1 dBm) is a little better than the 100 Gbps DP-MB-OFDM channel (BER~$2.4x10^{-5}$ at $P_{IN\ SPAN}$ ~ 0 dBm) both in terms of BER and optimal span input power. Also, in the "WDM" configuration, DP-QPSK (BER~$6x10^{-5}$ at $P_{IN\ SPAN}$ ~ 0 dBm) is still slightly better than DP-MB-OFDM (BER~$1.7x10^{-4}$ at $P_{IN\ SPAN}$ ~0 dBm). This indicates a slightly higher sensitivity of the 100 Gbps DP-MB-OFDM format to nonlinear effects when compared to 100 Gbps DP-QPSK. This observation is related to the exacerbation of FWM that occurs between OFDM subcarriers [Low07]. However, in this case, this effect is controlled due to the continuous accumulation of chromatic dispersion along the line in this "DCF-free" transmission configuration: the phase matching conditions which are mandatory to exacerbate inter-band FWM are rarely met, and this limits in turn the FWM impact [Liu09].

It should be noted at this point that no algorithm for fiber nonlinearities compensation or limitation was implemented or even considered here. Algorithms for nonlinear compensation can be found in [Shi08] and [Liu09].

5.2.2.2 Experimental Results: BER Vs OSNR

On the left and right hand sides of Figure 5-6, we present the same results as previously but with a different mode of representation. The BER is plotted as a function of the received OSNR measured in 0.5 nm for the two 100 Gbps DP-QPSK and 100 Gbps DP-MB-OFDM channels, respectively. As explained above, this mode of representation is particularly valuable because it permits to superimpose the sensitivity curves obtained after transmission with the ones measured in back-to-back, allowing to immediately measure the OSNR penalty induced by the transmission.

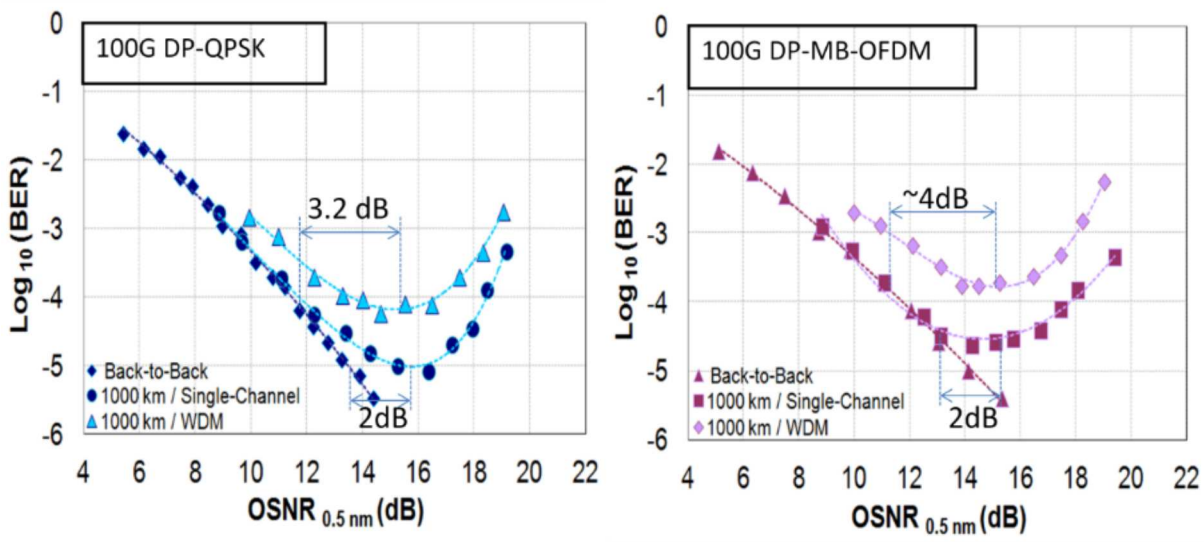

Figure 5-6: BER vs. received OSNR $_{0.5\ nm}$ for 100 Gbps DP-MB-OFDM (right fig) and DP-QPSK (left fig) after 1000 km of transmission over the DCF-free G.652 fiber line in "Single-Channel" and "WDM" configurations and after the back-to-back design.

Under "Single-Channel" configuration, for the two systems under study, the OSNR penalties are very similar, ~ 2dB at the optimum span input power for both 100 Gbps DP-QPSK and 100 Gbps DP-MB-OFDM formats, respectively. However, as already noticed, the BERs of the 100 Gbps DP-MB-OFDM and DP-QPSK channels are slightly different and better for the DP-QPSK format. These results confirm our previous interpretations. Note as well that globally the 1 dB channel power increase at the span inputs results in 1 dB OSNR improvement, but sometimes there is some imperfections due to power fluctuations in time of the power of the 100 Gbps channels at the transmitter side. It is thus the fit of the curve which is important, and not the curve which passes by each measurement points.

In the "WDM" configuration, at the optimum span input power, the transmission OSNR penalties are equal to ~ 3.2 dB for DP-QPSK and ~ 4 dB for DP-MB-OFDM. This 0.8-dB extra-penalty confirms that the 100 Gbps DP-MB-OFDM channel is slightly more sensitive to fiber nonlinearities than the 100 Gbps DP-QPSK channel.

5.3 Mixed 100 Gbps DP-MB-OFDM and 100 Gbps DP-QPSK transmission over dispersion-managed (DM) fiber line without the presence of 10 Gbps NRZ-OOK channels

The same multiplexing scheme as previously presented in Figure 5-3 is used here. However, hereafter the transmission is carried out over a DM G.652 fiber line. The DM transmission line shown in Figure 5-7 is constituted of a pre-compensation stage of -1000 ps/nm at 1550 nm, followed by ten spans of 100 km of G.652 SSMF, separated by double-stage EDFAs with 30 dB gain and a 5.5 dB noise figure, whose inter-stage is equipped with a DCM adapted to 90 km SSMF spans. In the middle of our transmission line, a DGE is inserted in order to flatten the multiplex power after 1000 km. A post-compensation stage of -700 ps/nm brings back to ~0 ps/nm the cumulated dispersion of the channel at 1550 nm.

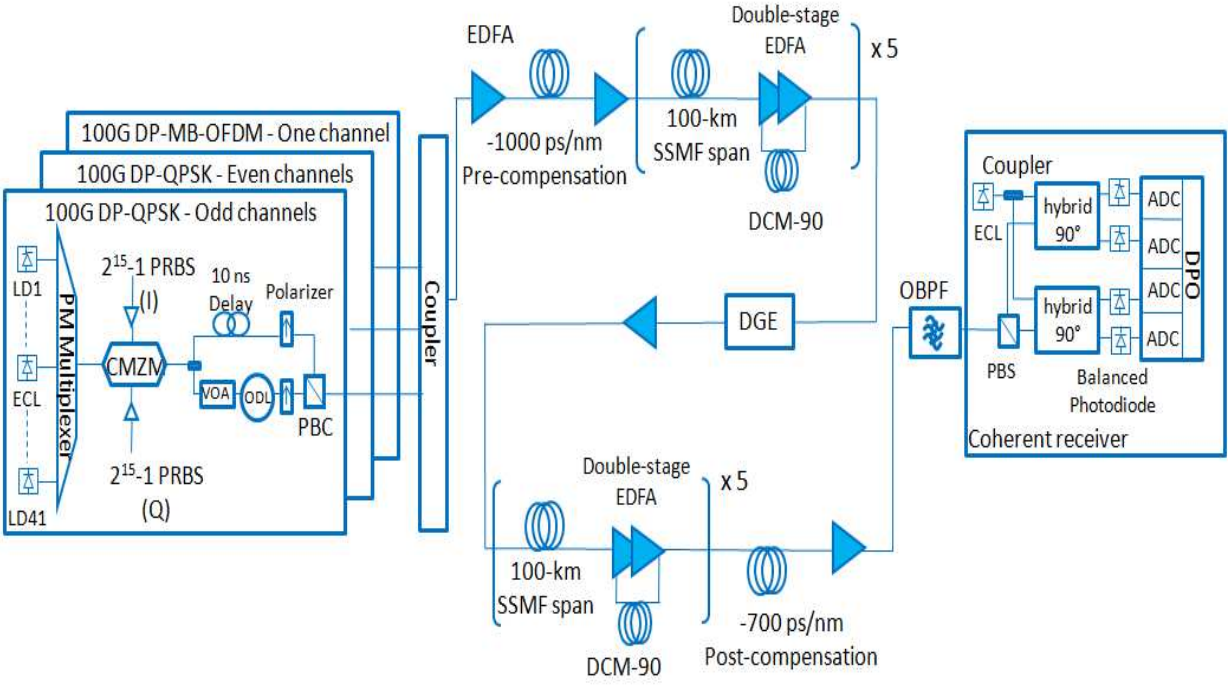

Figure 5-7: Set-up of the 100 Gbps DP-MB-OFDM and DP-QPSK transmitters, 1000 km DCF transmission line and coherent receiver.

Figure 5-8 shows the chromatic dispersion map. Note that this dispersion management is typical of the dispersion management currently used over the legacy 10 Gbps WDM systems.

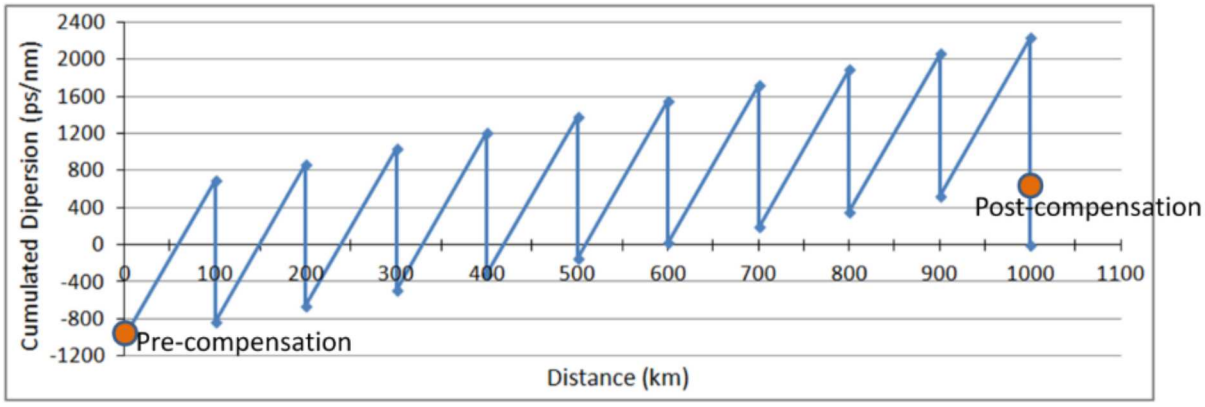

Figure 5-8: Evolution of the chromatic dispersion at 1550 nm.

In the following, the dispersion management and DCF-free schemes are denoted by "**DM/Single-Channel**" and "**Single-Channel**" for single channel transmission and by "**DM/WDM**" and "**WDM**" for QPSK WDM transmission, respectively.

5.3.1 Transmission performance comparison of the "Single-Channel" configuration with and without dispersion management

The first configuration evaluated is the "Single-Channel" configuration, in which the channel at 1552.93 nm carries the 100 Gbps DP-MB-OFDM signal and the channel at 1548.11 nm carries the 100 Gbps DP-QPSK signal. As previously, in this "Single-Channel" configuration; the other channels are present but not modulated. The two modulated channels and the thirty-eight unmodulated wavelengths are transmitted over the already described 10x100 km dispersion-managed G.652 fiber line.

In Figure 5-9 are plotted the BER as a function of the $P_{IN\ SPAN}$ for the 100 Gbps DP-QPSK (left fig) and 100 Gbps DP-MB-OFDM (right fig) channels. As reference, we have also plotted on this figure the results corresponding to the "Single-Channel" configuration previously obtained over the DCF-free line. The dispersion management and DCF-free schemes are denoted respectively on Figure 5-9 by "DM /Single-Channel" and "Single-Channel".

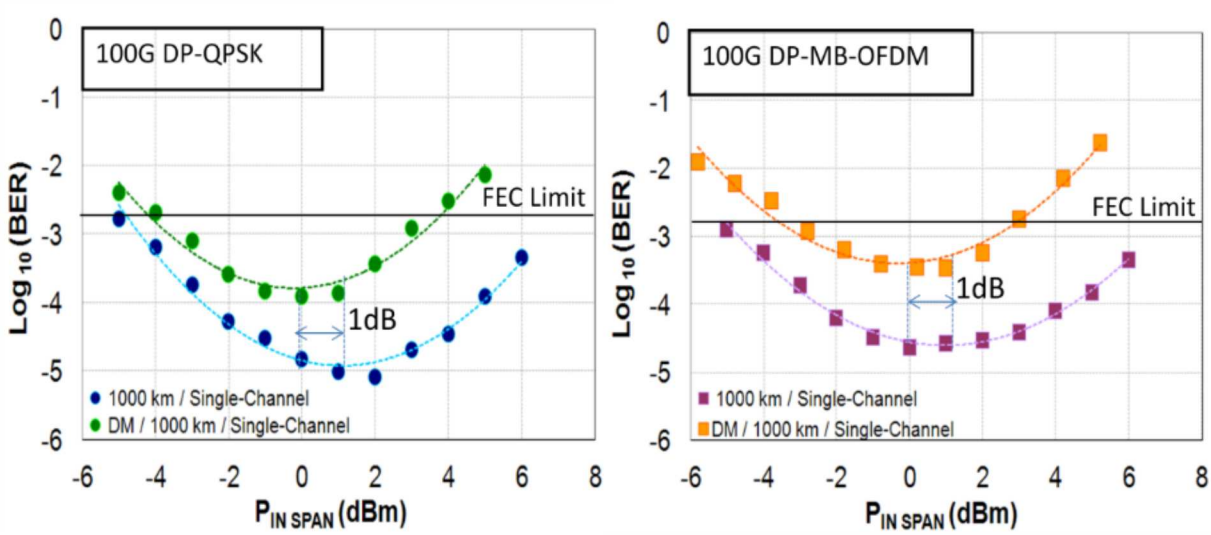

Figure 5-9: BER vs. span input power per channel for 100 Gbps DP-MB-OFDM (right fig) and DP-QPSK (left fig) after 1000 km of transmission over the DCF and DCF free G.652 fiber line in "Single-Channel" configuration.

Inspection of Figure 5-9 clearly shows that the introduction of dispersion management significantly degrades the transmission performance both in terms of BER (~1 decade is lost due to dispersion management) and optimal span input power per channel (which has to be decreased by 1 dB when dispersion management is used). Clearly, dispersion management exacerbates fiber nonlinearities, as soon as the "Single-Channel" configuration is considered. Let us now consider Figure 5-10 below, which illustrates the waveform evolution of a phase-modulated signal along the transmission line, first at the transmitter side, then in the middle of the link, and finally at the receiver side, for both the DCF-free (top of Figure 5-10) and dispersion-managed (bottom of Figure 5-10) cases, respectively. It can be observed that the envelope of the signal waveform changes with the accumulation of the chromatic dispersion, and that the location of the power peaks evolves with this last one. Consequently, fiber nonlinearities (in particular here SPM) acts homogeneously over all the parts of the signal and are averaged over all the duration of the signal and does not affect more particularly a special location of the waveform. At the opposite, in the dispersion management configuration, the power peaks are always located at the same time instants in the signal waveform as far as a given location of the dispersion map is considered. Consequently, SPM affects periodically always the same locations of the signal waveform, destroying progressively this waveform due to accumulation of nonlinear phase shifts in special waveform locations. Even if the PAPR of the signal waveform is higher over the DCF-free than over the dispersion-managed line, the transmission performance is better in the DCF-free case for the above reasons. Another explanation is the regular presence all along the line of DCF fiber in which nonlinearities are also slightly exacerbated in spite of a DCF input power per channel which is tuned so as to limit their impact.

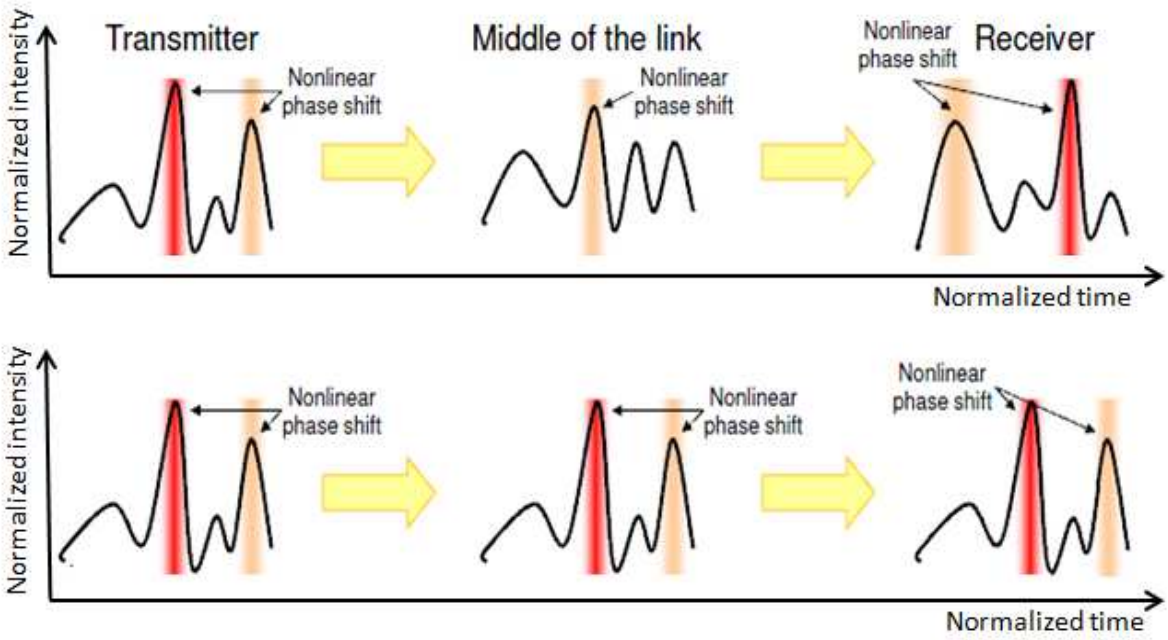

Figure 5-10: Waveform evolution of a phase-modulated signal along a transmission over DCF-free line (top fig) and over dispersion-managed line (bottom fig) [Jan12].

In spite of the fact that the two channels undergo the same nonlinearities accumulation over the 1000-km transmission of dispersion-managed G.652 fiber line, DP-QPSK performs slightly better (BER~$1x10^{-4}$ at $P_{IN\ SPAN}$ ~ 1 dBm) than DP-MB-OFDM (BER~$4x10^{-4}$ at $P_{IN\ SPAN}$ ~ 0 dBm), due probably (as there is no other WDM channels) to a stronger contribution of FWM and XPM interplays inside DP-MB-OFDM channel than in the DP-QPSK channel, in particular in the dispersion-managed configuration.

5.3.2 Performance comparison between "dispersion-managed WDM", "Single-Channel" and "WDM" configurations

The second configuration evaluated here is the "WDM" configuration over the dispersion-managed transmission line, denominated here by the "DM/WDM" acronym in the following plots. As represented on Figure 5-7, all the channels are modulated with 100 Gbps DP-QPSK, except the channel at 1552.93 nm which carries the 100 Gbps DP-MB-OFDM signal. This configuration does not correspond to any industrial 100 Gbps deployment case, but is interesting from a scientific point of view to identify the limitations of 100 Gbps DP-MB-OFDM transmission. The BER as a function of $P_{IN\ SPAN}$ for each of the two channels under measurements is plotted in Figure 5-11 and superimposed with the sensitivity curves already measured previously in the DCF-free configuration.

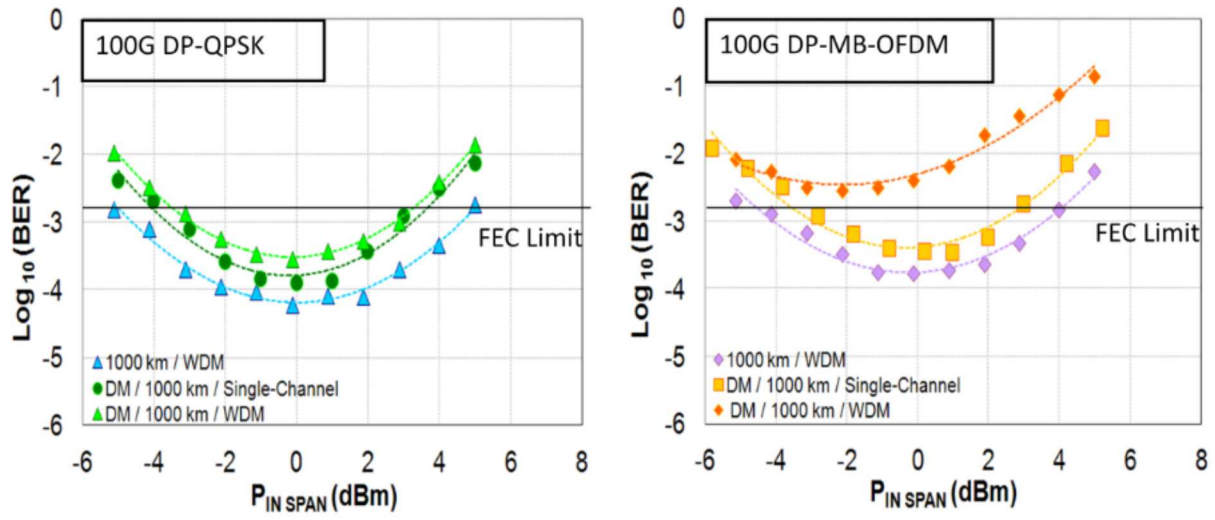

Figure 5-11: BER vs. span input power per channel for 100 Gbps DP-MB-OFDM (right fig) and DP-QPSK (left fig) after 1000 km of transmission over the DCF and DCF free G.652 fiber line in "WDM" configuration and over DCF fiber line in "Single-Channel" configuration.

Observation of Figure 5-11 shows that WDM transmission is very unfavorable to the 100 Gbps DP-MB-OFDM modulation over the DM line when compared to 100 Gbps DP-QPSK. In particular, compared to the previously measured "Single-Channel" case, the performance degradation is less than 2/10 of decades with 100 Gbps DP-QPSK and ~ 9/10 of decades with 100 Gbps DP-MB-OFDM, pointing out the higher sensitivity to cross-nonlinearities (XPM & XPolM) of 100 Gbps DP-MB-OFDM with respect to 100 Gbps DP-QPSK. Now compared to the "WDM" configuration over the DCF-free transmission line, the performance degradation over the DM line is ~1/2 BER decade with 100 Gbps DP-QPSK and 1.3 decades with 100 Gbps DP-MB-OFDM, pointing out the higher detrimental influence of the dispersion management over the 100 Gbps DP-MB-OFDM when compared to 100 Gbps DP-QPSK in this "WDM" configuration.
Two different interpretations can be then delivered to explain these behaviors. The explanations introduced in the previous part for the "Single-Channel" configuration are still valid to justify the better transmission performance of the DCF-free configuration over the "DM" one. The "WDM" configuration emphasizes the impact of nonlinearities because what has been explained in the previous paragraph for one channel is now de-multiplied by the presence of the other channels. But what is new here is the higher sensitivity to nonlinearities exacerbated by the dispersion management of 100 Gbps DP-MB-OFDM with respect to 100 Gbps DP-QPSK in the "WDM" configuration. The higher PAPR of OFDM over QPSK cumulated over all the WDM channels is a possible explanation of this difference of behavior between the 100 Gbps DP-MB-OFDM and 100 Gbps DP-QPSK in this "WDM" configuration over the DM line. This higher PAPR further exacerbates all the nonlinear effects which arise in the OFDM transmission: SPM, XPM, XPolM, and FWM.

The curves BER vs. OSNR shown in Figure 5-12 confirm this last interpretation. The OSNR penalties, which globally increase when we switch from the "Single-Channel" case to the "WDM" one, are significantly increased for the 100 Gbps DP-MB-OFDM modulation when compared to 100 Gbps DP-QPSK: while the OSNR penalty increases from 2.1 dB to 3.8 dB with 100 Gbps DP-QPSK, 100 Gbps MB-DP-OFDM experiences an OSNR penalty increase from 3 dB to 5 dB between the "Single-Channel" and the "WDM" configurations.

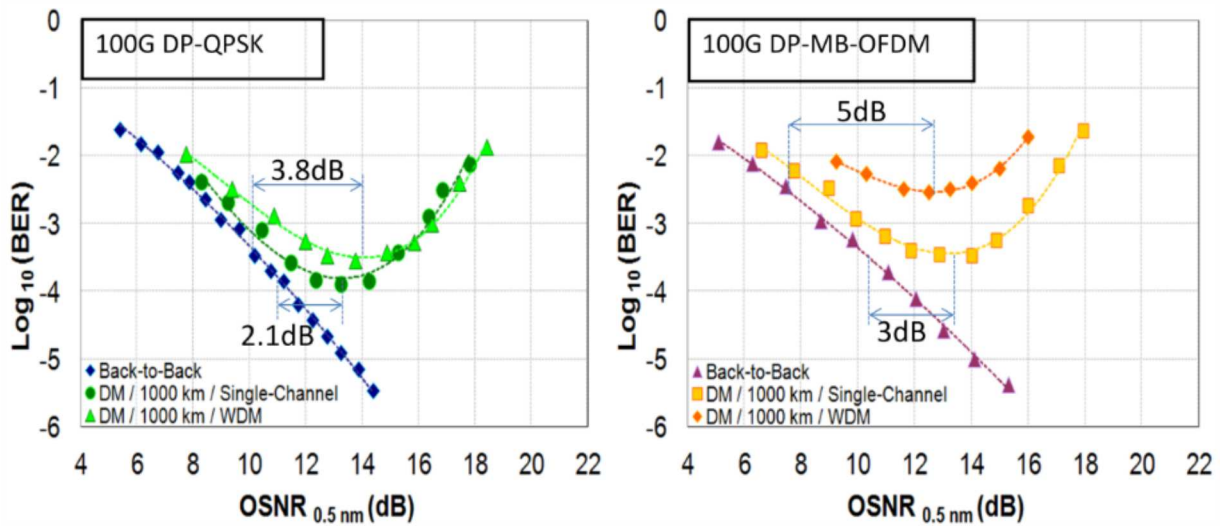

Figure 5-12: BER vs. received OSNR $_{0.5\ nm}$ for 100 Gbps DP-MB-OFDM (right fig) and DP-QPSK (left fig) after 1000 km of transmission over DCF G.652 fiber line in "Single-Channel" and "WDM" configurations and after the back-to-back design.

5.4 100 Gbps DP-MB-OFDM and 100 Gbps DP-QPSK transmission over legacy infrastructure including dispersion-managed (DM) fiber line and presence of 10 Gbps NRZ-OOK channels

The last configuration studied here, denoted by "**10G WDM**", corresponds to the case in which the 100 Gbps channels are deployed over an existing saturated 10 Gbps WDM transmission systems. By switching-off some 10 Gbps NRZ-OOK channels and replacing them by 100 Gbps channels, the system capacity can be gradually increased. Nonetheless, such 100 Gbps upgrade of a legacy 10 Gbps system results in drawbacks that will be pointed out in the following paragraphs.

Let us first describe the experimental set-up. The 100 Gbps DP-MB-OFDM transmitter operating at 1552.93 nm and the channel at 1548.11 nm carrying a 100 Gbps DP-QPSK signal are combined with a multiplex of 78 wavelengths spaced by 50 GHz and modulated at 10.7 Gbps by NRZ-OOK. The 78 NRZ channels at 10.7 Gbps are fed by standard laser diodes (LD) with wavelengths ranging from 1529.16 nm to 1560.61 nm. The 78 odd and even 10 Gbps channels are firstly encoded with an RS(255, 239) FEC code, separately multiplexed, independently modulated with de-correlated 2^{31}-1 PRBS, and then coupled with the two 100 Gbps channels. The DM transmission line has not been changed with respect to what has been previously described.

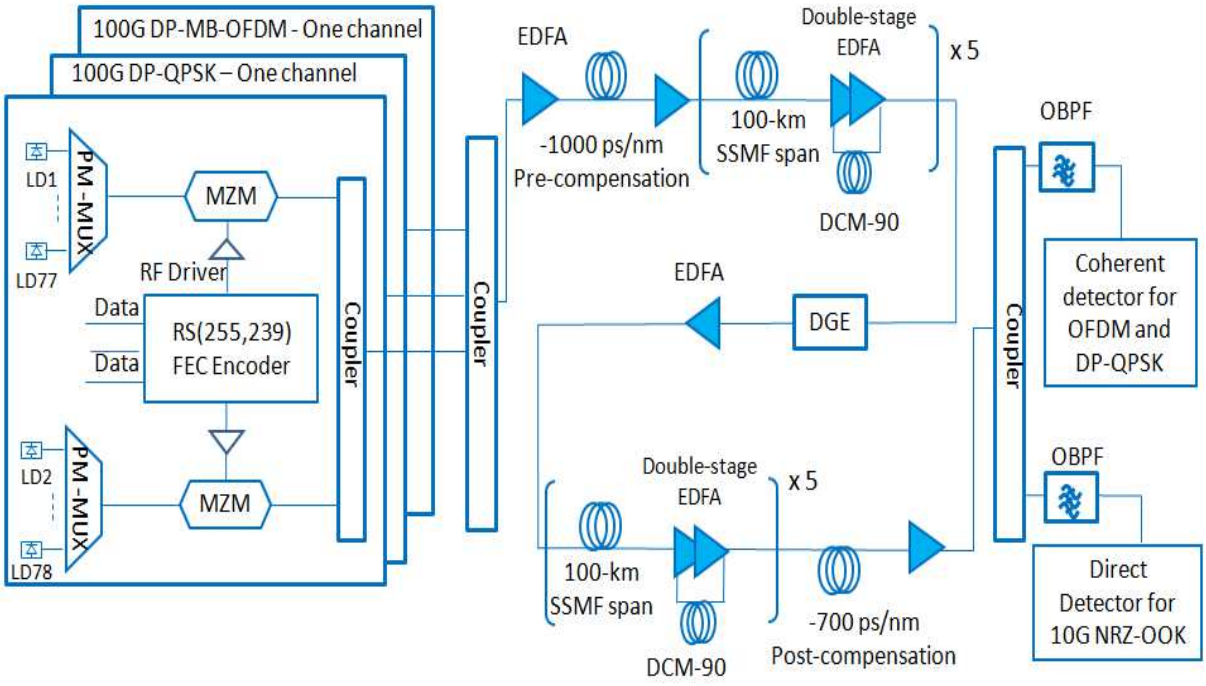

Figure 5-13:Set-up of the 100 Gbps DP MB-OFDM, 100 Gbps DP-QPSK, 10.7 Gbps NRZ-OOK transmitters, 10×100 km G.652 fiber transmission line, coherent receiver and direct detector with RS (Reed-Solomon).

At the receiver side, the 100 Gbps DP-MB-OFDM and DP-QPSK signals are selected by a square flat top OBPF of 0.4 nm bandwidth, and detected by a polarization diversity coherent receiver using a ~100 kHz bandwidth ECL as LO. The signals are converted back to the digital domain using a 50 GSa/s real-time DPO. The 10.7 Gbps NRZ channel under measurement is selected by a Gaussian OBPF of 0.25 nm bandwidth, detected by a 10 GHz photo-receiver, which feeds the FEC decoder and a 10.7 GHz clock and data recovery (CDR). The FEC card sends the decoded □□ □ □PBRS to a 9.95 Gbps BER tester (BERT).

5.4.1 Impact of the insertion of a guard band between the 10 Gbps NRZ-OOK channels and the 100 Gbps channels

Figure 5-14 below shows very well that, with both 100 Gbps DP-QPSK and 100 Gbps DP-MB-OFDM, the 10x100 km transmission over the G.652 fiber DM line is not error-free. The impact of cross-nonlinearities such as XPM and XPolM between the 100 Gbps channels and the 10 Gbps NRZ-OOK ones considerably degrades the transmission performance of 100 Gbps signals. Furthermore one can observe that the performance degradation is more important in this configuration than in the previous one, namely with the DM line and only 100 Gbps DP-QPSK and 100 Gbps DP-MB-OFDM channels. The intensity modulation of 10 Gbps NRZ-OOK neighbors impacts more the quality of transmission of 100 Gbps channels than the phase modulation of 100 Gbps DP-QPSK neighbors (transformed into intensity fluctuations by the chromatic dispersion).

In order to limit the impact of FWM, XPM and its XPolM corollary between the 10 Gbps NRZ channels and the 100 Gbps ones [Xie09], a first scheme has been tested, that consists in inserting a guard band of 100 GHz and 150 GHz, corresponding to one and two 10 Gbps channels switched-off from each side of the measured 100 Gbps channels ("GB=100 GHz" &

"GB=150 GHz" configurations). The BER vs $P_{IN\ SPAN}$ is plotted for both systems over Figure 5-14.
This option slightly improves the BER of 100 Gbps channels while increasing the optimum span input power per channel of both 100 Gbps DP-QPSK and 100 Gbps DP-MB-OFDM, but not sufficiently to be below the FEC limit. Note also that increasing the guard band width from 100 GHz to 150 GHz does not further improve transmission performance.

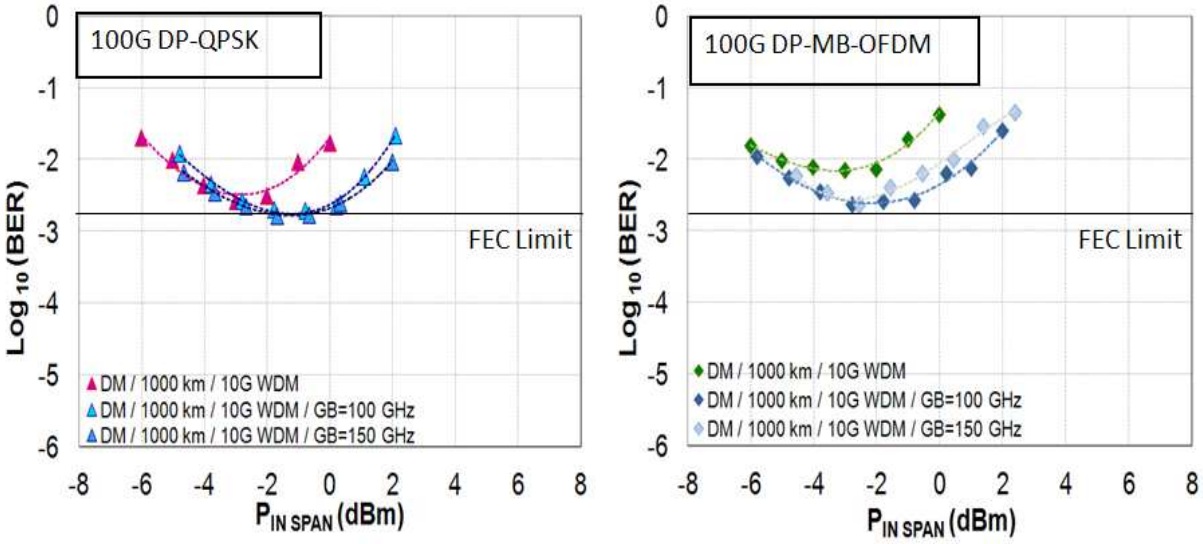

Figure 5-14: BER vs. span input power per channel for 100 Gbps DP-MB-OFDM (right fig) and DP-QPSK (left fig) after 1000 km of transmission over the DCF legacy fiber infrastructure in "WDM" configuration with and without adding a guard band between the 10 G and 100 G channels.

5.4.2 Impact of the insertion of a power dissymmetry between the 10 Gbps NRZ-OOK channels and the 100 Gbps channels

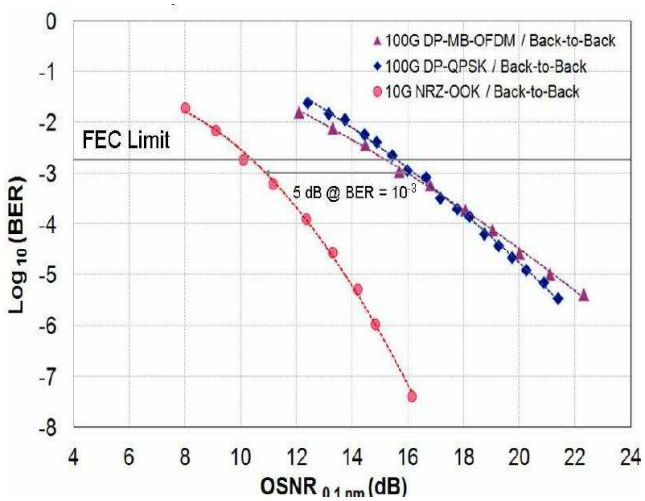

Figure 5-15: BER versus OSNR (in 0.1 nm) measured in back-to-back for the 124 Gbps DP-MB-OFDM, 112 Gbps DP-QPSK, and 10.7 Gbps NRZ-OOK signals.

Another possibility to reduce the impact of inter-channel nonlinearities between the 10 Gbps NRZ-OOK channels and the 100 Gbps ones is the reduction of the power in the 10 Gbps channels. In order to check the feasibility of this second solution, we have plotted in Figure

5-15 the BER as a function of the OSNR measured in 0.1 nm in back-to-back configuration for the three different modulation formats used in the WDM system: 100 Gbps DP-MB-OFDM, 100 Gbps DP-QPSK and 10 Gbps NRZ-OOK. As already shown, 100 Gbps DP-QPSK and 100 Gbps DP-MB-OFDM have the same OSNR sensitivity curves in the back-to-back configuration. But the more interesting thing is that 10 Gbps NRZ-OOK signal has 5 dB OSNR advantage over the 100 Gbps DP-QPSK and 100 Gbps DP-MB-OFDM in back-to-back near the FEC limit. This 5 dB advantage of 10 Gbps NRZ-OOK channels in back-to-back can be used to reduce the impact of fiber nonlinearities. Provided that transmission is error-free for these 10 Gbps NRZ-OOK channels after the 10x100 km G.652 fiber line, we reduce the power of the 10 Gbps channels of 5 dB with respect to that of the two 100 Gbps channels under study at the transmitter side. As a consequence, the power of 10 Gbps channels at the beginning of the fiber spans is also reduced by 5 dB. After the FEC decoding, we do not notice any error for the 10 Gbps channels after the 1000-km transmission. We start then the measurement of the performance of our two 100 Gbps DP-QPSK and 100 Gbps DP-MB-OFDM channels.

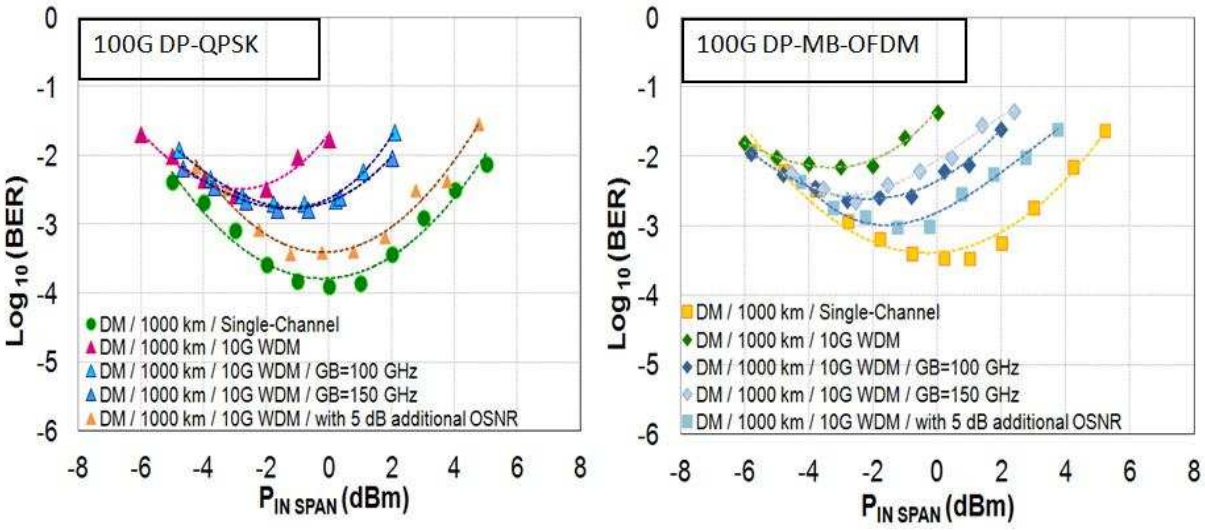

Figure 5-16: BER versus span input power per channel after the dispersion-managed 10×100-km G.652 fiber line for the 112 Gbps DP-QPSK and the 124 Gbps DP-MB-OFDM signals for the various configurations under study.

So, provided that the 10 Gbps NRZ channels have an advantage of 5 dB in terms of back-to-back OSNR sensitivity over both 100 Gbps DP-MB-OFDM and DP-QPSK signals, in the transmitter, the power of the 10 Gbps channels is reduced by 5 dB with respect to that of the 100 Gbps signals ("P(100G)-P(10G)= 5 dB" configuration). This solution improves the BER of 100 Gbps DP-QPSK and DP-MB-OFDM significantly: nearly one decade is gained with respect to the previous configurations where a guard-band of 100 GHz and 150 GHz was introduced. At the same time, the optimum span input power per channel is enhanced by 3 dB for DP-QPSK and by 2 dB for DP-MB-OFDM when compared to the "No Guard-Band" configuration, pointing out a decreased impact of the nonlinearities caused by the interactions between the 10 Gbps NRZ-OOK channels and the 100 Gbps ones.

This configuration permits the recovery of system margins and ensures an error-free 1000-km transmission, suggesting that the 10 Gbps channel power reduction option is a viable solution to limit the impact of XPM, XPolM, and FWM in such legacy infrastructure. Nonetheless, the BER obtained in the "Single-Channel" configuration in which the intra-channel nonlinearities are only excited is not recovered. Note that no error has been detected for the two 10 Gbps nearest neighbors of the 100 Gbps DP-MB-OFDM and DP-QPSK

channels (at the optimum span input power per channel over the curves of Figure 5-16). Figure 5-16 also points out that the 100 Gbps DP-QPSK shows a slightly higher performance than the 100 Gbps DP-MB-OFDM, which is less than half a BER decade in the various configurations under study. The optimum span input power per channel is also slightly higher (up to 1 dB) in the DP-QPSK case, indicating an upper resistance of 100 Gbps DP-QPSK over 100 Gbps DP-MB-OFDM to inter-channel nonlinear effects.

5.5 Conclusion

We have experimentally demonstrated that DP-MB-OFDM is a credible solution for modern DCF-free 100 Gbps WDM transmission systems. At the opposite of what is currently reported, in such a DCF-free configuration, 100 Gbps OFDM has performance comparable to the industrial 100 Gbps DP-QPSK solution. These results are really new, and should requalify OFDM as a credible solution for next generation of WDM systems working at data rate higher than 100 Gbps.

Furthermore, our experiments have confirmed that dispersion management is very detrimental for OFDM transmission in the absence or in the presence of 10 Gbps NRZ-OOK channels. When the 10 Gbps NRZ-OOK channels are present in the DM transmission system, the transmission of 100 Gbps DP-QPSK and 100 Gbps DP-MB-OFDM cannot be error-free. One has then to modify the architecture of the transmission system to recover some margins and restore the performance. The first tested solution has consisted in inserting a guard-band between the 10 Gbps and 100 Gbps channels. Unfortunately, this solution does not sufficiently improve the transmission performance to reach the FEC limit: inserting a guard-band of 100 or 150 GHz does not make the transmission error-free. In contrast, we have shown in this chapter that reducing the power of 10 Gbps NRZ-OOK channels by 5 dB with respect to the power of 100 Gbps channels is a relevant solution to restore the performance and realize error-free transmission of 100 Gbps DP-QPSK and 100 Gbps DP-MB-OFDM signals. We also show that, even in this configuration, the difference of performance between the 100 Gbps DP-QPSK and 100 Gbps DP-MB-OFDM channels is less than half a decade in BER. It is thus possible to introduce 100 Gbps DP-QPSK and 100 Gbps DP-MB-OFDM channels over a legacy WDM transmission system using G.652 fiber, dispersion management and 10 Gbps NRZ-OOK channels.

As a general conclusion, we can notice that, even if the performance of coherent 100 Gbps DP-MB-OFDM is slightly worse than that of coherent 100 Gbps DP-QPSK, the results are very encouraging when considering the next generation of 400 Gbps or 1 Tbps WDM systems based on OFDM technology.

Bibliography

[Alc] A.-L. 1. P. Brochure. www.alcatel-lucent.com ; Ciena 6500 product data sheet, www.ciena.com..

[Jan12] S. L. Jansen, "Multi-Carrier approaches for next-generation transmission: why, where and how?," in *OFC tutorial*, 2012.

[Liu09] X. Liu, F. Buchali, and R. W. Tkach, "Improving the nonlinear tolerance of polarization-division-multiplexed CO-OFDM in long-haul fiber transmission," 2009.

[Low07] A. J. Lowery, S. Wang, and M. Premaratne, "Calculation of power limit due to fiber nonlinearity in optical OFDM systems," 2007.

[LyG06] D.-S. Ly-Gagnon, S. Tsukamoto, K. Katoh, and K. Kikuchi, "Coherent detection of optical quadrature phase-shift keying signals with carrier phase estimation," 2006.

[Sav08] S. J. Savory, "Digital filters for coherent optical receivers," 2008.

[Shi08] W. Shieh, H. Bao, and T. Tang, "Coherent optical OFDM: theory and design," *Optics Express*, 2008.

[Xie09] C. Xie, "WDM coherent PDM-QPSK systems with and without inline optical dispersion compensation," 2009.

6 Conclusion

Chapter 6

CONCLUSION

This thesis lays out several experimental set-ups carried out in order to build for the first time in France an OFDM transceiver operating at 100 Gbps and to validate the different digital signal processing steps necessary to recover the transmitted data. It then establishes a performance assessment of the OFDM signal with respect to the single-carrier QPSK signal, for a transmission over 1000 km of G.652 fiber line.

The nominal data rate of 100 Gbps, increased up to 128 Gbps to account for the various transmission overheads (7% for FEC, 6% for protocol, 7.03% for cyclic prefix, 5% for training symbols, and 2.9% for pilot tones), is split between four polarization-multiplexed OFDM sub-bands. Each sub-band carries ~32 Gbps in a bandwidth of ~8 GHz while the sub-band spacing is 10 GHz.

A comb generator comprising a MZM driven by an RF frequency, followed by the combination of 20 GHz and 40 GHz polarization-maintaining delay line interferometers has allowed the generation of 4 combs of sub-carriers that feed 4 optical modulators each driven by the I and Q components of the 4 OFDM signals. The signals at the outputs of CMZMs are polarization multiplexed and then filtered.
However several stages in the transmitter structure can cause an IQ mismatch, e.g., a gain difference between the I and Q arms, a deviation from the □□□phase-shift between the two paths, and/or a time delay mismatch between the I and Q tributaries of the OFDM signals. We have proposed a simple method to finely tune the transmitter. It is based on the observation of the OFDM signal spectrum and consists in suppressing the optical power contained in the lower side-band when just the upper-band carries data or vice versa.

On the receiver side, the signal is detected by a polarization diversity coherent receiver using a ~100 kHz bandwidth ECL as local oscillator. The signal is converted back to the digital domain using a 50 GSa/s real-time oscilloscope (DPO). The offline digital signal processing (DSP) is then performed with four basic steps: synchronization according to the algorithm developed by Minn & Bhargava, which also allows the estimation of a frequency offset (CFO) in the range of $\pm 2\Delta f$ (Δf being the sub-carrier spacing); however, the CFO can exhibit high values that result in intecarrier interferences (ICI) and performance impairment of the transmission system when it is not compensated for. The estimation of the CFO is achieved through the implementation of a new and simple method. The CFO is found just by determining the frequency shift of the last filled OFDM sub-carrier located just before the zero or empty sub-carriers area, which is required in order to isolate the OFDM signal from the aliasing products generated by the digital-to-analogue converters (DAC); improved channel estimation combining time and frequency-domain averaging, followed by 2x2 MIMO zero-forcing equalization; and finally compensation of the common phase noise generated by the ECLs using the pilot sub-carriers.

The performance of the 100 Gbps DP-MB-OFDM system is compared to the performance of 100 Gbps DP-QPSK single-carrier system in back-to-back configuration. We observe that both systems have the same performances.

Also the impact of CD and PMD on the OFDM system performance has been investigated. The 100 Gbps coherent DP-MB-OFDM system was stressed by -10000 ps/nm of CD, 180 ps of FOPMD, and 8220 ps^2 of SOPMD while the SOP variation speed was fixed to 70°/ms.

We have shown that the impact of these effects on the OFDM performance is negligible for BER worse than $1x10^{-4}$.

After evaluating the impact of CD and PMD on the system performance, the 100 Gbps DP-MB-OFDM and 100 Gbps DP-QPSK are transmitted over 10 spans of 100 km of G.652 fiber, with or without dispersion management, in presence or in absence of 10 Gbps neighbors. We have experimentally demonstrated that DP-MB-OFDM is a credible solution for modern DCF-free 100 Gbps WDM transmission. 100 Gbps coherent DP-QPSK and DP-MB-OFDM transmission over legacy infrastructure (with dispersion management and presence of 10 Gbps neighbors) is possible over 1000 km of G.652 fiber, but under the condition to decrease the 10 Gbps channel power with respect to 100 Gbps channels by 5 dB. In such realistic conditions, 100 Gbps DP-MB-OFDM and DP-QPSK have a nearly similar performance. Even if the OFDM performance is slightly worse than that of 100 Gbps DP-QPSK, these results are very encouraging when considering the next generation of 400 Gbps or 1 Tbps WDM systems based on OFDM technology.

Perspectives

As network traffic, driven by high-bandwidth digital applications is growing exponentially, the capacity of WDM system will reach its scalability limits. To meet the ever increased growth in capacity, several solutions can be helpful.
The first solution relies on the use of a polarization-multiplexed high QAM constellation. However, accumulations of both ASE noise and fiber nonlinearities prevent the use of high QAM modulation and limit the maximum transmission distance of the signal. Even if several techniques have been proposed for the electronic compensation of the impact of nonlinear effects, for example, digital back-propagation (DBP), its compensation is at the expense of a high computational complexity. Moreover, the implementation of those techniques will not be practical as it requires knowledge of the optical path. To cope with the fiber nonlinearities, an ultra low loss, and super large effective area fibre can be strongly recommended to reduce nonlinear effects and ASE noise accumulation.
A second solution is provided by replacing the EDFA by Raman amplification. Raman amplification is able to distribute the gain into the line fiber permitting a significant improvement in the received OSNR at the end of the WDM link, and thus also increases significantly the maximum reach of the WDM transmission system and allows the use of higher order modulation since the fiber nonlinearities may be reduced. Furthermore, the Raman amplification opens a bandwidth of ~100 nm by extending the WDM bandwidth over S, C and L bands.

Another potentially strong solution to scale up the capacity of optical transport networks further, is spatial division multiplexing (SDM). An SDM system uses M parallel transmission paths per wavelength, and thus multiplies the available capacity of a given link by a factor of M. These parallel optical paths could be multiple cores within a multi-core fiber, or multiple modes within a multi-mode waveguide. Importantly, SDM is highly scalable since M can potentially be chosen to be very large. This creates high hopes for the use of SDM as a method to satisfy the data traffic growth for the next decade and beyond. After the integration of SDM, non-negligible crosstalk between multiple parallel transmission paths is introduced, so multiple-input multiple-output (MIMO) signal processing techniques should be used. However this solution is not yet mature: it requires the development of new fibers and amplifiers for space-division multiplexing (SDM).

In addition to any of those possible solutions, the use of super-channels which reduces the frequency guard interval between the sub-channels allowing thus the bit rates to be further increased is fundamental. The concept of the super-channel has been proposed to enable an overall capacity per WDM channel of 400 Gbps or 1 Tbps over long transmission distances by using a set of very compact sub-channels with spacing close or equal to the symbol rate. Nyquist wavelength-division multiplexing (N-WDM) and OFDM are both suitable formats for achieving high spectral efficiency super channels.

The first format achieves a high spectral efficiency by applying electrical or optical Nyquist filtering to the single-carrier signal in order to have an ideally rectangular spectrum with a bandwidth equal to the symbol rate. Consequently, as there is no spectral overlap between the neighbouring sub-channels, inter-channel crosstalk is removed. Quasi-Nyquist wavelength-division multiplexing (QN-WDM) transmission can also be achieved by relaxing the Nyquist condition and using a filter that approximates the ideal case with a channel spacing which is slightly larger than the symbol rate.

The alternative format, OFDM, has a narrow optical spectrum without the use of sharp cut-off filters. Several descendants of this kind of modulation are under study for optical transmission. Among these, we can mention the Reduced Guard Interval (RGI) CO-OFDM and DFT spread OFDM. In the proposed RGI CO-OFDM scheme, the cyclic prefix duration is reduced. Its duration is sufficient to prevent ISI, induced by an error on the estimation of the beginning of the signal, or by fiber polarization-mode dispersion (PMD). However CD is compensated for prior to OFDM signal processing at the receiver. This approach enables the reduction of the CP and then the increase of spectral efficiency. Conversely, DFT-Spread-OFDM is a technique used in wireless communication (LTE for uplink applications) and offers lower peak-to-average-power-ratio (PAPR) than conventional OFDM at the expense of higher complexity, since a DFT and IDFT are also implemented at the transmitter and receiver side, respectively. It has recently been adopted in optical transmission, and has shown higher nonlinear tolerance over conventional OFDM, especially with a dispersion managed transmission scheme.

The two formats would be expected to achieve similar maximum transmission distances and similar high spectral efficiency. However, which is the format that will be considered for long-haul transmission distances? Which type of fiber must be retained? Will we continue to keep the same fiber infrastructure and adopt Raman amplification? Or will the potential technology include ultra low loss and super large area fiber, multi-mode or multi-core fibers? Maybe different, low-loss and large effective area fibers combined with Raman amplification would solve the need for an ever-increasing optical fiber capacity and for reaching transmission distances beyond 1500 km.
The answer to these questions will be provided in the very near future.

Publications and patents

Publications:

[1] J. Karaki, E. Giacoumidis, D. Grot, T. Guillossou, C. Gosset, R. L. Bidan, T. L. Gall, Y. Jaouen and E. Pincemin, "Dual-Polarization Multi-Band OFDM versus Single-Carrier DP-QPSK for 100 Gbps long-haul WDM transmission over legacy fiber"," in *Optics Express* 2012.

[2] J. Karaki, E. Pincemin, D. Grot, T. Guillossou, Y. Jaouen, R. L. Bidan and T. L. Gall, "Dual-Polarization Multi-Band OFDM versus Single-Carrier DP-QPSK for 100 Gbps long-haul WDM transmission over legacy fiber"," in *ECOC* 2012.

[3] E. Giacoumidis, J. Karaki, E. Pincemin, C. Gosset, R. L. Bidan, E. Awwad and Y. Jaouen, "100 Gb/s coherent optical polarization multiplexed multi-band-OFDM (MB-OFDM) transmission for long-haul applications," in *ICTON*, 2012.

[4] E. Pincemin, J. Karaki, M. Selmi, D. Grot, T. Guillossou, C. Gosset, Y. Jaouen and P. Ciblat, "100 Gbps DP-QPSK performance over DCF-Free and legacy system infrastructure," in *IEEE Photonics conference*, 2012.

[5] J. Karaki, E. Pincemin, D. Grot, T. Guillossou, Y. Jaouen and R. L. Bidan, "Performance comparison between multi-band OFDM and single-carrier DP-QPSK for 100 Gbps long-haul WDM transmission," in *SPPCOM*, 2012.

[6] J. Karaki, E. Pincemin, Y. Jaouen and R. L. Bidan, "Frequency offset estimation robustness in a polarization-multiplexed coherent OFDM system stressed by chromatic dispersion and PMD," in *CLEO US*, 2012.

[7] J. Karaki, E. Pincemin, Y. Jaouen and R. L. Bidan, "First and Second-Order PMD impact over 100 Gbps polarisation multiplexed multi-band coherent OFDM system under realistic "field" conditions," in *IEEE Photonics conference*, 2011.

[8] E. Pincemin, J. Karaki, Y. Loussouarn, H. Poignant, C. Betoule, G. Thouenon and R. L. Bidan, "Challenges of 40/100 Gbps and beyond deployments over long-haul transport networks," *Optical Fiber Technology*, 2011.

[9] J. Karaki, E. Pincemin, T. Guillosou, Y. Jaouen and R. L. Bidan, "Approche multi-bandes pour la transmission WDM longue distance à 100 Gbps de signaux OFDM cohérents multiplexés en polarisation," in *JNOG*, 2011.

[10] S. Blouza, J. Karaki, N. Brochier, E. L. Rouzic, E. Pincemin and B. Cousin, "Multi-Band OFDM networking concepts," *Eurocon*, 2011.

Patents:

a) „*Procédé et dispositif de filtrage optique coupe-bande et dispositif d'insertion/extraction de sous-bande optique multiplexée en fréquence dans un signal optique*' Patent N° 11 51082 FR, Feb. 2011

b) 'Procédé de traitement d'un signal multi-porteuse reçu, procédé de réception d'un signal optique, programme d'ordinateur et dispositif de traitement correspondants' Patent N° 21199 FR, 2012